The Extracellular Matrix to Bind Them All:

Interactions Between ECM and Cells in Lung Fibrosis and Influences Thereof

Mehmet Nizamoglu

The Extracellular Matrix to Bind Them All: Interactions Between ECM and Cells in Lung Fibrosis and Influences Thereof

Mehmet Nizamoglu

The studies presented in this thesis were performed within an industrial collaborative PhD program between University Medical Center Groningen (UMCG) and Boehringer Ingelheim.

The printing of this thesis was financially supported by the University of Groningen, Graduate School of Medical Sciences, the Dutch Society for Matrix Biology (NVMB) and Boehringer Ingelheim.

ISBN (printed): 978-94-6483-345-4

Cover design: Albano Tosato
Layout: Wouter Aalberts | www.persoonlijkproefschrift.nl
Print: Ridderprint | www.ridderprint.nl

university of groningen

University Medical Center Groningen

NVMB
Dutch Society for Matrix Biology

university of groningen

The Extracellular Matrix to Bind Them All: Interactions Between ECM and Cells in Lung Fibrosis and Influences Thereof

PhD thesis

to obtain the degree of PhD at the
University of Groningen
on the authority of the
Rector Magnificus Prof. J.M.A. Scherpen
and in accordance with
the decision by the College of Deans.

This thesis will be defended in public on

Wednesday 27 September 2023 at 14.30 hours

by

Mehmet Nizamoğlu

born on 29 June 1992
in Kadıköy, Istanbul, Turkey

Supervisors
Prof. J.K. Burgess
Prof. H.I. Heijink
Prof. B.N. Melgert

Assessment Committee
Prof. R.A. Bank
Prof. G. Westergren-Thorsson
Prof. M. Kolb

Paranymphs
Mugdha M. Joglekar
Roderick H. J. de Hilster

"The head may err, but never the blood."

Nakajima Atsushi, in *Light, Wind and Dreams*

TABLE OF CONTENTS

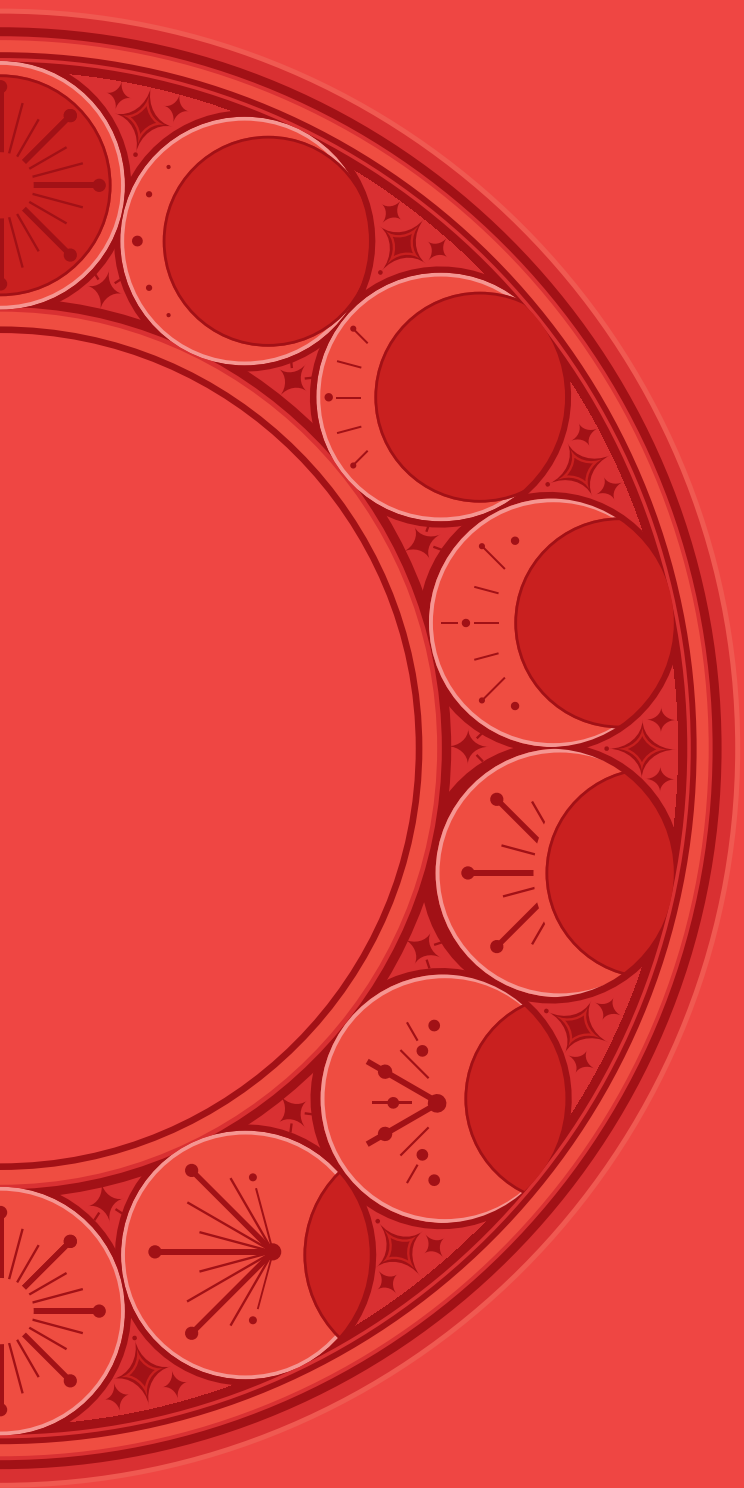

CHAPTER 1

General Introduction

Lung fibrosis encompasses several different pulmonary diseases, all of which result in fibrotic scar tissue accumulation in the lung interstitium, the region between the alveolar epithelium and blood vessels [1]. The most common type is idiopathic pulmonary fibrosis (IPF) which has an unknown etiology and is mainly characterized by progressive fibrosis and a poor prognosis [2]. The survival rate for patients with IPF is very low: a recent meta-analysis reported an overall median survival of 3.2 years [3]. Despite the fact that IPF is the most common type of lung fibrosis, it is still classified as a rare disease with a prevalence of 3-45 in 100,000 [4]. The current school of thought suggests that the IPF originates from repeating (micro)injuries in the alveolar epithelium of lung tissue, followed by an aberrant wound repair response involving the recruitment of the (myo)fibroblasts to the injured area [5]. Unfortunately, to date, there is no permanent cure for IPF except for lung transplantation [6]. The only two available therapeutics, Nintedanib and Pirfenidone, merely slow the progression of fibrosis, increase the median survival rate but cannot reverse or cure established disease [7, 8]. One of the main reasons for a lack of new treatment strategies is the lack of thorough knowledge of the mechanisms underlying disease progression, as the fibrotic process is already, usually, at a very late stage at the time of diagnosis. Another roadblock is the lack of adequate laboratory and animal models to investigate the complex disease mechanisms of IPF [9].

The formation of aberrant extracellular matrix (ECM), deposited as scar tissue, is a key disease mechanism not only for IPF but for all fibrotic lung diseases [10]. Forming the immediate environment around the cells, the ECM is composed of a plethora of proteins, proteoglycans and glycosaminoglycans [11]. ECM provides a mechanical scaffold for the resident cells to attach; moreover, it provides bioactive cues through its own composition, as well as the growth factors that are stored in it [12]. Lung ECM is of vital importance for lung function through providing structural support and elasticity [13]. In fibrotic lung diseases, including IPF, the native ECM is disrupted with respect to its composition, mechanics and organization [14]. These collective changes during fibrosis result in a stiff and rigid scaffold instead of a soft and elastic network [15, 16]. In the last decade, our thoughts on how ECM plays a role in biological processes, has evolved drastically from an inert scaffold towards a bioactive and instructive network. Parallel to these revelations, our understanding on the realms of how ECM might be involved in the progression of a fibrotic response in lung diseases has also improved. We now know that the presence of fibrotic ECM alone, *in vitro,* guides cells towards a more pro-fibrotic state in a positive feedback loop, possibly resulting in generation of more fibrotic ECM [17-19]. Together with aberrant composition, disorganized fibers and altered mechanics, abnormal cells

in fibrotic ECM mark the four neighboring regions with complex relationships with the realms of fibrotic ECM (**Figure 1**).

"*One Ring to rule them all, One Ring to find them,*
One Ring to bring them all, and in the darkness bind them." – *J.R.R. Tolkien.*

However, the details of the overruling capacity of ECM among the interactions between the ECM and the resident cells are still uncharted. By investigating and characterizing the interactions between the ECM and cells, which are already imprinted by the fibrotic ECM *in vivo*, we can broaden our horizons on how the pro-fibrotic cycle continues towards further activation of cells or disruption of composition, organization and mechanics of ECM.

■ **Figure 1: The landscape and influence of the Realms of Extracellular Matrix (ECM).** Aberrant composition, disorganized fibers, altered biomechanics and abnormal cells are important areas that regulate the interactions between the (fibrotic) ECM and resident cells are shaped during the course of the fibrotic response.

AIM AND OUTLINE OF THIS THESIS

The overarching aim of this thesis was to investigate and characterize the interactions between the fibrotic ECM and cells, to elucidate how these contribute to subsequent pro-fibrotic reactions.

In Chapter 2, I outlined the changes in the composition, mechanics and organization of ECM during lung fibrosis and summarize the recent advances regarding how these changes might pave the way to a better understanding of fibrotic responses.

In Chapter 3, I reported how collagen type XIV, an ECM protein, is involved in fibrotic lungs. While its role in the organization of fibrillar collagens was previously demonstrated, the status of collagen type XIV in IPF was not described prior. In this study, I investigated how the relative proportion of collagen type XIV protein is different in lungs of patients with IPF at the whole tissue level, as Ill as in specific tissue compartments.

In Chapter 4, I critically summarized the cutting-edge technologies used to mimic lung microenvironments in three-dimensional (3D) *in vitro* conditions. After reviewing different *in vitro* tools, and their advantages and disadvantages, I discussed the challenges associated with such models. Moreover, I provided a detailed overview of the recent translational applications for each model and characterizations of such models.

In Chapter 5, I investigated regenerative responses of cells isolated from the lungs of IPF patients and compared them to cells isolated from non-IPF lungs using an organoid model system. I hypothesized that supportive cells from the stromal niche/microenvironment imprinted by a fibrotic ECM carry over their "lessons" and result in a dysregulated regenerative response of epithelial cells. I compared the number and size of organoids developed from unfractionated cells obtained from non-IPF lungs to IPF lungs. In addition, I isolated epithelial cells from these unfractionated cell populations to test their regenerative capacity without the influence of additional cells.

In Chapter 6, I described the state-of-the-art status of 3D *in vitro* models used to mimic lung ECM. I explained the advantages of 3D over two-dimensional (2D) culture systems and exemplified the most commonly used materials to create a 3D *in vitro* lung microenvironment.

In Chapter 7, I provided a perspective on recent developments in lung ECM-derived hydrogels. After a brief review of the innovative science utilizing such hydrogels, I deliberated on the path towards developing new technologies based on ECM-derived hydrogels.

In Chapter 8, I harnessed the potential of lung ECM-derived hydrogels by artificially introducing fiber crosslinking. I hypothesized that applying additional fiber crosslinking would result in increased stiffness, and in turn would trigger cellular changes that are also observed during the fibrosis process. I investigated the changes in hydrogel mechanics and fiber organization, and examined cellular responses with respect to fibroblast activation. By creating an *in vitro* model that represents changes in the mechanical properties of fibrotic ECM alone, I succeeded in separating the mechanical influence of fibrotic ECM from the biomechanical influence on cells.

In Chapter 9, I examined ECM and cell interactions using both IPF and non-IPF human lung ECM-derived hydrogels and human primary lung fibroblasts. I hypothesized that the origin of microenvironment would overrule the origin of the fibroblasts, and that IPF matrix can drive fibrotic responses in fibroblasts from normal lungs. I tested this hypothesis by comparing the influence of the microenvironment with the influence of the cell origin by combining IPF or non-IPF ECM-derived hydrogels with IPF or non-IPF fibroblasts, ultimately resulting in a combinatorial comparison. I characterized changes in collagen amount and collagen fiber organization, glycosaminoglycan content as well as mechanical properties of hydrogels with and without fibroblasts to compare the instructiveness of non-IPF and IPF microenvironments.

In Chapter 10, the outcomes of the individual chapters of this thesis are integrated and discussed. The future perspectives of our findings with respect to interactions between ECM and cells in IPF are also included in this discussion. In the context of cellular functions, mechanical forces and fibrillar organization, this section concludes with how ECM *brings them all, binds them all,* and ultimately, *rules them all.*

REFERENCES

1. Wijsenbeek M, Suzuki A, Maher TM. Interstitial lung diseases. *Lancet* 2022: 400(10354): 769-786.
2. Khor YH, Ng Y, Barnes H, Goh NSL, McDonald CF, Holland AE. Prognosis of idiopathic pulmonary fibrosis without anti-fibrotic therapy: a systematic review. *Eur Respir Rev* 2020: 29(157): 190158.
3. Ryerson CJ, Kolb M. The increasing mortality of idiopathic pulmonary fibrosis: fact or fallacy? *Eur Respir J* 2018: 51(1): 1702420.
4. Podolanczuk AJ, Thomson CC, Remy-Jardin M, Richeldi L, Martinez FJ, Kolb M, Raghu G. Idiopathic Pulmonary Fibrosis: State of the Art for 2023. *Eur Respir J* 2023: 2200957.
5. Martinez FJ, Collard HR, Pardo A, Raghu G, Richeldi L, Selman M, Swigris JJ, Taniguchi H, Wells AU. Idiopathic pulmonary fibrosis. *Nat Rev Dis Primers* 2017: 3(1): 17074.
6. Lederer DJ, Martinez FJ. Idiopathic Pulmonary Fibrosis. *N Engl J Med* 2018: 378(19): 1811-1823.
7. Guenther A, Krauss E, Tello S, Wagner J, Paul B, Kuhn S, Maurer O, Heinemann S, Costabel U, Barbero MAN, Muller V, Bonniaud P, Vancheri C, Wells A, Vasakova M, Pesci A, Sofia M, Klepetko W, Seeger W, Drakopanagiotakis F, Crestani B. The European IPF registry (eurIPFreg): baseline characteristics and survival of patients with idiopathic pulmonary fibrosis. *Respir Res* 2018: 19(1): 141.
8. Behr J, Prasse A, Wirtz H, Koschel D, Pittrow D, Held M, Klotsche J, Andreas S, Claussen M, Grohe C, Wilkens H, Hagmeyer L, Skowasch D, Meyer JF, Kirschner J, Glaser S, Kahn N, Welte T, Neurohr C, Schwaiblmair M, Bahmer T, Oqueka T, Frankenberger M, Kreuter M. Survival and course of lung function in the presence or absence of antifibrotic treatment in patients with idiopathic pulmonary fibrosis: long-term results of the INSIGHTS-IPF registry. *Eur Respir J* 2020: 56(2): 1902279.
9. Moss BJ, Ryter SW, Rosas IO. Pathogenic Mechanisms Underlying Idiopathic Pulmonary Fibrosis. *Annu Rev Pathol* 2022: 17(1): 515-546.
10. Upagupta C, Shimbori C, Alsilmi R, Kolb M. Matrix abnormalities in pulmonary fibrosis. *Eur Respir Rev* 2018: 27(148): 180033.
11. Burgstaller G, Oehrle B, Gerckens M, White ES, Schiller HB, Eickelberg O. The instructive extracellular matrix of the lung: basic composition and alterations in chronic lung disease. *Eur Respir J* 2017: 50(1).
12. Theocharis AD, Skandalis SS, Gialeli C, Karamanos NK. Extracellular matrix structure. *Adv Drug Deliv Rev* 2016: 97: 4-27.
13. Burgess JK, Harmsen MC. Chronic lung diseases: entangled in extracellular matrix. *Eur Respir Rev* 2022: 31(163): 210202.
14. Herrera J, Henke CA, Bitterman PB. Extracellular matrix as a driver of progressive fibrosis. *J Clin Invest* 2018: 128(1): 45-53.

15. Booth AJ, Hadley R, Cornett AM, Dreffs AA, Matthes SA, Tsui JL, Weiss K, Horowitz JC, Fiore VF, Barker TH, Moore BB, Martinez FJ, Niklason LE, White ES. Acellular normal and fibrotic human lung matrices as a culture system for in vitro investigation. *Am J Respir Crit Care Med* 2012: 186(9): 866-876.

16. de Hilster RHJ, Sharma PK, Jonker MR, White ES, Gercama EA, Roobeek M, Timens W, Harmsen MC, Hylkema MN, Burgess JK. Human lung extracellular matrix hydrogels resemble the stiffness and viscoelasticity of native lung tissue. *Am J Physiol Lung Cell Mol Physiol* 2020: 318(4): L698-L704.

17. Parker MW, Rossi D, Peterson M, Smith K, Sikstrom K, White ES, Connett JE, Henke CA, Larsson O, Bitterman PB. Fibrotic extracellular matrix activates a profibrotic positive feedback loop. *J Clin Invest* 2014: 124(4): 1622-1635.

18. Philp CJ, Siebeke I, Clements D, Miller S, Habgood A, John AE, Navaratnam V, Hubbard RB, Jenkins G, Johnson SR. Extracellular Matrix Cross-Linking Enhances Fibroblast Growth and Protects against Matrix Proteolysis in Lung Fibrosis. *Am J Respir Cell Mol Biol* 2018: 58(5): 594-603.

19. Liu F, Lagares D, Choi KM, Stopfer L, Marinkovic A, Vrbanac V, Probst CK, Hiemer SE, Sisson TH, Horowitz JC, Rosas IO, Fredenburgh LE, Feghali-Bostwick C, Varelas X, Tager AM, Tschumperlin DJ. Mechanosignaling through YAP and TAZ drives fibroblast activation and fibrosis. *Am J Physiol Lung Cell Mol Physiol* 2015: 308(4): L344-357.

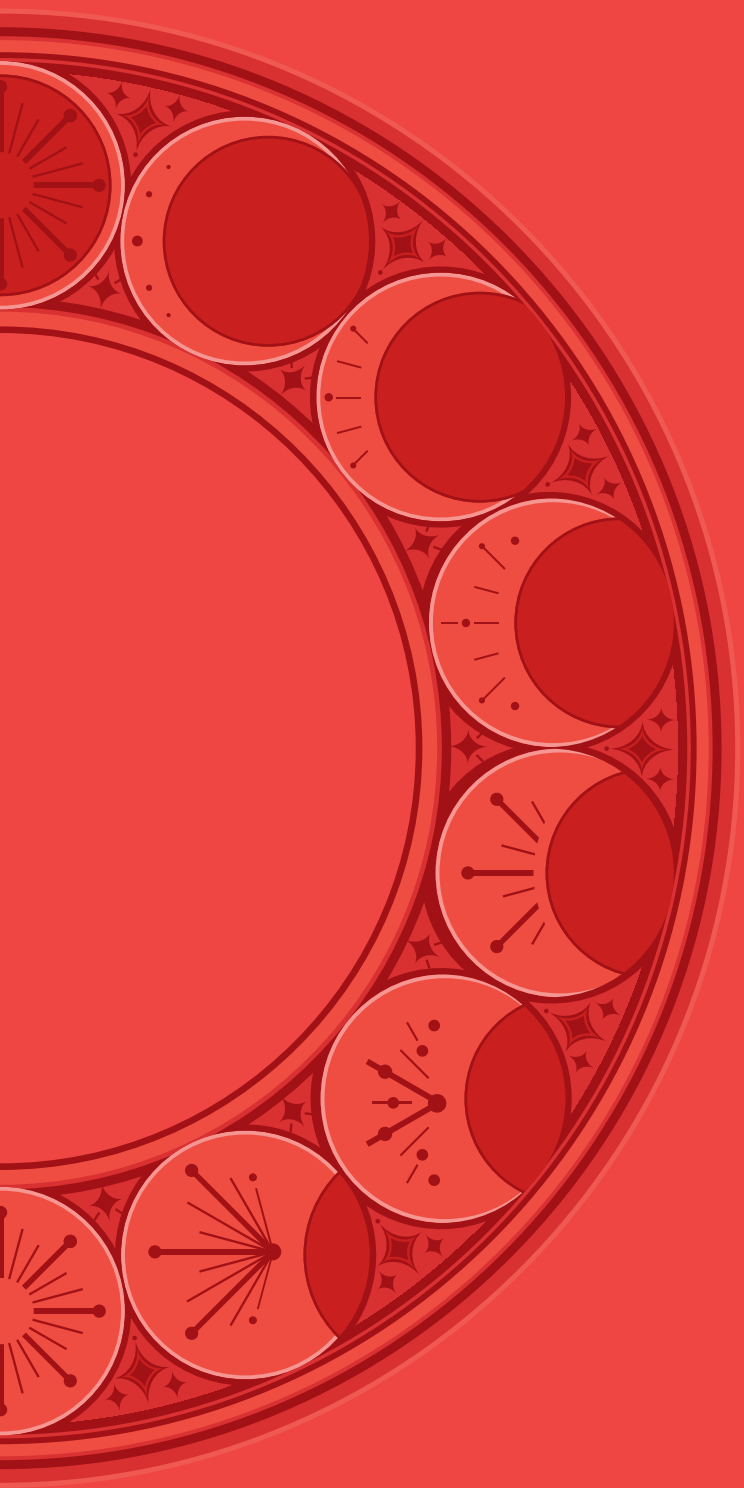

CHAPTER 2

The multi-faceted extracellular matrix: unlocking its secrets for understanding the perpetuation of lung fibrosis

Mehmet Nizamoglu & Janette K. Burgess

Reproduced with permission from Springer Nature from the publication in *Current Tissue Microenvironment Reports*:

Nizamoglu, M., & Burgess, J. K. (2021). The multi-faceted extracellular matrix: Unlocking its secrets for understanding the perpetuation of lung fibrosis. *Current Tissue Microenvironment Reports*, *2*(4), 53–71.
https://doi.org/10.1007/s43152-021-00031-2

ABSTRACT

Purpose of review: Lung fibrosis is currently thought to stem from an aberrant wound healing response after recurring (micro) injuries in the lung epithelium, together with disrupted crosstalk between epithelial and stromal cells. An important factor in lung fibrosis is the abnormal deposition of extracellular matrix (ECM). In this review, we extend the view of ECM to summarize how aberrant structural organization and degradation of ECM contributes to (perpetuation of) lung fibrosis.

Recent findings: Fibrotic changes in ECM including altered composition, such as increased collagens, coupled with mechanical properties, such as increased stiffness or abnormal fiber crosslinking, promote pro-fibrotic responses in cells in this microenvironment. Similarly, changes in matrix degrading enzymes and release of degradation products from ECM proteins also perpetuate cellular fibrotic responses.

Summary: In lung fibrosis, irreversible ECM structure, organization and architectural alterations drive a perpetuating fibrotic response. Targeting strategies abrogating the abnormal ECM or ECM-degrading enzymes accompanied by prognostic and/or diagnostic approaches based on ECM fragments may provide novel alternatives to current therapeutic approaches for lung fibrosis.

INTRODUCTION

Lung fibrosis is a common characteristic of the heterogeneous group of interstitial lung diseases (ILDs). Of these the most common is idiopathic pulmonary fibrosis (IPF), which is a chronic, progressive lung disease, with a very poor survival rate (median: 3–5 years) [1]. Currently, there is no cure for IPF, other than lung transplantation, and while there are two therapeutic agents, pirfenidone and nintedanib, that can slow the disease progression, these therapies are not effective in all patients and have adverse, sometimes severe side effects [2]. Lung fibrosis is currently thought to result from an aberrant wound healing response following recurrent microinjuries to the alveolar epithelium, augmented by aberrant cross-talk between the fibroblasts and epithelial cells resulting in an excessive and abnormal deposition of extracellular matrix (ECM) proteins [3–5].

Under normal physiological conditions, ECM is composed of a multitude of different proteins, glycosaminoglycans (GAGs), and glycoproteins (collagen types I, III, IV and VI, fibronectin, laminin, periostin, and hyaluronic acid are a few examples), forming a dynamic network that provides support to the cells embedded within it [6, 7]. In addition to its structural support function, ECM is a bioactive component of the tissue and it provides cues to all cells to influence/instruct their behavior. In fibrosis, deposition of several different ECM proteins such as collagens and fibronectin is increased, while others are decreased, changing the biochemical composition of the tissue [8]. As a natural consequence of the changes in the protein composition and organization, the biomechanical properties of fibrotic lung tissues are also altered: fibrotic lungs are stiffer, have a greater degree of collagen crosslinking and altered topography [9–11]. This catalogue of changes was previously thought to only be the result of the fibrotic process within the tissue; however, a plethora of recent studies have illustrated the changes in the ECM are an emerging contributor to the disease progression process itself, influencing different cell types and cellular mechanisms [12–17]. Moreover, with the advances in the single-cell RNA sequencing methods, lung resident cell populations are shown to have great heterogeneity in lung fibrosis, compared to healthy lungs, which would also impact the diversity of ECM changes in fibrosis [18–21]. Interestingly, it has recently been suggested (in the context of embryonic development) that each cell type expresses its own unique ECM gene profile (indicative of the production of an individual ECM protein profile) that becomes more refined as the cells differentiate towards end-stage cells such as fibroblasts [22]. This finding implies the importance of the ECM microenvironment, which is disrupted in fibrosis, for the maintenance of a homeostatic status in tissue. However, the detailed mechanisms regarding how altered properties of ECM affect cellular responses or contribute to the cellular heterogeneity present in fibrosis and the consequent influence upon the disease outcome are yet to be investigated completely.

In this review, we summarize the varied aspects of the contribution of ECM in lung fibrosis and how ECM influences cellular responses. First, we focus on updates for understanding how changes in ECM composition, coupled with altered mechanical properties, impact cellular responses. Then, we look beyond the ECM scaffold to illustrate how ECM degradation and the released bioactive ECM fragments play a role in lung fibrosis. Finally, we reflect on how targeting (changes in) ECM can be leveraged to provide new avenues for managing lung fibrosis.

ECM CHANGES IN FIBROSIS AND THEIR FUNCTIONAL CONSEQUENCES

Composition and Crosslinking

In pulmonary fibrosis, changes in the quantities of ECM proteins have been extensively described [6, 9, 23] : including, but not limited to, increased collagen types I and III, fibronectin, periostin, and hyaluronic acid. One of the most important pieces of evidence illustrating how fibrotic ECM induces fibrotic responses in fibroblasts, as a result of the feedback in two dimensional (2D) cell culture models, was described by Parker et al [14]. In concert, primary lung fibroblasts cultured on scaffolds made with stacked sections of decellularized IPF lung were shown to produce a protein output that mirrored the fibrotic matrix composition compared to the fibroblasts cultured on scaffolds made with control lung tissue [24]. By comparing the decellularized fibrotic and alveolar tissue-derived sections of mouse *ex vivo* lung tissue scaffolds, the fibrotic microenvironment was found to decrease the spontaneous movement speed of immortalized mouse fibroblasts, compared to healthy mouse tissue [13]. The effect of the microenvironment was shown to also influence responses in other cells: Monocyte-derived macrophages in the fibroblastic-foci were found to perpetuate the fibrotic response, suggesting the fibrotic microenvironmental cues were guiding these cellular responses [25]. Similarly, pericytes were also shown to have higher gene and protein expression of α smooth muscle actin (α-SMA) when cultured on decellularized IPF lung samples compared to decellularized control lung samples [26]. Interestingly, culturing alveolar epithelial cells on IPF lung derived decellularized matrices was found to protect alveolar epithelial cells from transforming growth factor β (TGF-β) induced apoptosis, while additionally strengthening the profibrotic response of IPF lung-derived decellularized matrix-seeded fibroblasts to TGF-β via engagement of integrin α2β1, compared with cells seeded on non-disease control lung derived decellularized matrices [27]. These studies collectively show the influence of the fibrotic ECM on different cells, illustrating the different responses of the cells to the changing microenvironment in lung fibrosis.

Along with the changes in the biochemical distribution of the ECM proteins in fibrosis, post-translational modifications of these proteins are also altered. Collagen protein synthesis starts within the rough endoplasmic reticulum, with post-translational modifications adding hydroxyl groups to proline and lysine residues **(Figure 1)** [28]. Individual collagen molecules come together within the Golgi to form the triple helical structure, forming the procollagen molecule. This trimer then is secreted from the Golgi into the extracellular space, where its pro-collagen ends at both the C- and N-terminals are cleaved to generate the mature collagen molecule. The collagen molecules self-assemble to begin forming fibrils before lysyl oxidases (LOX), LOX-like enzymes (LOXLs) and transglutaminases (TGs) actively crosslink the triple helices to each other, forming the collagen fibers [28]. Increased expression and amount of LOXL1 and LOXL2 was reported in IPF lung tissue compared with non-disease control lung tissue [11]. In concert, fibrotic fibroblasts were found to have higher expression of TG2 compared with healthy fibroblasts *in vitro* [29]. Crosslinking of the collagen fibers by LOX/LOXL has also been shown to promote the TGF-β induced stiffening of the microenvironment [11]. ECM deposited by from IPF-lung derived fibroblasts increased the expression of LOXL3 and TG2; and in turn, the increased crosslinking of this ECM was demonstrated to boost fibroblast proliferation and adhesion [29]. These data together suggest that the increased collagen crosslinking, and dysregulation of the crosslinking enzyme amounts in pulmonary fibrosis could contribute to the positive feedback loop which Parker et al. first described [14].

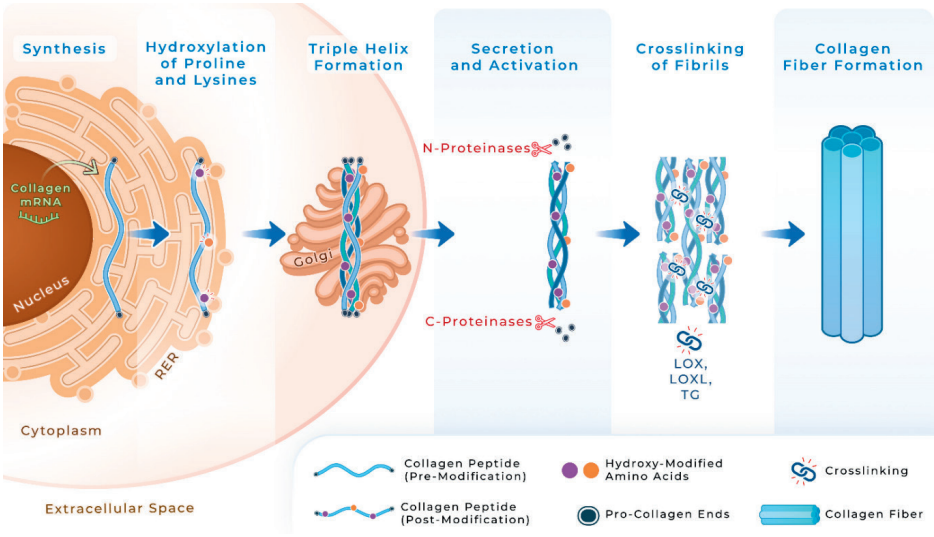

■ **Figure 1: Schematic illustration of synthesis, secretion and crosslinking of collagen fibrils.**
RER: Rough endoplasmic reticulum; LOX: lysyl oxidase; LOXL: LOX-like; TG: transglutaminase.

Stiffness and Viscoelasticity

Changes in the biomechanics of fibrotic lung tissue result directly from the altered and abnormal distribution and modification of the ECM proteins in lung fibrosis. Lung ECM has a viscoelastic nature that can dissipate the stress applied to it via various sources, such as mechanical forces changing with breathing in and out [10]. Among many biomechanical parameters, stiffness of the tissue is strongly associated with lung fibrosis and has been well-documented: native IPF lung samples were shown to have higher stiffness than control lung samples (1.96 ± 0.13 kPA vs 16.52 ± 2.25 kPA) and this difference remained similar also in decellularized lung samples (IPF lung sample: 7.34 ± 0.6 kPa, control lung sample: 1.6 ± 0.08 kPA) [9, 10]. Stiffness, like many other mechanotransducers, induces the Hippo pathway through yes-associated protein (YAP) – PDZ-binding motif (TAZ) signaling, resulting in the perpetuation of fibrosis [30]. Several *in vitro* models have been developed to assess the effect of stiffness on lung cells: fibroblasts cultured on 2D hydrogels with higher stiffness were shown to migrate faster, along with a greater cell spread area, compared to the fibroblasts cultured on hydrogels with lower (more physiological-like) stiffness [31]. Similarly, a stiffer 2D culture environment was shown to increase fibroblast activation via chromatin remodeling compared to softer surfaces, accompanied by increased nuclear volume in these fibroblasts [32]. Higher stiffness of fibronectin coated polyacrylamide hydrogels was shown to decrease fibroblast activating protein expression while increasing the cell spreading area and αSMA expression in murine lung fibroblasts compared with softer hydrogels; on the other hand, changes in the stiffness of collagen type I coated polyacrylamide hydrogels did not change the cellular response [33]. Likewise, comparing the effect of different stiffness values of polyacrylamide hydrogels and incorporation of solubilized matrix from healthy or IPF lungs on pericytes seeded on these hydrogels showed that increased cell area and higher expression of αSMA resulted from the increase in the stiffness of the hydrogel rather than the ECM composition [26]. Interestingly, a study by Matera et al. suggested opposing effects of stiffness on lung fibroblasts in 2D and 3D cultures: higher stiffness of 2D cultures promoted myofibroblast differentiation while stiffer 3D cultures limited the differentiation of the lung fibroblasts [12]. Lastly, blocking the YAP – TAZ pathway of mechanotransduction in IPF lung-derived fibroblasts resulted in decreased expression of ECM proteins while ECM-degradation enzyme gene expression levels increased compared to the untreated IPF fibroblasts [34]. All of these studies together indicate different effects of stiffness on cells. It is highly possible that the combination of altered composition and increased stiffness induces different cellular responses in different cells. More investigation on separating the contribution of altered composition and stiffness of the fibrotic microenvironment

could improve our understanding and help identify novel therapeutic approaches for targeting the progression of lung fibrosis.

Another emerging parameter among the biomechanical properties of ECM is the viscoelasticity, which is the ability to dissipate an applied stress through time [35]. The importance of the viscoelasticity of ECM both in healthy and diseased conditions has been recently reviewed elsewhere [36]. Similar to many other tissues and organs, lung ECM has viscoelastic properties and the loss of viscoelastic relaxation in fibrotic tissues has recently been established by our group [10]. The implications of (the loss of) viscoelasticity on cellular function *in vivo* is yet to be clarified; however, it is known that changes in the viscoelasticity of the microenvironment can affect cell migration, proliferation and ECM deposition by the cells [36]. All of these cellular functions are recognized as being altered in lung fibrosis, so now the challenge lies in separating the individual contributions of these different mechanical stimuli to the perpetuation of the fibrotic response. Promisingly, a recent study revealed the possibility of modifying stiffness and viscoelasticity independently of each other [37]. Developing advanced *in vitro* culture systems will further our understanding of viscoelasticity and its contribution to the progression of the lung fibrosis.

Topography

Topography of the ECM influences many cellular responses including migration and proliferation, as recently reviewed by Ouellette et al. [38]. While the altered composition alone could influence the topography of the ECM in lung fibrosis, the increased crosslinking and abnormal alignment of the fibers in the ECM are two other important factors changing the topography. In lung fibrosis, the topography of the ECM is drastically altered (**Figure 2**), due to the increased mature and organized collagen content, compared to the healthy lungs [11].

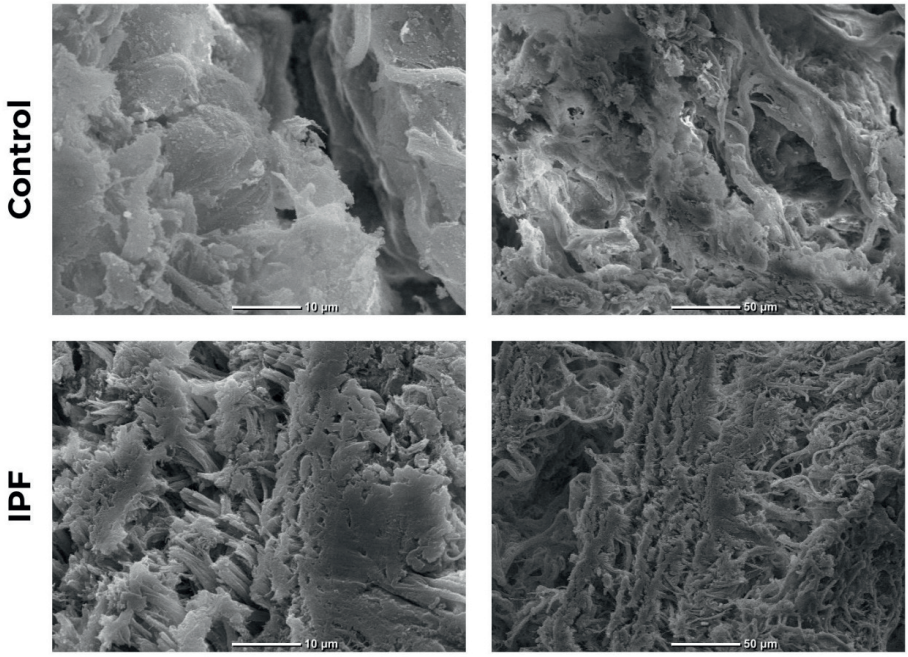

Figure 2: Representative scanning electron microscopy (SEM) images of decellularized lung parenchyma from non-disease control donors (upper row) and IPF patients (lower row).

One of the mechanisms by which abnormal topography plays a role in lung fibrosis is the altered microstructures in the protein organization. In a study by Seo et al., comparison of adipose-derived stromal cells seeded on collagen type I networks with thin fibers and low pore size to cells seeded on networks with thick fibers and bigger pore size revealed that changing the microstructure increased differentiation of these stromal cells to myofibroblasts ~1.5X [39]. Along with fiber thickness and pore size, fiber alignment is an important parameter in ECM topography. Increased migration speed of primary lung fibroblasts seeded on collagen type I -methacrylated gelatin hydrogels was observed in highly aligned network samples, compared to hydrogels with less aligned networks [40]. In another study, increasing fiber density independent of the stiffness resulted in higher surface area of seeded dermal fibroblasts in 3D *in vitro* culture [41]. While collagen type I hydrogels with different stiffness values were used to test the effect of microstructure in the study by Seo et al., it is difficult to conclude the stiffness-independent contribution of the microstructure. As the abovementioned changes (stiffness, viscoelasticity and topography) in the fibrotic ECM occur simultaneously during fibrosis, more studies using advanced biomaterials are required to examine the individual contributions of such properties to the perpetuation of the fibrotic response.

Storage of growth factors in the ECM

As the non-cellular part of the tissue microenvironment, the ECM serves as a storage depot for many different growth factors and other soluble proteins, many of which are important for regulating the fibrotic response. Within the ECM, it is predominantly the glycosaminoglycans (GAGs) that serve as a reservoir for growth factors in the extracellular space. The negatively charged residues within the GAGs provide multiple binding sites for the positively charged amino acids within many growth factors. Through these binding interactions the growth factors are bound to the ECM, protecting them from degradation and conserving them until they are required for local signaling [42, 43]. The changing protein content and organization in fibrotic lung diseases is likely to alter the presence, amount, and the availability of the factors stored within ECM. Among these ECM proteins, fibronectin can bind many growth factors and soluble proteins, including latent TGF-β-binding protein-1 (LTBP-1) [44]. Increased amounts of fibronectin and LTBP-1 in fibrosis could lead to a greater storage capacity of ECM for TGF-β. Activation of the stored TGF-β can be directed via mechanical stimuli due to prestress on the ECM, applied by cells or decreased viscoelastic relaxation of the ECM itself [45]. TGF-β activation is also regulated by mechanisms driven by other proteins including fibulin-1, an ECM glycoprotein, which is also found in greater amounts in the lung tissues of IPF patients [46, 47].

The binding of growth factors important for lung development and repair, including TGF-β, fibroblast growth factor (FGF) 1 and FGF2 and hepatocyte growth factor (HGF), and their interaction with their relevant receptors are dependent on the sulfation state of GAGs such as heparan sulfate, dermatan sulfate and chondroitin sulfate [42, 48]. Using hydrogels established using decellularized lung ECM (which is devoid of most GAGs) combined with heparan sulfate, dermatan sulfate or chondroitin sulfate with either TGF-β, FGF2 or HGF, Uhl and colleagues recently illustrated that matrix associated growth factor-dependent and -independent GAG effects in parallel with GAG-dependent and -independent matrix-associated growth factor effects are important for regulating cellular responses in lung *in vitro* models [48]. There is an increase in heparan sulfate, chondroitin sulfate, dermatan sulfate and hyaluronan in IPF lungs compared to controls [49], suggesting a greater capacity for anchoring important growth factors for regulating reparative or fibrotic processes in these tissues. Analyses of the sulfation state of the GAGs in the IPF tissues found that the highly sulfated GAGs were located predominantly in the regions of interaction between the fibrotic and less fibrotic tissues, potentially indicating a central role for the GAGs in providing growth factors for promoting the high fibrotic activity within these regions.

Table 1: Summary of recent studies illustrating changes related to ECM in fibrosis and their impacts on cell responses.

Category	Changes in ECM	Cellular Response	Reference
ECM Crosslinking	Pan-inhibition of LO activity	Lower rates of TGF-β induced collagen remodeling and ECM stiffness in human primary lung fibroblasts seeded on decellularized cell-derived ECM	[11]
	Increased ECM crosslinking by TG2	Higher rates of proliferation in human primary lung fibroblasts seeded on decellularized IPF cell-derived ECM	[29]
	Knock out of LOXL3 by siRNA	Lower rates of fibroblast-to-myofibroblast differentiation in normal human lung fibroblasts	[50]
	Deficiency of LOXL1	Lower expressions of TGF-β, collagen type I and αSMA in TGF-β overexpression mice model of fibrosis at day 35 compared to wild type mice of the same model	[51]
Stiffness	Increased stiffness in 2D polyacrylamide hydrogels	Faster migration and higher spread area normal human lung fibroblasts	[31]
	Increased stiffness in 2D collagen type I-coated culture	higher rate of activation and higher nuclear volume in murine primary lung fibroblasts	[32]
	Increased stiffness of fibronectin coated polyacrylamide hydrogels	Higher αSMA expression in murine lung fibroblasts	[33]
	Increased stiffness of polyacrylamide hydrogels functionalized with solubilized matrix from lungs	Higher cell area and higher αSMA expression in human primary microvascular pericytes	[26]
	Increased stiffness in 2D dextran-based hydrogels functionalized with MMP-cut sites	Higher myofibroblast differentiation in normal human lung fibroblasts	[12]
	Increased stiffness in 3D dextran-based hydrogels functionalized with MMP-cut sites	Lower myofibroblast differentiation in normal human lung fibroblasts	[12]
Topography	Thicker collagen fibers in 3D collagen type I hydrogels	Higher myofibroblast differentiation in human adipose derived stromal cells	[39]
	Increased alignment of collagen type I -methacrylated gelatin hydrogel networks	Increased migration speed in human primary lung fibroblasts in 2D	[40]
	Increasing fiber density in 3D dextran-based hydrogels functionalized with MMP-cut sites	Higher myofibroblast differentiation, cell spread area, YAP translocation and proliferation rate in normal human lung fibroblasts	[12]

LO: Lysyl oxidase, ECM: Extracellular matrix, TG: Transglutaminase, LOXL: Lysyl oxidase-like, TGF-β: Transforming growth factor β, αSMA: α Smooth muscle actin, MMP: Matrix metalloproteinase, YAP: Yes-associated protein

It is not unlikely that the ECM in fibrotic lung disease would have enhanced storage capacity for bioactive factors as a result of the increased amount of the abovementioned ECM proteins, among others, and the activation and release of these factors from the ECM would be boosted by the biomechanical changes in the tissues in lung fibrosis. Further investigations regarding the ECM-stored bioactive factors are necessary for improving our understanding of the contribution of the repository function of the ECM to the progression of lung fibrosis.

Collective impact of the altered ECM scaffold in fibrotic lung disease

All in all, the altered ECM in fibrosis generates diverse influences which impact cellular phenotypes; as summarized in **Table 1**. While the biochemical changes in the fibrotic microenvironment have been demonstrated with proteomics analyses via mass spectrometry [6], the accompanying biomechanical changes, such as increase in stiffness or loss of viscoelastic relaxation [10], require further investigation. While these changes could be simply the result of the altered biochemical composition, there are other emerging contributing factors such as collagen crosslinking that require further clarification. With the new developments in the field of biomaterials, advanced *in vitro* culture systems will be generated to mimic the specific biomechanical properties of the fibrotic microenvironment. Such systems will further improve our understanding of how the biomechanical properties of the ECM, either individually or collectively, contribute to the perpetuation of fibrotic disease in the lung. Eventually, such knowledge should illuminate how such properties could be targeted via therapeutic intervention for treatment of lung fibrosis.

BEYOND THE ECM SCAFFOLD

The role of ECM degrading enzymes and their regulators

The ECM is a dynamic microenvironment that is constantly being remodeled as elements are degraded and newly deposited during normal tissue maintenance and particularly under conditions of disease pathogenesis. While all cell types synthesize, secrete and orchestrate deposition of ECM (including epithelial cells, mesenchymal cells, endothelial cells and immune cells), the fibroblasts are recognized as the major ECM producing cell type in fibrotic tissues. Leukocytes and macrophages, but also mesenchymal and epithelial cells produce enzymes that regulate the degradation of the ECM. The most well recognized group are the matrix metalloproteinases (MMPS), but also serine or cysteine proteases have a role in maintaining a healthy homeostasis within the ECM [52, 53]. Activity of the enzymes that degrade the ECM is tightly balanced by endogenous inhibitors (tissue inhibitors of MMPs (TIMPs)), serpins or cystatins [54–56].

In fibrotic lung disease, an easy assumption would be that there would be reduced levels of matrix degradative enzymes, in particular MMPs, as this is where the greatest amount of research has focused, as an explanation as to why there is increased ECM deposition. However, multiple studies report increased levels of several MMPs associated with fibrotic lung disease, reviewed in [53, 57, 58]. While this appears paradoxical, it is important to realize that in addition to degrading ECM proteins, the range of substrates MMPs can process and activate includes cell receptors, chemokines and growth factors [59]. Through the generation of chemotactic gradients or activation of specific proinflammatory or profibrotic factors, in cooperation with disruption of basement membranes and other physical barriers within the tissue, MMPs can influence the influx of inflammatory cells into the site of tissue injury, which in turn then contribute to the development / perpetuation of fibrosis [60, 61]. A number of MMPs have been specifically linked to fibrosis in the lungs, summarized in **Table 2**. A selection of MMPs associated with fibrotic lung disease, particularly IPF, are highlighted herein.

MMP1

MMP1, considered a "classic" collagenase, cleaves interstitial collagens including collagen type I and III. MMP1 protein levels are increased in bronchial alveolar lavage and gene and protein expression levels are increased lung tissue from IPF, compared to non-fibrotic, patients [63, 69, 79, 96]. A single nucleotide polymorphism, within the AP-1 binding domain of the MMP1 promoter (which increases transcription of MMP1) is observed more frequently in patients with IPF who smoke, than those who do not [97]. In a murine system, MMP1 enhanced cellular migration, increased wound closure rate, and protected cells from apoptosis. Increased MMP1 in alveolar epithelial cells repressed mitochondrial respiration, reduced the production of reactive oxygen species (both total and mitochondrial) and also, under normoxic conditions, increased expression of hypoxia-inducible factor-1α (HIF-1α) [98]. The fact that MMP1 was upregulated via increased HIF-1α induction under hypoxic conditions in the alveolar epithelial cells suggests a role for MMP1 in bidirectional cross talk regulating alveolar epithelial cell functions in fibrosis.

Intriguingly, MMP1 has recently been reported to be part of a set of signature genes illustrating the link between IPF and lung cancer. MMP1 was suggested to be a promising candidate gene driving significant expression changes through the transition from healthy tissue to IPF and non-small cell carcinoma [99]. MMP1 is primarily located in reactive bronchial epithelial cells, hyperplastic type 2 pneumocytes in honeycomb cysts and in alveolar macrophages, with little to no expression being observed in interstitial mesenchymal cells, suggesting that the localization of the increased MMP1 in fibrotic lung tissue does not facilitate the degradation of the fibrotic deposits [69].

■ **Table 2: Different types of MMPs, their origins, involvement in lung fibrosis and possible mechanisms of action.** Substrates for cleavage sourced primarily from [62].

MMP	Source *in vivo*	Localization in lung tissue	Profile in lung fibrosis	Substrates for Cleavage	Possible mechanism of action	References
MMP1 Collagenase 1	Bronchial and AECs Macrophages	Reactive bronchial epithelial cells, hyperplastic type 2 pneumocytes in honeycomb cysts and in alveolar macrophages	↑ in plasma, serum & BAL from IPF, ↑ gene and protein in IPF lung tissue	ECM substrates: Collagen types I, II, III, VII and X; gelatins; aggrecan; link protein; entactin; tenascin; perlecan Non-ECM substrates α2-M; α1-PI; α1-antichymotrypsin; IGFBP-2, 3, 5; proIL-1β; CTGF	Regulates AEC migration, wound closure and resistance to apoptosis. Possible bidirectional cross talk (via HIF1α) regulating AEC functions in fibrosis	[63–67]
MMP2 Gelatinase A	Bronchial and AECs, Fibroblasts and fibrocytes	Subepithelial myofibroblasts foci, close to basement membrane disruption. In ECM surrounding fibroblast foci. AECs and basal bronchiolar epithelial cells	↑ in plasma and BAL from IPF ↑ protein in IPF lung tissue	ECM substrates Gelatins; collagen types IV, V, VII, X and XI; Ln; Fn; elastin; aggrecan; link protein Non-ECM substrates ProTGF-β; FGF receptor I; MCP-3; IGFBP-5; proIL-1β; galectin-3; plasminogen	Postulated disrupted integrity of sub-epithelial/endothelial basement membrane resulting in infiltration of factors and interstitial cells to the alveolar space promoting fibro-proliferative response	[67–71]
MMP3 Stromelysin 1	Bronchial and AECs, Alveolar Macrophages, and fibroblasts	Regions of bronchiolization close to aberrant ECM deposits Weaker expression in lymphoid aggregates	↑ in plasma and BAL from IPF ↑ gene and protein in IPF lung tissue	ECM substrates Aggrecan; decorin; gelatins; Fn; Ln; collagen types III, IV, IX and X; tenascin; link protein; perlecan Non-ECM substrates lamin, casein, IGFBP-3; proIL-1β; HB-EGF; CTGF; E-cadherin; α1-antichymotrypsin; α1-PI; α2-M; plasminogen; uPA; proMMP-1, 7, 8, 9, 13	Regulating activation of TGF-β through release from latency associated peptide and latent TGF-β binding protein 1 Induction of CTGF	[67, 72–77]

Table 2: Different types of MMPs, their origins, involvement in lung fibrosis and possible mechanisms of action. Substrates for cleavage sourced primarily from [62]. (continued)

MMP	Source *in vivo*	Localization in lung tissue	Profile in lung fibrosis	Substrates for Cleavage	Possible mechanism of action	References
MMP7 Matrilysin	Bronchial epithelial cells, aberrantly activated AECs, mononuclear phagocytes and fibrocytes	Aberrant activated AECs and in bronchiolar epithelial cells	↑ in plasma and serum from IPF ↑ gene and protein in IPF lung tissue	ECM substrates Aggrecan; gelatins; Fn; Ln; elastin; entactin; collagen type IV; tenascin; decorin; link protein, Non-ECM substrates osteopontin, β4 integrin, E-cadherin, syndecan, FasL, plasminogen, Proα-defensin; proTNFα; CTGF; HB-EGF; RANKL; IGFBP-3; plasminogen	Regulating neutrophil transepithelial influx, via the shedding of syndecan-i-CXCL1 complexes, Protecting the fibroblast from undergoing apoptosis vis removal of FasL from their surfaces	[63, 65–68, 72, 78–82]
MMP8 Collagenase 2	Bronchial epithelial cells, neutrophils, macrophages	Bronchial epithelial cells in regions of moderately severe and severe fibrosis, macrophages Type II AECs are positive for MMP-8 in control lung tissue but there is minimal or no staining in these cells in regions of moderately severe and severe fibrosis in IPF lungs	↑ in plasma and BAL from IPF ↑ gene and protein in lung homogenates and tissue from IPF	ECM substrates Collagen types I, II and III; gelatins; aggrecan; link protein Non-ECM substrates α1-PI	Promotes fibrocyte migration	[58, 66–68, 72, 83, 84]
MMP9 Gelatinase B	AECs, neutrophils, macrophages, fibrocytes and fibroblasts in fibroblastic foci	Metaplastic AECs, alveolar and interstitial macrophages and fibroblasts in fibrotic foci	↑ in plasma from IPF ↑ gene and protein in lung tissue from IPF	ECM substrates Gelatins; collagen types III, IV and V; aggrecan; elastin; entactin; link protein, vitronectin; N-telopeptide of collagen type I Non-ECM substrates ProTGF-β; IL-2 receptor α; Kit-L; IGFBP-3; proIL-1β; ICAM-1; α1-PI; galectin-3; plasminogen	Fibroblasts in healthy lung tissue express Thy-1 (a glycophosphatidylinositol-linked glycoprotein) which suppresses MMP9 expression. IPF fibroblasts lack Thy-1 leading to expression of MMP9, which correlates with regions of active fibrogenesis, suggesting a role for MMP9 in induction of fibrosis. Activation of TGF-β1 in the extracellular space	[67–69, 72, 79, 85]

■ **Table 2: Different types of MMPs, their origins, involvement in lung fibrosis and possible mechanisms of action. Substrates for cleavage sourced primarily from [62]. (continued)**

MMP	Source *in vivo*	Localization in lung tissue	Profile in lung fibrosis	Substrates for Cleavage	Possible mechanism of action	References
MMP10 Stromelysin 2	Bronchial and AECs and alveolar macrophages	AECs, macrophages, and peripheral bronchiolar epithelial cells	↑ in serum and BAL from IPF ↑ protein in lung tissue from IPF	ECM substrates Aggrecan; Fn; Ln; collagen types III, IV and V; link protein, gelatin, Non-ECM substrates lamin, casein, Pro-1, 8, 10	Possible role in regulation of macrophage migration and polarization driving fibrotic response	[58, 86–88]
MMP12 Macrophage elastase	macrophages, and lung stromal cells	Not available	↑ in plasma and BAL from IPF ↑ fragment from collagen type IV released after MMP12 degradation in IPF	ECM substrates Elastin; aggrecan; Fn; collagen type IV; osteonectin; Ln; nidogen Non-ECM substrates Plasminogen; apolipoprotein(a)	Postulated disrupted integrity of sub-epithelial/ endothelial basement membrane resulting in infiltration of factors and interstitial cells to the alveolar space promoting fibro-proliferative response	[67, 89, 90]
MMP13 Collagenase 3	Bronchial and AECs, alveolar macrophages and fibroblasts	Bronchial and AECs and alveolar macrophages	↑ in plasma from IPF ↑ protein in lung homogenates from IPF	ECM substrates Collagen types I, II, III, IV, IX, X and XIV; aggrecan; Fn; tenascin; osteonectin; Ln; Perlecan Non-ECM substrates CTGF; ProTGF-β; MCP-3; α1-antichymotrypsin	Not known as yet	[67, 91]
MMP14 MT1-MMP	AECs, alveolar macrophages and endothelial cells.	AECs and alveolar macrophages	↑ gene and protein in lung tissue from IPF	ECM substrates Collagen types I, II and III; gelatins; aggrecan; Fn; Ln; fibrin; Ln-5 Non-ECM substrates ProMMP-2; proMMP-13; CD44; MCP-3; tissue, transglutaminase	Facilitates fibroblast migration through disruption of ECM barriers	[69, 70, 92]

Table 2: Different types of MMPs, their origins, involvement in lung fibrosis and possible mechanisms of action. Substrates for cleavage sourced primarily from [62]. (continued)

MMP	Source *in vivo*	Localization in lung tissue	Profile in lung fibrosis	Substrates for Cleavage	Possible mechanism of action	References
MMP15 MT2-MMP	AECs and endothelial cells	AECs	↑ gene and protein in lung tissue from IPF	ECM substrates Fn; tenascin; nidogen; aggrecan; perlecan; Ln ProMMP-2; tissue transglutaminase	Not known as yet	[70]
MMP16 MT3-MMP	AECs and fibroblasts	AECs and fibroblasts in fibroblastic foci	↑ gene and protein in lung tissue from IPF	ECM substrates Collagen type III; Fn; gelatin Non-ECM substrates ProMMP-2; tissue transglutaminase	Not known as yet	[70]
MMP19	Monocytes, macrophages, fibroblasts, and endothelial cells	Hyperplastic AECs overlying fibrotic areas	↑ gene in lung tissue from IPF	ECM substrates Collagen type IV; gelatin; Fn; tenascin; aggrecan; COMP; Ln; nidogen Non-ECM substrates IGFBP-3	Stimulates epithelial cell wound healing and migration Promotes fibroblast migration, proliferation and ECM component synthesis	[93]
MMP28 Epilysin	bronchial and AECs	Bronchial and AECs	↑ in serum from IPF ↑ gene and protein in lung tissue from IPF	ECM substrates Unknown Non-ECM substrates Casein	Promoting M2 macrophage programming	[64, 94, 95]

AEC – alveolar epithelial cells; TGF – transforming growth factor; α2-M, α2-macroglobulin; α1-PI, α1-proteinase inhibitor; COMP, cartilage oligomeric matrix protein; CTGF, connective tissue growth factor; Fas-L, Fas ligand; FGF, fibroblast growth factor; Fn, fibronectin; HB-EGF, heparin-binding epidermal growth factor like growth factor; IGFBP, insulin-like growth factor binding protein; ICAM-1, inter-cellular adhesion molecule 1; Kit-L, kit ligand; Ln, laminin; MCP-3, monocyte chemotactic protein-3; MMP, matrix metalloproteinases; MT-MMP, membrane-type MMP; PG, proteoglycan; proIL-1β, pro interleukin-1β ; Pro, proteinase type; proTNF-α, pro tumor necrosis factor-α; proTGF-β, pro transforming growth factor β; ProMMP, latent MMP; RASI-1, rheumatoid arthritis synovium inflamed-1; RANKL, receptor activator for nuclear factor κB ligand; uPA, urokinase plasminogen activator

MMP3

MMP3, also known as stromelysin-1, can degrade a variety of ECM proteins including collagen types II, III, IV, IX, and X, proteoglycans, fibronectin, elastin, and laminin. MMP3 levels are increased in IPF patients with progressive disease who died within three years of follow-up, compared to those who survived [72]. Both MMP3 gene and protein expression are increased in IPF patients' lung tissue and serum compared to controls [73, 74]. MMP3 is predominantly expressed in regions of bronchiolization close to aberrant ECM deposits within the IPF lung tissue, with some evidence of weaker expression in lymphoid aggregates [74]. MMP3 is important for regulating the activation of the profibrotic growth factor TGF-β through facilitating the release of TGF-β homodimer from the latency associated peptide and latent TGF-β binding protein 1 [75]. Also of importance for the development of fibrosis in the lungs, MMP3 can induce gene and protein expression of connective tissue growth factor (CTGF/CCN2), independent of its proteolytic activity [76, 77].

MMP7

Increased levels of MMP7, referred to as matrilysin, have been recognized as a biomarker for IPF [100, 101]. Increases in serum and plasma protein levels and in lung tissue gene and protein expression are well documented in IPF patients compared to healthy controls or other forms of fibrotic lung disease [63, 65, 67, 78, 79]. Two MMP7 promoter polymorphisms (rs11568818 and rs11568819), which result in higher levels of MMP7 in plasma, have been associated with IPF [102]. MMP7 is synthesized and released from lung bronchial epithelial cells and aberrantly activated alveolar epithelial cells, mononuclear phagocytes and circulating fibrocytes [65, 68]. It has proteolytic activity against a wide range of ECM proteins including collagen type IV, laminin, elastin and fibronectin. In addition, it cleaves gelatin, osteopontin (a multifunctional cytokine which controls cell adhesion and migration), transmembrane tumor necrosis factor α (pro-TNF-α), β4 integrin, E-cadherin, syndecan, FAS ligand (FasL), plasminogen and insulin-like growth factor binding protein-3 (IGFBP-3), among others [57, 103]. MMP7 colocalizes with osteopontin in alveolar epithelial cells in IPF tissues and has an important role in regulating neutrophil transepithelial influx via the shedding of syndecan-1-CXCL1 complexes, thereby facilitating epithelial cell damage which then promotes fibrosis [80, 81]. The cleavage of FasL from the IPF fibroblast surface (releasing sFasL into the circulatory system), and thus protecting the fibroblast from undergoing apoptosis induced by T cells, has also recently been suggested as a mechanism by which MMP7 contributes to the development of fibrosis [82].

MMP28

MMP28 (epilysin), the newest member of the MMP family, has recently been identified as a possible biomarker for IPF [94]. Unlike other MMPs MMP28 is constitutively expressed in healthy tissue, including lung, leading to the suggestion that it has a role in maintenance of tissue homeostasis [104-106]. It is localized in bronchial and alveolar epithelial cells in IPF lung tissues [95] with the gene and protein levels being increased in IPF lung tissues, compared to other fibrotic lung diseases or normal controls, and the protein levels are increased in serum of IPF patients [66, 94, 95]. MMP28 is also expressed in macrophages and has been shown to reduce proinflammatory (M1) macrophage functions while promoting anti-inflammatory / profibrotic (M2) programming, thereby supporting development of lung fibrosis [107].

Interestingly, MMPs diffuse along ECM protein fibers, with different MMPs having affinity for different collagen fiber structures (for example MMP1, 8 or 13 unwind and cleave collagen fibers at specific internal sites within the fibers, whereas MMP2 and 9 will move along the fibers and digest predominantly at the termini) [108]. Through these patterns of behavior, the MMPs orchestrate a programmed functional outcome within a tissue environment. In a fibrotic environment, where the topography and arrangement of the ECM fibers is disrupted, the regulated function of the MMPs is predicted to be adversely affected.

ECM FRAGMENTS IN LUNG FIBROSIS

The resultant products from endogenous enzyme activity in the fibrotic lung environment, while often overlooked, are potentially key players in the disease process. These released fragments, called matricryptins or matrikines or ECM fragments (the term by which they will be referred to in this review), are bioactive and have been reported to regulate processes as diverse as cell signaling, gene expression, angiogenesis, adipogenesis, tumor growth and metastasis, wound healing and fibrosis. The ECM fragments can interact with growth factor receptors, toll-like receptors, integrins and other diverse cell surface receptors through which they actively induce cellular responses that often differ from events induced by their parent molecule. ECM fragments can also act as proteolytic enzymes or inhibitors of enzyme activity themselves or can be involved in the process of proenzyme activation. In all these functional capacities, ECM fragments may contribute to the disrupted ECM remodeling that is characteristic of the fibrotic lung, as summarized in **Table 3**.

Table 3: List of bio-active ECM fragments with (potential) roles in pulmonary fibrosis.

Parent ECM molecule	ECM fragment name	Molecular mass (kDa)	Evidence for alterations in pulmonary fibrosis	Mechanism of action	Other comments	References
Collagen type I	Proline-glycine-proline (PGP) (can also be found in Collagen III & IV)	0.269	Not detectable in BAL of IPF patients Administration of PGP to bleomycin challenged mice is protective from development of fibrosis	Enhances MMP9 and neutrophil elastase secretion Chemoattractant for leukocytes Promotes repair of epithelial cells, and neo-angiogenesis	Engages CXCR1/2	[109–111]
Collagen type I α1	Product from cleavage between amino acid positions 1158/1159			Promotes ECM deposition, fibroblast migration		[112]
Collagen type IV	Arresten (α1 chain)	26	Increased in serum of IPF patients. Increased fragment from collagen IV released after MMP12 degradation in IPF Higher levels related to mortality in ILD. Tumstatin and Lamstatin absent in lung tissues of patients with UIP but present in controls	Inhibits angiogenesis	Turnover is predictive of mortality in COPD	[90, 113–118]
	Canstatin (α2 chain)	24		Promotes fibrosis, MMP2 expression Inhibits lung fibroblast migration, myofibroblast contraction		
	Tumstatin (α3 chain)	27		Inhibits fibroblast proliferation & migration and angiogenesis		
	Tetrastatin (α4 chain)	25 20 AA		Inhibits tumurogenesis (probably via inhibiting angiogenesis)		
	Lamstatin / Pentastatin (α5 chain)	25 2.45		Inhibits lymphangiogenesis Inhibits tumorigenesis (probably via inhibiting angiogenesis)		
	Hexastatin (α6 chain)	25		Inhibits migration and survival of endothelial cells		

■ **Table 3: List of bio-active ECM fragments with (potential) roles in pulmonary fibrosis. (continued)**

Parent ECM molecule	ECM fragment name	Molecular mass (kDa)	Evidence for alterations in pulmonary fibrosis	Mechanism of action	Other comments	References
Collagen type VI	Endotrophin (α3 chain)	5.8	Elevated in serum of IPF patients	Increases expression of collagen and LOX family genes Regulates TGF-β Promotes fibrosis	High levels predict mortality in COPD High levels predict pulmonary fibrosis progression	[119–122]
Collagen XVIII	Endostatin (α1 chain)	21	Increased in serum, plasma and BAL of IPF patients	Anti-fibrotic activity in *in vitro* and *in vivo* models of fibrosis Regulates angiogenesis, adipogenesis, autophagy. Inhibits activation and activity of MMPs	Interacts with integrins and VEGFR2	[123–126]
Fibronectin	Fibstatin (C-terminal heparin binding domain)	29	Increased in plasma of ILD patients	Domains 12–14 (C-terminus) abolishes agonist activity		[127]
	Fragment containing FN III EDA Anastellin			Agonist for TLR 4: Domains 9–11 (N-terminus) increases agonist activity of TLR4		[128]
Perlecan	Endorepellin	85	Parent molecule increased in lung tissue from IPF patients	Counteracts endostatin's regulation of angiogenesis.	Interacts with integrins and VEGFR2	[49, 129, 130]
Fibulin-1	Fibulin-1C1		Increased in serum and lung tissue of IPF patients	Regulates fibrosis and activation of TGFβ	Interacts with LTBP-1, collagen and fibronectin	[46, 47, 131, 132]

BAL: Bronchoalveolar lavage, COPD: Chronic obstructive pulmonary disease, CXCR: CXC chemocine receptor, FN III EDA: Fibronectin extra domain A, ILD: Interstitial lung disease, IPF: Idiopathic pulmonary fibrosis, LOX: Lysyl oxidase, LTBP: Latent TGF-β binding protein, MMP: Matrix metalloproteinase, TGF-β: Transforming growth factor β, TLR: Toll-like receptor, UIP: Usual interstitial pneumonia, VEGFR: Vascular endothelial growth factor receptor

ROLE OF ECM FRAGMENTS IN THE FIBROTIC PROCESS

Active ECM fragments are generated throughout all phases of tissue repair and may contribute to the ongoing fibrotic process [117]. These fragments have roles in the regulation of the inflammatory responses (which have recently been reviewed in [111, 133], but will not be the subject of this review), angiogenic and fibrogenic responses. The altered ECM landscape in the fibrotic lung contains an increased proportion of many ECM molecules that yield active fragments that regulate angiogenesis (see **Table 3**). Given that angiogenesis generally precedes fibrosis in an area of tissue undergoing repair, these regulatory ECM fragments may impact the tissue repair as a result of the altered structure of the fibrotic ECM. In turn, the consequential sprouting of fresh vessels from pre-existing vasculature within the damaged tissues may also impact the dysregulated and aberrant ECM composition and the continuing production of active ECM fragments.

Fibroblasts are recognized as the key active cell during the fibrogenic phase of the repair process. Aberrant fibroblast responses to the altered ECM environment that they encounter in the fibrotic lung may lead to overabundant ECM fragment production, which would further compound the matrix remodeling driving progressive fibrosis. The role of the ECM scaffold in IPF lung tissues has been elegantly illustrated [9, 24] as a driver of cellular responses; however, how this environment impacts the release of active ECM fragments has yet to be explored.

Collagen type I

The smallest identified ECM active fragment (PGP) comes predominantly from collagen type I but is also present in collagens type III and IV. The role of this fragment has been well characterized in inflammatory processes, as reviewed in [111], but less is known about its potential roles in regulating other processes in the angiogenic or fibrogenic responses.

The collagen type I α1 fragment released following MMP 2 and 9 cleavage between amino acids 1158/1159 induces fibroblast migration and enhances deposition of a variety of ECM proteins, contributing to the fibrotic response [112].

Collagen type IV

The six α chains that generate the heterotrimers of collagen type IV have all been characterized to release active ECM fragments, which are predominantly active in the regulation of neo-angiogenesis and -lymphangiogenesis. In addition to these functions these ECM active fragments also regulate the activity of mesenchymal

cells. While most of the information about these functions have been elucidated in the cancer field, emerging evidence points to key roles for these fragments in pulmonary diseases.

Arresten (α1 non-collagenous region 1 (NC1)) binds to integrin α1β1 to inhibit angiogenesis through impacting endothelial cell migration, proliferation and the ability to form tubes. These actions occur in part by blocking its parent molecule binding to the same integrin. [134]. Arresten may also interact with heparan sulfate proteoglycans to further enhance its effects. Arresten is increased in lung tissue of patients with usual interstitial pneumonia (UIP) [118].

Canstatin (α2 NC1) binds to integrins αvβ1, αvβ3 and αvβ5 on endothelial cells to inhibit tumor associated angiogenesis through disrupting cell-matrix interactions. Some studies suggest that interactions with αvβ3 and αvβ5 induces apoptosis, while inhibiting migration and proliferation in the endothelial cells [135]. Canstatin is also increased in lung tissue of patients with usual interstitial pneumonia (UIP) [118].

Tumstatin (α3 NC1) binds to the CD47/αvβ3 integrin complex to inhibit proliferation of melanoma and epithelial cells. It inhibits neo-angiogenesis but also has antitumorigenic activities that are associated with distinct regions within this active ECM fragment [136]. Tumstatin binds to airway smooth muscle cells to influence the ECM they deposit, which in turns impacts the migration of endothelial or inflammatory cells within this matrix environment [137, 138]. The levels of tumstatin are reduced in airway tissues from individuals with asthma and lymphangioleiomyomatosis [114, 139], and recently were reported to undetectable in lung tissues from patients with UIP [118].

Similarly, tetrastatin (α4 NC1) and hexastatin (α6 NC1) also bind to integrins (αvβ3 and αvβ1, αvβ3 and αvβ5 respectively). While the direct integrin that lamstatin/pentatstatin (α5 NC1) interacts with has not been reported, it is reasonable to assume this active ECM fragment will also interact in a similar manner to its family members. Similar to tumstatin, lamstatin/pentastatin has been reported to be absent in lung tissues from patients with lymphangioleiomyomatosis and UIP [118, 139].

Arresten, canstatin and tumstatin all interact directly with fibroblasts to exert organ-specific effects on migration and proliferation [140], with induction of migration being noted in cardiac fibroblasts but inhibition in lung fibroblasts [118, 141]. In the lung fibroblasts, TGF-β induced conversion of fibroblasts to myofibroblasts was linked with canstatin release.

Fibronectin

Fibronectin is recognized to have central roles in regulating fibroblast migration when incorporated in the ECM, while the released active fragments of fibronectin also regulate fibroblast functions, including their phenotype differentiation [117]. These fragments also regulate endothelial cell responses, particularly during wound healing and possibly fibrosis. Anastellin, a peptide derived from the first type III module in fibronectin, helps orchestrate fibronectin fibriilogenesis and is anti-angiogenic but promotes fibroblast survival [142].

Fibulin-1

Fibulin-1 usually acts as a bridging molecule in the ECM facilitating the assembly of the larger structural proteins to which it binds, including collagen type I, elastin and fibronectin. *In vitro* studies have identified a peptide from fibulin-1 that activates lung-derived fibroblasts, inducing attachment, enhanced viability, proliferation and mitochondrial activity [131]. Fibulin-1 levels are increased in serum and lung tissues of IPF patients, with high levels being related to disease progression [47]. Mice that lack the fibulin-1C isoform are protected from the development of pulmonary fibrosis, through regulation of TGF-β activation via interactions with latent TGF-β binding protein [46, 132], but the levels of circulating fragments from fibulin-1 have not been measured in these animals.

Perlecan

When incorporated in the basement membrane, perlecan is recognized to have a pro-angiogenic function. However, when the active fragment, endorepellin, is released from its parent molecule, it has the opposite effect. Through binding to integrin α2β1 on endothelial cells, endorepellin mediates interruption of cell migration, via disruption of cytoskeletal arrangement and focal adhesions [143]. Endorepellin cooperates with endostatin, a polypeptide derived from the carboxy-terminus of collagen type XVIII, to enhance the effectiveness of each ECM fragment [130]. It also interacts with fibroblasts, protecting them from apoptosis, hence possibly mediating a role in fibrosis through this promotion of fibroblast survival [129].

ECM fragments as (bio)markers of an active fibrotic process

In addition to being active contributors to the pathological processes occurring during lung fibrosis, ECM fragments can also serve as sentinel indicators of these processes. During the cleavage processes that result in the release of ECM fragments from the deposited ECM in lung tissues, or indeed during the processes that enable the ECM fibers to be incorporated into the ECM bed, neo-epitopes are exposed on these fragments. Monitoring of the exposure of these neo-epitopes, or the levels of

the recognized ECM fragments, including those discussed above, released from lung tissues has the potential to inform us about the fibrotic processes that are active in a patient. Such fragments can be considered as possible biomarkers for fibrotic lung disease.

In a population-based multi-ethnic study, Madahar and colleagues reported that levels of two collagen fragments, carboxyl-terminal telopeptide of collagen type I (ICTP) and amino-terminal propeptide of procollagen type III (PIIINP), were associated with sub-clinical interstitial lung disease (interstitial lung abnormalities) detected through computed tomography screening [144]. These associations were not influenced by sex, race or smoking status. This report suggests that these ECM fragments represent a sensitive indication of fibrotic activity that can be detected well before lung function parameters can register disease activity.

In the PROFILE study, ECM degradation markers were found to have significantly different levels between controls and IPF patients [145]. When assessed longitudinally, changes in the levels of six neoepitopes (MMP -degraded-collagen type I (C1M), -collagen type III (C3M), -collagen type VI (C6M) and -C-reactive protein (CRPM), collagen type III degraded by ADAMTS-1/4/8 (C3A) and citrullinated vimentin degraded by MMP-2/8 (VICM)) were indicative of IPF patients with a greater likelihood of disease progression compared to those with stable disease. The baseline levels of C1M and C3A were associated with increased mortality. The levels of markers of ECM synthesis, neoepitope of collagen type III (PRO-C3) and collagen type VI (PRO-C6), were also elevated in IPF patients compared to healthy controls and again were increased in progressive disease compared to stable [146]. In addition, during exacerbations, patients with idiopathic interstitial pneumonia, including IPF, had increased levels of MMP-degraded collagen type IV (C4M) and C6M but decreased levels of MMP7-degraded elastin (ELM7) and MMP-degraded versican (VCANM) compared to patients with stable disease. Lower VCANM levels during exacerbation were associated with increased mortality [147]. Serum levels of laminin, collagen type IV, PIIINP and hyaluronic acid were also higher in a cohort of IPF and connective tissue disease patients, compared to controls, and were associated with mortality [116].

The serial measurement of ECM fragment or neoepitope markers in serum has the potential to inform about parameters important for clinical management of disease in these patients. These markers may bring manifestation of precision medicine in pulmonary fibrosis one step closer.

CONCLUSION

There is an urgent need for establishing effective processes for diagnosing patients with fibrotic lung diseases, and an even greater need for being able to accurately identify the underlying pathological cause to then be able to effectively manage these patients, without causing further harm. The ultimate goal is to enable the development of therapeutic approaches that are able to reverse the destructive changes in the lung tissue to regenerate effective gas exchange units and to return the longevity and quality of life for these patients. Thinking about the ECM as an active contributory element within the disease process has the potential to provide far reaching opportunities for novel advances in identifying disease-modifying mechanisms for pulmonary fibrosis. A consideration of the diversity of "hidden" changes within the ECM milieu that go far beyond the well-recognized changes in the composition and amount of ECM in a fibrotic lesion within lung tissues augments the novel directions that can be pursued when searching for future therapeutic targets (**Figure 3**). Future studies using emerging novel *in vitro* models that incorporate dimensionality and mechanical elements that exist in the lung, coupled with state-of-the-art transcriptomic and spatial proteomic profiling of fibrotic lung tissues, have the potential to ensure exciting developments in our understanding and management of pulmonary fibrosis in the near future.

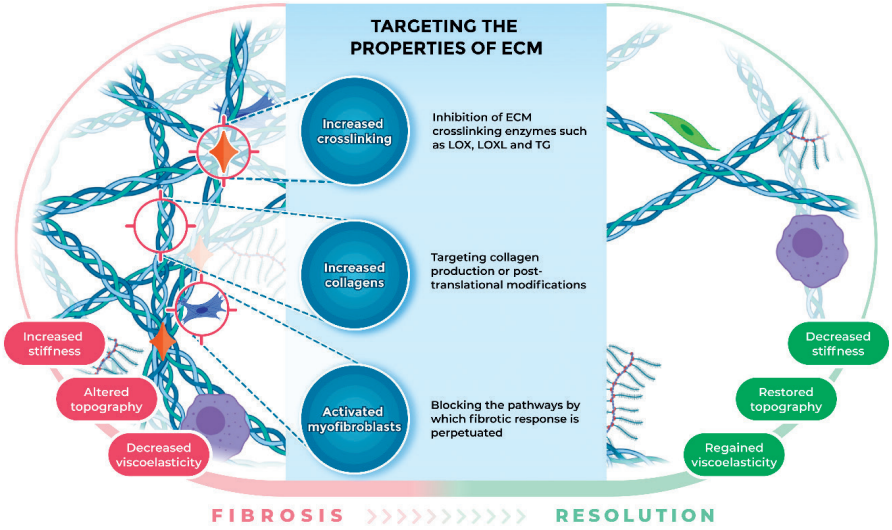

■ **Figure 3: ECM changes and potential therapeutic targeting sites/points.** ECM: Extracellular matrix; LOX: Lysyl oxidase; LOXL: Lysyl oxidase-like; TG: Transglutaminase.

Disclosures

MN and JKB receive unrestricted research funds from Boehringer Ingelheim.

ACKNOWLEDGEMENTS

JKB was funded by a Rosalind Franklin Fellowship co-funded by the EU and the University of Groningen. The authors thank Albano Tosato for the assistance with figure preparation; they also thank Gavin Tjin and the Sydney Microscopy and Microanalysis Facility at the University of Sydney, Australia for the SEM images.

REFERENCES

1. Martinez FJ, Collard HR, Pardo A, Raghu G, Richeldi L, Selman M, Swigris JJ, Taniguchi H, Wells AU. Idiopathic pulmonary fibrosis. *Nat Rev Dis Pri* 2017: 3(1): 17074.
2. Lederer DJ, Martinez FJ. Idiopathic Pulmonary Fibrosis. *N Engl J Med* 2018: 378(19): 1811-1823.
3. Jenkins G. Demystifying pulmonary fibrosis. *Am J Physiol Lung Cell Mol Physiol* 2020: 319(3): L554-L559.
4. Spagnolo P, Kropski JA, Jones MG, Lee JS, Rossi G, Karampitsakos T, Maher TM, Tzouvelekis A, Ryerson CJ. Idiopathic pulmonary fibrosis: Disease mechanisms and drug development. *Pharmacol Ther* 2021: 222: 107798.
5. Selman M, Pardo A. When things go wrong: exploring possible mechanisms driving the progressive fibrosis phenotype in interstitial lung diseases. *Eur Respir J* 2021: 58(3): 2004507.
6. Burgstaller G, Oehrle B, Gerckens M, White ES, Schiller HB, Eickelberg O. The instructive extracellular matrix of the lung: basic composition and alterations in chronic lung disease. *Eur Respir J* 2017: 50(1).
7. Karamanos NK, Theocharis AD, Piperigkou Z, Manou D, Passi A, Skandalis SS, Vynios DH, Orian-Rousseau V, Ricard-Blum S, Schmelzer CEH, Duca L, Durbeej M, Afratis NA, Troeberg L, Franchi M, Masola V, Onisto M. A guide to the composition and functions of the extracellular matrix. *FEBS J* 2021: 288(24): 6850-6912.
8. Burgess JK, Mauad T, Tjin G, Karlsson JC, Westergren-Thorsson G. The extracellular matrix - the under-recognized element in lung disease? *J Pathol* 2016: 240(4): 397-409.
9. Booth AJ, Hadley R, Cornett AM, Dreffs AA, Matthes SA, Tsui JL, Weiss K, Horowitz JC, Fiore VF, Barker TH, Moore BB, Martinez FJ, Niklason LE, White ES. Acellular normal and fibrotic human lung matrices as a culture system for in vitro investigation. *Am J Respir Crit Care Med* 2012: 186(9): 866-876.
10. de Hilster RHJ, Sharma PK, Jonker MR, White ES, Gercama EA, Roobeek M, Timens W, Harmsen MC, Hylkema MN, Burgess JK. Human lung extracellular matrix hydrogels resemble the stiffness and viscoelasticity of native lung tissue. *Am J Physiol Lung Cell Mol Physiol* 2020: 318(4): L698-L704.
11. Tjin G, White ES, Faiz A, Sicard D, Tschumperlin DJ, Mahar A, Kable EPW, Burgess JK. Lysyl oxidases regulate fibrillar collagen remodelling in idiopathic pulmonary fibrosis. *Dis Model Mech* 2017: 10(11): 1301-1312.
12. Matera DL, DiLillo KM, Smith MR, Davidson CD, Parikh R, Said M, Wilke CA, Lombaert IM, Arnold KB, Moore BB, Baker BM. Microengineered 3D pulmonary interstitial mimetics highlight a critical role for matrix degradation in myofibroblast differentiation. *Sci Adv* 2020: 6(37).
13. Burgstaller G, Sengupta A, Vierkotten S, Preissler G, Lindner M, Behr J, Konigshoff M, Eickelberg O. Distinct niches within the extracellular matrix dictate fibroblast function in (cell free) 3D lung tissue cultures. *Am J Physiol Lung Cell Mol Physiol* 2018: 314(5): L708-L723.
14. Parker MW, Rossi D, Peterson M, Smith K, Sikstrom K, White ES, Connett JE, Henke CA, Larsson O, Bitterman PB. Fibrotic extracellular matrix activates a profibrotic positive feedback loop. *J Clin Invest* 2014: 124(4): 1622-1635.

15. McQuattie-Pimentel AC, Ren Z, Joshi N, Watanabe S, Stoeger T, Chi M, Lu Z, Sichizya L, Aillon RP, Chen CI, Soberanes S, Chen Z, Reyfman PA, Walter JM, Anekalla KR, Davis JM, Helmin KA, Runyan CE, Abdala-Valencia H, Nam K, Meliton AY, Winter DR, Morimoto RI, Mutlu GM, Bharat A, Perlman H, Gottardi CJ, Ridge KM, Chandel NS, Sznajder JI, Balch WE, Singer BD, Misharin AV, Budinger GRS. The lung microenvironment shapes a dysfunctional response of alveolar macrophages in aging. *J Clin Invest* 2021: 131(4).

16. Blokland KEC, Pouwels SD, Schuliga M, Knight DA, Burgess JK. Regulation of cellular senescence by extracellular matrix during chronic fibrotic diseases. *Clin Sci* 2020: 134(20): 2681-2706.

17. Vasse GF, Nizamoglu M, Heijink IH, Schleputz M, van Rijn P, Thomas MJ, Burgess JK, Melgert BN. Macrophage-stroma interactions in fibrosis: biochemical, biophysical, and cellular perspectives. *J Pathol* 2021: 254(4): 344-357.

18. Adams TS, Schupp JC, Poli S, Ayaub EA, Neumark N, Ahangari F, Chu SG, Raby BA, DeIuliis G, Januszyk M, Duan Q, Arnett HA, Siddiqui A, Washko GR, Homer R, Yan X, Rosas IO, Kaminski N. Single-cell RNA-seq reveals ectopic and aberrant lung-resident cell populations in idiopathic pulmonary fibrosis. *Sci Adv* 2020: 6(28): eaba1983.

19. Habermann AC, Gutierrez AJ, Bui LT, Yahn SL, Winters NI, Calvi CL, Peter L, Chung MI, Taylor CJ, Jetter C, Raju L, Roberson J, Ding G, Wood L, Sucre JMS, Richmond BW, Serezani AP, McDonnell WJ, Mallal SB, Bacchetta MJ, Loyd JE, Shaver CM, Ware LB, Bremner R, Walia R, Blackwell TS, Banovich NE, Kropski JA. Single-cell RNA sequencing reveals profibrotic roles of distinct epithelial and mesenchymal lineages in pulmonary fibrosis. *Sci Adv* 2020: 6(28): eaba1972.

20. Tsukui T, Sun KH, Wetter JB, Wilson-Kanamori JR, Hazelwood LA, Henderson NC, Adams TS, Schupp JC, Poli SD, Rosas IO, Kaminski N, Matthay MA, Wolters PJ, Sheppard D. Collagen-producing lung cell atlas identifies multiple subsets with distinct localization and relevance to fibrosis. *Nat Commun* 2020: 11(1): 1920.

21. Valenzi E, Bulik M, Tabib T, Morse C, Sembrat J, Trejo Bittar H, Rojas M, Lafyatis R. Single-cell analysis reveals fibroblast heterogeneity and myofibroblasts in systemic sclerosis-associated interstitial lung disease. *Ann Rheum Dis* 2019: 78(10): 1379-1387.

22. Sacher F, Feregrino C, Tschopp P, Ewald CY. Extracellular matrix gene expression signatures as cell type and cell state identifiers. *bioRxiv* 2021: 2021.2003.2011.434939.

23. Germanguz I, Aranda E, Xiong JC, Kissel N, Nichols A, Gadee E, O'Neill JD. Fibrotic human lung extracellular matrix as a disease-specific substrate for 3D in-vitro models of pulmonary fibrosis. *J Respir Med Lung Dis* 2019: 4(1): 1-11.

24. Elowsson Rendin L, Lofdahl A, Ahrman E, Muller C, Notermans T, Michalikova B, Rosmark O, Zhou XH, Dellgren G, Silverborn M, Bjermer L, Malmstrom A, Larsson-Callerfelt AK, Isaksson H, Malmstrom J, Westergren-Thorsson G. Matrisome Properties of Scaffolds Direct Fibroblasts in Idiopathic Pulmonary Fibrosis. *Int J Mol Sci* 2019: 20(16).

25. Joshi N, Watanabe S, Verma R, Jablonski RP, Chen CI, Cheresh P, Markov NS, Reyfman PA, McQuattie-Pimentel AC, Sichizya L, Lu Z, Piseaux-Aillon R, Kirchenbuechler D, Flozak AS, Gottardi CJ, Cuda CM, Perlman H, Jain M, Kamp DW, Budinger GRS, Misharin AV. A spatially restricted fibrotic niche in pulmonary fibrosis is sustained by M-CSF/M-CSFR signalling in monocyte-derived alveolar macrophages. *Eur Respir J* 2020: 55(1).

26. Sava P, Ramanathan A, Dobronyi A, Peng X, Sun H, Ledesma-Mendoza A, Herzog EL, Gonzalez AL. Human pericytes adopt myofibroblast properties in the microenvironment of the IPF lung. *JCI Insight* 2017: 2(24).

27. Agarwal M, Goheen M, Jia S, Ling S, White ES, Kim KK. Type I Collagen Signaling Regulates Opposing Fibrotic Pathways through alpha(2) beta(1) Integrin. *Am J Respir Cell Mol Biol* 2020: 63(5): 613-622.

28. Sorushanova A, Delgado LM, Wu Z, Shologu N, Kshirsagar A, Raghunath R, Mullen AM, Bayon Y, Pandit A, Raghunath M, Zeugolis DI. The Collagen Suprafamily: From Biosynthesis to Advanced Biomaterial Development. *Adv Mater* 2019: 31(1): e1801651.

29. Philp CJ, Siebeke I, Clements D, Miller S, Habgood A, John AE, Navaratnam V, Hubbard RB, Jenkins G, Johnson SR. Extracellular Matrix Cross-Linking Enhances Fibroblast Growth and Protects against Matrix Proteolysis in Lung Fibrosis. *Am J Respir Cell Mol Biol* 2018: 58(5): 594-603.

30. Tschumperlin DJ, Lagares D. Mechano-therapeutics: Targeting Mechanical Signaling in Fibrosis and Tumor Stroma. *Pharmacol Ther* 2020: 212: 107575.

31. Asano S, Ito S, Takahashi K, Furuya K, Kondo M, Sokabe M, Hasegawa Y. Matrix stiffness regulates migration of human lung fibroblasts. *Physiol Rep* 2017: 5(9).

32. Jones DL, Meridew JA, Link PA, Ducharme MT, Lydon KL, Choi KM, Caporarello N, Tan Q, Diaz Espinosa AM, Xiong Y, Lee JH, Ye Z, Yan H, Ordog T, Ligresti G, Varelas X, Tschumperlin DJ. ZNF416 is a pivotal transcriptional regulator of fibroblast mechanoactivation. *J Cell Biol* 2021: 220(5).

33. Avery D, Govindaraju P, Jacob M, Todd L, Monslow J, Pure E. Extracellular matrix directs phenotypic heterogeneity of activated fibroblasts. *Matrix Biol* 2018: 67: 90-106.

34. Haak AJ, Kostallari E, Sicard D, Ligresti G, Choi KM, Caporarello N, Jones DL, Tan Q, Meridew J, Diaz Espinosa AM, Aravamudhan A, Maiers JL, Britt RD, Jr., Roden AC, Pabelick CM, Prakash YS, Nouraie SM, Li X, Zhang Y, Kass DJ, Lagares D, Tager AM, Varelas X, Shah VH, Tschumperlin DJ. Selective YAP/TAZ inhibition in fibroblasts via dopamine receptor D1 agonism reverses fibrosis. *Sci Transl Med* 2019: 11(516).

35. Cantini M, Donnelly H, Dalby MJ, Salmeron-Sanchez M. The Plot Thickens: The Emerging Role of Matrix Viscosity in Cell Mechanotransduction. *Adv Healthc Mater* 2020: 9(8): e1901259.

36. Chaudhuri O, Cooper-White J, Janmey PA, Mooney DJ, Shenoy VB. Effects of extracellular matrix viscoelasticity on cellular behaviour. *Nature* 2020: 584(7822): 535-546.

37. Vining KH, Stafford A, Mooney DJ. Sequential modes of crosslinking tune viscoelasticity of cell-instructive hydrogels. *Biomaterials* 2019: 188: 187-197.

38. Ouellette JN, Drifka CR, Pointer KB, Liu Y, Lieberthal TJ, Kao WJ, Kuo JS, Loeffler AG, Eliceiri KW. Navigating the Collagen Jungle: The Biomedical Potential of Fiber Organization in Cancer. *Bioengineering* 2021: 8(2).

39. Seo BR, Chen X, Ling L, Song YH, Shimpi AA, Choi S, Gonzalez J, Sapudom J, Wang K, Andresen Eguiluz RC, Gourdon D, Shenoy VB, Fischbach C. Collagen microarchitecture mechanically controls myofibroblast differentiation. *Proc Natl Acad Sci USA* 2020: 117(21): 11387–11398.

40. Tisler M, Alkmin S, Chang HY, Leet J, Bernau K, Sandbo N, Campagnola PJ. Analysis of fibroblast migration dynamics in idiopathic pulmonary fibrosis using image-based scaffolds of the lung extracellular matrix. *Am J Physiol Lung Cell Mol Physiol* 2020: 318(2): L276–L286.

41. Matera DL, Wang WY, Smith MR, Shikanov A, Baker BM. Fiber Density Modulates Cell Spreading in 3D Interstitial Matrix Mimetics. *ACS Biomater Sci Eng* 2019: 5(6): 2965–2975.

42. Costa DSd, Reis RL, Pashkuleva I. Sulfation of Glycosaminoglycans and Its Implications in Human Health and Disorders. *Annu Rev Biomed Eng* 2017: 19(1): 1–26.

43. Vallet SD, Clerc O, Ricard-Blum S. Glycosaminoglycan–Protein Interactions: The First Draft of the Glycosaminoglycan Interactome. *J Histochem Cytochem* 2021: 69(2): 93–104.

44. Klingberg F, Chau G, Walraven M, Boo S, Koehler A, Chow ML, Olsen AL, Im M, Lodyga M, Wells RG, White ES, Hinz B. The fibronectin ED-A domain enhances recruitment of latent TGF-beta-binding protein-1 to the fibroblast matrix. *J Cell Sci* 2018: 131(5).

45. Klingberg F, Chow ML, Koehler A, Boo S, Buscemi L, Quinn TM, Costell M, Alman BA, Genot E, Hinz B. Prestress in the extracellular matrix sensitizes latent TGF-beta1 for activation. *J Cell Biol* 2014: 207(2): 283–297.

46. Liu G, Cooley MA, Jarnicki AG, Borghuis T, Nair PM, Tjin G, Hsu AC, Haw TJ, Fricker M, Harrison CL, Jones B, Hansbro NG, Wark PA, Horvat JC, Argraves WS, Oliver BG, Knight DA, Burgess JK, Hansbro PM. Fibulin-1c regulates transforming growth factor-beta activation in pulmonary tissue fibrosis. *JCI Insight* 2019: 5(16).

47. Jaffar J, Unger S, Corte TJ, Keller M, Wolters PJ, Richeldi L, Cerri S, Prele CM, Hansbro PM, Argraves WS, Oliver RA, Oliver BG, Black JL, Burgess JK. Fibulin-1 predicts disease progression in patients with idiopathic pulmonary fibrosis. *Chest* 2014: 146(4): 1055–1063.

48. Uhl FE, Zhang F, Pouliot RA, Uriarte JJ, Rolandsson Enes S, Han X, Ouyang Y, Xia K, Westergren-Thorsson G, Malmström A, Hallgren O, Linhardt RJ, Weiss DJ. Functional role of glycosaminoglycans in decellularized lung extracellular matrix. *Acta Biomater* 2020: 102: 231–246.

49. Westergren-Thorsson G, Hedstrom U, Nybom A, Tykesson E, Ahrman E, Hornfelt M, Maccarana M, van Kuppevelt TH, Dellgren G, Wildt M, Zhou XH, Eriksson L, Bjermer L, Hallgren O. Increased deposition of glycosaminoglycans and altered structure of heparan sulfate in idiopathic pulmonary fibrosis. *Int J Biochem Cell Biol* 2017: 83: 27–38.

50. Aumiller V, Strobel B, Romeike M, Schuler M, Stierstorfer BE, Kreuz S. Comparative analysis of lysyl oxidase (like) family members in pulmonary fibrosis. *Sci Rep* 2017: 7(1): 149.

51. Bellaye PS, Shimbori C, Upagupta C, Sato S, Shi W, Gauldie J, Ask K, Kolb M. Lysyl Oxidase-Like 1 Protein Deficiency Protects Mice from Adenoviral Transforming Growth Factor-beta1-induced Pulmonary Fibrosis. *Am J Respir Cell Mol Biol* 2018: 58(4): 461-470.

52. Wolters PJ, Chapman HA. Importance of lysosomal cysteine proteases in lung disease. *Respir Res* 2000: 1(3): 170-177.

53. Mahalanobish S, Saha S, Dutta S, Sil PC. Matrix metalloproteinase: An upcoming therapeutic approach for idiopathic pulmonary fibrosis. *Pharmacol Res* 2020: 152: 104591.

54. Chakraborti S, Sarkar J, Pramanik PK, Chakraborti T. Role of Proteases in Lung Disease: A Brief Overview. Proteases in Human Diseases Proteases in Human Diseases. Springer Singapore, 2017; pp. 333-374.

55. Askew DJ, Silverman GA. Intracellular and extracellular serpins modulate lung disease. *J Perinatol* 2008: 28 Suppl 3(Suppl 3): S127-135.

56. Buhling F, Waldburg N, Reisenauer A, Heimburg A, Golpon H, Welte T. Lysosomal cysteine proteases in the lung: role in protein processing and immunoregulation. *Eur Respir J* 2004: 23(4): 620-628.

57. Pardo A, Cabrera S, Maldonado M, Selman M. Role of matrix metalloproteinases in the pathogenesis of idiopathic pulmonary fibrosis. *Respir Res* 2016: 17(1): 23.

58. Craig VJ, Zhang L, Hagood JS, Owen CA. Matrix metalloproteinases as therapeutic targets for idiopathic pulmonary fibrosis. *Am J Respir Cell Mol Biol* 2015: 53(5): 585-600.

59. Gill SE, Parks WC. Metalloproteinases and their inhibitors: regulators of wound healing. *Int J Biochem Cell Biol* 2008: 40(6-7): 1334-1347.

60. Butler GS, Overall CM. Matrix metalloproteinase processing of signaling molecules to regulate inflammation. *Periodontol 2000* 2013: 63(1): 123-148.

61. Parks WC, Wilson CL, Lopez-Boado YS. Matrix metalloproteinases as modulators of inflammation and innate immunity. *Nat Rev Immunol* 2004: 4(8): 617-629.

62. Shiomi T, Lemaître V, D'Armiento J, Okada Y. Matrix metalloproteinases, a disintegrin and metalloproteinases, and a disintegrin and metalloproteinases with thrombospondin motifs in non-neoplastic diseases. *Pathol Int* 2010: 60(7): 477-496.

63. Morais A, Beltrão M, Sokhatska O, Costa D, Melo N, Mota P, Marques A, Delgado L. Serum metalloproteinases 1 and 7 in the diagnosis of idiopathic pulmonary fibrosis and other interstitial pneumonias. *Respir Med* 2015: 109(8): 1063-1068.

64. Pardo A, Selman M, Kaminski N. Approaching the degradome in idiopathic pulmonary fibrosis. *Int J Biochem Cell Biol* 2008: 40(6-7): 1141-1155.

65. Zuo F, Kaminski N, Eugui E, Allard J, Yakhini Z, Ben-Dor A, Lollini L, Morris D, Kim Y, DeLustro B, Sheppard D, Pardo A, Selman M, Heller RA. Gene expression analysis reveals matrilysin as a key regulator of pulmonary fibrosis in mice and humans. *Proc Natl Acad Sci USA* 2002: 99(9): 6292-6297.

66. Rosas IO, Richards TJ, Konishi K, Zhang Y, Gibson K, Lokshin AE, Lindell KO, Cisneros J, Macdonald SD, Pardo A, Sciurba F, Dauber J, Selman M, Gochuico BR, Kaminski N. MMP1 and MMP7 as potential peripheral blood biomarkers in idiopathic pulmonary fibrosis. *PLoS Med* 2008: 5(4): e93.

67. Todd JL, Vinisko R, Liu Y, Neely ML, Overton R, Flaherty KR, Noth I, Newby LK, Lasky JA, Olman MA, Hesslinger C, Leonard TB, Palmer SM, Belperio JA, investigators I-PR. Circulating matrix metalloproteinases and tissue metalloproteinase inhibitors in patients with idiopathic pulmonary fibrosis in the multicenter IPF-PRO Registry cohort. *BMC Pulm Med* 2020: 20(1): 64.

68. Garcia-de-Alba C, Becerril C, Ruiz V, Gonzalez Y, Reyes S, Garcia-Alvarez J, Selman M, Pardo A. Expression of matrix metalloproteases by fibrocytes: possible role in migration and homing. *Am J Respir Crit Care Med* 2010: 182(9): 1144-1152.

69. Selman M, Ruiz V, Cabrera S, Segura L, Ramirez R, Barrios R, Pardo A. TIMP-1, -2, -3, and -4 in idiopathic pulmonary fibrosis. A prevailing nondegradative lung microenvironment? *Am J Physiol Lung Cell Mol Physiol* 2000: 279(3): L562-574.

70. Garcia-Alvarez J, Ramirez R, Sampieri CL, Nuttall RK, Edwards DR, Selman M, Pardo A. Membrane type-matrix metalloproteinases in idiopathic pulmonary fibrosis. *Sarcoidosis Vasc Diffuse Lung Dis* 2006: 23(1): 13-21.

71. Nguyen M, Arkell J, Jackson CJ. Human endothelial gelatinases and angiogenesis. *Int J Biochem Cell Biol* 2001: 33(10): 960-970.

72. McKeown S, Richter AG, O'Kane C, McAuley DF, Thickett DR. MMP expression and abnormal lung permeability are important determinants of outcome in IPF. *Eur Respir J* 2009: 33(1): 77-84.

73. Yamashita CM, Dolgonos L, Zemans RL, Young SK, Robertson J, Briones N, Suzuki T, Campbell MN, Gauldie J, Radisky DC, Riches DW, Yu G, Kaminski N, McCulloch CA, Downey GP. Matrix metalloproteinase 3 is a mediator of pulmonary fibrosis. *Am J Pathol* 2011: 179(4): 1733-1745.

74. DePianto DJ, Chandriani S, Abbas AR, Jia G, N'Diaye EN, Caplazi P, Kauder SE, Biswas S, Karnik SK, Ha C, Modrusan Z, Matthay MA, Kukreja J, Collard HR, Egen JG, Wolters PJ, Arron JR. Heterogeneous gene expression signatures correspond to distinct lung pathologies and biomarkers of disease severity in idiopathic pulmonary fibrosis. *Thorax* 2015: 70(1): 48-56.

75. Maeda S, Dean DD, Gomez R, Schwartz Z, Boyan BD. The First Stage of Transforming Growth Factor β1 Activation is Release of the Large Latent Complex from the Extracellular Matrix of Growth Plate Chondrocytes by Matrix Vesicle Stromelysin-1 (MMP-3). *Calcif Tissue Int* 2002: 70(1): 54-65.

76. Muromachi K, Kamio N, Narita T, Annen-Kamio M, Sugiya H, Matsushima K. MMP-3 provokes CTGF/CCN2 production independently of protease activity and dependently on dynamin-related endocytosis, which contributes to human dental pulp cell migration. *J Cell Biochem* 2012: 113(4): 1348-1358.

77. Eguchi T, Kubota S, Kawata K, Mukudai Y, Uehara J, Ohgawara T, Ibaragi S, Sasaki A, Kuboki T, Takigawa M. Novel Transcription Factor-Like Function of Human Matrix Metalloproteinase 3 Regulating the CTGF/CCN2 Gene. *Mol Cell Biol* 2008: 28(7): 2391-2413.

78. Selman M, Pardo A, Barrera L, Estrada A, Watson SR, Wilson K, Aziz N, Kaminski N, Zlotnik A. Gene expression profiles distinguish idiopathic pulmonary fibrosis from hypersensitivity pneumonitis. *Am J Respir Crit Care Med* 2006: 173(2): 188-198.

79. Cui Y, Ji J, Hou J, Tan Y, Han X. Identification of Key Candidate Genes Involved in the Progression of Idiopathic Pulmonary Fibrosis. *Molecules* 2021: 26(4): 1123.

80. Pardo A, Gibson K, Cisneros J, Richards TJ, Yang Y, Becerril C, Yousem S, Herrera I, Ruiz V, Selman M, Kaminski N. Up-regulation and profibrotic role of osteopontin in human idiopathic pulmonary fibrosis. *PLoS Med* 2005: 2(9): e251.

81. Li Q, Park PW, Wilson CL, Parks WC. Matrilysin shedding of syndecan-1 regulates chemokine mobilization and transepithelial efflux of neutrophils in acute lung injury. *Cell* 2002: 111(5): 635-646.

82. Nareznoi D, Konikov-Rozenman J, Petukhov D, Breuer R, Wallach-Dayan SB. Matrix Metalloproteinases Retain Soluble FasL-mediated Resistance to Cell Death in Fibrotic-Lung Myofibroblasts. *Cells* 2020: 9(2): 411-411.

83. Stijn W, Stijn E, Bart M, Marijke W, Christophe D, Jonas Y, Jana S, Eric K, Geert M, Wim A. Multiplex protein profiling of bronchoalveolar lavage in idiopathic pulmonary fibrosis and hypersensitivity pneumonitis. *Ann Thorac Med* 2013: 8(1): 38-45.

84. Craig VJ, Polverino F, Laucho-Contreras ME, Shi Y, Liu Y, Osorio JC, Tesfaigzi Y, Pinto-Plata V, Gochuico BR, Rosas IO, Owen CA. Mononuclear phagocytes and airway epithelial cells: novel sources of matrix metalloproteinase-8 (MMP-8) in patients with idiopathic pulmonary fibrosis. *PLoS One* 2014: 9(5): e97485.

85. Hagood JS, Prabhakaran P, Kumbla P, Salazar L, MacEwen MW, Barker TH, Ortiz LA, Schoeb T, Siegal GP, Alexander CB, Pardo A, Selman M. Loss of fibroblast Thy-1 expression correlates with lung fibrogenesis. *Am J Pathol* 2005: 167(2): 365-379.

86. Sokai A, Handa T, Tanizawa K, Oga T, Uno K, Tsuruyama T, Kubo T, Ikezoe K, Nakatsuka Y, Tanimura K, Muro S, Hirai T, Nagai S, Chin K, Mishima M. Matrix metalloproteinase-10: a novel biomarker for idiopathic pulmonary fibrosis. *Respir Res* 2015: 16(1): 120.

87. Murray MY, Birkland TP, Howe JD, Rowan AD, Fidock M, Parks WC, Gavrilovic J. Macrophage migration and invasion is regulated by MMP10 expression. *PLoS One* 2013: 8(5): e63555.

88. Rohani MG, McMahan RS, Razumova MV, Hertz AL, Cieslewicz M, Pun SH, Regnier M, Wang Y, Birkland TP, Parks WC. MMP-10 Regulates Collagenolytic Activity of Alternatively Activated Resident Macrophages. *J Invest Dermatol* 2015: 135(10): 2377-2384.

89. Matute-Bello G, Wurfel MM, Lee JS, Park DR, Frevert CW, Madtes DK, Shapiro SD, Martin TR. Essential role of MMP-12 in Fas-induced lung fibrosis. *Am J Respir Cell Mol Biol* 2007: 37(2): 210-221.

90. Sand JM, Larsen L, Hogaboam C, Martinez F, Han M, Rossel Larsen M, Nawrocki A, Zheng Q, Karsdal MA, Leeming DJ. MMP mediated degradation of type IV collagen alpha 1 and alpha 3 chains reflects basement membrane remodeling in experimental and clinical fibrosis--validation of two novel biomarker assays. *PLoS One* 2013: 8(12): e84934.

91. Nkyimbeng T, Ruppert C, Shiomi T, Dahal B, Lang G, Seeger W, Okada Y, D'Armiento J, Günther A. Pivotal Role of Matrix Metalloproteinase 13 in Extracellular Matrix Turnover in Idiopathic Pulmonary Fibrosis. *PLoS One* 2013: 8(9): e73279.

92. Rowe RG, Keena D, Sabeh F, Willis AL, Weiss SJ. Pulmonary fibroblasts mobilize the membrane-tethered matrix metalloprotease, MT1-MMP, to destructively remodel and invade interstitial type I collagen barriers. *Am J Physiol Lung Cell Mol Physiol* 2011: 301(5): L683-692.

93. Yu G, Kovkarova-Naumovski E, Jara P, Parwani A, Kass D, Ruiz V, Lopez-Otín C, Rosas IO, Gibson KF, Cabrera S, Ramírez R, Yousem SA, Richards TJ, Chensny LJ, Selman M, Kaminski N, Pardo A. Matrix Metalloproteinase-19 Is a Key Regulator of Lung Fibrosis in Mice and Humans. *Am J Respir Crit Care Med* 2012: 186(8): 752-762.

94. Maldonado M, Buendía-Roldán I, Vicens-Zygmunt V, Planas L, Molina-Molina M, Selman M, Pardo A. Identification of MMP28 as a biomarker for the differential diagnosis of idiopathic pulmonary fibrosis. *PLoS One* 2018: 13(9): e0203779.

95. Maldonado M, Salgado-Aguayo A, Herrera I, Cabrera S, Ortíz-Quintero B, Staab-Weijnitz CA, Eickelberg O, Ramírez R, Manicone AM, Selman M, Pardo A. Upregulation and Nuclear Location of MMP28 in Alveolar Epithelium of Idiopathic Pulmonary Fibrosis. *Am J Respir Cell Mol Biol* 2018: 59(1): 77-86.

96. Konishi K, Gibson KF, Lindell KO, Richards TJ, Zhang Y, Dhir R, Bisceglia M, Gilbert S, Yousem SA, Song JW, Kim DS, Kaminski N. Gene expression profiles of acute exacerbations of idiopathic pulmonary fibrosis. *Am J Respir Crit Care Med* 2009: 180(2): 167-175.

97. Checa M, Ruiz V, Montano M, Velazquez-Cruz R, Selman M, Pardo A. MMP-1 polymorphisms and the risk of idiopathic pulmonary fibrosis. *Hum Genet* 2008: 124(5): 465-472.

98. Herrera I, Cisneros J, Maldonado M, Ramírez R, Ortiz-Quintero B, Anso E, Chandel NS, Selman M, Pardo A. Matrix Metalloproteinase (MMP)-1 Induces Lung Alveolar Epithelial Cell Migration and Proliferation, Protects from Apoptosis, and Represses Mitochondrial Oxygen Consumption. *J Biol Chem* 2013: 288(36): 25964-25975.

99. Leng D, Yi J, Xiang M, Zhao H, Zhang Y. Identification of common signatures in idiopathic pulmonary fibrosis and lung cancer using gene expression modeling. *BMC Cancer* 2020: 20(1): 986.

100. Jee AS, Sahhar J, Youssef P, Bleasel J, Adelstein S, Nguyen M, Corte TJ. Review: Serum biomarkers in idiopathic pulmonary fibrosis and systemic sclerosis associated interstitial lung disease – frontiers and horizons. *Pharmacol Ther* 2019: 202: 40-52.

101. White ES, Xia M, Murray S, Dyal R, Flaherty CM, Flaherty KR, Moore BB, Cheng L, Doyle TJ, Villalba J, Dellaripa PF, Rosas IO, Kurtis JD, Martinez FJ. Plasma Surfactant Protein-D, Matrix Metalloproteinase-7, and Osteopontin Index Distinguishes Idiopathic Pulmonary Fibrosis from Other Idiopathic Interstitial Pneumonias. *Am J Respir Crit Care Med* 2016: 194(10): 1242-1251.

102. Richards TJ, Park C, Chen Y, Gibson KF, Peter Di Y, Pardo A, Watkins SC, Choi AM, Selman M, Pilewski J, Kaminski N, Zhang Y. Allele-specific transactivation of matrix metalloproteinase 7 by FOXA2 and correlation with plasma levels in idiopathic pulmonary fibrosis. *Am J Physiol Lung Cell Mol Physiol* 2012: 302(8): L746-754.

103. Dancer RCA, Wood AM, Thickett DR. Metalloproteinases in idiopathic pulmonary fibrosis. *Eur Respir J* 2011: 38(6): 1461–1467.

104. Lohi J, Wilson CL, Roby JD, Parks WC. Epilysin, a novel human matrix metalloproteinase (MMP-28) expressed in testis and keratinocytes and in response to injury. *J Biol Chem* 2001: 276(13): 10134–10144.

105. Rodgers UR, Kevorkian L, Surridge AK, Waters JG, Swingler TE, Culley K, Illman S, Lohi J, Parker AE, Clark IM. Expression and function of matrix metalloproteinase (MMP)-28. *Matrix Biol* 2009: 28(5): 263–272.

106. Illman SA, Lohi J, Keski-Oja J. Epilysin (MMP-28) – structure, expression and potential functions. *Exp Dermatol* 2008: 17(11): 897–907.

107. Gharib SA, Johnston LK, Huizar I, Birkland TP, Hanson J, Wang Y, Parks WC, Manicone AM. MMP28 promotes macrophage polarization toward M2 cells and augments pulmonary fibrosis. *J Leukoc Biol* 2014: 95(1): 9–18.

108. Van Doren SR. Matrix metalloproteinase interactions with collagen and elastin. *Matrix Biol* 2015: 44–46: 224–231.

109. O'Reilly PJ, Ding Q, Akthar S, Cai G, Genschmer KR, Patel DF, Jackson PL, Viera L, Roda M, Locy ML, Bernstein EA, Lloyd CM, Bernstein KE, Snelgrove RJ, Blalock JE. Angiotensin-converting enzyme defines matrikine-regulated inflammation and fibrosis. *JCI Insight* 2017: 2(22).

110. Hahn CS, Scott DW, Xu X, Roda MA, Payne GA, Wells JM, Viera L, Winstead CJ, Bratcher P, Sparidans RW, Redegeld FA, Jackson PL, Folkerts G, Blalock JE, Patel RP, Gaggar A. The matrikine N-α-PGP couples extracellular matrix fragmentation to endothelial permeability. *Sci Adv* 2015: 1(3): e1500175.

111. Patel DF, Snelgrove RJ. The multifaceted roles of the matrikine Pro-Gly-Pro in pulmonary health and disease. *Eur Respir Rev* 2018: 27(148): 180017.

112. Lindsey ML, Iyer RP, Zamilpa R, Yabluchanskiy A, Deleon-Pennell KY, Hall ME, Kaplan A, Zouein FA, Bratton D, Flynn ER, Cannon PL, Tian Y, Jin Y-F, Lange RA, Tokmina-Roszyk D, Fields GB, De Castro Brás LE. A Novel Collagen Matricryptin Reduces Left Ventricular Dilation Post-Myocardial Infarction by Promoting Scar Formation and Angiogenesis. *J Am Coll Cardiol* 2015: 66(12): 1364–1374.

113. Ronnow SR, Sand JMB, Langholm LL, Manon-Jensen T, Karsdal MA, Tal-Singer R, Miller BE, Vestbo J, Leeming DJ. Type IV collagen turnover is predictive of mortality in COPD: a comparison to fibrinogen in a prospective analysis of the ECLIPSE cohort. *Respir Res* 2019: 20(1): 63.

114. Burgess JK, Boustany S, Moir LM, Weckmann M, Lau JY, Grafton K, Baraket M, Hansbro PM, Hansbro NG, Foster PS, Black JL, Oliver BG. Reduction of tumstatin in asthmatic airways contributes to angiogenesis, inflammation, and hyperresponsiveness. *Am J Respir Crit Care Med* 2010: 181(2): 106–115.

115. Weckmann M, Moir LM, Heckman CA, Black JL, Oliver BG, Burgess JK. Lamstatin--a novel inhibitor of lymphangiogenesis derived from collagen IV. *J Cell Mol Med* 2012: 16(12): 3062–3073.

116. Su Y, Gu H, Weng D, Zhou Y, Li Q, Zhang F, Zhang Y, Shen L, Hu Y, Li H. Association of serum levels of laminin, type IV collagen, procollagen III N-terminal peptide, and hyaluronic acid with the progression of interstitial lung disease. *Medicine (Baltimore)* 2017: 96(18): e6617.

117. De Castro Brás LE, Frangogiannis NG. Extracellular matrix-derived peptides in tissue remodeling and fibrosis. *Matrix Biol* 2020: 91-92: 176-187.

118. Urushiyama H, Terasaki Y, Nagasaka S, Terasaki M, Kunugi S, Nagase T, Fukuda Y, Shimizu A. Role of α1 and α2 chains of type IV collagen in early fibrotic lesions of idiopathic interstitial pneumonias and migration of lung fibroblasts. *Lab Invest* 2015: 95(8): 872-885.

119. Zhao Y, Gu X, Zhang N, Kolonin MG, An Z, Sun K. Divergent functions of endotrophin on different cell populations in adipose tissue. *Am J Physiol Endocrinol Metabol* 2016: 311(6): E952-E963.

120. Park J, Scherer PE. Adipocyte-derived endotrophin promotes malignant tumor progression. *J Clin Invest* 2012: 122(11): 4243-4256.

121. Sun K, Park J, Gupta OT, Holland WL, Auerbach P, Zhang N, Goncalves Marangoni R, Nicoloro SM, Czech MP, Varga J, Ploug T, An Z, Scherer PE. Endotrophin triggers adipose tissue fibrosis and metabolic dysfunction. *Nat Commun* 2014: 5(1): 3485.

122. Rønnow SR, Langholm LL, Karsdal MA, Manon-Jensen T, Tal-Singer R, Miller BE, Vestbo J, Leeming DJ, Sand JMB. Endotrophin, an extracellular hormone, in combination with neoepitope markers of von Willebrand factor improves prediction of mortality in the ECLIPSE COPD cohort. *Respir Res* 2020: 21(1).

123. Sumi M, Satoh H, Kagohashi K, Ishikawa H, Sekizawa K. Increased serum levels of endostatin in patients with idiopathic pulmonary fibrosis. *J Clin Lab Anal* 2005: 19(4): 146-149.

124. Richter AG, McKeown S, Rathinam S, Harper L, Rajesh P, McAuley DF, Heljasvaara R, Thickett DR. Soluble endostatin is a novel inhibitor of epithelial repair in idiopathic pulmonary fibrosis. *Thorax* 2009: 64(2): 156-161.

125. Ricard-Blum S, Vallet SD. Proteases decode the extracellular matrix cryptome. *Biochimie* 2016: 122: 300-313.

126. Yamaguchi Y, Takihara T, Chambers RA, Veraldi KL, Larregina AT, Feghali-Bostwick CA. A peptide derived from endostatin ameliorates organ fibrosis. *Sci Transl Med* 2012: 4(136): 136ra171.

127. Moodley YP, Corte TJ, Oliver BG, Glaspole IN, Livk A, Ito J, Peters K, Lipscombe R, Casey T, Tan DBA. Analysis by proteomics reveals unique circulatory proteins in idiopathic pulmonary fibrosis. *Respirology* 2019: 24(11): 1111-1114.

128. Julier Z, Martino MM, de Titta A, Jeanbart L, Hubbell JA. The TLR4 agonist fibronectin extra domain A is cryptic, exposed by elastase-2; use in a fibrin matrix cancer vaccine. *Sci Rep* 2015: 5(1): 8569.

129. Poluzzi C, Iozzo RV, Schaefer L. Endostatin and endorepellin: A common route of action for similar angiostatic cancer avengers. *Adv Drug Del Rev* 2016: 97: 156-173.

130. Mongiat M, Sweeney SM, San Antonio JD, Fu J, Iozzo RV. Endorepellin, a novel inhibitor of angiogenesis derived from the C terminus of perlecan. *J Biol Chem* 2003: 278(6): 4238-4249.

131. Ge Q, Chen L, Jaffar J, Argraves WS, Twal WO, Hansbro P, Black JL, Burgess JK, Oliver B. Fibulin1C peptide induces cell attachment and extracellular matrix deposition in lung fibroblasts. *Sci Rep* 2015: 5(1): 9496.

132. Liu G, Cooley MA, Jarnicki AG, Hsu AC, Nair PM, Haw TJ, Fricker M, Gellatly SL, Kim RY, Inman MD, Tjin G, Wark PA, Walker MM, Horvat JC, Oliver BG, Argraves WS, Knight DA, Burgess JK, Hansbro PM. Fibulin-1 regulates the pathogenesis of tissue remodeling in respiratory diseases. *JCI Insight* 2016: 1(9).

133. Herrera J, Henke CA, Bitterman PB. Extracellular matrix as a driver of progressive fibrosis. *J Clin Invest* 2018: 128(1): 45-53.

134. Sudhakar A, Boosani CS. Signaling mechanisms of endogenous angiogenesis inhibitors derived from type IV collagen. *Gene Regul Syst Bio* 2007: 1: 217-226.

135. Magnon C, Galaup A, Mullan B, Rouffiac V, Bouquet C, Bidart JM, Griscelli F, Opolon P, Perricaudet M. Canstatin acts on endothelial and tumor cells via mitochondrial damage initiated through interaction with alphavbeta3 and alphavbeta5 integrins. *Cancer Res* 2005: 65(10): 4353-4361.

136. Hamano Y, Kalluri R. Tumstatin, the NC1 domain of alpha 3 chain of type IV collagen, is an endogenous inhibitor of pathological angiogenesis and suppresses tumor growth. *Biochem Biophys Res Commun* 2005: 333(2): 292-298.

137. Harkness LM, Weckmann M, Kopp M, Becker T, Ashton AW, Burgess JK. Tumstatin regulates the angiogenic and inflammatory potential of airway smooth muscle extracellular matrix. *J Cell Mol Med* 2017: 21(12): 3288-3297.

138. Nissen G, Hollaender H, Tang FSM, Wegmann M, Lunding L, Vock C, Bachmann A, Lemmel S, Bartels R, Oliver BG, Burgess JK, Becker T, Kopp MV, Weckmann M. Tumstatin fragment selectively inhibits neutrophil infiltration in experimental asthma exacerbation. *Clin Exp Allergy* 2018: 48(11): 1483-1493.

139. Weckmann M, Svolos M, Boustany S, Oliver BG, Burgess JK, Moir LM, Black J. Lamstatin And Tumstatin - Novel Inhibitors Of Lymphatic Cell Proliferation Are Absent In Lymphangioleiomyomatosis. *Am J Respir Crit Care Med* 2010: 181: A2093.

140. Urushiyama H, Terasaki Y, Nagasaka S, Kokuho N, Terasaki M, Kunugi S, Mikami Y, Noguchi S, Horie M, Nagahama K, Yamauchi Y, Shimizu A, Nagase T. Role of canstatin in early fibrotic lesions of idiopathic interstitial pneumonias and migration of lung fibroblasts. *Int J Clin Exp Pathol* 2016: 9(12): 12714-12722.

141. Okada M, Murata N, Yamawaki H. Canstatin stimulates migration of rat cardiac fibroblasts via secretion of matrix metalloproteinase-2. *Am J Physiol Cell Physiol* 2017: 312(3): C199-C208.

142. Ambesi A, McKeown-Longo PJ. Anastellin, the angiostatic fibronectin peptide, is a selective inhibitor of lysophospholipid signaling. *Mol Cancer Res* 2009: 7(2): 255-265.

143. Bix G, Fu J, Gonzalez EM, Macro L, Barker A, Campbell S, Zutter MM, Santoro SA, Kim JK, HöÖK M, Reed CC, Iozzo RV. Endorepellin causes endothelial cell disassembly of actin cytoskeleton and focal adhesions through $\alpha 2\beta 1$ integrin. *J Cell Biol* 2004: 166(1): 97-109.

144. Madahar P, Duprez DA, Podolanczuk AJ, Bernstein EJ, Kawut SM, Raghu G, Barr RG, Gross MD, Jacobs DR, Jr., Lederer DJ. Collagen biomarkers and subclinical interstitial lung disease: The Multi-Ethnic Study of Atherosclerosis. *Respir Med* 2018: 140: 108-114.

145. Jenkins RG, Simpson JK, Saini G, Bentley JH, Russell AM, Braybrooke R, Molyneaux PL, McKeever TM, Wells AU, Flynn A, Hubbard RB, Leeming DJ, Marshall RP, Karsdal MA, Lukey PT, Maher TM. Longitudinal change in collagen degradation biomarkers in idiopathic pulmonary fibrosis: an analysis from the prospective, multicentre PROFILE study. *Lancet Respir Med* 2015: 3(6): 462-472.

146. Organ LA, Duggan A-MR, Oballa E, Taggart SC, Simpson JK, Kang'Ombe AR, Braybrooke R, Molyneaux PL, North B, Karkera Y, Leeming DJ, Karsdal MA, Nanthakumar CB, Fahy WA, Marshall RP, Jenkins RG, Maher TM. Biomarkers of collagen synthesis predict progression in the PROFILE idiopathic pulmonary fibrosis cohort. *Respir Res* 2019: 20(1).

147. Sand JMB, Tanino Y, Karsdal MA, Nikaido T, Misa K, Sato Y, Togawa R, Wang X, Leeming DJ, Munakata M. A Serological Biomarker of Versican Degradation is Associated with Mortality Following Acute Exacerbations of Idiopathic Interstitial Pneumonia. *Respir Res* 2018: 19(1): 82.

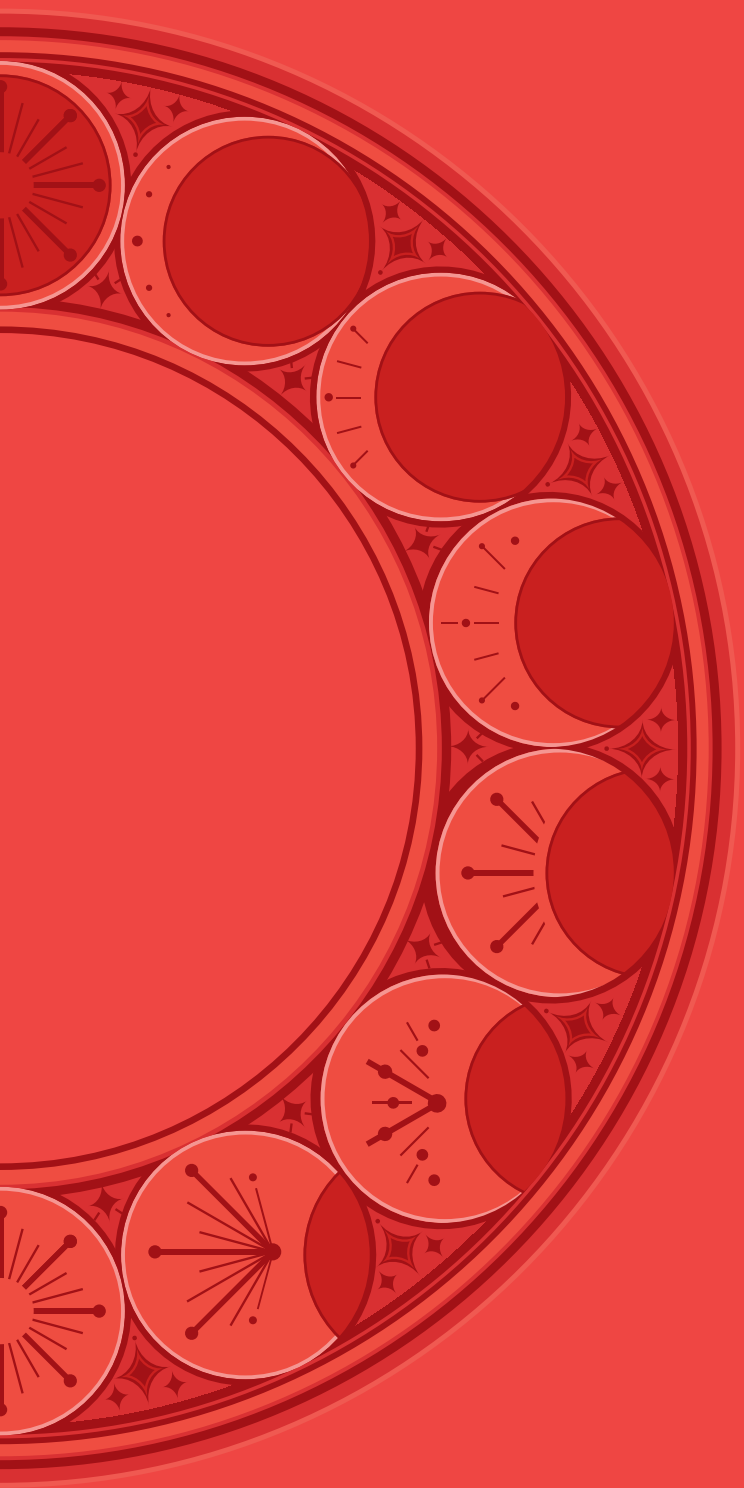

CHAPTER 3

Abnormal collagen structure resulting from lack of contribution of collagen type XIV in lungs of patients with idiopathic pulmonary fibrosis

Mehmet Nizamoglu *, Maunick Lefin Koloko Ngassie *, Rhode A. Meuleman, Martin Banchero, Theo Borghuis, Wim Timens, Martijn C. Nawijn, Barbro N. Melgert, Irene H. Heijink, Corry-Anke Brandsma, Janette K. Burgess

* Equal contributions

Submitted

ABSTRACT

Abnormal deposition of extracellular matrix (ECM) in lung tissue is a characteristic of idiopathic pulmonary fibrosis (IPF). Increased collagen deposition in lung ECM is accompanied by altered collagen organization. Collagen type XIV, a fibril-associated collagen, supports collagen fibril organization. Its status in IPF has not been described at the protein level yet. In this study, we utilized publicly available datasets for single-cell RNA-sequencing for characterizing collagen type XIV expression at the gene level. For protein level comparison, we applied immunohistochemical staining for collagen type XIV on lung tissue sections from IPF patients and compared it to lung tissue sections from never smoking and ex-smoking donors. Analyzing the relative amounts of collagen type XIV at the whole tissue level as well as in parenchyma, airway wall and bronchial epithelium, we found consistently lower proportions of collagen type XIV in all compartments across IPF samples. Our study suggests proportionally lower collagen type XIV in IPF lung tissues may have implications for the assembly of the ECM fibers which may contribute to progression of fibrosis.

INTRODUCTION

Idiopathic pulmonary fibrosis (IPF) is the result of aberrant deposition of extracellular matrix (ECM) in the alveolar septa, causing restricted breathing in patients [1]. Currently, the median survival time of patients with IPF is less than for many cancers, and there is no available cure [1]. As the lung ECM structure in IPF is drastically altered and provides a feedback loop that perpetuates disease progression [2, 3], investigating the underlying matrix pathology is expected to improve our understanding of the disease.

Deposition of collagens in the altered ECM in IPF has been well documented, including an increase in collagen types I and III, as well as changes in the organization of collagen fibrils [4, 5]. Among other types of collagens, collagen type XIV (COL14) is a fibril-associated collagen with interrupted triple-helices (FACIT) that plays a crucial role in the organization of the collagen network in ECM [6]. Unlike abnormal collagen deposition and organization in IPF which has been described in detail, the role of FACITs in this process or, more specifically, involvement of COL14 in IPF, remains unknown. Previously, in a mouse model of fibrosis, higher levels of COL14 deposition were shown in bleomycin-treated mice compared to control mice [7]. However, the time for development of fibrosis in this model compared to IPF and/or species differences can influence how these results translate to humans. Accordingly, in the current study we aimed to investigate whether there are differences in the COL14 gene expression and protein levels in lung tissue from patients with (end stage) IPF compared to normal lung tissue.

MATERIALS AND METHODS

Data analysis of publicly available single-cell RNA-sequencing datasets

Cell-type specific *COL14A1* gene expression levels in lung tissue of patients with IPF and non-IPF donors were analyzed using publicly available single-cell RNA sequencing datasets from the Human Lung Cell Atlas (HCLA) consortium and the IPF atlas dataset from Adams et al. [8, 9]. These datasets were analyzed and clustered using HCLA annotations for 4 major cell groups: endothelial, epithelial, immune and stromal cells for analysis of the expression profile of the Collagen Type XIV Alpha 1 Chain (*COL14A1*) gene which encodes COL14 protein.

Immunohistochemical staining (IHC)

IHC was used to quantify proteins of interest in lung tissue. Control lung tissues were obtained through resections from patients undergoing surgery for lung cancer, taken from as far away from the tumor region as possible and were macroscopically normal tissue as assessed by pathologists. Fibrotic lungs were obtained from explanted material following transplantations (**Table 1**). Formalin fixed and paraffin embedded tissue sections of 6 µm thickness were obtained from never-smoker (n=9), ex-smoker (n=9) and IPF (n=12) lungs and were stained for COL14A1 using polyclonal rabbit anti-COL14A1 antibody (HPA023781; Atlas antibodies Inc.). Secondary polyclonal Goat Anti-Rabbit antibody (P0488, Dako, Denmark) was visualized using NovaRED® Substrate (SK-4800, Vector Laboratories, Canada). Counterstaining was done using hematoxylin. Slides were scanned using a Hamamatsu NanoZoomer digital scanner (Hamamatsu Photonic K.K., Shizuoka, Japan) as described previously [10].

The study protocol was consistent with the Research Code of the University Medical Center Groningen (research code UMCG (umcgresearch.org) and national ethical and professional guidelines ("Code of conduct for Health Research (only in Dutch): Gedragscode-Gezondheidsonderzoek-2022.pdf (coreon.org). Lung tissues used in this study were derived from leftover lung material after lung surgery and transplant procedures. All samples and clinical information were coded before experiments were performed. This material was not subject to the Medical Research Human Subjects Act in the Netherlands; all biological samples are from archival materials that are exempt from consent in compliance with applicable laws and regulations (Dutch laws: Medical Treatment Agreement Act (WGBO) art 458 / GDPR art 9/ UAVG art 24) .

Table 1: Patient characteristics for the donors included in this study.

	Never smoker	Ex-smoker	IPF	P value	
				Never smoker vs IPF	Ex-smoker vs IPF
Age (median (min-max))	70 (50-82)	55 (43-62)	58.50 (37-67)	0.0213*	ns*
Sex (M/F)	1/8	3/6	9/3	0.075#	ns#
FEV1 (pred) † (%, (min-max))	107.5 (80-121)	103.6 (85-127)	49.35 (18-74.50)	0.0002 *	0.0002*

*: Tested using Mann-Whitney test, #: Tested using Fisher's exact test. †: Data was available only n=8 for all groups. IPF: Idiopathic pulmonary fibrosis, FEV1: Forced expiratory volume in 1 second. ns: not significant

Image analysis

The image analysis was performed for 4 different regions within the scanned images for percentage of positive area as previously described [10]. For whole tissue analysis, scanned images were used after removal of artifacts. For the parenchyma analysis, airways and blood vessels were removed from the whole tissue images. Additionally, specific parts of the airways including the airway wall and the epithelium were examined. Airways were extracted using Aperio ImageScope software (Leica Biosystems, Amsterdam, The Netherlands). Based on the localization of the staining, different parts of the airways were selected using Adobe Photoshop (Adobe, San Jose, California, USA). Artifacts and the remaining compartments of the airways which were not used for examination were removed during this step. In the case of IPF airway walls, which have no clear border between the end of the airway wall and the surrounding parenchyma, the distance between the epithelial layer and smooth muscle layer (E-SM distance) was measured. This distance then was multiplied by three to calculate distance from the outside of the smooth muscle layer till the (not visible) parenchyma (SM-P distance). The multiplication by three was calculated based on the ratio between measured E-SM and SM-P distances from IPF airways which were surrounded by still visible parenchyma. The approach is illustrated in *Supplementary Figure 1*.

Next, the total tissue area positive for COL14 was quantified by applying color deconvolution to separate the different staining colors [10]. The quantification of the staining was automatically processed using FIJI Image J. Afterwards, the raw data was sorted in RStudio, from which the percentage of area of the tissue present that stained positive for the protein of interest was calculated. The formula used to calculate the percentage of area stained positive for the protein is as follows:

$$Area(\%) = \frac{Area\ (Nova\ Red)}{Area\ (Total)} \times 100\%$$

Statistical analysis

Differences between never-smoker non-IPF, ex-smoker non-IPF and IPF groups were tested using a Kruskal-Wallis test for whole tissue and parenchyma regions. For airway wall and bronchial epithelium regions, a mixed model analysis was used to test the statistical differences between patients incorporating multiple airway wall and bronchial epithelium images per patient. $p < 0.05$ was considered significant.

RESULTS

We observed *COL14A1* expression in epithelial and stromal cells from control lung tissue in the HLCA dataset (**Figure 1A**), while expression of *COL14A1* in the IPF atlas was mainly restricted to stromal cells (**Figure 1B**). Pseudobulk analysis performed on this dataset revealed that *COL14A1* expression in bronchial epithelium, fibroblasts and myofibroblasts of IPF lungs was significantly higher compared to the same cells in non-IPF tissue (**Figure 1C**).

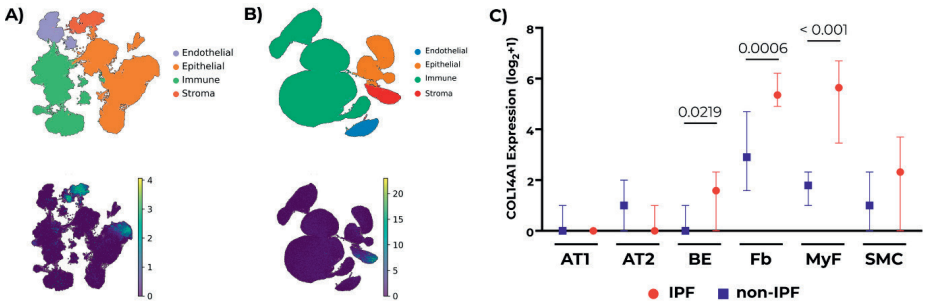

■ **Figure 1: Gene expression profile of COL14A1 in IPF and non-IPF lungs.** A) COL14A1 expression in healthy lungs (data reconstructed from single-cell RNA-sequencing data obtained from Sikkema et al. [8]. B) COL14A1 expression in IPF and non-IPF lungs (reconstructed from single-cell RNA-sequencing data obtained from Adams et al. [9]), C) Comparison of COL14A1 counts in IPF and non-IPF lungs across relevant cell types: alveolar type 1 (AT1) and type 2 (AT2), bronchial epithelial cells (BE), fibroblasts (Fb), myofibroblasts (MyF) and smooth muscle cells (SMC). Data is represented as median ± 95% confidence interval. Applied statistical test: Mann-Whitney test. N=28 for non-IPF, n=32 for IPF.

Immunohistochemical staining of the human lung tissue showed COL14A1 in control tissue, which was mainly localized in airways and parenchyma (**Figure 2**). Image analysis of whole lung tissue sections from IPF and non-IPF donors revealed relatively lower percentages of COL14A1 positive area in tissue from patients with IPF compared to those from both never and ex-smoker controls (**Figure 3A**). When focusing on specific regions, we also observed a relative lower percentage of positively-stained area in lung parenchyma of patients with IPF compared to both non-IPF control groups (**Figure 3B**), Lastly, the analysis of airways revealed a relative lower percentage of positive-stained area of COL14A1 in both airway wall (**Figure 3C**) and bronchial epithelium (**Figure 3D**) of IPF-derived lung tissue compared to non-IPF controls (both groups). In the whole tissue analysis and analyses of specific tissue compartments, there were no differences in relative positively-stained area between never-smoker and ex-smoker non-IPF tissues.

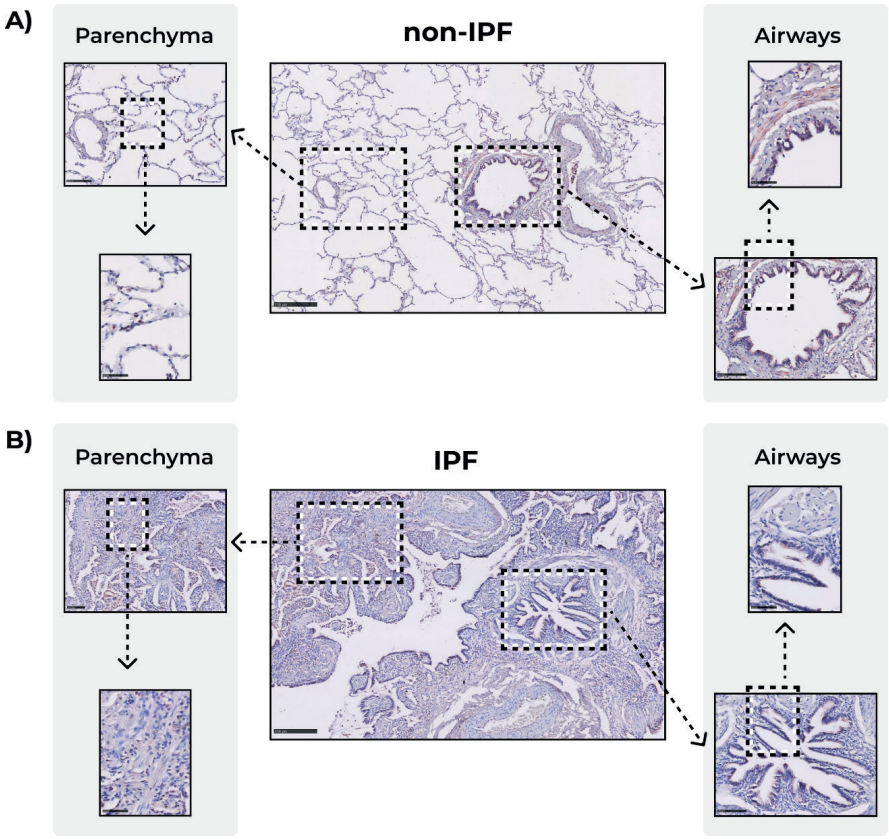

Figure 2: Example images of COL14A1 staining in whole tissue, lung parenchyma, and airways in A) non-IPF and B) IPF lung samples. Scale bars for intact images: 250 µm, for first level zoom-in: 100 µm and for second level zoom-in: 50 µm. IPF: Idiopathic pulmonary fibrosis.

DISCUSSION

Collectively, our results show proportionally lower COL14 protein expression relative to other ECM components that make up lung tissue in patients with IPF compared to both ex-smoker and never-smoker non-IPF controls. To the best of our knowledge, this is the first report of protein level changes related to spatial location of COL14 in human lung tissue in IPF. In this study, we examined the relative proportion of COL14 to tissue present in each sample and not the absolute amount, therefore it is possible that there may be an overall increase in the amount of COL14 in IPF lung tissues. As the total amount of tissue present in IPF lung sections is higher than in controls, it is conceivable there is an increase in absolute amount of COL14, while the proportion of COL14 in comparison to other ECM components is reduced. A previous report of

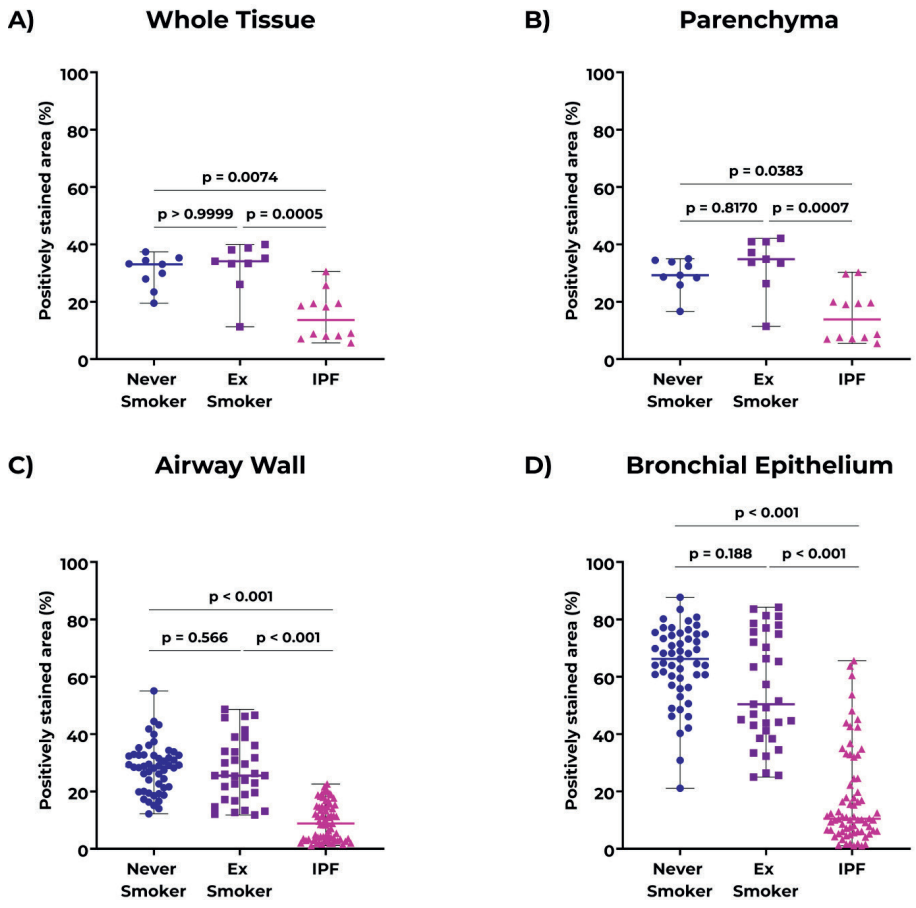

■ **Figure 3: Percentage area stained positive for COL14A1 in: A) whole lung tissue, B) lung parenchyma, C) airway wall, D) bronchial epithelium.** For panels A and B, each data point represents individual donors; data were tested using Kruskal–Wallis test with Dunn's multiple comparisons test for panels. N=9 for never smoker and ex-smoker groups, n=12 for IPF. For panels C and D, each data point represents individual airway wall or bronchial epithelial region within airways (n = 1–7 regions per donor); data were tested using mixed-model analysis to account for multiple airways per donor. N=9 for never smoker and ex-smoker groups, n=12 for IPF. IPF: Idiopathic pulmonary fibrosis.

higher mass spectrometry counts of COL14 in IPF lungs compared to non-IPF lungs [11] suggests that such an absolute increase is likely, being cons 297 istent with the RNA findings in myofibroblasts in our current study.

How COL14 is involved in the regulation of human lung ECM structure and how changes in its proportional expression influence fibrotic responses in IPF is currently

unknown. As FACITs regulate the structural organization of fibrillar collagens, it can be argued that lower proportions of COL14 in IPF lungs contribute to the reported imbalance between organized and disorganized fibrillar collagen in IPF [5]. More research correlating fibrillar collagen organization with FACITs such as COL14 will increase understanding of the involvement of COL14 in the development and/or progression of fibrotic responses. A recent study using mice deficient in *COL14A1* found increased stiffness and abnormal collagen fibril organization in the corneas of *COL14A1*-knockout mice compared to wildtypes [12]. These observations parallel well-documented increases in the stiffness of lungs from patients with IPF [11]. Together with our observations reported here, it is tempting to speculate that COL14 protein levels in IPF lungs do not mirror the increase in other ECM proteins in lung tissue during fibrosis, thereby leading to more disorganized collagen fibers with higher stiffness in lungs of patients with IPF.

ACKNOWLEDGEMENTS

The stainings of COL14A1 on lung tissue analyzed in this manuscript were conducted as part of the HOLLAND (HistopathOLogy of Lung Aging aNd COPD) project. The HOLLAND project was initiated and supervised by Corry-Anke Brandsma, Wim Timens, and Janette Burgess, technical support was provided by Marjan Reinders-Luinge, Anja Bakker and Theo Borghuis, and image analyses pipelines were developed by Theo Borghuis, Maunick Lefin Koloko Ngassie and Niek Bekker. MN, BNM, IHH and JKB receive unrestricted research funds from Boehringer Ingelheim. JKB also acknowledges support from the NWO (Aspasia 015.013.010). This work was supported by the Chan Zuckerberg Initiative, LLC Seed Network grant CZF2019-002438 "Lung Cell Atlas 1.0"

SUPPLEMENTARY FIGURES

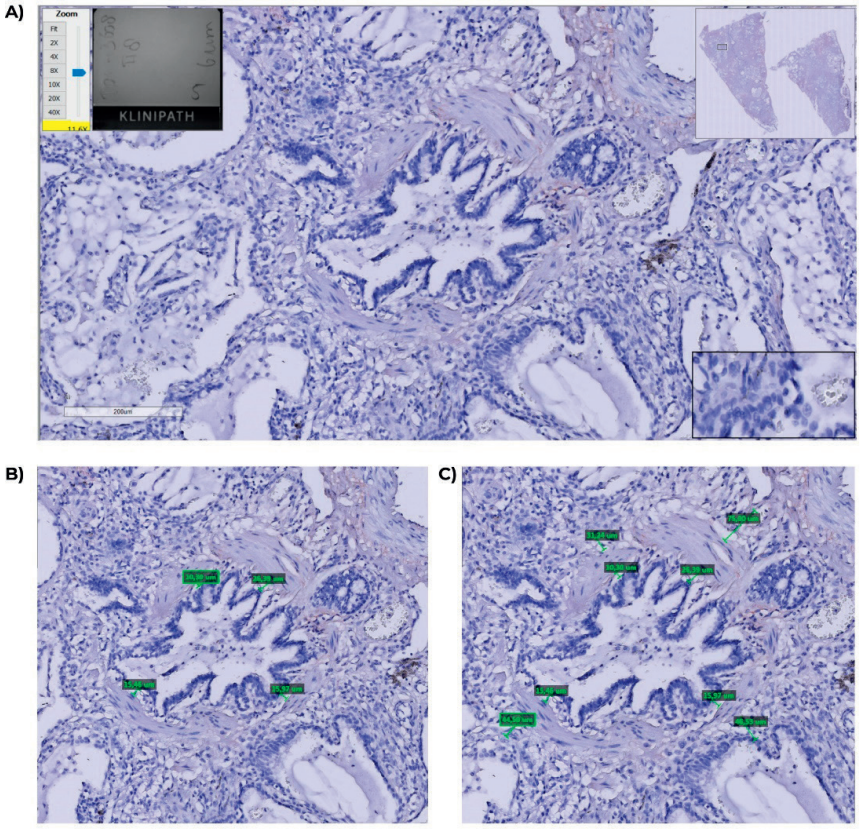

Supplementary Figure 1: Example of how to determine SM-P distances of a fibrotic airway. (A) Measurements were performed on the airway in the Aperio ImageScope program. (B) The airway with measured E-SM distances. (C) The airway with both measured E-SM distances and calculated SM-P distances. The SM-P distances are measured starting from the outside of the smooth muscle layer.

REFERENCES

1. Martinez FJ, Collard HR, Pardo A, Raghu G, Richeldi L, Selman M, Swigris JJ, Taniguchi H, Wells AU. Idiopathic pulmonary fibrosis. *Nat Rev Dis Pri* 2017: 3(1): 17074.
2. Parker MW, Rossi D, Peterson M, Smith K, Sikstrom K, White ES, Connett JE, Henke CA, Larsson O, Bitterman PB. Fibrotic extracellular matrix activates a profibrotic positive feedback loop. *J Clin Invest* 2014: 124(4): 1622-1635.
3. Nizamoglu M, Burgess JK. The Multi-Faceted Extracellular Matrix: Unlocking Its Secrets for Understanding the Perpetuation of Lung Fibrosis. *Curr Tissue Microenviron Rep* 2022: 2(4): 53-71.
4. Burgstaller G, Oehrle B, Gerckens M, White ES, Schiller HB, Eickelberg O. The instructive extracellular matrix of the lung: basic composition and alterations in chronic lung disease. *Eur Respir J* 2017: 50(1).
5. Tjin G, White ES, Faiz A, Sicard D, Tschumperlin DJ, Mahar A, Kable EPW, Burgess JK. Lysyl oxidases regulate fibrillar collagen remodelling in idiopathic pulmonary fibrosis. *Dis Model Mech* 2017: 10(11): 1301-1312.
6. Ansorge HL, Meng X, Zhang G, Veit G, Sun M, Klement JF, Beason DP, Soslowsky LJ, Koch M, Birk DE. Type XIV Collagen Regulates Fibrillogenesis. *J Biol Chem* 2009: 284(13): 8427-8438.
7. Tzortzaki EG, Tischfield JA, Sahota A, Siafakas NM, Gordon MK, Gerecke DR. Expression of FACIT collagens XII and XIV during bleomycin-induced pulmonary fibrosis in mice. *Anat Rec A Discov Mol Cell Evol Biol* 2003: 275(2): 1073-1080.
8. Sikkema L, Strobl D, Zappia L, Madissoon E, Markov NS, Zaragosi L, Ansari M, Arguel M, Apperloo L, Bécavin C, Berg M, Chichelnitskiy E, Chung M, Collin A, Gay ACA, Hooshiar Kashani B, Jain M, Kapellos T, Kole TM, Mayr C, von Papen M, Peter L, Ramírez-Suástegui C, Schniering J, Taylor C, Walzthoeni T, Xu C, Bui LT, de Donno C, Dony L, Guo M, Gutierrez AJ, Heumos L, Huang N, Ibarra I, Jackson N, Kadur Lakshminarasimha Murthy P, Lotfollahi M, Tabib T, Talavera-Lopez C, Travaglini K, Wilbrey-Clark A, Worlock KB, Yoshida M, Desai T, Eickelberg O, Falk C, Kaminski N, Krasnow M, Lafyatis R, Nikolíc M, Powell J, Rajagopal J, Rozenblatt-Rosen O, Seibold MA, Sheppard D, Shepherd D, Teichmann SA, Tsankov A, Whitsett J, Xu Y, Banovich NE, Barbry P, Duong TE, Meyer KB, Kropski JA, Pe'er D, Schiller HB, Tata PR, Schultze JL, Misharin AV, Nawijn MC, Luecken MD, Theis F. An integrated cell atlas of the human lung in health and disease. *bioRxiv* 2022: 2022.2003.2010.483747.
9. Adams TS, Schupp JC, Poli S, Ayaub EA, Neumark N, Ahangari F, Chu SG, Raby BA, Deluliis G, Januszyk M, Duan Q, Arnett HA, Siddiqui A, Washko GR, Homer R, Yan X, Rosas IO, Kaminski N. Single-cell RNA-seq reveals ectopic and aberrant lung-resident cell populations in idiopathic pulmonary fibrosis. *Sci Adv* 2020: 6(28): eaba1983.
10. Koloko Ngassie ML, De Vries M, Borghuis T, Timens W, Sin DD, Nickle D, Joubert P, Horvatovich P, Marko-Varga G, Teske JJ, Vonk JM, Gosens R, Prakash YS, Burgess JK, Brandsma CA. Age-associated differences in the human lung extracellular matrix. *Am J Physiol Lung Cell Mol Physiol* 2023: 324(6): L799-L814.

11. Booth AJ, Hadley R, Cornett AM, Dreffs AA, Matthes SA, Tsui JL, Weiss K, Horowitz JC, Fiore VF, Barker TH, Moore BB, Martinez FJ, Niklason LE, White ES. Acellular normal and fibrotic human lung matrices as a culture system for in vitro investigation. *Am J Respir Crit Care Med* 2012: 186(9): 866–876.

12. Sun M, Zafrullah N, Adams S, Devaux F, Avila MY, Ziebarth N, Margo CE, Koch M, Espana EM. Collagen XIV Is an Intrinsic Regulator of Corneal Stromal Structure and Function. *Am J Pathol* 2021: 191(12): 2184–2194.

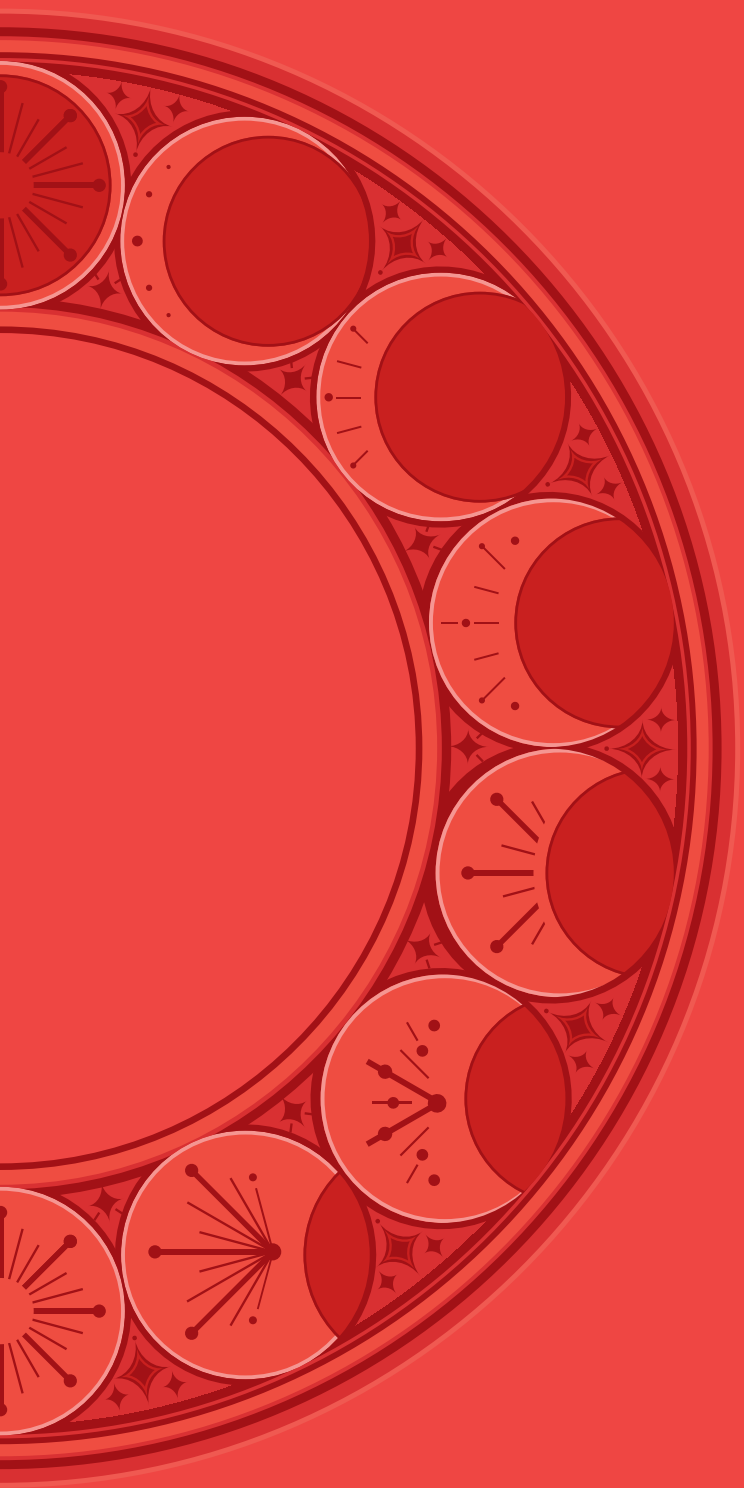

CHAPTER 4

Innovative 3D models for understanding mechanisms underlying lung diseases: powerful tools for translational research

Mehmet Nizamoglu [#], Mugdha M. Joglekar [#], Catarina R. Almeida, Anna-Karin Larsson Callerfelt, Isabelle Dupin, Olivier T. Guenat, Pauline Henrot, Lisette van Os, Jorge Otero, Linda Elowsson, Ramon Farre, Janette K. Burgess

[#] Equal contributions

Published in *European Respiratory Review* under a CC BY-NC 4.0 license as: **Nizamoglu, M.***, Joglekar M.M.*, Almeida C.A., Larsson Callerfelt, A.K., Dupin, I., Guenat, O.T., Henrot, P., van Os, L., Otero, J., Elowsson, L., Farre, R,. & Burgess, J.K. (2023). Innovative 3D models for understanding mechanisms underlying lung diseases: powerful tools for translational research. *European Respiratory Review* 2023; 32: 230042.
https://doi.org/10.1183/16000617.0042-2023

ABSTRACT

Chronic lung diseases result from alteration and/or destruction of lung tissue, inevitably causing decreased breathing capacity and quality of life for patients. While animal models have paved the way towards understanding pathobiology and developing therapeutic strategies for disease management, their translational capacity is limited. Therefore, the need for developing innovative *in vitro* models to reflect chronic lung diseases, facilitating mechanism investigation and advancement of new treatment strategies is well recognised. In the last decades, lungs, in healthy and diseased conditions, have been modelled using precision-cut lung slices, organoids, extracellular matrix-derived hydrogels and lung-on-chip systems. These three-dimensional models together provide a wide spectrum of applicability and mimicry of the lung microenvironment. While each system has its own limitations, their advantages over traditional two-dimensional culture systems, or even over animal models, increases the value of *in vitro* models. Generating new and advanced models with increased translational capacity will not only benefit our understanding of the pathobiology of lung diseases but should also quicken the timelines required for discovery and generation of new therapeutics. This article summarises and provides an outline of the European Respiratory Society (ERS) Research Seminar: "Innovative 3D models for understanding mechanisms underlying lung diseases: powerful tools for translational research" in Lisbon, Portugal in April 2022. Current *in vitro* models developed for recapitulating healthy and diseased lungs are outlined and discussed with respect to the challenges associated with them, efforts to develop best practices for model generation, characterisation and utilisation of models, as well as state-of-the-art translational potential.

KEY TERMS

Click chemistry: Fast, simple, and high-yielding reactions used for joining molecular entities through a simple action like snapping things together

Cross-linked/ing: Formation of bonds between two molecular chains to link them together

Cryopreservation: Storing of cells, tissues or organs through freezing in protective substances that enable the frozen object to be retrieved in a living state

Decellularised/Decellularisation: Removal of cells and cellular content from any given tissue or organ

Elastic modulus/Stiffness: Measure of mechanical properties that defines the compressive elastic deformation of materials

Extracellular matrix (ECM): A bioactive and dynamic 3 dimensional network composed of proteins, glycosaminoglycans, glycoproteins, and proteoglycans. It provides structure and support to the cells, being present in all tissues and organs

Feeder (layer): A layer of cells which do not grow themselves but provide support for other cells

Lyophilisation: Removal of frozen water from frozen tissues or organs under vacuum conditions

Microenvironment: The local environment surrounding a cell, composed of the ECM, other cells, and factors that dynamically interact with one another to affect the cell directly or indirectly.

Pluripotent stem cells: Cells that have the capacity to self-renew and are able to differentiate into all different types of cells in the body

Remodelling: Series of changes in the content and organization of the components (of the extracellular matrix)

Resident progenitor cells: self-renewing cells resident in a tissue that are activated during injury to participate in the repair process through differentiating to tissue-specific cell types

Thermosensitive: Responsive to changes in temperature

Viscoelastic (stress) relaxation: Measure of the decrease in the accumulated load (stress) in the structure through both viscous (fluid) and elastic (solid) manners

INTRODUCTION

Chronic lung diseases contribute significantly to the global burden of healthcare [1]. Asthma, chronic obstructive pulmonary disease (COPD), lung fibrosis, pulmonary hypertension, and lung cancer are some common examples [1]. Structural alterations and cellular damage in these chronic diseases can be the result of (combinations of) prolonged exposure to environmental factors such as smoke (cigarette or other sources), air pollution, and pathogens or genetic predisposition [2]. As a result, chronic diseases are often characterised by excessive mucus secretion [3, 4], reduced mucociliary clearance [3, 4], and aberrant remodelling of the airways, pulmonary vasculature and distal parenchymal tissue [5]. Subsequently, airflow limitation and alveolar tissue destruction results in the loss of lung function [3-5]. Localised repair and regeneration in the lung can be facilitated by resident progenitor cells [2, 6], but these progenitor cells can be functionally impaired in disease conditions [6]. Therefore, for most end-stage lung diseases, the only definitive treatment is lung transplantation [7].

Developing appropriate treatments for chronic lung diseases can be bolstered through thorough understanding of disease mechanisms. In spite of the abundance and advancement in knowledge, the pathogenesis and progression of most chronic diseases remains unclear. Much knowledge has been obtained from rodent studies, which often do not completely recapitulate human diseases [8]. Traditional two dimensional (2D) *in vitro* cell culture approaches have played a fundamental role in advancement of current knowledge of cell behaviour and fate. However, these approaches lack a range of essential cell-cell and cell-extracellular matrix (ECM) interactions that have been shown to define cell signalling and function [9]. Bioengineering has promoted the development of innovative *in vitro* systems for modelling diseases in lung research [10]. Hence, three-dimensional (3D) models containing one or more matrix components and multiple cell types are becoming the sought-after standard for *in vitro* studies. These models support the growth of cells in all directions and allow for interaction with their surroundings. The use of models emulating human disease will not only aid in increased understanding of disease processes, but new models can also improve the drug development process and safety testing.

This review extensively describes the state-of-the-art for *in vitro* models developed for *ex vivo* engineering in lung research as a summary and postscript of the presentations and discussions that took place during the European Respiratory Society (ERS) Research Seminar: "Innovative 3D models for understanding mechanisms underlying lung diseases: powerful tools for translational research" in Lisbon, Portugal in April 2022. A synopsis of various traditional and novel methods for characterisation of these

models along with a comprehensive overview of the advantages and disadvantages of each model are presented. Furthermore, the translational potential of *in vitro* systems supplemented with potential challenges are reviewed.

GENERATION OF (3D) INNOVATIVE *IN VITRO* LUNG MODELS

Currently, translation of respiratory therapies from bench to bedside remains limited in part due to the lack of relevant *in vitro and in vivo* models. The need for more accurate and physiologically representative models of the lung is thus clearly established. Various approaches to develop new models range from models using exclusively the source material of the lung like precision cut lung slices (PCLS) to fully engineered environments like the lung-on-chip (LOC). This article will focus on disease modelling in four main types of *in vitro* lung models: PCLS, organoids, lung ECM-derived hydrogels, and LOC. Each of these models have their strengths and weaknesses as presented in **Figure 1**.

The common ground in the above-mentioned models is the development of a cellular environment away from stiff and non-physiological plastic culture dishes, proposing instead a transition towards softer materials, with the possibility of inclusion of ECM proteins and/or reproduction of the structural arrangement, biochemical, and biomechanical properties of the lung. To recapitulate the lung microenvironment, several different factors are important. The main factors are biomechanics (mechanics of breathing and stiffness), lung ECM (structure and composition), and lung cell composition (cell types and cell source). Other factors that may be added include, but are not limited to, an immune component, hypoxic and normoxic regions, and blood flow (perfusion).

These *in vitro* models can be used to investigate the influence of individual mechanical parameters and immune cell interactions on disease origin and progression, along with screening for druggable targets and developing therapies. Animal models remain an indispensable tool for research as *in vitro* models cannot yet mimic the complex structures of tissues and systemic effects. However, there is an evolving role for these preclinical systems for modelling *in vivo* conditions and screening therapeutics to reduce the burden on *in vivo* systems.

Each model has different advantages and disadvantages, and the choice of model is highly dependent on the research question to be addressed and the availability of source material. This review section will highlight some of the innovative *in vitro* lung models and their recent developments.

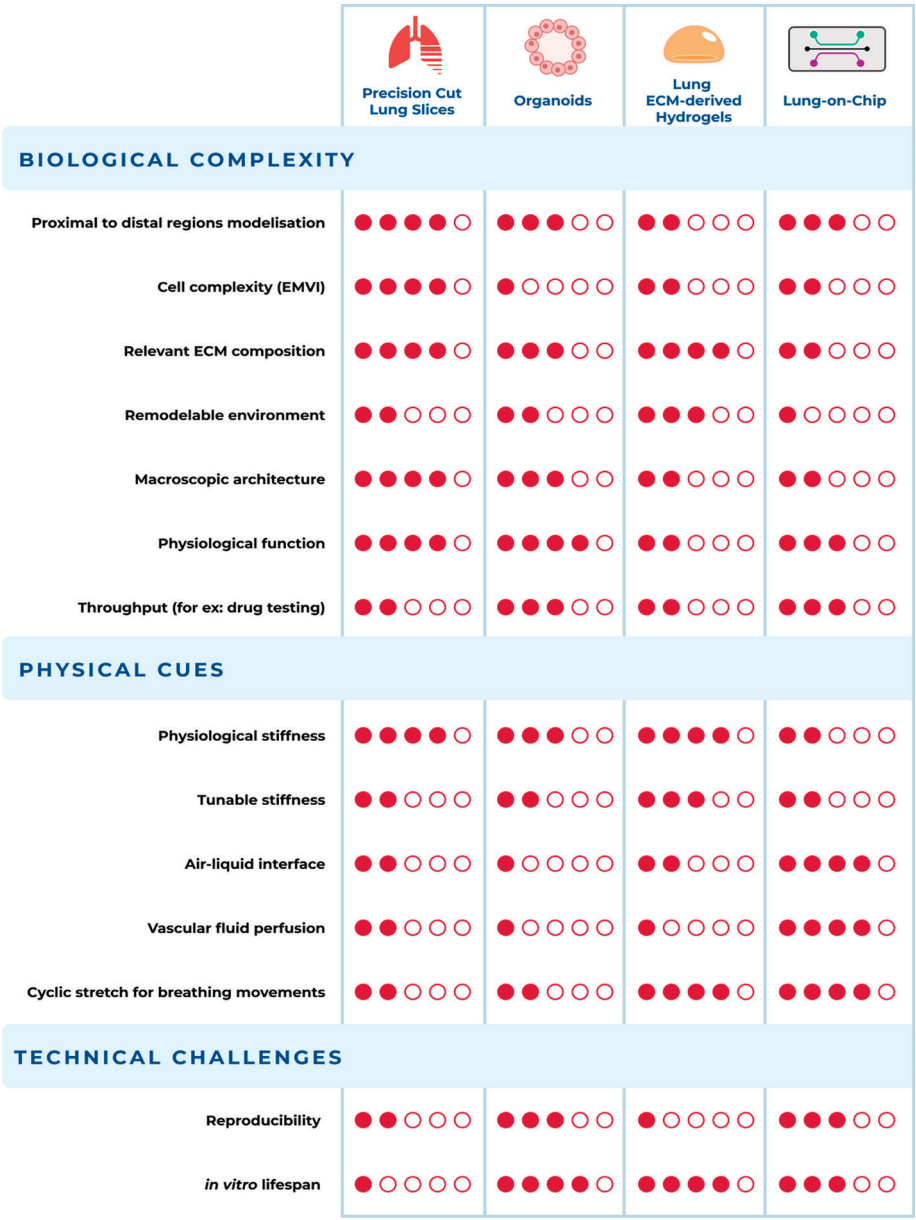

■ **Figure 1: A general comparison of *in vitro* models used for modelling the lung: precision cut lung slices (PCLS), organoids, lung extracellular matrix (ECM)-derived hydrogels and lung-on-chip (LOC).** E/M/V/I: Epithelial cells, Mesenchymal cells, Vascular cells, Immune cells. The proportion of filled dots reflects the score, on a scale of 5, of the model to fulfil the stated criterion from least representative (1 filled dot) to a complete lung *in vitro* (5 filled dots). Lung ECM-derived hydrogel comparisons were based on cell-seeded hydrogels. Reported scores reflect the opinion of the authors and the meeting attendees rather than an objective scoring.

PRECISION CUT LUNG SLICES (PCLS)

PCLS are a unique translational *ex vivo* model of peripheral lung tissue that have applicability for many different research approaches including drug discovery and toxicity screenings [11, 12]. The slice lung model was first introduced as a pharmacological model by Dandurand et al. [13]. Unlike tissue fragments obtained by cutting or shredding explanted tumour resections [14], PCLS are well-defined models with standardised protocols for preparation and use in experiments. Upon collection, the lungs are filled via the trachea in animals or bronchi/bronchioles in human lung explants with a low melting agarose solution (0.75% - 3%) and then cut into slices of 200 - 500 µm thickness [15, 16]. The slices consist of distal airways and vessels with their intact lung architecture, maintaining cell-cell interactions and ECM. It is possible to sequentially study various lung cell populations in airways and vessels of different sizes and anatomical locations from a healthy or diseased lung, thus optimally utilizing available resources. Such an approach provides opportunities for specialised screening of the responses of alveoli, bronchioles, vessels, and surrounding ECM. Calcium fluxes and ciliary beat frequency can be followed and visualised in the small airways [16, 17], with smaller airways being known to respond to a greater extent to bronchoconstrictors than larger airways [15, 18]. In some instances, the thickness of the slices may be a concern as the readouts and functionality can differ depending on the thickness. Therefore, it is important to describe slice thickness, area of the slices, and lumen size of airways and pulmonary vessels when reporting generated data. Moreover, cutting and embedding the lung tissues in agarose can trigger repair and regenerative responses that can subsequently affect further experiments. Thorough washing and resting periods prior to experimental procedures can considerably reduce the effect of the processing steps. The viable culture period (5-28 days) is dependent on the type of analysis to be performed and should always be specified to enable replication of the studies. Cryopreservation of PCLS is a way forward to maximise the number of slices that can be used per lung and the possibility to share valuable material, however current protocols under development for cryopreservation need further improvement to enhance PCLS viability and functionality upon revival. PCLS can also be modified to mimic disease with different approaches and protocols either by treating the animal prior to harvesting of the lung or by directly treating the PCLS. Examples of applications of such models include allergic asthma [19, 20], emphysema [21, 22], acute respiratory distress syndrome (ARDS) [23], fibrosis [24, 25]. PCLS can also be decellularised and used as lung scaffolds with native ECM architecture for 3D cell culture studies with and without cyclic stretch [26-28]. Material availability and viable culture duration limits the use of PCLS, however, these models provide unmatched

resemblance of the physiological architecture and multicellularity of the lung. These models represent the status of the lung at a given time of harvest, thus providing excellent tools to study different stages of disease progression. Overcoming the current restrictions, combined with facilitating immune cell recruitment, would aid in unlocking the true potential of PCLS.

ORGANOIDS

Organoid cultures are defined as 3D cultures grown from pluripotent stem cells (PSCs) or adult progenitor cells that self-organise to form structures histologically similar to human organs [29, 30]. The requirements for 3D cultures to be considered as an organoid are self-renewing capacity and the replication of some function specific to the mimicked organ (such as the mucociliary function in the case of bronchial organoids) [29, 30]. In contrast to organoids, spheroids are typically cell aggregates grown scaffold-free from a single or a mix of multiple cell types and have a lower complexity while recapitulating native tissue [31]. While organoids modelling bronchial epithelium have been rapidly instituted, those for alveoli have been more challenging to establish [32]. Early efforts employed flow cytometry sorting of murine alveolar type II epithelial cells co-cultured with mesenchymal cells [33]. To date, the minimal composition of lung organoids built from adult progenitor cells comprises bronchial epithelial cells that are embedded in a 3D ECM-based hydrogel with a complex combination of growth factors [34]. This gives rise to spherical organoids often filled with secretions, that are classified into tracheospheres [35], bronchospheres [36], or alveolospheres [33, 37], depending on the source of epithelial cells. More recently, isolation (often with selection of EpCAM+ cells, via flow cytometry [38] or magnetic bead-based selection [39]) of epithelial cells, coupled with culture with or without mitomycin restricted feeder fibroblasts has been described for alveolar organoid culture [40, 41]. Moreover, generating alveolar organoids without the presence of a feeder cell population has also recently become possible [42, 43]. Research using organoids has progressed exponentially during the last decade, and results obtained have been reviewed in detail elsewhere [44, 45]. Relatively simple to obtain, human airway organoids derived from epithelial cells and adult stem cells have been successfully used to study important processes such as respiratory virus infections including respiratory syncytial virus (RSV) [46] and influenza viruses [47] respectively. Donor-specific organoids can be generated from progenitor cells purified from human lung tissue to model the healthy state and various respiratory diseases (see Table 1). In contrast, PSC-derived lung organoids rely on a complex manipulation of developmental signalling pathways, to form a lung bud

organoid that can develop into branching airways with primitive alveoli [48]. PSC and in particular induced PSC (iPSC)-based organoids have great potential thanks to their potential for combining multiple cell types such as epithelial, smooth muscle cells and fibroblasts [49], but due to their intrinsic immature nature, generating disease models is not straightforward, except for monogenic disorders such as cystic fibrosis (CF) [50]. All in all, lung organoids have rapidly shown their value for respiratory research, thanks to their physiologically relevant properties, the possibility to recreate and understand lung development, and regeneration mechanisms. Organoid amplification [46] and cryopreservation of organoids opens a world of possibilities for the establishment of biobanks to facilitate greater availability of progenitors for organoid development for biomedical research and personalised medicine [51].

LUNG EXTRACELLULAR MATRIX (ECM)-DERIVED HYDROGELS

Hydrogels are hydrophilic polymers physically or chemically cross-linked to form a 3D network [52]. Hydrogels can hold copious amounts of fluids while maintaining their structural integrity and represent the hydrated nature of physiological ECM. Individual ECM components or derivatives of them such as collagen, gelatine, fibronectin, fibrin, and hyaluronic acid have frequently been used to form hydrogels to mimic the ECM and provide bioactive components in cell culture [53]. However, they do not fully recapitulate the physiological complexity of the ECM and its macrostructure. Organ-derived ECM recapitulates the tissue-specific biochemical and biophysical complexity of the native tissue [54]. Thus, cell-seeded seeded lung ECM-derived hydrogels have since emerged as an important *in vitro* system to model the lung microenvironment. The first lung ECM-derived hydrogel was reported by Pouliot et al. in 2016, using porcine lung ECM [55], which was followed by human lung-derived ECM [54, 56] for establishing such models. Lung tissue can be decellularised using different methods, including chemical detergents, freezing/thawing, sonication, enzymatic digestion [53, 57], and recently developed apoptosis-associated approaches [58], followed by lyophilisation and milling into fine power [54] or homogenising using mortar and pestle [53]. The decellularised ECM is solubilised using pepsin in acidic conditions with constant agitation for 24-72 hours [53]. Pepsin preserves the ultrastructure of collagens by cleaving collagen triple helices only at their telopeptide bonds [53], although the digestion time has been shown to affect hydrogel properties and morphology and metabolic activity of cells seeded onto the hydrogels [53, 59]. The pH of the solution is neutralised, followed by buffering with PBS to generate a self-assembling and thermosensitive ECM pre-gel that forms a hydrogel at 37°C [54]. Ultrasonic cavitation has also been

used to solubilise milled ECM of porcine trachea [60], as an alternative to pepsin digestion, which also solves the unsolved challenge of leftover pepsin in the lung ECM-derived hydrogels. Despite these rigorous treatments, ECM-derived hydrogels retain most of the native composition and reflect mechanical properties of the lung ECM both in healthy and diseased states [54]. Interestingly, a recent report illustrates organ-specific elasticity, viscoelastic relaxation and gelling properties of ECM-derived hydrogels [56]. These studies highlight the importance of mimicking the underlying architectural and mechanical properties of the ECM that are disease and organ-specific and can thus differentially regulate cellular responses. To this end, multiple studies have demonstrated alterations in cellular morphology or phenotype [61, 62], differentiation [63, 64] and gene and protein expression [61, 65] in cells cultured on or harvested from within ECM-derived hydrogels. Further investigation into individual biomechanical properties in studies using novel tools such as click chemistry for modulating elastic modulus [66], ECM-derived and synthetic material hybrid hydrogels to modulate stiffness [67], or applying fibre cross-linking to native lung ECM-derived hydrogels to increase stiffness and decrease viscoelastic stress relaxation [68], have provided novel insights as to the role of the lung microenvironment in driving disease processes. Lung ECM-derived hydrogels are an innovative and powerful tool that can be manipulated. Through the addition of cyclic stretch to mimic breathing, this model has the potential to further mimic the lung microenvironment *in vivo* [62, 69], thus being among the models that most closely represent physiological conditions. A challenge yet to be addressed effectively is the capacity to mimic the physiological architecture of peripheral lung tissue. Through the employment of this model system, the outcomes of cell-ECM interactions in the lung are slowly becoming evident.

LUNG-ON-CHIP (LOC)

LOC devices are microphysiological systems that model part of the lung and provide the possibility to combine physiological flow, mechanical stretching, multi-compartment co-culture, drug/particle exposure and ECM material in an *in vitro* system. The LOC models began with 2 or 2.5D systems, however, they have now advanced to multicellular and multidimensional 3D systems. Microfluidic devices offer many possibilities that have recently been used to develop different LOC devices and some relevant LOC devices are highlighted here. The first LOC with physiological flow and mechanical stretch was developed by the Ingber group [70]. This alveolus-on-chip, with lung epithelial cells and endothelial cells, was perfused with neutrophils to mimic an infection, and later expanded to initiate coronavirus disease (COVID-19)

research on the chip [71, 72]. Diseases like asthma and COPD have been modelled in LOC mimicking small airways [73, 74]. In addition, a stromal layer can be included, combining LOC technology with hydrogel culture [75]. LOC technology has evolved further and recently, a LOC with a stretch regimen that is closer to physiological stretch was developed. This platform uses a micro-diaphragm that stretches the cell culture membrane in three-dimensions [76, 77]. It can be used with immortalised primary alveolar cells for nanoparticle exposure and lipopolysaccharide challenge [78]. To create a more *in vivo*-like environment, the polymer membrane of the LOC was replaced by a collagen-elastin membrane spread by surface tension on an ultra-thin grid with holes the size of alveoli enabling the creation of an array of alveoli [79]. Lung microvasculature and vascular diseases are also modelled with microfluidics. For example, side effects of the IPF drug Nintedanib [80], effects of physiological stretch on the endothelium [81], or combined effects of hypoxia and cyclic stretch [82] have been investigated. A challenge with LOC experiments is the incorporation of primary material that presents wide heterogeneity. This has been tackled by generating type II alveolar epithelial cells (AECII) organoids to enable expansion of primary lung alveolar cells in hydrogels before culture in a LOC [42]. Another challenge is the complicated fabrication of LOC devices, which often requires highly specialised equipment. A recent study showed that it is possible to develop a LOC to study ventilation-induced injury solely by using a simple 3D printer and syringe pump [83]. In spite of these challenges, LOC as a technology has been successfully commercialised by multiple startups, such as Emulate [71], AlveoliX [78], and Mimetas [84] that support research on a wide-range of human (lung) diseases. Often, these companies offer customization of chips allowing easy technology transfer and adaptation of LOC systems, thus enabling rapid uptake of LOC without the limitation of the requirement of development and manufacture in-house by various research groups. However, the scalability and costs of these systems remain an important challenge. The LOC field is still young and exciting with new developments continuously occurring. Overall, LOC technology is promising for modelling lung diseases and drug efficacy/safety screening with the advantage of being able to model the complexity of the different compartments of the lung in one system.

PERSPECTIVES AND FUTURE DIRECTIONS

A summary of recent applications of the use of PCLS, organoids, ECM-derived hydrogels and LOC as *in vitro* systems for lung disease modelling is presented in **Table 1.** Excitingly, the development of lung *in vitro* models continues to rapidly advance. In

the future, there is the potential for different models highlighted in this perspective to be combined to create an optimal *in vitro* model that can utilize the advantages of different models in concert. For example, by combining LOC technology with porcine lung ECM hydrogels, a physiomimetic acute respiratory distress syndrome model incorporating primary rat mesenchymal stromal cells and AECII has recently been developed [62]. Furthermore, these *in vitro* models can be improved using techniques such as 3D bioprinting that is rapidly offering several new opportunities such as bioinks with bioactive components and tuneable mechanical properties [85, 86]. The cellular and ECM diversity in the lungs and an increase in the use of human material in research calls for the use of spatio-specific material for defined research questions. An indispensable feature of animal models that is yet to be recapitulated in *in vitro* models, is the systemic responses that arise from a functioning immune system. The inclusion of immune cells in *in vitro* models developed for testing novel cellular and molecular interventions will aid in advancing knowledge about local and systemic immune responses associated with lung diseases [87]. Furthermore, development of advanced *in vitro* models will reduce the dependency on animal models for scientific research. However, to reach this point, adequate characterisation of *in vitro* models is necessary, which will be discussed in the next section.

■ **Table 2: Overview of the use of the different 3D *in vitro* systems to model healthy and diseased human lungs.**

	Precision Cut Lung Slices (PCLS)	Organoids#	Lung Extracellular Matrix (ECM)-derived hydrogels*	Lung-on-chip
Healthy	**Both alveolar and airway:** Bronchoconstriction assay [18, 88], Response to drugs or industrial chemicals [89], Long-term (14 days) [90, 91], Indacaterol efficacy [92]	**Airway:** From adult stem cells [93, 94] From PSCs [49, 95], With bronchial epithelial cells, lung fibroblasts and endothelial cells [96] Alveolar: From PSCs [97–99] Both alveolar and airway: Human foetal-lung derived organoids [100]	Both alveolar and airway: Human lung ECM hydrogels and comparison to native tissue [54]	Airway: With epithelial cells only [101], epithelial-vascular interface [102], With fibroblast compartment [103], Epithelial-ECM-smooth muscle interface [104], Epithelial-ECM-vascular interface [105], Cell extravasation [106] Alveolar: Alveolar-capillary interface [70], Alveolar acini with immune compartment [107], With micro-diaphragm [76], With inverse opal gelatine hydrogel [108], With biological and stretchable membrane [79], With fibroblast compartment [75]
Asthma	Airway only: Effect of soluble guanylate cyclase on bronchodilation [109], asthma mediators [110], ß2-agonist efficacy modulated by steroids [111], Rhinovirus infection: increased IL-13, IL-25 and thymic stromal lymphopoietin [112]	Airway only: Notch2 role in goblet cell metaplasia [113]		Airway only: IL-13 induced asthma [102], IL-13 and viral-induced exacerbations [114]
Chronic Obstructive Pulmonary Disease	Alveolar only: CS model +/- viral exacerbations FZD4 inhibitor efficiency in COPD patients PCLS [115], Wnt/β-catenin signal activation efficiency [22]	Alveolar only: COPD-patient derived epithelial cell organoids [116], Emphysematous alveolar epithelial cells [42]	Both alveolar and airway: COPD lung ECM hydrogels and comparison to native tissue [54]	Airway: With COPD epithelial cells, poly-IC-induced [102], Cigarette smoke-induced [73, 117] Alveolar: Cigarette smoke-induced [108], With emphysematous cells [42]

■ **Table 2: Overview of the use of the different 3D *in vitro* systems to model healthy and diseased human lungs. (continued)**

	Precision Cut Lung Slices (PCLS)	Organoids#	Lung Extracellular Matrix (ECM)-derived hydrogels*	Lung-on-chip
Cystic fibrosis		Airway: From patient-derived adult stem cells [46], From patient-derived PSCs [50, 118] From multipotent human foregut stem cells with cystic fibrosis transmembrane conductance regulator mutation [119] Not categorised: Nasospheres for drug testing [120, 121]		Both alveolar and airway: With epithelial cells from patients with cystic fibrosis [103]
Lung Fibrosis	Alveolar only: IPF model with cytokines [24], From IPF patients [25]	Alveolar only: Hermansky–Pudlak syndrome [48], Hermansky–Pudlak syndrome mutation in embryonic stem cell-derived organoids [122]	Both alveolar and airway: IPF lung ECM hydrogels and comparison to native tissue [54],	Both alveolar and airway: With IPF fibroblasts [103] Alveolar: With epithelial cells (wound-healing and stretch) [123]
Cancer	Not categorised: Kras mutation model [124] Non-small cell lung cancer [125] T cells infiltration [126]	Not categorised: From patient-derived adult stem cells [46], Patients-derived organoids: Non-small cell [127], adenocarcinoma [128], five different subtypes [129], Co-cultured with endogenous tumour infiltrating lymphocytes [130]		Not categorised: Non-small-cell lung cancer [131, 132], Mesothelioma [131], Safety studies [133]

Only the studies using human-origin cells and ECM were included in the table. #Studies using the following terminology were included under the "organoids" section: spheroids, tracheosphere, bronchosphere, alveolosphere, nasosphere and organoids. *Studies aiming at building lung tissues for transplantation were not included in this table. **PSC:** pluripotent stem cell, **iPSC:** induced pluripotent stem cell, **ECM:** extracellular matrix, **COPD:** chronic obstructive pulmonary disease, **IPF:** idiopathic pulmonary fibrosis, **PCLS:** precision cut lung slice, **TGF-β:** transforming growth factor beta.

CHALLENGES ASSOCIATED WITH 3D *IN VITRO* MODELS

In vitro models including PCLS, organoids, lung ECM-derived hydrogels, and LOC are powerful methods for employment in the quest to decipher the *in vivo* status of lung diseases at the cellular and ECM level. A comprehensive overview of the challenges associated with the above-mentioned *in vitro* models is presented in **Table 2**. In addition to the challenges specific for each model, there are overarching challenges for *in vitro* models in general. As research using such models progresses, the materials utilised, methods applied, and outcomes tested also diversify. As one of the primary outcomes of the "ERS Research Seminar 2022: Innovative 3D models for understanding mechanisms underlying lung diseases: powerful tools for translational research", the participants were invited to contribute to a discussion on defining best practices when using these models and resources to improve reporting and reproducibility of data generated with these models. The main take-home message from these discussions was the need for clear and detailed methodology sections when reporting outcomes and open communication. Additionally, several other important issues were highlighted.

Best practices for handling patient samples: All participants were appreciative of the opportunities and importance of using precious human samples; however, the limitations of this practice were also recognised. The variability in the results caused by sample processing can be addressed by suggesting optimal windows of time between explanting of tissues and processing and clarity of methodologies for processing when working with human material [134]. Extensive information, about each protocol used by investigators, in the materials and methods sections would improve the potential for accurate comparisons to be made between different studies. Primary lung tissue material is generally seen as the optimal choice of source for cell and ECM material, but access to such primary tissue is limited and not equally distributed between research centres. Obtaining ethical board permissions to use the sparse human-sourced material is a challenge [135], and the establishment of local exchange networks has aided in tackling this. However, a European network currently does not exist, which limits optimal distribution of primary samples. Moreover, limited-to-no access to "true" healthy lung samples hinders how we can model truly "normal" tissues, resulting in potential bias in the data generated. Extensive descriptions of the details of obtaining and processing animal-sourced materials used in combination with patient-derived material for *in vitro* models would stimulate cumulative research.

Best practices for (description of) the methods applied: Different *in vitro* models require different methods for production. The development of innovative and novel techniques is encouraged by the interdisciplinary nature of lung disease research, which is supported by the fields of cell biology, pulmonology, biomaterials, and bioengineering. As a result, various research groups are developing different methods for generating *in vitro* models dependent upon available resources and applicability to the research questions explored. This however results in diversity and hence variability in the outcomes obtained from *in vitro* models, making comparison between different studies challenging. As we attempt to build on existing knowledge, the lack of unified approaches renders our efforts more complex. Agreeing on minimum parameters to define the steps required to create each version of these models, preparing such guidelines for the community and encouraging clear communication are important starting points for tackling this conundrum [136].

Best practices for measuring and reporting end points: Different research questions require the generation and measuring of different outcomes. Characterisation of end points can be performed with different methodologies which can provide information that speaks towards similar end points. While the separate measurements will ideally provide data that can be informative for comparisons, differences in the sample processing and individual experimental setups are likely to influence the outcomes, generating difficulties when it comes to making subsequent comparisons between different studies. Defining certain standards or establishing recommendations for reporting of specific details where variances may occur that influence the outcomes (for example number of cells used, exact media composition, timing for all culture steps of experiment) would greatly benefit the field. Such an approach will enable the field to move forward as it would bring different studies performed at different locations and/or times to a comparable basis.

Establishing best practices for the materials used, methods applied for generation of *in vitro* models, and the end points tested will be a difficult task. However, this newly advancing topic would strongly benefit from starting the discussions regarding the best practices for above-mentioned criteria. Enforcing "gold standards" to be met with each model system prematurely would potentially result in missing development opportunities represented by the many innovative pioneering studies. It must also be noted that these standards might vary based on the research question. One way to start such discussions is creating awareness of the need to follow best practices by providing detailed information for other influential elements of academic research. Engaging editors and journals regarding the development of good practices for the field would be an ideal starting point. The development of

agreements such as minimum information about a microarray experiment (MIAME) [137], Animal Research: Reporting of *in vivo* Experiments (ARRIVE) [138], and the FDA Modernization Act 2.0 [139] provide guidelines intended to improve quality and reproducibility of scientific reports involving microarrays, animal research, and alternative methods used to test drug safety and effectiveness. These agreements are advanced to ensure unified evaluation and interpretation of results and better reproducibility of experiments, moving towards new standards for certifying new methodologies for drug development. Such initiatives could subsequently be moved forward by engaging with reviewers about what to look out for when presented with manuscripts reporting such methodologies, as well as providing information for the research community. Together with a scientific community working harmoniously, reviewers and editors of journals paying attention and looking to apply such standards would greatly benefit the advancements made in generating and using innovative *in vitro* models for translational research [140, 141].

■ **Table 3: Main challenges associated with the four different *in vitro* culture systems for modelling lung environment in health and disease**

Precision Cut Lung Slices (PCLS)	Organoids	Lung Extracellular matrix (ECM)-derived hydrogels	Lung-on-chip
	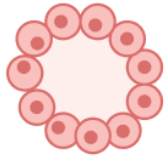		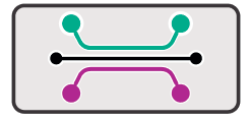
• Patient-to-patient variations	• Heterogeneity in number and sizes (due to intra- and inter-patient variations and various culture modalities)	• Patient-to-patient variations influencing ECM hydrogel properties	• Challenges associated with incorporation of cells (only for closed lung-on-chip systems)
• Heterogeneity in the diseased regions, resulting in intra and inter-slice differences	• Closed architecture with limited access to the lumen, which is filled with liquid instead of air	• Heterogeneity in the diseased regions and in decellularisation methods	• Restriction of the morphogenesis to predefined geometry
• Absence of easy air-liquid interface setting	• Presence of necrotic cores	• Macroscopic architecture differing from native lung	• Non-permissive environment that cannot be remodelled
• Need for fresh starting material that limits lifespan of various cells and the tissue *in vitro*	• Difficult to obtain fully differentiated lung cell types	• Pepsin removal currently not possible	• Non-physiological stiffness of the device
• Snapshot of the cell populations in the tissue and absence of access to infiltrating cells,	• Lack of vascularisation and difficult to introduce perfusion or immune cells	• Incorporation of cells is challenging	• Challenges associated with translation of observations from microscale to *in vivo* systems
• Difficult to preserve arteriole morphology and function	• Limited inclusion of mechanical forces associated with breathing	• Limited inclusion of mechanical forces associated with breathing	• For non-commercialised lung-on-chips: rather long production time of the microfluidic devices with a small throughput
• Cellular behaviour likely impacted by processing and agarose embedding	• Limitations in hydrogel types to develop organoid culture systems	• Lack of vascularization and difficult to introduce perfusion	

CHARACTERISATION OF *IN VITRO* MODELS

Today the use of complex 3D systems has made it possible to undertake translational studies in models that more closely mimic the *in vivo* situation. State-of-the-art characterisation of these 3D *in vitro* models is thereby of importance. The characterisation of experimental 3D models such as PCLS, organoids, (cell-seeded) ECM-derived hydrogels and decellularised lung matrices, and LOC, presents different challenges, with appropriate ways for characterising biological and physical aspects within the models dependent on the research question being addressed. These research questions might include different conditions, including but not limited to basal levels, challenged and stimulated. Here we present a non-exhaustive summary of recent advances in characterization of these *in vitro* models.

Imaging

Imaging is a major methodology used for characterisation of the macroscopic architecture and spatial localisation of specific proteins or cells, as well as cell-cell and cell-ECM interactions [142]. Light sheet fluorescence microscopy (LSFM) is an emerging technique for imaging larger 3D samples with high spatiotemporal resolution [143]. LSFM has been used extensively for organoid development studies, where visualisation is essential for understanding the cellular complexity [144] and airway development [145]. LSFM, however, requires fixation of the sample and optical clearing which is a challenge when working with 3D structures with different thickness such as PCLS. This is due to the difficulty with optical clearing in thicker PCLS that render blurry images at ≥100 µm depth. Scanning electron microscopy (SEM) has also been used to characterize cellular structures in PCLS [146], lung organoids [46, 147], and LOC [108]; or fibre structure of empty lung ECM-derived hydrogels [56]. Second harmonic generation microscopy [148, 149] has greatly facilitated the characterisation of ECM components in a PCLS model [146]; however, it has yet to be applied to other model systems for characterization of cells and microenvironment. The imaging technique employed depends on several properties of the particular *in vitro* model, thus limiting the applicability of different microscopic approaches to certain 3D models. Some important considerations while choosing an imaging technique for an *in vitro* model include: the thickness and size of the sample, effect on live cells, and fixation methods.

Protein and Gene Level Characterizations

Recent advances in sensitivity and resolution of mass spectrometry allow for deeper characterisation of all 3D models [26, 150] and have been commonly used for the characterisation of ECM composition, ECM remodelling, and cell phenotyping [151].

Isotope-labelled amino acids that tag chemical, metabolic, and enzymatic processes have been used to differentiate, in combination with mass spectrometry, between *de novo* ECM synthesis and native ECM proteins in decellularised PCLS [26, 152]. While mass spectrometry analysis on regional and disease-specific empty lung ECM hydrogels has been recently performed [153], employing such analysis on cell-seeded lung ECM-derived hydrogels is yet to be completed. Parallel to mass spectrometry, Raman spectroscopy is a label-free method that allows investigation of biochemical composition of ECM based models such as PCLS, decellularised PCLS, and hydrogels [154]. Regarding gene level characterization, RNA-sequencing approaches have been successfully applied to PCLS [155], organoid [46], and LOC systems [156]. Single-cell RNA-sequencing, a method based on capturing the mRNA content of each cell at a single cell resolution has been recently applied to lung organoid samples [157]; however, it has yet to be implemented on the remaining systems. Metabolomics approaches have also been applied to PCLS [146] and iPSC-derived epithelial progenitor cells [158]; however, no application of these approaches to other model systems has been reported.

Mechanical Characterization

Lung diseases are often characterised by an alteration in physiological mechanical properties of the ECM, and thus of the lung tissue as a whole. These changes in turn affect cellular behaviour. Importantly, the macroscopic stiffness of a tissue is rarely the same as the local microscopic stiffness which is sensed by cells through their cell surface focal adhesions [159]. Mechanical properties of *in vitro* models (mainly hydrogel based) can be manipulated to mimic disease conditions and characterised using various methods including rheometry [85], low-load compression testing [54, 68, 160] and atomic force microscopy (AFM) [61]. On a cellular, and thus a micrometre-scale, spatial elastic modulus can be measured using Brillouin microscopy. Brillouin light scattering allows for live measurements of viscoelastic properties over the surface of the sample and can be applied on bioprinted cells and 3D *in vitro* models [161, 162]. Innovative use of 4D traction force microscopy and an open source MATLAB software package represents an emerging method to measure and calculate traction forces exerted by cells in 3D hydrogel cultures over time [163]. On a microscopic scale, AFM has been commonly used to both measure stiffness and viscoelastic properties which allows for a local assessment of the material properties [164]. Cells in the lungs experience dynamic forces and are under constant cyclic stretching, which is exaggerated in patients being mechanically ventilated [165]. Additionally, cells also receive biomechanical cues from the local microenvironment [166, 167]. A novel approach using AFM was highlighted as a way to measure microrheology of tissue exposed to different levels of stretch [168].

All of these methodologies have the potential to be applied for examining PCLS, organoids, cultures with ECM-derived hydrogels and decellularised lung matrices, or LOC. Generation of such information will further our understanding of how altered mechanical conditions in lung disease impact cellular behaviour in the 3D environment [169].

TRANSLATIONAL POTENTIAL OF *IN VITRO* MODELS

The high number of failures of new drugs for respiratory diseases in clinical trials might be related to limitations in preclinical studies [170, 171]. Many of these trials fail in phase III: while the therapy is not toxic, its efficacy cannot be demonstrated. One of the main problems with the preclinical models that are currently used, is the lack of attention given to the physical aspects that are characteristic of the lung and (spatial) organization of different cells [172, 173]. Because 3D models can be implemented with human cells, they can more closely resemble human physiology, which has resulted in a growing number of studies using 3D models to study lung development and lung disease pathogenesis. Furthermore, these models have the potential as screening tools for pharmacological drugs being developed to treat pathologies such as lung fibrosis and other rare lung diseases. **Figure 2** illustrates currently available models for most common lung diseases while highlighting the models that have yet to be developed for these diseases.

Mechanopharmacology is emerging as one of the key fields associated with the development of 3D models and harvesting their potential in translational research, as it investigates the effects of mechanics in dictating the efficacy of drugs and vice versa. Pioneering studies on healthy and asthmatic subjects [174, 175] highlighted the difference on the mechanical properties of the airways and the relation with strains produced by deep inhalations [176-178]. In IPF, it has been shown that transforming growth factor (TGF)-β signalling [179] is involved in an aberrant feedback loop, as the composition of ECM [180], and stiffening of the microenvironment activates TGF-β, which further promotes production and cross-linking of fibrillar collagen [181]. Experiments performed with IPF fibroblasts cultured on either stiff tissue culture plastic, in CytoSoft® plates (2 kPa) or in soft spheroids (0.4 kPa) showed that softer materials induced expression of cycloxygenase-2 (COX-2), suggesting that higher stiffness reduced COX-2 expression while activating TGF-β [182].

Human airway organoids have been explored with respect to their translational potential for cell therapy [93]. However, dissociating such organoids into single-

cell suspensions for subsequent therapeutic application remains a challenge for advancing their use in cell therapy, as well as the development of platforms for high-throughput drug screening. As an example, in the rare disease primary ciliary dyskinesia (PCD) [183], cultures of basal epithelial cells from patients have been performed in 96 well plates for the screening of different drugs from a reduced starting cell number [184]. Methods to promote the expansion and differentiation of epithelial cells within 3D organoids, only requiring low cell numbers, provide novel opportunities to investigate how these cells behave in health and disease [185].

The translational capacity of preclinical models has recently been highlighted as a discussion point. As 92% of the preclinical trials fail for new lung cancer treatments, it is clear that there is a need to increase the preclinical "confidence" [186]. Therefore, New Approach Methodologies (NAMs) are needed [187]. The main steps that must

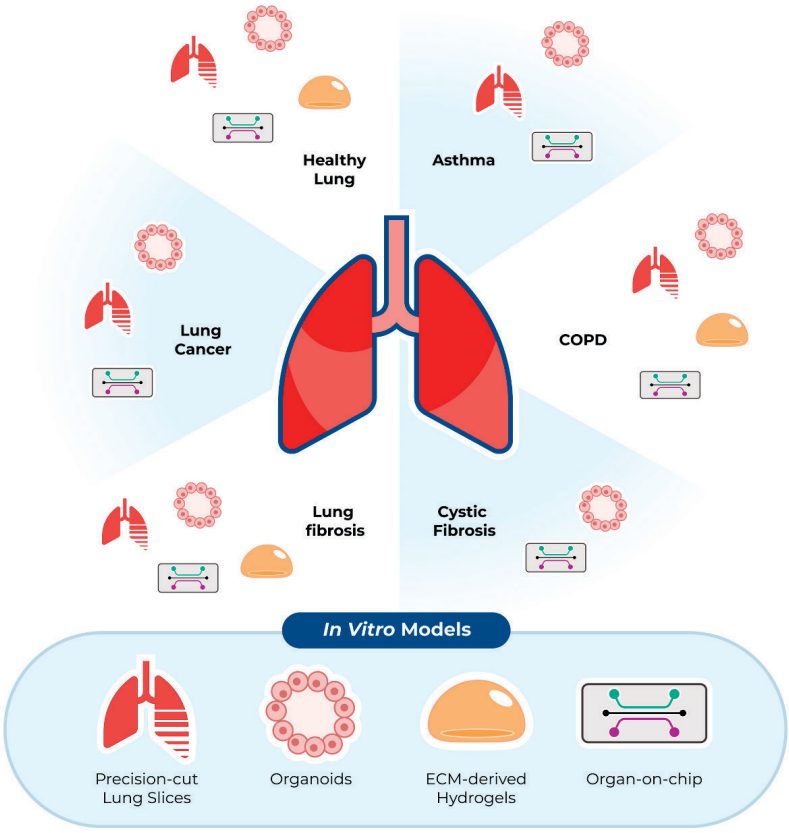

■ **Figure 2: Summary of the state-of-the-art status of different models used for modelling of different diseases.** COPD: Chronic obstructive pulmonary disease

be considered when developing NAMs are: (1) a detailed methodological description; (2) consideration of the diseased organ anatomy, control of the cell/cell ratio; (3) overcome the uncertainty due to interspecies differences, by using human cells, no animal-derived proteins, and including the microbiome; (4) exposure conditions and time points [188, 189]. Primarily driven from cancer research, these lessons can be applied to develop innovative 3D *in vitro* models described here to investigate disease pathogenesis, progression, and therapeutic targets for chronic lung diseases.

CONCLUSIONS

In vitro models with 3D structures are powerful tools that provide variability and versatility for both basic and translational research in lung diseases. PCLS, organoids, lung ECM-derived hydrogels and LOC systems present a wide spectrum of tuneability and biomimicry. Each of these models have advantages and limitations, and selection and application of the models for different studies requires a thorough understanding of their strengths and disadvantages. The future of these models, moving towards increased complexity to better represent the lung physiological conditions, will be built upon refinement of the currently developed model versions, by defining best practices for the materials used, the characterisation methods applied, and how the reported readouts can be compared. Similarly, combinations of these models to create increasingly tailored models for specific research questions would also increase the lung mimicking capacity of the models. By improving the currently existing models, generating new and innovative alternatives, as well as developing creative combinations of these systems, the translational capacity of *in vitro* research for lung preclinical studies will be greatly enhanced. The path to achieve more applicable and accepted models lies in open communication, clear descriptions of all materials/components used, and methods applied, as well as educating all parts of the scientific community. It is not unlikely that in the near future advanced *in vitro* models will replace several animal models that do not accurately reflect the diseased microenvironment of some lung diseases.

Points for Future Research:

- Exploring opportunities for combining elements from precision-cut lung slices, organoids, lung ECM-derived hydrogels and lung-on-chip models to expand 3D models for mimicking lung homeostasis and pathogenesis will advance the field.
- Establishing best practices for reporting the materials used, methods applied for generation of *in vitro* models, and the end points tested, based on the research question and model used, would greatly benefit the field. Thorough and cross-

platform characterizations of different *in vitro* models have great potential in furthering our understanding of how altered biochemical and mechanical conditions in lung disease impact cellular behaviour in the 3D environment.

- New Approach Methodologies (NAMs) for *in vitro* models are required to increase the preclinical confidence in these models.

Acknowledgements:

MMJ is funded by the Graduate School of Medical Sciences of the University of Groningen. MN and JKB receive unrestricted research funds from Boehringer Ingelheim. JKB also acknowledges support from the Nederlandse Organisatie voor Wetenschappelijk Onderzoek (NWO) (Aspasia 015.013.010). AKLC acknowledges support from the Swedish Heart Lung Foundation (grant 20210382). LvO and OG thank the H2020 ITN network EUROoC, project Nr.812954 for its financial support. RF acknowledges partial support from the Spanish Ministry of Science and Innovation (PID2020-113910RB-I00-AEI/10.13039/501100011033). JO acknowledges partial support from the Spanish Ministry of Science and Innovation (PGC2018-097323-A-I00).

REFERENCES

1. Labaki WW, Han MK. Chronic respiratory diseases: a global view. *Lancet Respir Med* 2020: 8(6): 531–533.
2. Melo-Narvaez MC, Stegmayr J, Wagner DE, Lehmann M. Lung regeneration: implications of the diseased niche and ageing. *Eur Respir Rev* 2020: 29(157).
3. Hough KP, Curtiss ML, Blain TJ, Liu RM, Trevor J, Deshane JS, Thannickal VJ. Airway Remodeling in Asthma. *Front Med* 2020: 7: 191.
4. Zhou-Suckow Z, Duerr J, Hagner M, Agrawal R, Mall MA. Airway mucus, inflammation and remodeling: emerging links in the pathogenesis of chronic lung diseases. *Cell Tissue Res* 2017: 367(3): 537–550.
5. Khedoe P, Wu X, Gosens R, Hiemstra PS. Repairing damaged lungs using regenerative therapy. *Curr Opin Pharmacol* 2021: 59: 85–94.
6. Petersen TH, Calle EA, Niklason LE. Strategies for lung regeneration. *Mater Today* 2011: 14(5): 196–201.
7. van der Mark SC, Hoek RAS, Hellemons ME. Developments in lung transplantation over the past decade. *Eur Respir Rev* 2020: 29(157): 190132.
8. Miller AJ, Spence JR. In Vitro Models to Study Human Lung Development, Disease and Homeostasis. *Physiology (Bethesda)* 2017: 32(3): 246–260.
9. Burgess JK, Harmsen MC. Chronic lung diseases: entangled in extracellular matrix. *Eur Respir Rev* 2022: 31(163): 210202.
10. Moreira A, Muller M, Costa PF, Kohl Y. Advanced In Vitro Lung Models for Drug and Toxicity Screening: The Promising Role of Induced Pluripotent Stem Cells. *Adv Bio (Weinh)* 2022: 6(2): e2101139.
11. Sanderson MJ. Exploring lung physiology in health and disease with lung slices. *Pulm Pharmacol Ther* 2011: 24(5): 452–465.
12. Liu G, Betts C, Cunoosamy DM, Aberg PM, Hornberg JJ, Sivars KB, Cohen TS. Use of precision cut lung slices as a translational model for the study of lung biology. *Respir Res* 2019: 20(1): 162.
13. Dandurand RJ, Wang CG, Phillips NC, Eidelman DH. Responsiveness of individual airways to methacholine in adult rat lung explants. *J Appl Physiol* 1993: 75(1): 364–372.
14. Voabil P, de Bruijn M, Roelofsen LM, Hendriks SH, Brokamp S, van den Braber M, Broeks A, Sanders J, Herzig P, Zippelius A, Blank CU, Hartemink KJ, Monkhorst K, Haanen J, Schumacher TN, Thommen DS. An ex vivo tumor fragment platform to dissect response to PD-1 blockade in cancer. *Nat Med* 2021: 27(7): 1250–1261.
15. Martin C, Uhlig S, Ullrich V. Videomicroscopy of methacholine-induced contraction of individual airways in precision-cut lung slices. *Eur Respir J* 1996: 9(12): 2479–2487.
16. Bergner A, Sanderson MJ. Acetylcholine-induced calcium signaling and contraction of airway smooth muscle cells in lung slices. *J Gen Physiol* 2002: 119(2): 187–198.
17. Delmotte P, Sanderson MJ. Ciliary beat frequency is maintained at a maximal rate in the small airways of mouse lung slices. *Am J Respir Cell Mol Biol* 2006: 35(1): 110–117.

18. Wohlsen A, Martin C, Vollmer E, Branscheid D, Magnussen H, Becker WM, Lepp U, Uhlig S. The early allergic response in small airways of human precision-cut lung slices. *Eur Respir J* 2003: 21(6): 1024-1032.

19. Kim DS, Park JH, Park BK, Lee JS, Nicholson AG, Colby T. Acute exacerbation of idiopathic pulmonary fibrosis: frequency and clinical features. *Eur Respir J* 2006: 27(1): 143-150.

20. Donovan C, Bailey SR, Tran J, Haitsma G, Ibrahim ZA, Foster SR, Tang ML, Royce SG, Bourke JE. Rosiglitazone elicits in vitro relaxation in airways and precision cut lung slices from a mouse model of chronic allergic airways disease. *Am J Physiol Lung Cell Mol Physiol* 2015: 309(10): L1219-1228.

21. Van Dijk EM, Culha S, Menzen MH, Bidan CM, Gosens R. Elastase-Induced Parenchymal Disruption and Airway Hyper Responsiveness in Mouse Precision Cut Lung Slices: Toward an Ex vivo COPD Model. *Front Physiol* 2016: 7: 657.

22. Uhl FE, Vierkotten S, Wagner DE, Burgstaller G, Costa R, Koch I, Lindner M, Meiners S, Eickelberg O, Königshoff M. Preclinical validation and imaging of Wnt-induced repair in human 3D lung tissue cultures. *Eur Respir J* 2015: 46: 1150-1166.

23. Nonaka PN, Falcones B, Farre R, Artigas A, Almendros I, Navajas D. Biophysically Preconditioning Mesenchymal Stem Cells Improves Treatment of Ventilator-Induced Lung Injury. *Arch Bronconeumol (Engl Ed)* 2020: 56(3): 179-181.

24. Alsafadi HN, Staab-Weijnitz CA, Lehmann M, Lindner M, Peschel B, Konigshoff M, Wagner DE. An ex vivo model to induce early fibrosis-like changes in human precision-cut lung slices. *Am J Physiol Lung Cell Mol Physiol* 2017: 312(6): L896-L902.

25. Lofdahl A, Wenglen C, Rydell-Tormanen K, Westergren-Thorsson G, Larsson-Callerfelt AK. Effects of 5-Hydroxytryptamine Class 2 Receptor Antagonists on Bronchoconstriction and Pulmonary Remodeling Processes. *Am J Pathol* 2018: 188(5): 1113-1119.

26. Rosmark O, Ahrman E, Muller C, Elowsson Rendin L, Eriksson L, Malmstrom A, Hallgren O, Larsson-Callerfelt AK, Westergren-Thorsson G, Malmstrom J. Quantifying extracellular matrix turnover in human lung scaffold cultures. *Sci Rep* 2018: 8(1): 5409.

27. Rosmark O, Ibanez-Fonseca A, Thorsson J, Dellgren G, Hallgren O, Larsson Callerfelt AK, Elowsson L, Westergren-Thorsson G. A tunable physiomimetic stretch system evaluated with precision cut lung slices and recellularized human lung scaffolds. *Front Bioeng Biotechnol* 2022: 10: 995460.

28. Mondonedo JR, Bartolak-Suki E, Bou Jawde S, Nelson K, Cao K, Sonnenberg A, Obrochta WP, Imsirovic J, Ram-Mohan S, Krishnan R, Suki B. A High-Throughput System for Cyclic Stretching of Precision-Cut Lung Slices During Acute Cigarette Smoke Extract Exposure. *Front Physiol* 2020: 11: 566.

29. Clevers H. Modeling Development and Disease with Organoids. *Cell* 2016: 165(7): 1586-1597.

30. Lancaster MA, Knoblich JA. Organogenesis in a dish: modeling development and disease using organoid technologies. *Science* 2014: 345(6194): 1247125.

31. Gunti S, Hoke ATK, Vu KP, London NR, Jr. Organoid and Spheroid Tumor Models: Techniques and Applications. *Cancers (Basel)* 2021: 13(4): 874.

32. Rock JR, Onaitis MW, Rawlins EL, Lu Y, Clark CP, Xue Y, Randell SH, Hogan BL. Basal cells as stem cells of the mouse trachea and human airway epithelium. *Proc Natl Acad Sci USA* 2009: 106(31): 12771-12775.

33. Barkauskas CE, Cronce MJ, Rackley CR, Bowie EJ, Keene DR, Stripp BR, Randell SH, Noble PW, Hogan BL. Type 2 alveolar cells are stem cells in adult lung. *J Clin Invest* 2013: 123(7): 3025-3036.

34. Li Y, Wu Q, Sun X, Shen J, Chen H. Organoids as a Powerful Model for Respiratory Diseases. *Stem Cells Int* 2020: 2020: 5847876.

35. Hynds RE, Butler CR, Janes SM, Giangreco A. Expansion of Human Airway Basal Stem Cells and Their Differentiation as 3D Tracheospheres. Methods Mol Biol. Springer New York, 2016; pp. 43-53.

36. Sprott RF, Ritzmann F, Langer F, Yao Y, Herr C, Kohl Y, Tschernig T, Bals R, Beisswenger C. Flagellin shifts 3D bronchospheres towards mucus hyperproduction. *Respir Res* 2020: 21(1): 222.

37. Loebel C, Weiner AI, Eiken MK, Katzen JB, Morley MP, Bala V, Cardenas-Diaz FL, Davidson MD, Shiraishi K, Basil MC, Ferguson LT, Spence JR, Ochs M, Beers MF, Morrisey EE, Vaughan AE, Burdick JA. Microstructured Hydrogels to Guide Self-Assembly and Function of Lung Alveolospheres. *Adv Mater* 2022: 34(28): e2202992.

38. Hu Y, Ng-Blichfeldt JP, Ota C, Ciminieri C, Ren W, Hiemstra PS, Stolk J, Gosens R, Konigshoff M. Wnt/beta-catenin signaling is critical for regenerative potential of distal lung epithelial progenitor cells in homeostasis and emphysema. *Stem Cells* 2020: 38(11): 1467-1478.

39. Ng-Blichfeldt JP, Schrik A, Kortekaas RK, Noordhoek JA, Heijink IH, Hiemstra PS, Stolk J, Konigshoff M, Gosens R. Retinoic acid signaling balances adult distal lung epithelial progenitor cell growth and differentiation. *EBioMedicine* 2018: 36: 461-474.

40. Wu X, van Dijk EM, Ng-Blichfeldt JP, Bos IST, Ciminieri C, Konigshoff M, Kistemaker LEM, Gosens R. Mesenchymal WNT-5A/5B Signaling Represses Lung Alveolar Epithelial Progenitors. *Cells* 2019: 8(10): 1147.

41. Kathiriya JJ, Wang C, Zhou M, Brumwell A, Cassandras M, Le Saux CJ, Cohen M, Alysandratos KD, Wang B, Wolters P, Matthay M, Kotton DN, Chapman HA, Peng T. Human alveolar type 2 epithelium transdifferentiates into metaplastic KRT5(+) basal cells. *Nat Cell Biol* 2022: 24(1): 10-23.

42. van Riet S, van Schadewijk A, Khedoe P, Limpens R, Barcena M, Stolk J, Hiemstra PS, van der Does AM. Organoid-based expansion of patient-derived primary alveolar type 2 cells for establishment of alveolus epithelial Lung-Chip cultures. *Am J Physiol Lung Cell Mol Physiol* 2022: 322(4): L526-L538.

43. Kim JH, An GH, Kim JY, Rasaei R, Kim WJ, Jin X, Woo DH, Han C, Yang SR, Kim JH, Hong SH. Human pluripotent stem-cell-derived alveolar organoids for modeling pulmonary fibrosis and drug testing. *Cell Death Discovery* 2021: 7(1): 48.

44. Fatehullah A, Tan SH, Barker N. Organoids as an in vitro model of human development and disease. *Nat Cell Biol* 2016: 18(3): 246-254.

45. Corro C, Novellasdemunt L, Li VSW. A brief history of organoids. *Am J Physiol Lung Cell Mol Physiol* 2020: 319(1): C151-C165.

46. Sachs N, Papaspyropoulos A, Zomer-van Ommen DD, Heo I, Bottinger L, Klay D, Weeber F, Huelsz-Prince G, Iakobachvili N, Amatngalim GD, de Ligt J, van Hoeck A, Proost N, Viveen MC, Lyubimova A, Teeven L, Derakhshan S, Korving J, Begthel H, Dekkers JF, Kumawat K, Ramos E, van Oosterhout MF, Offerhaus GJ, Wiener DJ, Olimpio EP, Dijkstra KK, Smit EF, van der Linden M, Jaksani S, van de Ven M, Jonkers J, Rios AC, Voest EE, van Moorsel CH, van der Ent CK, Cuppen E, van Oudenaarden A, Coenjaerts FE, Meyaard L, Bont LJ, Peters PJ, Tans SJ, van Zon JS, Boj SF, Vries RG, Beekman JM, Clevers H. Long-term expanding human airway organoids for disease modeling. *EMBO J* 2019: 38(4): e100300.

47. Zhou J, Li C, Sachs N, Chiu MC, Wong BH, Chu H, Poon VK, Wang D, Zhao X, Wen L, Song W, Yuan S, Wong KK, Chan JF, To KK, Chen H, Clevers H, Yuen KY. Differentiated human airway organoids to assess infectivity of emerging influenza virus. *Proc Natl Acad Sci USA* 2018: 115(26): 6822-6827.

48. Chen YW, Huang SX, de Carvalho A, Ho SH, Islam MN, Volpi S, Notarangelo LD, Ciancanelli M, Casanova JL, Bhattacharya J, Liang AF, Palermo LM, Porotto M, Moscona A, Snoeck HW. A three-dimensional model of human lung development and disease from pluripotent stem cells. *Nat Cell Biol* 2017: 19(5): 542-549.

49. Dye BR, Dedhia PH, Miller AJ, Nagy MS, White ES, Shea LD, Spence JR. A bioengineered niche promotes in vivo engraftment and maturation of pluripotent stem cell derived human lung organoids. *eLife* 2016: 5: e19732.

50. McCauley KB, Hawkins F, Serra M, Thomas DC, Jacob A, Kotton DN. Efficient Derivation of Functional Human Airway Epithelium from Pluripotent Stem Cells via Temporal Regulation of Wnt Signaling. *Cell Stem Cell* 2017: 20(6): 844-857 e846.

51. Dekkers JF, Berkers G, Kruisselbrink E, Vonk A, de Jonge HR, Janssens HM, Bronsveld I, van de Graaf EA, Nieuwenhuis EE, Houwen RH, Vleggaar FP, Escher JC, de Rijke YB, Majoor CJ, Heijerman HG, de Winter-de Groot KM, Clevers H, van der Ent CK, Beekman JM. Characterizing responses to CFTR-modulating drugs using rectal organoids derived from subjects with cystic fibrosis. *Sci Transl Med* 2016: 8(344): 344ra384.

52. Chai Q, Jiao Y, Yu X. Hydrogels for Biomedical Applications: Their Characteristics and the Mechanisms behind Them. *Gels* 2017: 3(1): 6.

53. Saldin LT, Cramer MC, Velankar SS, White LJ, Badylak SF. Extracellular matrix hydrogels from decellularized tissues: Structure and function. *Acta Biomater* 2017: 49: 1-15.

54. de Hilster RHJ, Sharma PK, Jonker MR, White ES, Gercama EA, Roobeek M, Timens W, Harmsen MC, Hylkema MN, Burgess JK. Human lung extracellular matrix hydrogels resemble the stiffness and viscoelasticity of native lung tissue. *Am J Physiol Lung Cell Mol Physiol* 2020: 318(4): L698-L704.

55. Pouliot RA, Link PA, Mikhaiel NS, Schneck MB, Valentine MS, Kamga Gninzeko FJ, Herbert JA, Sakagami M, Heise RL. Development and characterization of a naturally derived lung extracellular matrix hydrogel. *J Biomed Mater Res A* 2016: 104(8): 1922-1935.

56. Martinez-Garcia FD, de Hilster RHJ, Sharma PK, Borghuis T, Hylkema MN, Burgess JK, Harmsen MC. Architecture and Composition Dictate Viscoelastic Properties of Organ-Derived Extracellular Matrix Hydrogels. *Polymers* 2021: 13(18): 3113.

57. Heath DE. A Review of Decellularized Extracellular Matrix Biomaterials for Regenerative Engineering Applications. *Regen Eng Transl Med* 2019: 5(2): 155-166.

58. Song YH, Maynes MA, Hlavac N, Visosevic D, Daramola KO, Porvasnik SL, Schmidt CE. Development of novel apoptosis-assisted lung tissue decellularization methods. *Biomater Sci* 2021: 9(9): 3485-3498.

59. Pouliot RA, Young BM, Link PA, Park HE, Kahn AR, Shankar K, Schneck MB, Weiss DJ, Heise RL. Porcine Lung-Derived Extracellular Matrix Hydrogel Properties Are Dependent on Pepsin Digestion Time. *Tissue Eng Part C Methods* 2020: 26(6): 332-346.

60. Hussey GS, Nascari DG, Saldin LT, Kolich B, Lee YC, Crum RJ, El-Mossier SO, D'Angelo W, Dziki JL, Badylak SF. Ultrasonic cavitation to prepare ECM hydrogels. *Acta Biomater* 2020: 108(1878-7568 (Electronic)): 77-86.

61. Falcones B, Sanz-Fraile H, Marhuenda E, Mendizabal I, Cabrera-Aguilera I, Malandain N, Uriarte JJ, Almendros I, Navajas D, Weiss DJ, Farre R, Otero J. Bioprintable Lung Extracellular Matrix Hydrogel Scaffolds for 3D Culture of Mesenchymal Stromal Cells. *Polymers* 2021: 13(14): 2350.

62. Marhuenda E, Villarino A, Narciso ML, Camprubi-Rimblas M, Farre R, Gavara N, Artigas A, Almendros I, Otero J. Lung Extracellular Matrix Hydrogels Enhance Preservation of Type II Phenotype in Primary Alveolar Epithelial Cells. *Int J Mol Sci* 2022: 23(9): 4888.

63. Beachley V, Ma G, Papadimitriou C, Gibson M, Corvelli M, Elisseeff J. Extracellular matrix particle-glycosaminoglycan composite hydrogels for regenerative medicine applications. *J Biomed Mater Res A* 2018: 106(1): 147-159.

64. Ravindra A, D'Angelo W, Zhang L, Reing J, Johnson S, Myerburg M, Badylak SF. Human Bronchial Epithelial Cell Growth on Homologous Versus Heterologous Tissue Extracellular Matrix. *J Surg Res* 2021: 263: 215-223.

65. Saldin LT, Klimak M, Hill RC, Cramer MC, Huleihel L, Li X, Quidgley-Martin M, Cardenas D, Keane TJ, Londono R, Hussey G, Kelly L, Kosovec JE, Lloyd EJ, Omstead AN, Zhang L, Nieponice A, Jobe B, Hansen K, Zaidi AH, Badylak SF. The effect of normal, metaplastic, and neoplastic esophageal extracellular matrix upon macrophage activation. *J Immunol Regen Med* 2021: 13(2468-4988 (Electronic)).

66. Petrou CL, D'Ovidio TJ, Bolukbas DA, Tas S, Brown RD, Allawzi A, Lindstedt S, Nozik-Grayck E, Stenmark KR, Wagner DE, Magin CM. Clickable decellularized extracellular matrix as a new tool for building hybrid-hydrogels to model chronic fibrotic diseases in vitro. *J Mater Chem B* 2020: 8(31): 6814-6826.

67. Saleh KS, Hewawasam R, Serbedzija P, Blomberg R, Noreldeen SE, Edelman B, Smith BJ, Riches DWH, Magin CM. Engineering Hybrid-Hydrogels Comprised of Healthy or Diseased Decellularized Extracellular Matrix to Study Pulmonary Fibrosis. *Cell Mol Bioeng* 2022: 15(5): 505-519.

68. Nizamoglu M, de Hilster RHJ, Zhao F, Sharma PK, Borghuis T, Harmsen MC, Burgess JK. An in vitro model of fibrosis using crosslinked native extracellular matrix-derived hydrogels to modulate biomechanics without changing composition. *Acta Biomater* 2022: 147: 50-62.

69. Falcones B, Soderlund Z, Ibanez-Fonseca A, Almendros I, Otero J, Farre R, Rolandsson Enes S, Elowsson Rendin L, Westergren-Thorsson G. hLMSC Secretome Affects Macrophage Activity Differentially Depending on Lung-Mimetic Environments. *Cells* 2022: 11(12): 1866.

70. Huh D, Matthews BD, Mammoto A, Montoya-Zavala M, Hsin HY, Ingber DE. Reconstituting organ-level lung functions on a chip. *Science* 2010: 328(5986): 1662-1668.

71. Si L, Bai H, Rodas M, Cao W, Oh CY, Jiang A, Moller R, Hoagland D, Oishi K, Horiuchi S, Uhl S, Blanco-Melo D, Albrecht RA, Liu WC, Jordan T, Nilsson-Payant BE, Golynker I, Frere J, Logue J, Haupt R, McGrath M, Weston S, Zhang T, Plebani R, Soong M, Nurani A, Kim SM, Zhu DY, Benam KH, Goyal G, Gilpin SE, Prantil-Baun R, Gygi SP, Powers RK, Carlson KE, Frieman M, tenOever BR, Ingber DE. A human-airway-on-a-chip for the rapid identification of candidate antiviral therapeutics and prophylactics. *Nat Biomed Eng* 2021: 5(8): 815-829.

72. Thacker VV, Sharma K, Dhar N, Mancini GF, Sordet-Dessimoz J, McKinney JD. Rapid endotheliitis and vascular damage characterize SARS-CoV-2 infection in a human lung-on-chip model. *EMBO Rep* 2021: 22(6): e52744.

73. Benam KH, Novak R, Nawroth J, Hirano-Kobayashi M, Ferrante TC, Choe Y, Prantil-Baun R, Weaver JC, Bahinski A, Parker KK, Ingber DE. Matched-Comparative Modeling of Normal and Diseased Human Airway Responses Using a Microengineered Breathing Lung Chip. *Cell Syst* 2016: 3(5): 456-466 e454.

74. Hajipouran Benam K, Novak R, Villenave R, Lucchesi C, Hubeau C, Nawroth J, Hirano-Kobayashi M, Ferrante TC, Choe Y, Prantil-Baun R, Weaver JC, Hamilton GA, Bahinski A, Ingber DE. Human small airway-on-a-chip: A novel microphysiological system to model lung inflammation, accelerate drug development and enable inhalational toxico-analysis. 51 Airway Pharmacology and Treatment. European Respiratory Society, 2016.

75. Varone A, Nguyen JK, Leng L, Barrile R, Sliz J, Lucchesi C, Wen N, Gravanis A, Hamilton GA, Karalis K, Hinojosa CD. A novel organ-chip system emulates three-dimensional architecture of the human epithelia and the mechanical forces acting on it. *Biomaterials* 2021: 275: 120957.

76. Stucki AO, Stucki JD, Hall SR, Felder M, Mermoud Y, Schmid RA, Geiser T, Guenat OT. A lung-on-a-chip array with an integrated bio-inspired respiration mechanism. *Lab Chip* 2015: 15(5): 1302-1310.

77. Stucki JD, Hobi N, Galimov A, Stucki AO, Schneider-Daum N, Lehr CM, Huwer H, Frick M, Funke-Chambour M, Geiser T, Guenat OT. Medium throughput breathing human primary cell alveolus-on-chip model. *Sci Rep* 2018: 8(1): 14359.

78. Sengupta A, Roldan N, Kiener M, Froment L, Raggi G, Imler T, de Maddalena L, Rapet A, May T, Carius P, Schneider-Daum N, Lehr CM, Kruithof-de Julio M, Geiser T, Marti TM, Stucki JD, Hobi N, Guenat OT. A New Immortalized Human Alveolar Epithelial Cell Model to Study Lung Injury and Toxicity on a Breathing Lung-On-Chip System. *Front Toxicol* 2022: 4: 840606.

79. Zamprogno P, Wuthrich S, Achenbach S, Thoma G, Stucki JD, Hobi N, Schneider-Daum N, Lehr CM, Huwer H, Geiser T, Schmid RA, Guenat OT. Second-generation lung-on-a-chip with an array of stretchable alveoli made with a biological membrane. *Commun Biol* 2021: 4(1): 168.

80. Zeinali S, Bichsel CA, Hobi N, Funke M, Marti TM, Schmid RA, Guenat OT, Geiser T. Human microvasculature-on-a chip: anti-neovasculogenic effect of nintedanib in vitro. *Angiogenesis* 2018: 21(4): 861-871.

81. Zeinali S, Thompson EK, Gerhardt H, Geiser T, Guenat OT. Remodeling of an in vitro microvessel exposed to cyclic mechanical stretch. *APL Bioeng* 2021: 5(2): 026102.

82. Campillo N, Jorba I, Schaedel L, Casals B, Gozal D, Farre R, Almendros I, Navajas D. A Novel Chip for Cyclic Stretch and Intermittent Hypoxia Cell Exposures Mimicking Obstructive Sleep Apnea. *Front Physiol* 2016: 7: 319.

83. Tas S, Rehnberg E, Bölükbas DA, Beech JP, Kazado LN, Svenningsson I, Arvidsson M, Sandberg A, Dahlgren KA, Edthofer A, Gustafsson A, Isaksson H, Wood JA, Tegenfeldt JO, Wagner DE. 3D printed lung on a chip device with a stretchable nanofibrous membrane for modeling ventilator induced lung injury. Cold Spring Harbor Laboratory, 2021.

84. Jung O, Tung YT, Sim E, Chen YC, Lee E, Ferrer M, Song MJ. Development of human-derived, three-dimensional respiratory epithelial tissue constructs with perfusable microvasculature on a high-throughput microfluidics screening platform. *Biofabrication* 2022: 14(2): 025012.

85. De Santis MM, Alsafadi HN, Tas S, Bölükbas DA, Prithiviraj S, Da Silva IAN, Mittendorfer M, Ota C, Stegmayr J, Daoud F, Königshoff M, Swärd K, Wood JA, Tassieri M, Bourgine PE, Lindstedt S, Mohlin S, Wagner DE. Extracellular-Matrix-Reinforced Bioinks for 3D Bioprinting Human Tissue. *Adv Mater* 2020: 33(3): 2005476.

86. Dabaghi M, Carpio MB, Moran-Mirabal JM, Hirota JA. 3D (bio)printing of lungs: past, present, and future. *Eur Respir J* 2023: 61(1): 2200417.

87. Campillo N, Falcones B, Otero J, Colina R, Gozal D, Navajas D, Farre R, Almendros I. Differential Oxygenation in Tumor Microenvironment Modulates Macrophage and Cancer Cell Crosstalk: Novel Experimental Setting and Proof of Concept. *Front Oncol* 2019: 9: 43.

88. Banerjee A, Trivedi CM, Damera G, Jiang M, Jester W, Hoshi T, Epstein JA, Panettieri RA, Jr. Trichostatin A abrogates airway constriction, but not inflammation, in murine and human asthma models. *Am J Respir Cell Mol Biol* 2012: 46(2): 132-138.

89. Lauenstein L, Switalla S, Prenzler F, Seehase S, Pfennig O, Forster C, Fieguth H, Braun A, Sewald K. Assessment of immunotoxicity induced by chemicals in human precision-cut lung slices (PCLS). *Toxicol In Vitro* 2014: 28(4): 588-599.

90. Neuhaus V, Schaudien D, Golovina T, Temann UA, Thompson C, Lippmann T, Bersch C, Pfennig O, Jonigk D, Braubach P, Fieguth HG, Warnecke G, Yusibov V, Sewald K, Braun A. Assessment of long-term cultivated human precision-cut lung slices as an ex vivo system for evaluation of chronic cytotoxicity and functionality. *J Occup Med Toxicol* 2017: 12: 13.

91. Temann A, Golovina T, Neuhaus V, Thompson C, Chichester JA, Braun A, Yusibov V. Evaluation of inflammatory and immune responses in long-term cultured human precision-cut lung slices. *Hum Vaccin Immunother* 2017: 13(2): 351-358.

92. Sturton RG, Trifilieff A, Nicholson AG, Barnes PJ. Pharmacological characterization of indacaterol, a novel once daily inhaled 2 adrenoceptor agonist, on small airways in human and rat precision-cut lung slices. *J Pharmacol Exp Ther* 2008: 324(1): 270-275.

93. Butler CR, Hynds RE, Gowers KH, Lee Ddo H, Brown JM, Crowley C, Teixeira VH, Smith CM, Urbani L, Hamilton NJ, Thakrar RM, Booth HL, Birchall MA, De Coppi P, Giangreco A, O'Callaghan C, Janes SM. Rapid Expansion of Human Epithelial Stem Cells Suitable for Airway Tissue Engineering. *Am J Respir Crit Care Med* 2016: 194(2): 156-168.

94. Hild M, Jaffe AB. Production of 3-D Airway Organoids From Primary Human Airway Basal Cells and Their Use in High-Throughput Screening. *Curr Protoc Stem Cell Biol* 2016: 37(1): IE 9 1-IE 9 15.

95. Konishi S, Gotoh S, Tateishi K, Yamamoto Y, Korogi Y, Nagasaki T, Matsumoto H, Muro S, Hirai T, Ito I, Tsukita S, Mishima M. Directed Induction of Functional Multi-ciliated Cells in Proximal Airway Epithelial Spheroids from Human Pluripotent Stem Cells. *Stem Cell Rep* 2016: 6(1): 18-25.

96. Tan Q, Choi KM, Sicard D, Tschumperlin DJ. Human airway organoid engineering as a step toward lung regeneration and disease modeling. *Biomaterials* 2017: 113: 118-132.

97. Jacob A, Morley M, Hawkins F, McCauley KB, Jean JC, Heins H, Na CL, Weaver TE, Vedaie M, Hurley K, Hinds A, Russo SJ, Kook S, Zacharias W, Ochs M, Traber K, Quinton LJ, Crane A, Davis BR, White FV, Wambach J, Whitsett JA, Cole FS, Morrisey EE, Guttentag SH, Beers MF, Kotton DN. Differentiation of Human Pluripotent Stem Cells into Functional Lung Alveolar Epithelial Cells. *Cell Stem Cell* 2017: 21(4): 472-488 e410.

98. Zacharias WJ, Frank DB, Zepp JA, Morley MP, Alkhaleel FA, Kong J, Zhou S, Cantu E, Morrisey EE. Regeneration of the lung alveolus by an evolutionarily conserved epithelial progenitor. *Nature* 2018: 555(7695): 251-255.

99. Miller AJ, Dye BR, Ferrer-Torres D, Hill DR, Overeem AW, Shea LD, Spence JR. Generation of lung organoids from human pluripotent stem cells in vitro. *Nat Protoc* 2019: 14(2): 518-540.

100. Nikolic MZ, Caritg O, Jeng Q, Johnson JA, Sun D, Howell KJ, Brady JL, Laresgoiti U, Allen G, Butler R, Zilbauer M, Giangreco A, Rawlins EL. Human embryonic lung epithelial tips are multipotent progenitors that can be expanded in vitro as long-term self-renewing organoids. *eLife* 2017: 6: e26575.

101. Bol L, Galas JC, Hillaireau H, Le Potier I, Nicolas V, Haghiri-Gosnet AM, Fattal E, Taverna M. A microdevice for parallelized pulmonary permeability studies. *Biomed Microdevices* 2014: 16(2): 277-285.

102. Benam KH, Villenave R, Lucchesi C, Varone A, Hubeau C, Lee HH, Alves SE, Salmon M, Ferrante TC, Weaver JC, Bahinski A, Hamilton GA, Ingber DE. Small airway-on-a-chip enables analysis of human lung inflammation and drug responses in vitro. *Nat Methods* 2016: 13(2): 151-157.

103. Mejias JC, Nelson MR, Liseth O, Roy K. A 96-well format microvascularized human lung-on-a-chip platform for microphysiological modeling of fibrotic diseases. *Lab Chip* 2020: 20(19): 3601-3611.

104. Humayun M, Chow CW, Young EWK. Microfluidic lung airway-on-a-chip with arrayable suspended gels for studying epithelial and smooth muscle cell interactions. *Lab Chip* 2018: 18(9): 1298-1309.

105. Barkal LJ, Procknow CL, Alvarez-Garcia YR, Niu M, Jimenez-Torres JA, Brockman-Schneider RA, Gern JE, Denlinger LC, Theberge AB, Keller NP, Berthier E, Beebe DJ. Microbial volatile communication in human organotypic lung models. *Nat Commun* 2017: 8(1): 1770.

106. Punde TH, Wu WH, Lien PC, Chang YL, Kuo PH, Chang MD, Lee KY, Huang CD, Kuo HP, Chan YF, Shih PC, Liu CH. A biologically inspired lung-on-a-chip device for the study of protein-induced lung inflammation. *Integr Biol (Camb)* 2015: 7(2): 162-169.

107. Artzy-Schnirman A, Zidan H, Elias-Kirma S, Ben-Porat L, Tenenbaum-Katan J, Carius P, Fishler R, Schneider-Daum N, Lehr CM, Sznitman J. Capturing the Onset of Bacterial Pulmonary Infection in Acini-On-Chips. *Adv Biosyst* 2019: 3(9): e1900026.

108. Huang D, Liu T, Liao J, Maharjan S, Xie X, Perez M, Anaya I, Wang S, Tirado Mayer A, Kang Z, Kong W, Mainardi VL, Garciamendez-Mijares CE, Garcia Martinez G, Moretti M, Zhang W, Gu Z, Ghaemmaghami AM, Zhang YS. Reversed-engineered human alveolar lung-on-a-chip model. *Proc Natl Acad Sci USA* 2021: 118(19): e2016146118.

109. Ghosh A, Koziol-White CJ, Asosingh K, Cheng G, Ruple L, Groneberg D, Friebe A, Comhair SA, Stasch JP, Panettieri RA, Jr., Aronica MA, Erzurum SC, Stuehr DJ. Soluble guanylate cyclase as an alternative target for bronchodilator therapy in asthma. *Proc Natl Acad Sci USA* 2016: 113(17): E2355-2362.

110. Ressmeyer AR, Larsson AK, Vollmer E, Dahlen SE, Uhlig S, Martin C. Characterisation of guinea pig precision-cut lung slices: comparison with human tissues. *Eur Respir J* 2006: 28(3): 603-611.

111. Cooper PR, Panettieri RA, Jr. Steroids completely reverse albuterol-induced beta(2)-adrenergic receptor tolerance in human small airways. *J Allergy Clin Immunol* 2008: 122(4): 734-740.

112. Kennedy JL, Koziol-White CJ, Jeffus S, Rettiganti MR, Fisher P, Kurten M, Eze A, House S, Sikes JD, Askew E, Putt C, Panettieri RA, Jones SM, Kurten RC. Effects of rhinovirus 39 infection on airway hyperresponsiveness to carbachol in human airways precision cut lung slices. *J Allergy Clin Immunol* 2018: 141(5): 1887-1890 e1881.

113. Danahay H, Pessotti AD, Coote J, Montgomery BE, Xia D, Wilson A, Yang H, Wang Z, Bevan L, Thomas C, Petit S, London A, LeMotte P, Doelemeyer A, Velez-Reyes GL, Bernasconi P, Fryer CJ, Edwards M, Capodieci P, Chen A, Hild M, Jaffe AB. Notch2 is required for inflammatory cytokine-driven goblet cell metaplasia in the lung. *Cell Rep* 2015: 10(2): 239-252.

114. Nawroth JC, Lucchesi C, Cheng D, Shukla A, Ngyuen J, Shroff T, Varone A, Karalis K, Lee H-H, Alves S, Hamilton GA, Salmon M, Villenave R. A Microengineered Airway Lung Chip Models Key Features of Viral-induced Exacerbation of Asthma. *Am J Respir Cell Mol* 2020: 63(5): 591-600.

115. Skronska-Wasek W, Mutze K, Baarsma HA, Bracke KR, Alsafadi HN, Lehmann M, Costa R, Stornaiuolo M, Novellino E, Brusselle GG, Wagner DE, Yildirim AO, Konigshoff M. Reduced Frizzled Receptor 4 Expression Prevents WNT/beta-Catenin-driven Alveolar Lung Repair in Chronic Obstructive Pulmonary Disease. *Am J Respir Crit Care Med* 2017: 196(2): 172-185.

116. Kruk D, Wisman M, Noordhoek JA, Nizamoglu M, Jonker MR, de Bruin HG, Arevalo Gomez K, Ten Hacken NHT, Pouwels SD, Heijink IH. Paracrine Regulation of Alveolar Epithelial Damage and Repair Responses by Human Lung-Resident Mesenchymal Stromal Cells. *Cells* 2021: 10(11): 2860.

117. Benam KH, Novak R, Ferrante TC, Choe Y, Ingber DE. Biomimetic smoking robot for in vitro inhalation exposure compatible with microfluidic organ chips. *Nat Protoc* 2020: 15(2): 183-206.

118. Hirai H, Liang X, Sun Y, Zhang Y, Zhang J, Chen YE, Mou H, Zhao Y, Xu J. The sodium/glucose cotransporters as potential therapeutic targets for CF lung diseases revealed by human lung organoid swelling assay. *Mol Ther Methods Clin Dev* 2022: 24: 11-19.

119. Hannan NR, Sampaziotis F, Segeritz CP, Hanley NA, Vallier L. Generation of Distal Airway Epithelium from Multipotent Human Foregut Stem Cells. *Stem Cells Dev* 2015: 24(14): 1680-1690.

120. Calucho M, Gartner S, Barranco P, Fernandez-Alvarez P, Perez RG, Tizzano EF. Validation of nasospheroids to assay CFTR functionality and modulator responses in cystic fibrosis. *Sci Rep* 2021: 11(1): 15511.

121. Sette G, Lo Cicero S, Blacona G, Pierandrei S, Bruno SM, Salvati V, Castelli G, Falchi M, Fabrizzi B, Cimino G, De Maria R, Biffoni M, Eramo A, Lucarelli M. Theratyping cystic fibrosis in vitro in ALI culture and organoid models generated from patient-derived nasal epithelial conditionally reprogrammed stem cells. *Eur Respir J* 2021: 58(6): 2100908.

122. Strikoudis A, Cieślak A, Loffredo L, Chen Y-W, Patel N, Saqi A, Lederer DJ, Snoeck H-W. Modeling of Fibrotic Lung Disease Using 3D Organoids Derived from Human Pluripotent Stem Cells. *Cell Rep* 2019: 27(12): 3709-3723.e3705.

123. Felder M, Trueeb B, Stucki AO, Borcard S, Stucki JD, Schnyder B, Geiser T, Guenat OT. Impaired Wound Healing of Alveolar Lung Epithelial Cells in a Breathing Lung-On-A-Chip. *Front Bioeng Biotechnol* 2019: 7: 3.

124. van Rijt SH, Bolukbas DA, Argyo C, Datz S, Lindner M, Eickelberg O, Konigshoff M, Bein T, Meiners S. Protease-mediated release of chemotherapeutics from mesoporous silica nanoparticles to ex vivo human and mouse lung tumors. *ACS Nano* 2015: 9(3): 2377-2389.

125. Dong M, Philippi C, Loretz B, Nafee N, Schaefer UF, Friedel G, Ammon-Treiber S, Griese EU, Lehr CM, Klotz U, Murdter TE. Tissue slice model of human lung cancer to investigate telomerase inhibition by nanoparticle delivery of antisense 2'-O-methyl-RNA. *Int J Pharm* 2011: 419(1-2): 33-42.

126. Salmon H, Franciszkiewicz K, Damotte D, Dieu-Nosjean MC, Validire P, Trautmann A, Mami-Chouaib F, Donnadieu E. Matrix architecture defines the preferential localization and migration of T cells into the stroma of human lung tumors. *J Clin Invest* 2012: 122(3): 899-910.

127. Shi R, Radulovich N, Ng C, Liu N, Notsuda H, Cabanero M, Martins-Filho SN, Raghavan V, Li Q, Mer AS, Rosen JC, Li M, Wang YH, Tamblyn L, Pham NA, Haibe-Kains B, Liu G, Moghal N, Tsao MS. Organoid Cultures as Preclinical Models of Non-Small Cell Lung Cancer. *Clin Cancer Res* 2020: 26(5): 1162-1174.

128. Li Z, Qian Y, Li W, Liu L, Yu L, Liu X, Wu G, Wang Y, Luo W, Fang F, Liu Y, Song F, Cai Z, Chen W, Huang W. Human Lung Adenocarcinoma-Derived Organoid Models for Drug Screening. *iScience* 2020: 23(8): 101411.

129. Kim M, Mun H, Sung CO, Cho EJ, Jeon HJ, Chun SM, Jung DJ, Shin TH, Jeong GS, Kim DK, Choi EK, Jeong SY, Taylor AM, Jain S, Meyerson M, Jang SJ. Patient-derived lung cancer organoids as in vitro cancer models for therapeutic screening. *Nat Commun* 2019: 10(1): 3991.

130. Neal JT, Li X, Zhu J, Giangarra V, Grzeskowiak CL, Ju J, Liu IH, Chiou SH, Salahudeen AA, Smith AR, Deutsch BC, Liao L, Zemek AJ, Zhao F, Karlsson K, Schultz LM, Metzner TJ, Nadauld LD, Tseng YY, Alkhairy S, Oh C, Keskula P, Mendoza-Villanueva D, De La Vega FM, Kunz PL, Liao JC, Leppert JT, Sunwoo JB, Sabatti C, Boehm JS, Hahn WC, Zheng GXY, Davis MM, Kuo CJ. Organoid Modeling of the Tumor Immune Microenvironment. *Cell* 2018: 175(7): 1972-1988 e1916.

131. Ruppen J, Wildhaber FD, Strub C, Hall SR, Schmid RA, Geiser T, Guenat OT. Towards personalized medicine: chemosensitivity assays of patient lung cancer cell spheroids in a perfused microfluidic platform. *Lab Chip* 2015: 15(14): 3076-3085.

132. Yang X, Li K, Zhang X, Liu C, Guo B, Wen W, Gao X. Nanofiber membrane supported lung-on-a-chip microdevice for anti-cancer drug testing. *Lab Chip* 2018: 18(3): 486-495.

133. Kerns SJ, Belgur C, Petropolis D, Kanellias M, Barrile R, Sam J, Weinzierl T, Fauti T, Freimoser-Grundschober A, Eckmann J, Hage C, Geiger M, Ng PR, Tien-Street W, Manatakis DV, Micallef V, Gerard R, Bscheider M, Breous-Nystrom E, Schneider A, Giusti AM, Bertinetti-Lapatki C, Grant HS, Roth AB, Hamilton GA, Singer T, Karalis K, Moisan A, Bruenker P, Klein C, Bacac M, Gjorevski N, Cabon L. Human immunocompetent Organ-on-Chip platforms allow safety profiling of tumor-targeted T-cell bispecific antibodies. *eLife* 2021: 10: e67106.

134. Redrup MJ, Igarashi H, Schaefgen J, Lin J, Geisler L, Ben M'Barek M, Ramachandran S, Cardoso T, Hillewaert V. Sample Management: Recommendation for Best Practices and Harmonization from the Global Bioanalysis Consortium Harmonization Team. *AAPS J* 2016: 18(2): 290-293.

135. Sabroe I, Dockrell DH, Vogel SN, Renshaw SA, Whyte MK, Dower SK. Identifying and hurdling obstacles to translational research. *Nat Rev Immunol* 2007: 7(1): 77-82.

136. Curtis MJ, Alexander S, Cirino G, Docherty JR, George CH, Giembycz MA, Hoyer D, Insel PA, Izzo AA, Ji Y, MacEwan DJ, Sobey CG, Stanford SC, Teixeira MM, Wonnacott S, Ahluwalia A. Experimental design and analysis and their reporting II: updated and simplified guidance for authors and peer reviewers. *Br J Pharmacol* 2018: 175(7): 987-993.

137. Brazma A, Hingamp P, Quackenbush J, Sherlock G, Spellman P, Stoeckert C, Aach J, Ansorge W, Ball CA, Causton HC, Gaasterland T, Glenisson P, Holstege FC, Kim IF, Markowitz V, Matese JC, Parkinson H, Robinson A, Sarkans U, Schulze-Kremer S, Stewart J, Taylor R, Vilo J, Vingron M. Minimum information about a microarray experiment (MIAME)-toward standards for microarray data. *Nat Genet* 2001: 29(4): 365-371.

138. Percie du Sert N, Hurst V, Ahluwalia A, Alam S, Avey MT, Baker M, Browne WJ, Clark A, Cuthill IC, Dirnagl U, Emerson M, Garner P, Holgate ST, Howells DW, Karp NA, Lazic SE, Lidster K, MacCallum CJ, Macleod M, Pearl EJ, Petersen OH, Rawle F, Reynolds P, Rooney K, Sena ES, Silberberg SD, Steckler T, Wurbel H. The ARRIVE guidelines 2.0: Updated guidelines for reporting animal research. *BMC Vet Res* 2020: 16(1): 242.

139. "117th Congress (2021-2022)". S.5002 - FDA Modernization Act 2.0. *In:* 117th Congress (2021-2022), ed., 2022.

140. McGrath JC, Curtis MJ. BJP is changing its requirements for scientific papers to increase transparency. *Br J Pharmacol* 2015: 172(11): 2671-2674.

141. Reproducibility: let's get it right from the start. *Nat Commun* 2018: 9(1): 3716.

142. Liu AP, Chaudhuri O, Parekh SH. New advances in probing cell-extracellular matrix interactions. *Integrative Biology* 2017: 9(5): 383-405.

143. Stelzer EHK, Strobl F, Chang B-J, Preusser F, Preibisch S, McDole K, Fiolka R. Light sheet fluorescence microscopy. *Nat Rev Methods Primers* 2021: 1(1).

144. Dekkers JF, Alieva M, Wellens LM, Ariese HCR, Jamieson PR, Vonk AM, Amatngalim GD, Hu H, Oost KC, Snippert HJG, Beekman JM, Wehrens EJ, Visvader JE, Clevers H, Rios AC. High-resolution 3D imaging of fixed and cleared organoids. *Nat Protoc* 2019: 14(6): 1756-1771.

145. Salwig I, Spitznagel B, Wiesnet M, Braun T. Imaging lung regeneration by light sheet microscopy. *Histochem Cell Biol* 2021: 155(2): 271-277.

146. Khan MM, Poeckel D, Halavatyi A, Zukowska-Kasprzyk J, Stein F, Vappiani J, Sevin DC, Tischer C, Zinn N, Eley JD, Gudmann NS, Muley T, Winter H, Fisher AJ, Nanthakumar CB, Bergamini G, Pepperkok R. An integrated multiomic and quantitative label-free microscopy-based approach to study pro-fibrotic signalling in ex vivo human precision-cut lung slices. *Eur Respir J* 2021: 58(1): 2000221.

147. Vazquez-Armendariz AI, Heiner M, El Agha E, Salwig I, Hoek A, Hessler MC, Shalashova I, Shrestha A, Carraro G, Mengel JP, Gunther A, Morty RE, Vadasz I, Schwemmle M, Kummer W, Hain T, Goesmann A, Bellusci S, Seeger W, Braun T, Herold S. Multilineage murine stem cells generate complex organoids to model distal lung development and disease. *EMBO J* 2020: 39(21): e103476.

148. Chen X, Nadiarynkh O, Plotnikov S, Campagnola PJ. Second harmonic generation microscopy for quantitative analysis of collagen fibrillar structure. *Nat Protoc* 2012: 7(4): 654-669.

149. Abraham T, Hirota J, Elliot M, Kinght D, Hogg J. How Multiphoton and Harmonic Generation Microscopy Methods are Useful in Understanding Lung Structure and Related Diseases. *Microsc Microanal* 2017: 17(S2): 278-279.

150. Rozanova S, Barkovits K, Nikolov M, Schmidt C, Urlaub H, Marcus K. Quantitative Mass Spectrometry-Based Proteomics: An Overview. *In:* Marcus K, Eisenacher M, Sitek B, eds. Quantitative Methods in Proteomics. Springer US, New York, NY, 2021; pp. 85-116.

151. Marzi J, Brauchle EM, Schenke-Layland K, Rolle MW. Non-invasive functional molecular phenotyping of human smooth muscle cells utilized in cardiovascular tissue engineering. *Acta Biomater* 2019: 89: 193-205.

152. Elowsson Rendin L, Lofdahl A, Ahrman E, Muller C, Notermans T, Michalikova B, Rosmark O, Zhou XH, Dellgren G, Silverborn M, Bjermer L, Malmstrom A, Larsson-Callerfelt AK, Isaksson H, Malmstrom J, Westergren-Thorsson G. Matrisome Properties of Scaffolds Direct Fibroblasts in Idiopathic Pulmonary Fibrosis. *Int J Mol Sci* 2019: 20(16).

153. Hoffman ET, Uhl FE, Asarian L, Deng B, Becker C, Uriarte JJ, Downs I, Young B, Weiss DJ. Regional and disease specific human lung extracellular matrix composition. *Biomaterials* 2023: 293: 121960.

154. Bergholt MS, Serio A, Albro MB. Raman Spectroscopy: Guiding Light for the Extracellular Matrix. *Front Bioeng Biotechnol* 2019: 7: 303.

155. Stegmayr J, Alsafadi HN, Langwinski W, Niroomand A, Lindstedt S, Leigh ND, Wagner DE. Isolation of high-yield and -quality RNA from human precision-cut lung slices for RNA-sequencing and computational integration with larger patient cohorts. *Am J Physiol Lung Cell Mol Physiol* 2021: 320(2): L232-L240.

156. Bai Y, Krishnamoorthy N, Patel KR, Rosas I, Sanderson MJ, Ai X. Cryopreserved Human Precision-Cut Lung Slices as a Bioassay for Live Tissue Banking. A Viability Study of Bronchodilation with Bitter-Taste Receptor Agonists. *Am J Respir Cell Mol Biol* 2016: 54(5): 656-663.

157. Alysandratos KD, Garcia-de-Alba C, Yao C, Pessina P, Huang J, Villacorta-Martin C, Hix OT, Minakin K, Burgess CL, Bawa P, Murthy A, Konda B, Beers MF, Stripp BR, Kim CF, Kotton DN. Culture impact on the transcriptomic programs of primary and iPSC-derived human alveolar type 2 cells. *JCI Insight* 2023: 8(1).

158. Leibel SL, Tseu I, Zhou A, Hodges A, Yin J, Bilodeau C, Goltsis O, Post M. Metabolomic profiling of human pluripotent stem cell differentiation into lung progenitors. *iScience* 2022: 25(2): 103797.

159. Uriarte JJ, Meirelles T, Gorbenko Del Blanco D, Nonaka PN, Campillo N, Sarri E, Navajas D, Egea G, Farre R. Early Impairment of Lung Mechanics in a Murine Model of Marfan Syndrome. *PLoS One* 2016: 11(3): e0152124.

160. Migulina N, Tjin G, Faiz A, Borghuis T, Zhao F, Kaper HJ, Metzlar M, van Dijk E, Sharma PK, Timens W, Gosens R, Brandsma CA, Burgess JK. Differential roles for lysyl oxidase (like), family members in chronic obstructive pulmonary disease; from gene and protein expression to function. *FASEB J* 2022: 36(7): e22374.

161. Bevilacqua C, Hambura S, Wang L, Chan CJ, Eguren M, Gomez Elliff JM, Diz-Muñoz A, Prevedel R. High-resolution line-scanning Brillouin microscopy for fast and low phototoxicity live-imaging of mechanical properties in biology. SPIE, 2021.

162. Rad MA, Mahmodi H, Filipe EC, Cox TR, Kabakova I, Tipper JL. Micromechanical characterisation of 3D bioprinted neural cell models using Brillouin microspectroscopy. *Bioprinting* 2022: 25: e00179.

163. Barrasa-Fano J, Shapeti A, Jorge-Penas A, Barzegari M, Sanz-Herrera JA, Van Oosterwyck H. TFMLAB: A MATLAB toolbox for 4D traction force microscopy. *Softwarex* 2021: 15: 100723.

164. Alcaraz J, Otero J, Jorba I, Navajas D. Bidirectional mechanobiology between cells and their local extracellular matrix probed by atomic force microscopy. *Semin Cell Dev Biol* 2018: 73: 71-81.

165. Pugin J. Molecular mechanisms of lung cell activation induced by cyclic stretch. *Crit Care* 2003: 31(4 Suppl): S200-206.

166. Burgstaller G, Oehrle B, Gerckens M, White ES, Schiller HB, Eickelberg O. The instructive extracellular matrix of the lung: basic composition and alterations in chronic lung disease. *Eur Respir J* 2017: 50(1).

167. Nizamoglu M, Burgess JK. The Multi-Faceted Extracellular Matrix: Unlocking Its Secrets for Understanding the Perpetuation of Lung Fibrosis. *Curr Tissue Microenviron Rep* 2022: 2(4): 53–71.

168. Junior C, Narciso M, Marhuenda E, Almendros I, Farre R, Navajas D, Otero J, Gavara N. Baseline Stiffness Modulates the Non-Linear Response to Stretch of the Extracellular Matrix in Pulmonary Fibrosis. *Int J Mol Sci* 2021: 22(23): 12928.

169. Reimelt AM, Vasilescu DM, Beare R, Knudsen L, Grothausmann R. 3D image analysis of the alveolar shape in human lungs. *Eur Respir J* 2021: 58(suppl 65): PA1876.

170. Barnes PJ, Bonini S, Seeger W, Belvisi MG, Ward B, Holmes A. Barriers to new drug development in respiratory disease. *Eur Respir J* 2015: 45(5): 1197–1207.

171. Yamaguchi S, Kaneko M, Narukawa M. Approval success rates of drug candidates based on target, action, modality, application, and their combinations. *Clin Transl Sci* 2021: 14(3): 1113–1122.

172. Cook D, Brown D, Alexander R, March R, Morgan P, Satterthwaite G, Pangalos MN. Lessons learned from the fate of AstraZeneca's drug pipeline: a five-dimensional framework. *Nature Rev Drug Discov* 2014: 13(6): 419–431.

173. Sgalla G, Lerede M, Richeldi L. Emerging drugs for the treatment of idiopathic pulmonary fibrosis: 2020 phase II clinical trials. *Expert Opin Emerg Drugs* 2021: 26(2): 93–101.

174. Wilson JW, Li X, Pain MC. The lack of distensibility of asthmatic airways. *Am Rev Respir Dis* 1993: 148(3): 806–809.

175. Ward JE, Harris T, Bamford T, Mast A, Pain MCF, Robertson C, Smallwood D, Tran T, Wilson J, Stewart AG. Proliferation is not increased in airway myofibroblasts isolated from asthmatics. *Eur Respir J* 2008: 32(2): 362–371.

176. Chapman DG, King GG, Berend N, Diba C, Salome CM. Avoiding deep inspirations increases the maximal response to methacholine without altering sensitivity in non-asthmatics. *Respir Physiol Neurobiol* 2010: 173(2): 157–163.

177. Tschumperlin DJ, Dai G, Maly IV, Kikuchi T, Laiho LH, McVittie AK, Haley KJ, Lilly CM, So PT, Lauffenburger DA, Kamm RD, Drazen JM. Mechanotransduction through growth-factor shedding into the extracellular space. *Nature* 2004: 429(6987): 83–86.

178. Park JA, Tschumperlin DJ. Chronic intermittent mechanical stress increases MUC5AC protein expression. *Am J Respir Cell Mol Biol* 2009: 41(4): 459–466.

179. Stewart AG, Thomas B, Koff J. TGF-beta: Master regulator of inflammation and fibrosis. *Respirology* 2018: 23(12): 1096–1097.

180. Liu G, Cooley MA, Jarnicki AG, Borghuis T, Nair PM, Tjin G, Hsu AC, Haw TJ, Fricker M, Harrison CL, Jones B, Hansbro NG, Wark PA, Horvat JC, Argraves WS, Oliver BG, Knight DA, Burgess JK, Hansbro PM. Fibulin-1c regulates transforming growth factor-beta activation in pulmonary tissue fibrosis. *JCI Insight* 2019: 5(16).

181. Jones MG, Andriotis OG, Roberts JJ, Lunn K, Tear VJ, Cao L, Ask K, Smart DE, Bonfanti A, Johnson P, Alzetani A, Conforti F, Doherty R, Lai CY, Johnson B, Bourdakos KN, Fletcher SV, Marshall BG, Jogai S, Brereton CJ, Chee SJ, Ottensmeier CH, Sime P, Gauldie J, Kolb M, Mahajan S, Fabre A, Bhaskar A, Jarolimek W, Richeldi L, O'Reilly KM, Monk PD, Thurner PJ, Davies DE. Nanoscale dysregulation of collagen structure-function disrupts mechano-homeostasis and mediates pulmonary fibrosis. *eLife* 2018: 7.

182. Berhan A, Harris T, Jaffar J, Jativa F, Langenbach S, Lonnstedt I, Alhamdoosh M, Ng M, Lee P, Westall G, Wilson N, Wilson M, Stewart AG. Cellular Microenvironment Stiffness Regulates Eicosanoid Production and Signaling Pathways. *Am J Respir Cell Mol Biol* 2020: 63(6): 819-830.

183. Wallmeier J, Nielsen KG, Kuehni CE, Lucas JS, Leigh MW, Zariwala MA, Omran H. Motile ciliopathies. *Nat Rev Dis Pri* 2020: 6(1): 77.

184. Lee DDH, Cardinale D, Nigro E, Butler CR, Rutman A, Fassad MR, Hirst RA, Moulding D, Agrotis A, Forsythe E, Peckham D, Robson E, Smith CM, Somavarapu S, Beales PL, Hart SL, Janes SM, Mitchison HM, Ketteler R, Hynds RE, O'Callaghan C. Higher throughput drug screening for rare respiratory diseases: readthrough therapy in primary ciliary dyskinesia. *Eur Respir J* 2021: 58(4).

185. Hynds RE, Bonfanti P, Janes SM. Regenerating human epithelia with cultured stem cells: feeder cells, organoids and beyond. *EMBO Mol Med* 2018: 10(2): 139-150.

186. Pan E, Bogumil D, Cortessis V, Yu S, Nieva J. A Systematic Review of the Efficacy of Preclinical Models of Lung Cancer Drugs. *Front Oncol* 2020: 10: 591.

187. Paul SM, Mytelka DS, Dunwiddie CT, Persinger CC, Munos BH, Lindborg SR, Schacht AL. How to improve R&D productivity: the pharmaceutical industry's grand challenge. *Nature Rev Drug Discov* 2010: 9(3): 203-214.

188. Movia D, Prina-Mello A. Preclinical Development of Orally Inhaled Drugs (OIDs)-Are Animal Models Predictive or Shall We Move Towards In Vitro Non-Animal Models? *Animals (Basel)* 2020: 10(8).

189. Movia D, Bruni-Favier S, Prina-Mello A. In vitro Alternatives to Acute Inhalation Toxicity Studies in Animal Models-A Perspective. *Front Bioeng Biotechnol* 2020: 8: 549.

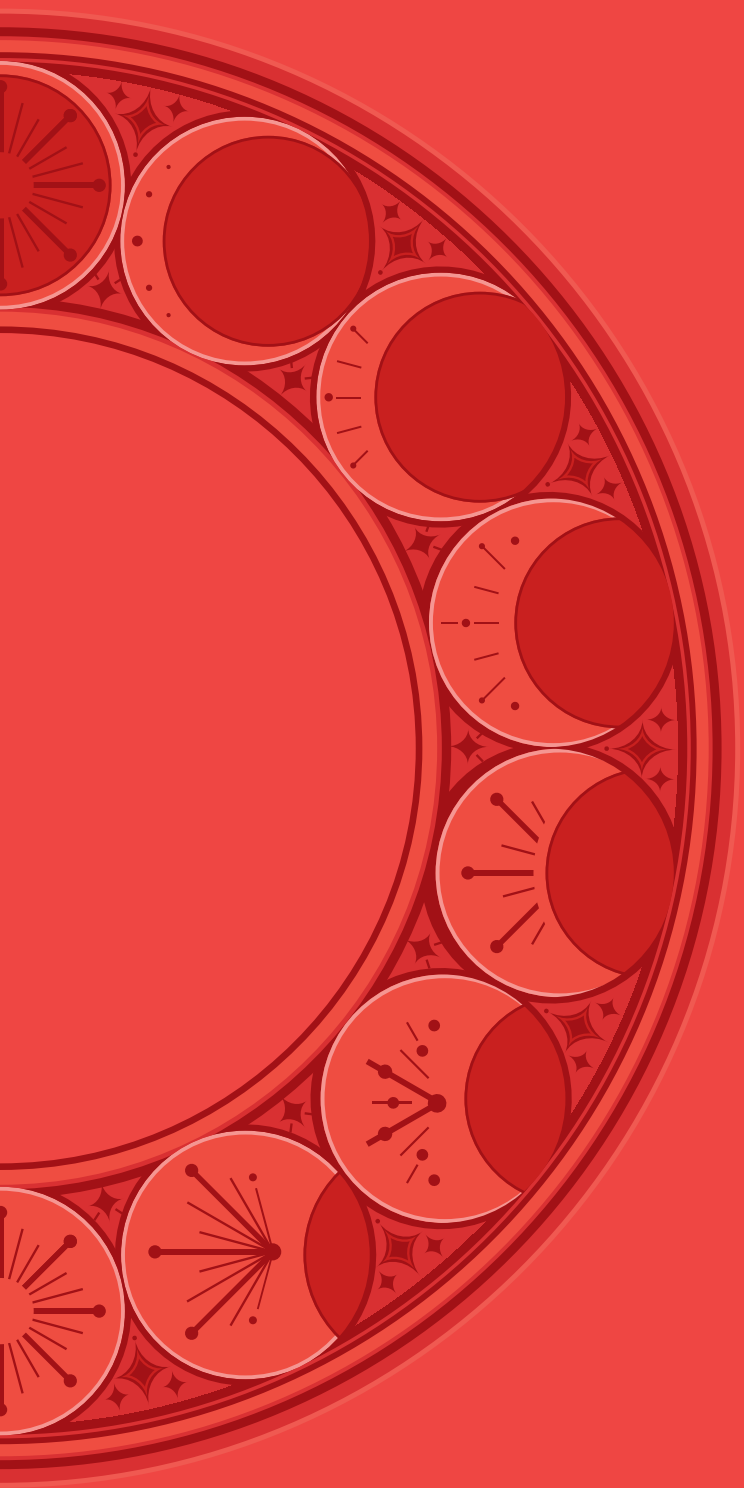

CHAPTER 5

Dysregulated cross talk between alveolar epithelial cells and stromal cells in IPF reduces epithelial regenerative capacity

Marissa Wisman † , **Mehmet Nizamoglu** † , Jacobien A. Noordhoek, Wim Timens, Janette K. Burgess, Irene H. Heijink

† These authors have contributed equally to this work and share first authorship.

Published in Frontiers in Medicine under a CC BY 4.0 license as:
Wisman, M.*, **Nizamoglu, M.***, Noordhoek, J. A., Timens, W., Burgess, J. K. & Heijink I. H. (2023). Dysregulated cross-talk between alveolar epithelial cells and stromal cells in IPF reduces epithelial regenerative capacity.
Frontiers in Medicine, 10.
https://doi.org/10.0.13.61/fmed.2023.1182368

ABSTRACT

In idiopathic pulmonary fibrosis (IPF) constant epithelial micro-injury and aberrant interactions within the stromal micro-environment lead to abnormal alveolar repair and fibrosis. We hypothesized that alveolar epithelial regenerative responses in IPF are impaired due to disturbed crosstalk between epithelial cells and their stromal niche. We established organoid cultures from unfractionated suspensions and isolated EpCAM$^+$ cells from distal lung tissue of patients with and without IPF. We observed significantly more organoids being formed from unfractionated suspensions compared to isolated EpCAM$^+$ cell cultures, indicating the presence of supportive cells in the unfractionated suspensions. Importantly, lower organoid numbers were observed in unfractionated cultures from IPF lungs compared to non-IPF lungs. This difference was not found when comparing organoid formation from isolated EpCAM$^+$ cells alone between IPF and non-IPF groups, suggesting that crosstalk between the supportive population and epithelial cells is impaired in lungs from IPF patients. Additionally, organoids grown from IPF lung-derived cells were larger in size compared to those from non-IPF lungs in both unfractionated and EpCAM$^+$ cultures, indicating an intrinsic abnormality in epithelial progenitors from IPF lungs. Together, our observations suggest that dysregulated crosstalk between alveolar progenitor cells and the stromal niche affects the regenerative capacity, potentially contributing to alveolar impairment in IPF.

INTRODUCTION

Idiopathic Pulmonary Fibrosis (IPF) is a progressive lung disease characterized by aberrant repair responses in the alveoli, leading to fibrosis and rapid lung function decline. A high mortality rate, while having no cure available, illustrates the urgent need to understand IPF pathogenesis to identify new therapeutic strategies [1]. The origin of the disease is still unknown, but ongoing alveolar epithelial micro-injury and aberrant interactions within the stromal micro-environment are thought to induce the abnormal alveolar regeneration and tissue repair [2]. The crosstalk between epithelial cells and their stromal niche composed of supportive cells and extracellular matrix (ECM) is critical for alveolar repair [3]. The stromal compartment includes fibroblasts, mesenchymal stromal cells, macrophages and endothelial cells, as well as ECM [4]. Emerging data suggests that stromal alterations in IPF lead to inadequate alveolar epithelial regeneration [5].

In this study we hypothesized that the crosstalk between alveolar epithelial cells and other cell types present in the fibrotic micro-environment of the lung is disrupted, resulting in reduced regenerative capacity of alveolar epithelial progenitors derived from IPF patients. We studied epithelial regenerative potential using an organoid model where alveolar epithelial progenitors were seeded into a 3-dimensional (3D) hydrogel (Matrigel) with stromal cells to recapitulate critical aspects of alveolar regeneration [6], including self-organization into 3D structures, proliferation and differentiation.

MATERIALS AND METHODS

Subjects

Parenchymal lung tissue was derived from 10 non-IPF donors undergoing tumour resection surgery and 4 IPF donors undergoing lung transplantation surgery (characteristics are shown in **Table 1**). Tissue derived from the non-IPF donors was taken from anatomically normal tissue as assessed by experienced pathologists, as far away from the tumour region as possible. This protocol was consistent with the Research Code of the University Medical Center Groningen (*https://www.umcg.nl/documents/770534/2183586/umcg-research-code-2018-en.pdf/9680a460-3feb-543d-7d58-bc9d4f7277de?t=1614951313016*) and national ethical and professional guidelines (*https://www.coreon.org/gedragscode-gezondheidsonderzoek*; Code of conduct - in Dutch)

Table 4: Characteristics of donors included in the study.

	Non-IPF (n=4)	IPF (n=4)	P value
Sex	3M/1F	3M/1F	>0.999#
Smoking history			0.0285#
Former	3	0	
Never	1	4	
Age (median (min-max))	55 (36-58)	61 (27-68)	0.3143†
FEV1% (Pred.) (median (min-max))	96.5 (70-111)	42.0 (17-64)	0.0286†

#Indicates p value as assessed by the Chi-square test. † indicates p value as assessed by the Mann-Whitney test. IPF: Idiopathic pulmonary fibrosis, FEV1 (pred.): Forced expiratory volume in 1 second (predicted).

Tissue dissociation

Unfractionated cell suspensions were obtained from parenchymal lung tissue without any visible airways present as previously described by Kruk et al [7]. Briefly, lung tissue was cut into small sections (1 cm^3) and treated overnight at 4 °C with Trypsin/EDTA (0.25%; Gibco, Waltham, MA), supplemented with 1% penicillin (100 U/mL) / streptomycin (100 µg/mL) (P/S) (Gibco), Collagenase A (2 mg/mL; Roche, Basel, Switzerland) and DNase (0.04 mg/mL; Sigma-Aldrich, Burlington, VT). Subsequently, EpCAM (CD326)$^+$ epithelial progenitors were isolated from this unfractionated cell suspension by negative selection for CD31 and CD45 to deplete endothelial cells and hematopoietic cells [8], followed by a positive selection for CD326 using magnetic beads (human anti-CD31, human anti-CD45, human anti-CD326) (Miltenyi Biotec, Bergisch Gladback, Germany) according to manufacturer's instructions. The cell suspensions were then resuspended in Small Airway Growth Medium (SAGM) (PromoCell, Heidelberg, Germany), counted manually and kept on ice until use.

Organoid culture

MRC-5 human foetal lung fibroblasts (ATCC, Manassas, VA) were cultured in Ham's F12 medium (Gibco) containing 10% foetal bovine serum (FBS) (Sigma-Aldrich) and 1% P/S. When confluent, cells were treated with Mitomycin C (0.01 mg/mL) (Sigma-Aldrich) for 2 hours to inhibit proliferation. Subsequently, cells were trypsinized and resuspended in SAGM, counted manually and kept on ice until use. To generate organoids, unfractionated lung cell suspensions or EpCAM$^+$ epithelial cells were mixed in a 1:1 ratio with MRC-5 cells. This cell mixture, diluted 2:1 with SAGM, was seeded in 100 µL Matrigel (8.4 mg/mL; Corning, New York, MA) on top of 6.5 mm Transwell inserts (0.4 µm pore size; Corning) and cultured for 7 days in SAGM medium

containing 1% FBS and 1% P/S in the basolateral compartment. At day 7, images of the organoid cultures were taken using a Nikon Eclipse Ti-E microscope (Brightfield; Nikon Instruments Europe, Amsterdam, Netherlands) and the organoid forming efficiency and organoid size (diameter) were quantified manually using Nikon Eclipse Ti software (Nikon Instruments).

Immunohistochemistry

Cytospin slides were prepared from the unfractionated cell suspension for immunohistochemical analyses. Slides were fixed with acetone (Merck, Darmstadt, Germany) and blocked with 5% bovine serum albumin (BSA) (Sigma-Aldrich) / 1X Phosphate Buffered Saline (PBS) (Gibco) and 0.25% Hydrogen Peroxide (Merck) / 1X PBS, both for 30 minutes at room temperature (RT). The slides were stained overnight with primary antibody solutions for EpCAM (1:1000; Invitrogen, Massachusetts, USA), endothelial cell marker CD31 (1:100; Immunotools, Friesoythe, Germany), stromal cell marker CD90 (1:100; Biolegend, San Diego, CA), or macrophage marker CD68 (1:100; Agilent Dako, Santa Clara, CA) in 1% BSA / 0.1% Triton-X (Merck) / 1X PBS). The next day, slides were washed with 1X PBS and incubated for 1 hour at RT with a secondary antibody solution (1:50 Rabbit-anti Mouse (Agilent Dako) in 1% BSA / 0.1% Triton-X / 1X PBS). After washing the slides with 1X PBS, they were incubated for1 hour at RT with a tertiary antibody solution (1:50 Goat-anti Rabbit (Agilent Dako) in 1% BSA / 0.1% Triton-X / 1X PBS) where after colour was developed using a NovaRed Substrate kit (Vector labs, Newark, CA) according to the company's manual. Haematoxylin solution (Sigma-Aldrich) was used to counterstain the nuclei. From a total cell count of, at minimum 150 cells, positive stained cells were counted manually. The presence of bronchiolization in IPF lung samples was identified in haematoxylin and eosin (H&E) - stained sections from paraffin embedded lung tissue taken near the site of tissue used for the organoid cultures.

Statistics

One-way ANOVA with Šídák's multiple comparisons test was used to assess for statistical differences after testing the normality of the data with Q-Q plots and Shapiro-Wilk test. In case of non-parametric data, the Mann-Whitney test was used for comparisons of two groups and the Kruskal–Wallis test for comparison of more than two groups. $P<0.05$ was considered statistically significant.

RESULTS

IPF lung-derived cells form a smaller number of organoids independent of the number of epithelial cells

Both IPF and non-IPF lung-derived cell suspensions were able to form organoids by day 7 (**Figure 1**). We first compared organoid formation efficiency between the IPF and IPF groups in isolated EpCAM$^+$ cell populations. The number of EpCAM$^+$ cells isolated from IPF lung tissue was significantly lower compared to the non-IPF group (*Supplementary Figure 1)*. Therefore, the number of organoids was normalized to the number of epithelial cells isolated per donor to correct for differences in epithelial cell counts. We observed that IPF and non-IPF-derived EpCAM$^+$ cells were equally well capable of forming organoids, as reflected by both the size of the organoids and the numbers (**Figure 2A**). Next, we assessed organoid formation efficiency of unfractionated suspensions. We normalized for the input of epithelial numbers based on the number of EpCAM$^+$ in the cytospins of these suspensions and observed that significantly more organoids formed from the unfractionated suspensions compared

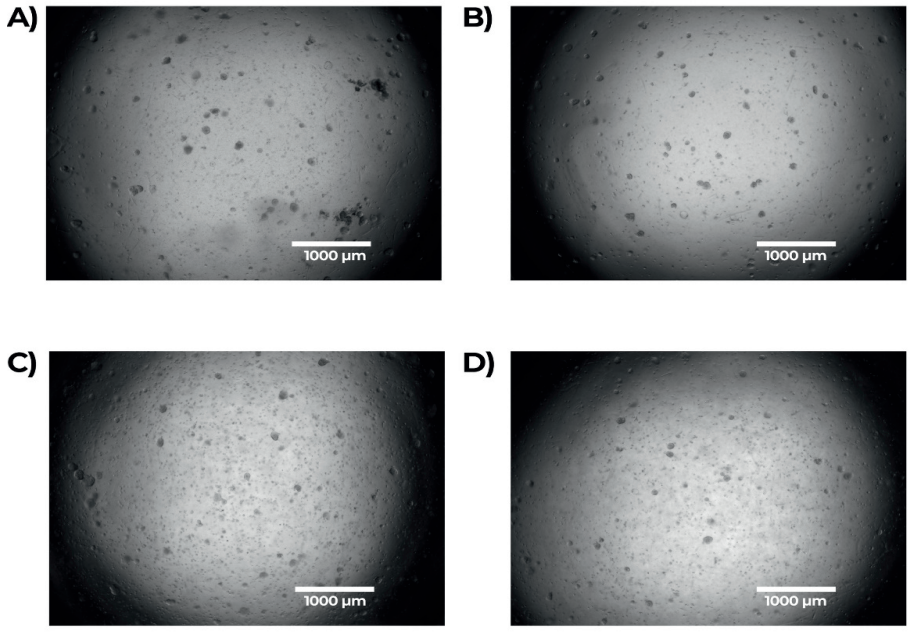

■ **Figure 1: Organoid formation by lung alveolar progenitor cells isolated from IPF and non-IPF lungs.** A) non-IPF (unfractionated), B) non-IPF EpCAM$^+$, C) IPF (unfractionated), D) IPF EpCAM$^+$. Brightfield images were taken on day 7 of the organoid cultures with a 2X magnification. Scale bar: 1000 µm. Representative images are shown.

to isolated EpCAM$^+$ cells (*Supplementary Figure 2*), suggesting the presence of a supportive cell population. Interestingly, when unfractionated organoid cultures were compared between the groups, we observed that significantly less organoids were formed from IPF lung-derived cells compared to non-IPF lung-derived cells (**Figure 2A**).

In addition to the number of organoids formed, the size distribution of the organoids was compared between the groups. Notably, IPF-derived cells formed significantly larger organoids compared to the non-IPF group, for both unfractionated (non-IPF organoids mean size 78.45 ± 8.00 µm, IPF organoids mean size 92.70 ± 26.83 µm) and EpCAM$^+$ (non-IPF organoids mean size 64.45 ± 1.47 µm, IPF organoids mean size 82.51 ± 14.42 µm) cultures . (**Figure 2B**).

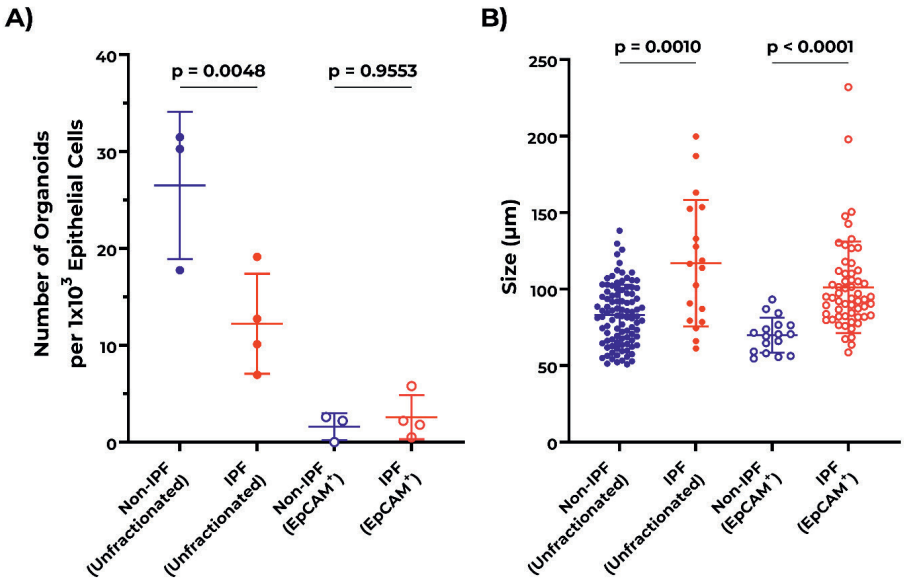

■ **Figure 2: Abnormalities in organoid formation of unfractionated lung cell suspensions from IPF patients.** A) Quantification of organoid numbers at day 7 comparing non-IPF (n=3) and IPF (n=4) unfractionated and EpCAM$^+$ cultures. Organoid counts were normalized to the number of EpCAM$^+$ cells to correct for differences in epithelial cell input during the organoid assay. Means ± SD are indicated. One-way ANOVA with Šídák's multiple comparisons test was used to assess for statistical differences after testing the data for normality with Q-Q plots and Shapiro-Wilk test. B) Quantification of organoid size distribution at day 7 comparing non-IPF (n=3) and IPF (n=4) unfractionated and EpCAM$^+$ cultures. The Kruskal–Wallis test was used to assess for statistical differences.

Cell fractions in unfractionated lung suspensions do not differ significantly between IPF and non-IPF groups

To investigate whether there were differences in the composition of cell types in the unfractionated suspensions between IPF and non-IPF lungs, cytospins of unfractionated suspensions were stained for several markers. As the stromal compartment of the lungs includes various major cell types, we stained for epithelial cells (EpCAM), stromal cells (CD90), macrophages (CD68) and endothelial cells (CD31), which have all been implicated in IPF pathology [3, 9]. We were able to identify CD90$^+$, CD68$^+$ and CD31$^+$ cells in the unfractionated suspensions, but we did not observe significant differences in the percentages of each type of cell between the non- IPF and IPF groups (**Figure 3**).

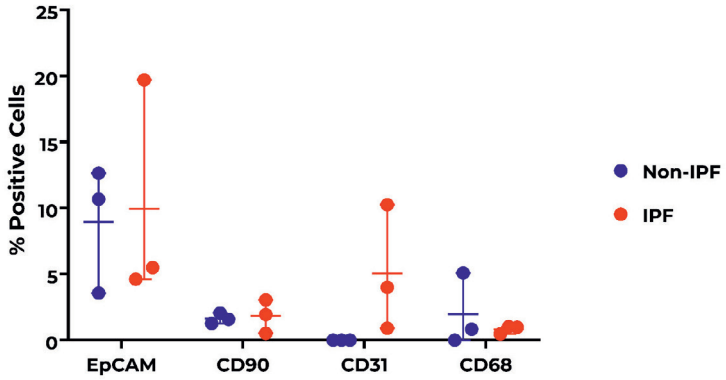

■ **Figure 3: Percentage of cells stained positive for EpCAM (epithelial cells), CD31 (endothelial cells), CD90 (mesenchymal cells) and CD68 (macrophages) in unfractionated cell suspension cytospins from IPF and non-IPF lungs.** Means ± SD values are shown. Statistical differences between IPF and non-IPF groups were tested using the unpaired t-test after verifying data normality with Q-Q plots and Shapiro-Wilk test.

DISCUSSION

In this study, we compared the organoid forming efficiency of EpCAM$^+$ epithelial cell populations and unfractionated cell suspensions from parenchymal regions of IPF and non-IPF lungs. Our results suggest the presence of a supportive cell population in the unfractionated lung suspensions. Of interest, we observed reduced organoid forming efficiency in the unfractionated suspensions from IPF compared to non-IPF lungs. This difference was not present in organoids formed from isolated EpCAM$^+$ cell populations from both IPF and non-IPF lungs, suggesting that dysregulated cross-

talk between epithelial cells and other supportive cell populations exists in IPF lungs. In addition to the reduced organoid forming capacity, the organoids derived from IPF lungs were significantly larger compared to non-IPF lung-derived organoids in both unfractionated suspensions and EpCAM$^+$ cell populations. To the best of our knowledge, this is the first report of lower organoid forming capacity in cells isolated from parenchymal tissue of lungs of patients with IPF.

Organoid forming efficiency as an indication of regenerative capacity has been demonstrated for several other lung diseases [10]. While fewer numbers of epithelial cells were isolated from the lungs from donors with IPF, our results show reduced numbers of organoids in IPF lung-derived cultures in the unfractionated groups independent of the number of epithelial cells. This was not observed in organoid cultures established from isolated EpCAM$^+$ epithelial cells. This observation does not align with the current school of thought that suggests that the loss of regenerative capacity (specifically their ability to self-renew) of epithelial cells stems from epithelial-mesenchymal transition or senescence in the epithelial cell population in IPF [11]. The comparable organoid forming efficiency seen in isolated EpCAM$^+$ cell populations in IPF and non-IPF groups, relative to the starting number of epithelial cells, indicates that the hampered repair capacity does not result directly from defects in the epithelial progenitor cells. Rather, it may be the result of defective interactions between cells within the stromal niche. However, we did not observe significant differences in the proportions of supporting cell types (stromal, endothelial or macrophage) present in the isolated cell populations between IPF and non-IPF. We did not examine the individual functioning of the cells from the stromal niche, thus it may be that the fibrotic microenvironment *in vivo* from which these cells were derived has imprinted cells towards different behaviour [12]; the observed differences in organoid supportive capacity might thus result from dysregulated crosstalk between the epithelial cells and stromal cells dictated by the imprinting from the IPF microenvironment.

The IPF organoid cultures, both unfractionated and EpCAM$^+$ populations, generated larger organoids compared to non-IPF cultures. This indicates that epithelial progenitors from IPF lungs display intrinsic differences with respect to proliferation or other characteristics that determine organoid size. The morphology of the epithelial cells in tissue sections adjacent to the regions from where we isolated cells from in the lungs of patients with IPF was checked. Previously published reports indicate bronchiolization of the epithelium in the alveolar region in patients with IPF [13], which may be related to the intrinsic differences observed in IPF-derived epithelial cells. When the H&E-stained sections of IPF lung tissue were examined,

presence of bronchiolization of the alveolar epithelium was observed in all IPF patients from whom cells were obtained (*Supplementary Figure 3*). This is relevant as this is indicative of an active bronchiolization process occurring in the alveolar region in the IPF tissues, which is a form of metaplasia, and the larger organoid formation, potentially due to aberrant proliferation or cell transitioning in the IPF organoids, may be a reflection of such metaplasia [14, 15]. Further studies on whether the IPF organoids contain more or larger cells, or more swelling due to reduced barrier function or more mucus production would be required to investigate the influence of bronchiolization in parenchymal lung tissue on the organoid forming process.

Our study reporting initial observations on alveolar regeneration in IPF has some limitations that should be recognized. The lack of differences in the numbers of different cell types in the unfractionated cell populations between the groups may be a consequence of the isolation method, which has been optimized for alveolar epithelial cells and not for other cell types. In addition, the generated cell counts may be an underestimation of the total numbers of cells present in the lung tissue as several of the surface markers are known to be sensitive to cleavage by the enzymatic treatment used to isolate cells. Nevertheless, sufficient cell numbers have been isolated in order to support organoid formation effectively, as indicated by our current findings. Further investigation of the involvement of cellular interactions during the initiation of organoid formation will be of interest in future studies, but was outside of the scope of this discovery study.

As mentioned above, the origin of larger organoids from IPF donors requires further investigation. The finding that the organoid forming efficiency differs between IPF and non-IPF lung-derived organoid cultures from unfractionated suspensions, but not isolated epithelial progenitors, suggests that altered interactions between different cell types derived from IPF lungs are responsible for the aberrations in the initiation phase of the organoid formation. Previous research has shown that WNT-signalling influences the ability of epithelial progenitor cells to self-renew and form organoids [16]. In mice it has been shown that epithelial progenitors reside in a stromal niche that provides WNT signals to maintain their stemness [17]. Thus, we speculate that the WNT signalling pathway might be dysregulated in IPF-derived organoids due to the disturbed crosstalk between epithelial progenitors and stromal cell types. Further studies are needed to investigate whether alterations in the release of WNT ligands from stromal cells, endothelial cells and/or macrophages or in their interaction with epithelial cells occur in IPF.

Conclusions

Overall, our observations indicate that aberrant crosstalk between (alveolar) epithelial cells and stromal cells changes the regenerative capacity of alveolar progenitors in IPF. This dysregulation may contribute to the abnormal alveolar repair in IPF, partly leading to bronchial and squamous metaplasia. In addition, this disturbance might also contribute to an abnormal alveolar micro-environment and ECM interactions in the lung in IPF. Further investigations regarding the contribution of specific stromal cells in epithelial regeneration will be necessary to understand the influence of aberrant alveolar repair in IPF pathophysiology. It will be of interest to investigate the behaviour of metaplastic bronchial epithelial cells in culture systems like organoids to provide further insight into abnormal alveolar repair in IPF. Future research using the combination of different epithelial cell types, as well their interaction with specific stromal cells, will deepen our understanding of IPF pathophysiology.

SUPPLEMENTARY FIGURES

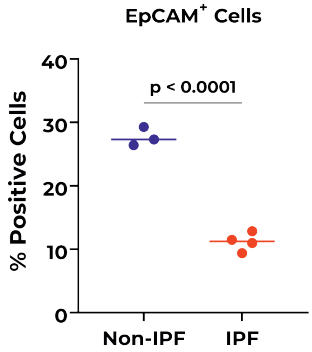

Supplementary Figure 1: Number of EpCAM⁺ positive cells isolated from non-IPF and IPF lung tissue. N=3 for non-IPF and n=4 for IPF samples. Statistical differences between non-IPF and IPF groups were tested using unpaired t-test after verifying normality with Q-Q plots and Shapiro-Wilk test.

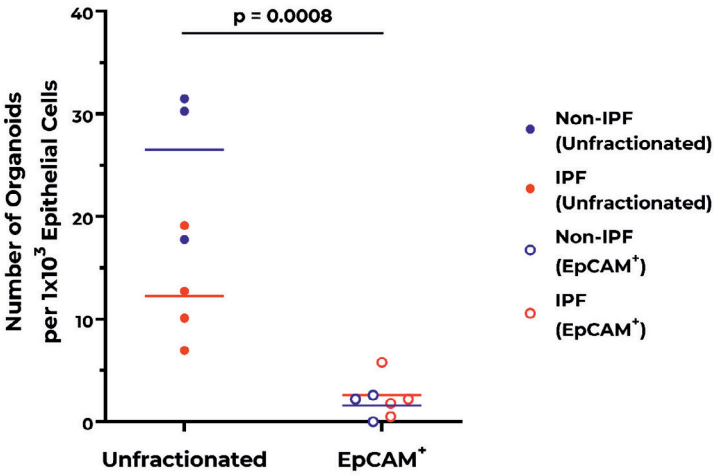

Supplementary Figure 2: Difference in organoid forming efficiency between unfractionated and EpCAM⁺ cell populations of IPF and non-IPF lung-derived epithelial cells. Quantification of organoid numbers at day 7 comparing unfractionated and EpCAM⁺ cultures (n=7 in total). Organoid counts were normalized to the number of EpCAM⁺ cells to correct for differences in epithelial cell input during the organoid assay. Means ±SD are indicated. Statistical differences between groups were tested using the unpaired t-test after verifying normality with Q-Q plots and Shapiro-Wilk test.

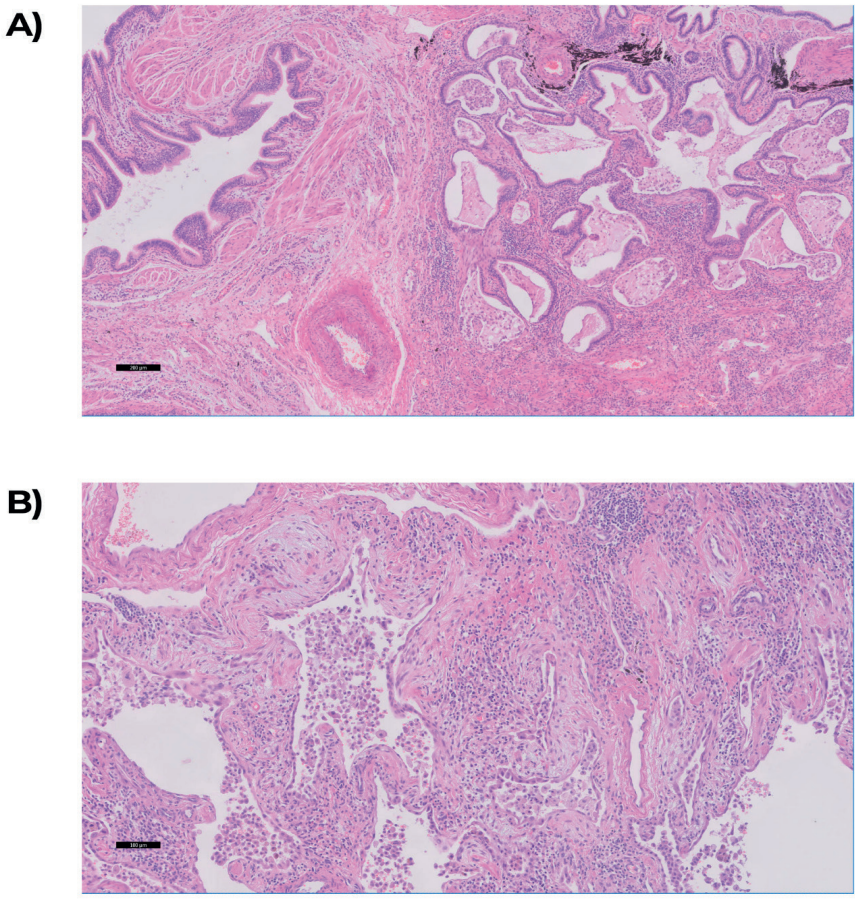

Supplementary Figure 3: Aberrances in alveolar structure in IPF lung tissue. A) Representative image showing the presence of bronchiolization (right) adjacent to a pre-existing bronchiole (left) in the lung parenchyma in IPF lung tissue (hematoxylin and eosin, scale bar is 200 µm). B) Extensive fibroblastic foci covered by cubic to flat squamous epithelium, bordering a remaining alveoli filled with macrophages (hematoxylin and eosin, scale bar is 100 µm).

REFERENCES

1. Chambers RC, Mercer PF. Mechanisms of alveolar epithelial injury, repair, and fibrosis. *Ann Am Thorac Soc* 2015: 12 Suppl 1(Suppl 1): S16-20.
2. Selman M, Pardo A. The leading role of epithelial cells in the pathogenesis of idiopathic pulmonary fibrosis. *Cell Signal* 2020: 66: 109482.
3. Kong J, Wen S, Cao W, Yue P, Xu X, Zhang Y, Luo L, Chen T, Li L, Wang F, Tao J, Zhou G, Luo S, Liu A, Bao F. Lung organoids, useful tools for investigating epithelial repair after lung injury. *Stem Cell Res Ther* 2021: 12(1): 95.
4. Nizamoglu M, Burgess JK. The Multi-Faceted Extracellular Matrix: Unlocking Its Secrets for Understanding the Perpetuation of Lung Fibrosis. *Curr Tissue Microenviron Rep* 2022: 2(4): 53-71.
5. Chapman HA. Epithelial-mesenchymal interactions in pulmonary fibrosis. *Annu Rev Physiol* 2011: 73(1): 413-435.
6. Barkauskas CE, Chung MI, Fioret B, Gao X, Katsura H, Hogan BL. Lung organoids: current uses and future promise. *Development* 2017: 144(6): 986-997.
7. Kruk D, Wisman M, Noordhoek JA, Nizamoglu M, Jonker MR, de Bruin HG, Arevalo Gomez K, Ten Hacken NHT, Pouwels SD, Heijink IH. Paracrine Regulation of Alveolar Epithelial Damage and Repair Responses by Human Lung-Resident Mesenchymal Stromal Cells. *Cells* 2021: 10(11): 2860.
8. Barkauskas CE, Cronce MJ, Rackley CR, Bowie EJ, Keene DR, Stripp BR, Randell SH, Noble PW, Hogan BL. Type 2 alveolar cells are stem cells in adult lung. *J Clin Invest* 2013: 123(7): 3025-3036.
9. Vasse GF, Nizamoglu M, Heijink IH, Schleputz M, van Rijn P, Thomas MJ, Burgess JK, Melgert BN. Macrophage-stroma interactions in fibrosis: biochemical, biophysical, and cellular perspectives. *J Pathol* 2021: 254(4): 344-357.
10. Hughes T, Dijkstra KK, Rawlins EL, Hynds RE. Open questions in human lung organoid research. *Front Pharmacol* 2022: 13: 1083017.
11. Confalonieri P, Volpe MC, Jacob J, Maiocchi S, Salton F, Ruaro B, Confalonieri M, Braga L. Regeneration or Repair? The Role of Alveolar Epithelial Cells in the Pathogenesis of Idiopathic Pulmonary Fibrosis (IPF). *Cells* 2022: 11(13): 2095.
12. Upagupta C, Shimbori C, Alsilmi R, Kolb M. Matrix abnormalities in pulmonary fibrosis. *Eur Respir Rev* 2018: 27(148): 180033.
13. Chakraborty A, Mastalerz M, Ansari M, Schiller HB, Staab-Weijnitz CA. Emerging Roles of Airway Epithelial Cells in Idiopathic Pulmonary Fibrosis. *Cells* 2022: 11(6): 1050.
14. Seibold MA, Smith RW, Urbanek C, Groshong SD, Cosgrove GP, Brown KK, Schwarz MI, Schwartz DA, Reynolds SD. The idiopathic pulmonary fibrosis honeycomb cyst contains a mucocilary pseudostratified epithelium. *PLoS One* 2013: 8(3): e58658.
15. Schruf E, Schroeder V, Le HQ, Schonberger T, Raedel D, Stewart EL, Fundel-Clemens K, Bluhmki T, Weigle S, Schuler M, Thomas MJ, Heilker R, Webster MJ, Dass M, Frick M, Stierstorfer B, Quast K, Garnett JP. Recapitulating idiopathic pulmonary fibrosis related alveolar epithelial dysfunction in a human iPSC-derived air-liquid interface model. *FASEB J* 2020: 34(6): 7825-7846.

16. Wu X, van Dijk EM, Ng-Blichfeldt JP, Bos IST, Ciminieri C, Konigshoff M, Kistemaker LEM, Gosens R. Mesenchymal WNT-5A/5B Signaling Represses Lung Alveolar Epithelial Progenitors. *Cells* 2019: 8(10): 1147.

17. Nabhan AN, Brownfield DG, Harbury PB, Krasnow MA, Desai TJ. Single-cell Wnt signaling niches maintain stemness of alveolar type 2 cells. *Science* 2018: 359(6380): 1118-1123.

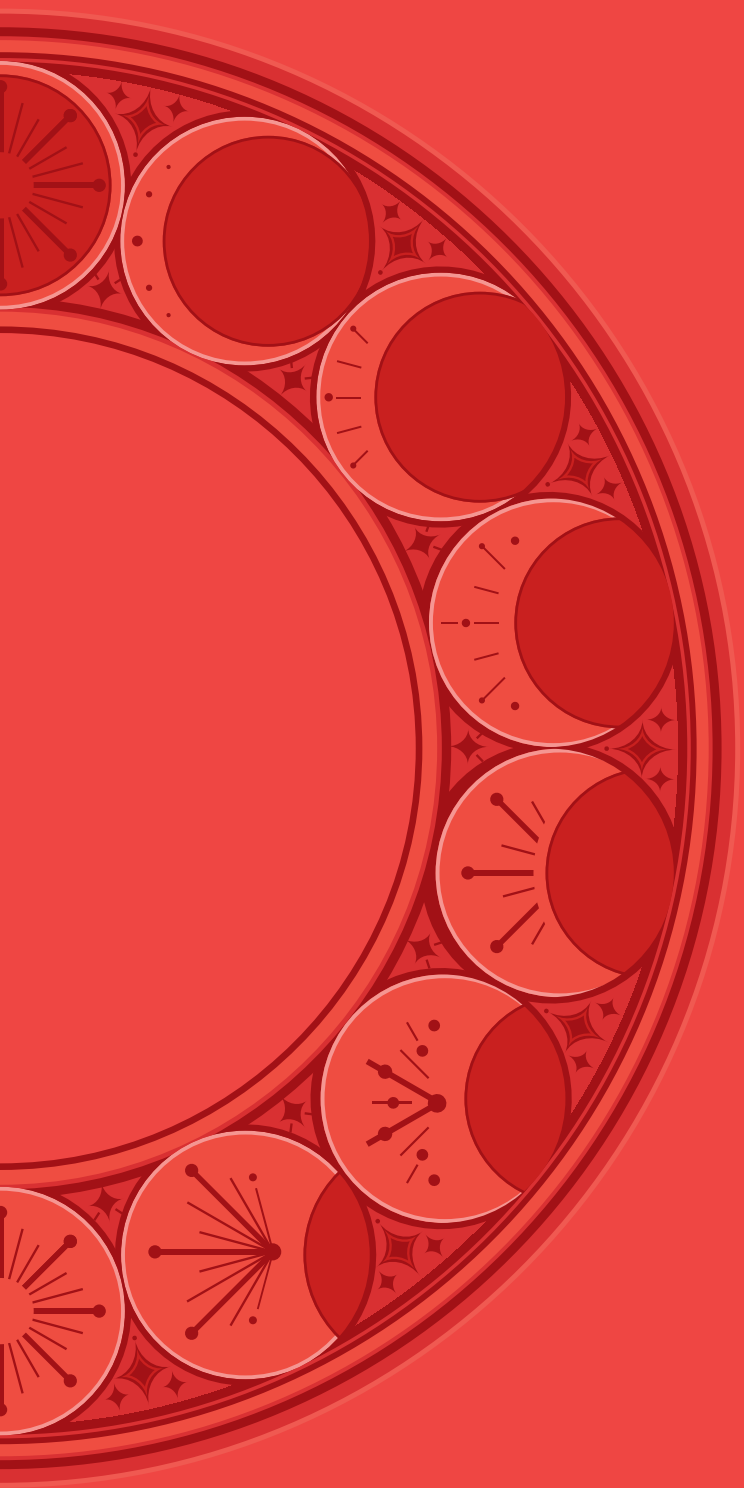

CHAPTER 6

3D lung models – 3D extracellular matrix models

Mehmet Nizamoglu, Mugdha M. Joglekar, Roderick H.J. de Hilster, Maunick Lefin Koloko Ngassie, Greta J. Teitsma, Nataliya Migulina, Kaj E.C. Blokland*, Janette K. Burgess*

* Equal contributions

Reproduced with permission from Springer Nature from the publication in *3D Lung Models for Regenerating Lung Tissue*:
Nizamoglu, M., Joglekar, M. M., de Hilster, R. H. J., Ngassie, M. L., Teitsma, G. J., Migulina, N., Blokland, K. E. C., & Burgess, J. K. (2022). Three dimensional lung models - three dimensional extracellular matrix models. 3D Lung Models for Regenerating Lung Tissue, 109–131.
https://doi.org/10.1016/b978-0-323-90871-9.00012-7

ABSTRACT

In vitro models for investigating mechanisms underlying repair and regeneration in lung disease have advanced greatly in the last decades. Of these models, 3-dimensional (3D) models are particularly interesting owing to their enhanced resemblance of the physiological conditions *in vivo*. 3D *in vitro* models can be created using natural or synthetic biomaterials; where utilizing the extracellular matrix (ECM) from the lung itself or ECM-derived biomaterials have improved our understanding of lung disease and repair mechanisms. Homeostasis of lung ECM is critically important for the function of the lungs for gas exchange, and disruption of the ECM occurs in most chronic lung diseases. Reflecting the complexity of the architecture of lung tissue, several different types of *in vitro* models based on ECM have been developed. Materials derived from collagen, gelatin, hyaluronic acid and their derivatives are among the most used single ECM protein-based models. Although these models lack the 3D architecture and organization of the native ECM, they facilitate the collection of extensive information via mimicking the lung microenvironment in health and disease. Decellularized lung matrices have been used as scaffolds for *in vitro* models enabling the preservation of native architecture and composition within the ECM. However, reintroducing and imaging to localize cells poses some novel challenges when working within these 3D models. Hydrogels prepared using these decellularized lung matrices are emerging as a new opportunity, bringing the native lung ECM composition and the ability to control the model shape together.

In this chapter, we discuss the ECM-based 3D *in vitro* models for lung disease, repair and regeneration. First, we briefly outline the lung ECM and the changes associated with chronic lung diseases. Then we summarize the progress and the state-of-the-art research performed using these models, discussing the advantages and challenges related to these models and summarizing the properties of an ideal 3D model.

INTRODUCTION

The non-cellular component in all tissues and organs is the extracellular matrix (ECM). The ECM fulfils an essential role acting as a physical scaffolding, while initiating critical biochemical and biomechanical cues for all cells that reside within it [1]. The ECM mainly consists of fiber-forming and interfibrillar molecules. Collagen and elastin are categorized as fiber-forming molecules, whereas proteoglycans and glycoproteins are considered interfibrillary molecules [2]. Healthy ECM is crucial for cells, as it modulates events such as migration and adhesion [3]. All tissues and organs have their own specific ECM, adapted to meet the individual needs to ensure that the organ can fulfil its defined roles. Within the lung, the ECM consists of two main compartments; the basal membrane, which is a specialized layer under the epithelial and endothelial cells, and the interstitial matrix [4]. Fibroblasts are recognized as the cell type responsible for the maintenance and majority of the ECM production [5]. During lung development, the ECM not only provides the developing organ structure but it is also important for the regulation of cell functions such as proliferation, migration and differentiation [6]. Fibroblasts are crucial during development and homeostasis, in their role as the gatekeepers responsible for production, deposition and maintenance of the ECM, residing throughout the organ [7, 8]. Dynamic changes within the ECM are associated with several chronic lung diseases, including chronic obstructive pulmonary disease (COPD) and idiopathic pulmonary fibrosis (IPF), illustrating the essential role of the ECM in the lung at all stages of life [9]. In addition to its role as a scaffold, the ECM has also been recognized as a key regulator of a myriad of biological processes including cell migration, growth, survival, differentiation and metabolism [8, 10].

The lung ECM consists of a multitude of macromolecules of which the major constituents include elastin, collagens, glycosaminoglycans (GAGs), proteoglycans (PGs) and glycoproteins (**Figure 1**). These macromolecules specifically fulfill roles contributing to the maintenance of the ECM biomechanical characteristics and function of the lung. Elastin is one of the principal constituents of lung ECM and represents 20-30, 7-16 and 3-5% dry weight of parenchyma, blood vessels and airways, respectively [11]; providing the lung its extension and recoil properties [12]. One of the most abundant ECM proteins in the lung is collagen, which comprises 28 different types categorized according to their structure and function as fibrils, fibril-associated collagens with interrupted triple helices, network-forming, beaded filaments and anchoring fibrils collagens [10, 13]. GAGs are polysaccharides with highly hydrophilic proprieties which contribute to the viscoelasticity of the lung [14]. Additionally, GAGs are known as regulators of immune responses, growth

factor activity and tissue modeling and remodeling [14, 15]. Four subfamilies of GAGs can be distinguished in the lung including heparan sulfate, hyaluronic acid, chondroitin sulfate/dermatan sulfate and keratan sulfate [16]. With the exception of hyaluronic acid, which is not synthesized as a PG, the other GAGs are synthesized as PGs, which consist of a protein backbone (referred to as the core protein) to which GAGs bind covalently [17]. Thus, major proteoglycan families can be classified based on their GAG composition, molecular weight and function [14]. Extracellular PGs can be classified in two groups, aggregating and small leucine-rich repeat PGs [16]. Known for their role in matrix-cell interactions, glycoproteins including fibronectin, laminins, vitronectin, thrombospondin, tenascin and nidogens play a crucial role in regulating cellular responses [18].

To investigate the role of the ECM in the development of lung pathologies, different *in vitro* experimental models such as traditional two-dimensional (2D) and more recently innovative three-dimensional (3D) cell culture systems have been developed. The 2D culture system is a wellestablished and broadly used system which (as discussed in Chapter 2), while having facilitated the generation of valuable data as the main workhouse of the *in vitro* lab for many years, has now been recognized to be limited in respect to its ability to mirror the physiological microenvironment from which cells are derived. Therefore, the importance of model systems that further mimic the natural physiological microenvironment of cells is necessary for a better understanding of cellular responses during homeostasis and disease.

In this chapter, we discuss the 3D *in vitro* models for representing lung disease, repair and regeneration. First, we outline the changes in the ECM during chronic lung diseases and summarize the major differences between 2D and 3D culture systems. Next, we describe the single ECM protein-based models used for advanced 3D lung modeling. Then, we illustrate state-of-the-art research that is performed using the complete lung ECM as a basis for the model. In conclusion, we discuss the limitations of actual conceptualized and available 3D culture systems, the encountered challenges and the novel approaches to improve the quality and robustness of 3D culture systems.

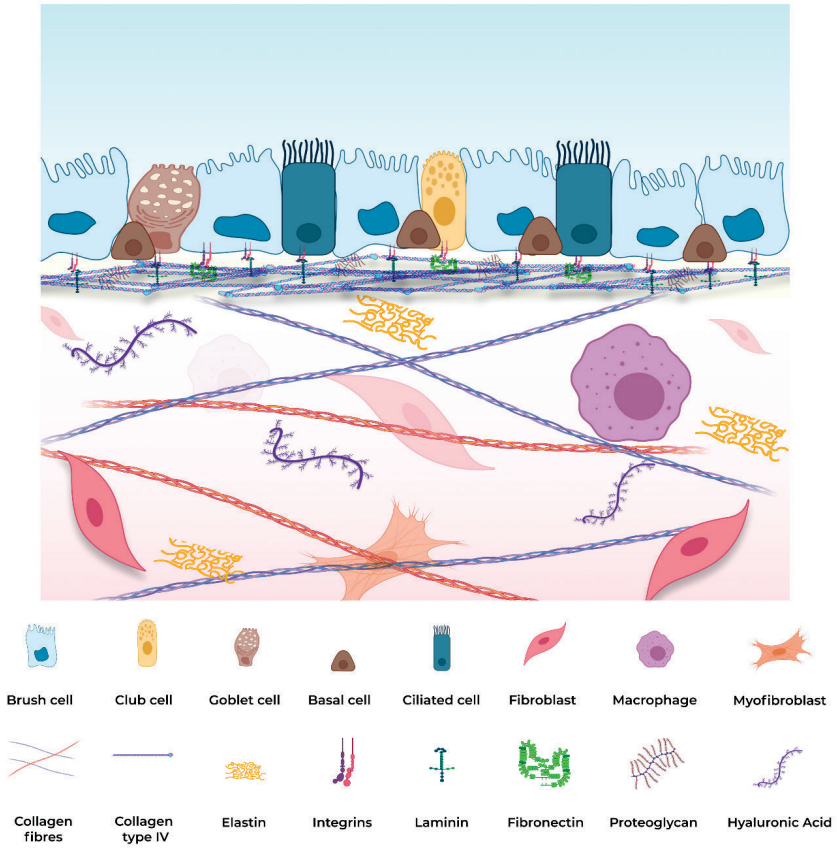

Figure 1: A schematic representation of lung extracellular matrix (ECM) and tissue structure. Lung epithelium is located above a basement membrane, which mainly consists of collagen type IV fibers and laminin. Below the basement membrane, the interstitial matrix is formed by various types of collagen fibers, proteoglycans and elastin.

ECM CHANGES IN CHRONIC LUNG DISEASES

The vital function of the lung is crucially dependent on maintenance of the homeostatic balance between the cells and the ECM in which these cells reside. While cellular mechanisms underlying the pathology of various (chronic) lung diseases have been thoroughly investigated to date; the pivotal functional impact of the changes observed in ECM during these diseases has recently been recognized. Of importance, the acknowledged heterogeneity of chronic lung diseases is thought to be reflected by changes in the ECM during the disease course. Changes in the composition,

organization and structure of the ECM consequently impact the biomechanics of the lung tissue at both the macro and microscales; influencing the biomechanics of breathing and gas exchange but also local forces and mechanotransduction experienced at the cellular level.

Asthma

The main characteristics of asthma include chronic inflammation and airway hyperresponsiveness, accompanied by airway remodeling which includes goblet cell hyperplasia [19–22]). Changes in the ECM structure in asthma include thickening of the basement membrane and increased deposition of ECM in and around the airway smooth muscle (ASM) layers. These changes have been summarized elegantly elsewhere [8, 22–27] and the complete details are outside the scope of this chapter. Specifically, fibronectin and (fragments of) elastic fibers have been found to be increased in the ASM layer in clinically severe asthma patients, compared to controls [20]. Similarly, the ASM layer contains less proteoglycans in severe asthma patients compared to patients with moderate asthma [28]. In addition, the collagen type IV in basement membrane has also been shown to decrease in asthma patients, despite the increase of the basement membrane thickness [29]. Interestingly, tumstatin, the degradation product of collagen type IV α3, was found to be absent in the lungs of asthma patients, compared to healthy controls [30]. Fibrillar collagen organization was also found to be disorganized in the airways of asthma patients, compared with healthy controls [31]. Higher levels of periostin were found both in the epithelial and subepithelial layers in asthma patients in comparison to controls [32]. Next to the deposited factors, soluble ECM proteins are contributors to the changes in ECM in asthma: Higher levels of Fibulin-1, a secreted glycoprotein, were found in asthma patients compared to the healthy controls [33] and the presence of this glycoprotein in the ECM was important for the regulation of ASM proliferation [33] and the development of airway wall fibrosis [34]. Considered together, these studies illustrate an altered ECM composition in the asthmatic airway wall.

Chronic Obstructive Pulmonary Disease (COPD)

COPD is a chronic lung disease characterized by airway obstruction caused by several factors including pulmonary inflammation accompanied by bronchitis, mucus hypersecretion, remodeling of the small airway wall and emphysema [35]. The last two phenotypes, airway wall remodeling and emphysema, are the consequences of the alteration of the lung ECM homeostasis [22, 23, 27]. Emphysema is caused by the degradation of elastic fibers and collagens by proteolytic enzymes, including matrix metalloproteinases (MMPs) and elastase [22]. Samples from different origins including sputum, bronchoalveolar lavage, lung parenchyma and lung cells showed

an increase in MMPs expression and their enzymatic activity in COPD subjects [36]. Merrilees et al. demonstrated that elastin fibers were decreased in alveoli of COPD lungs [37]. Comparably, immunohistochemical analysis demonstrated a reduction in fractional area of elastic fibers in COPD [38]. Additionally, degradation products of elastin were increased in urinary excretions of COPD patient compared with non-COPD controls [39]. The destruction of elastin fibers results in loss of lung elasticity, an alteration of the transpulmonary dissemination of the transpulmonary pressure resulting in lung hyperinflation [23]. Additionally, immunohistochemical analyses revealed that the fractional area of type I collagen was significantly reduced in the inner layer and muscle layer of the small airways in COPD when compared with non-smokers [38]. Interestingly, no changes were reported for other collagens including type III and IV or proteoglycans including decorin, biglycan and lumican [38]. This was in contrast to the findings of van Straaten et al. who reported reduced decorin and biglycan in the peribronchiolar regions from COPD patients with emphysema, compared to those of controls or lung fibrosis patients [40]. The levels of heparan sulphate were reduced in the airway walls of patients with both COPD and lung fibrosis. However, fibronectin was found elevated in the inner / outer layer, and muscle layer of the small airways in COPD patients in contrast to smokers and non-smokers patients, whilst tenascin was increased only in the inner layer of the small airways of COPD compared to controls [38]. Collagen organization also plays an important role in ECM remodeling and the regulation of cellular function. Using second harmonic generation, Tjin and colleagues demonstrated that the organization of type I collagen in the airway wall was significantly different in COPD lung tissue compared with non-disease controls [41]. There are excellent reviews summarizing the changes observed in the lung ECM of COPD subjects [15, 24, 26, 42].

Changes in the expression and organization of ECM molecules in the lung may have an important consequence for the mechanical properties of the lung ECM in the COPD lung. The stiffness of the tissue plays a critical role. Suki and colleagues extensively discussed the importance of collagen and elastin for the mechanical properties of lung parenchyma. Since the stiffness of elastin was demonstrated to be two fold smaller than that of collagen [43], a decrease of elastin may lead to an imbalance in ECM composition and an increase in lung stiffness, which in turn can negatively impact the lung function.

Idiopathic Pulmonary Fibrosis (IPF)

IPF is a chronic fibrotic lung disease of unknown etiology, characterized by abnormal deposition of ECM in the lung parenchymal regions [44]. While repeated micro-injuries to the epithelial layer are thought to be the initiator of an aberrant wound

healing response, miscommunication between the epithelial and stromal cells, senescence of these cells as well as increased number of pro-fibrotic cells such as myofibroblasts or pro-fibrotic macrophages, are all thought to contribute to the perpetuation of the fibrotic response in the lung tissue [45, 46]. The changes in ECM in IPF and their associated influences on the cells are reviewed elsewhere [22, 23, 47-51]. Among these changes, greater deposition of collagens type I, III and VI are well documented in IPF patients compared to healthy controls [52]. Similarly, elastic fibers are more abundant in lung parenchyma of IPF patients compared to non-IPF controls [53, 54]. In addition to the increased deposition of ECM proteins, post-translational modifications such as fiber crosslinking are more prominent in lung tissues of IPF patients compared to healthy controls [55, 56]. Lung biomechanical properties are altered as a result of changes in ECM structure: lung tissue of IPF patients are significantly stiffer compared to healthy tissue (16.52 ± 2.25 vs 1.96 ± 0.13 kPa), with an accompanying decrease in the viscoelastic relaxation properties (72.1 ± 13.1% vs 88.7 ± 10.4%)) [57, 58]. The instructiveness of ECM has been shown to provide a positive feedback loop between fibrotic ECM and fibroblasts [59-61]. Similar to other chronic lung diseases, secreted/released ECM fragments and growth factors deposited in ECM could also be playing crucial roles in the pathophysiology of IPF: increased TGF-β, latent TGF binding protein (LTBP) and several ECM protein degradation fragments have been found higher in IPF patients compared to healthy controls [62-64]. Likewise, IPF patients were found to have higher levels of fibulin-1 both in serum and lung tissue, compared to healthy controls [65]. In addition, the enzyme responsible for regulating crosslinking of collagen and elastin fibers, lysyl oxidases and transglutaminases are also recognized to be dysregulated in IPF [55, 60, 66]. In summary, the amounts and composition of ECM proteins present in the lung tissues are drastically altered in IPF, which also leads to biomechanical changes in the lung microenvironment.

2D VS 3D CELL CULTURE SYSTEMS

2D cell cultures have been used since the beginning of the 20th century. Basic 2D cell culture models include adherence of cells to petri dishes, tissue culture flasks or well plates made from glass or tissue-culture polystyrene. 2D culture systems described below do not consider suspension cell cultures. Classic 2D systems are simple to handle, easy to reproduce and facilitate the growth of large volumes of cells. Also, methods such as single-cell imaging and profiling of cells are easy to apply using such 2D-model culture systems. Moreover, 2D cell culture procedures are generally standardized and reproducible [67, 68] and these models are widely

applied for the study of mechanisms underlying lung diseases [69]. However, several limitations using 2D models have been identified when trying to replicate the 3D *in vivo* environment including differences in cell – cell and cell – ECM interactions, as summarized in **Table 1**. Other limitations of 2D models include adhesion of cells only in a 2D plane and induction of apical – basal polarity of the cells which can influence apoptosis signaling pathways [67, 70]. The stiffness of basic 2D culture surfaces, such as tissue culture plastic (TCP), is significantly higher than the *in vivo* microenvironment, resembling cartilage or bone tissue rather than soft lung tissue. Even in fibrotic diseases such as IPF, the increased Young's modulus is not as high as TCP which is 1 GPA compared to 16 kPa, respectively [49, 71]. Increased substrate stiffness leads to greater proliferation of cells and differentiation of fibroblasts to myofibroblasts [72, 73]. The highlighted differences between 2D and 3D culture models affect cell behavior, which contributes to cellular alterations that affect phenotype, differentiation, proliferation and gene and protein expression, cell signaling and behaviors [67, 68, 73]. Classical 2D models provide limited opportunities for studying cell migration and tissue remodeling; with perhaps the exception of information that can be garnered from "wound healing" experiments. However, in recent years, novel 2D models that feature properties that further reflect those of lung tissue have been developed. For example, to study the effects of mechanical properties on cell behaviors mechanically tunable polydimethylsiloxane substrates and polyacrylamide (PA) hydrogels can be used. Moreover, ECM proteins can be covalently cross-linked to the PA hydrogels [74]. The growth of cells on a basement membrane extract, such as Matrigel, provides signaling engagement, cell integrity and structural support which are unattainable in the basic 2D models [75]. Another semi 2D model that has been adopted is an air–liquid interface (ALI) culture system, where epithelial cells are grown on an upper surface of a porous membrane. The apical side of the membrane can be used to expose cells to air. The basal side is maintained in contact with the culture media to provide a continuing supply of nutrients. This model is commonly used for the culture of bronchial epithelial cells, which differentiae into pseudostratified mucociliated epithelial cells after exposure to air, to test the influence of external stimuli on these cells [76].

■ **Table 5: Comparison of 2- and 3-dimensinoal culture systems.**

	2D	3D
Adhesion	One plane	Three dimensional
Polarity	Basal-apical	No forced polarity
Stiffness	High stiffness (mega- to gigapascal range)	Variable stiffness (kilopascal range)
Soluble gradients	Absent	Present
Access to nutrients, GF, oxygen	Very accessible	More complicated with increasing thickness, similar to *in vivo*
ECM	One layer of matrix (coating)	Surrounded by matrix
Motion	Unconstrained spreading and migration	spreading and migration is hindered due to surrounding Matrix
Culturing Cost	Cheap	Expensive
Throughput	High	Low
Visualization	Easy	Difficult
Interactions	2D cell interaction, basolateral ECM interactions, no niches	2D and 3D cell interactions, cell-ECM/ scaffold, niches
Culture protocols	Simple, methods are known, various kits are available, easy to reproduce	Complex methods that are not standardized, not easy to reproduce, more difficult to maintain the culture
Reproduction of key aspects of the tissue	Stiffness ~100 MPa (stiffer than fibrotic tissue), cells change behavior (gene, RNA, protein expression, adhere more strongly, proliferation is higher)	Stiffness comparable to tissue and highly adaptable, cells behavior is closer to the behavior *in vivo*

2D: 2-dimensional, 3D: 3-dimensional, ECM: extracellular matrix, GF: growth factors

2D cell culture models have provided a wealth of knowledge and insight over the past decades into some of the physiological and pathophysiological mechanisms of human biology and disease [77–79]. Nevertheless, the lung, as well as all other organs, is a 3D tissue structure *in vivo*. The 3D structure of every tissue is highly reliant on its native ECM, which is specialized for that tissue and the mechanical stresses it must endure *in situ*. The cells residing in the lung naturally experience physical interactions with their relative ECM in either 2- or 3-D. The endothelial cells, as well as the alveolar and airway epithelium experience a 2D interaction with the basement membrane that lies beneath their basal surfaces, whereas the mesenchymal cells that reside in the interstitium experience 3D interactions with their surrounding ECM. When put together the whole model is a complex 3D structure with intricate interactions between the resident cells and the ECM. The inflow of transient immune cells is an element that is not within the scope of the models discussed in this chapter.

When culturing cells in a 3D environment using models such as hydrogels or matrices, the cells have the opportunity to adhere in all dimensions to the matrix fibers that surround them, and consequently do not experience forced polarity [77, 80, 81]. These engagements occur via the binding of cell surface integrins to defined motifs (e.g., arginine-glycine-aspartate (RGD) motifs on fibronectin)) present on ECM proteins. Through this binding, cells sense the stiffness of the surrounding ECM, a process referred to as mechanosensing [82–86]. The mechanical stimuli from the ECM are then converted into biochemical activity activating intracellular signaling pathways resulting in gene expression responsible for regulating cell survival, proliferation, differentiation, apoptosis, ECM protein synthesis and secretion [85]. In addition, matrix fibers sequester soluble factors (e.g. growth factors, cytokines, extracellular vesicles, chemokines) and nutrients through entrapment and binding to proteoglycans and GAGs, potentially exposing cells to a gradient of nutrients, growth factors and soluble factors [77, 79, 87, 88]. The addition of a third dimension is a logical step forward to make the models used for studying cell interactions in lung diseases more translational, and with the incorporation of the ECM these innovative models will allow the creation of more intricate co-culture systems to answer more complex questions about lung pathophysiology [89].

3D MODELS – 1: SINGLE-PROTEIN MODELS

Collagen

One of the most commonly used 3D models which consist of one ECM protein are models based on collagen type I. Collagen type I is commercially available, but it can also easily be derived from rodent, porcine, bovine or human sources, and can be relatively cheap to produce in large quantities [90]. Secondly, collagen can be used in different forms of biomaterials such as hydrogels or sponges [91]. Since collagen is the most abundant ECM molecule in native tissues, which modulates and supports the survival of different cell types, it makes collagen scaffolds a good model for mimicking *in vivo* tissue. Cells can be cultured in 3D collagen models for days and weeks. Cells grown in such an environment are likely to maintain similar behavior, migration, attachment through GFOGER, GVOGEA, GLOGEN and other sites and signaling pathways to those enacted in the lungs [92, 93] **(Figure 2)**. Recently, 3D collagen scaffolds have been used for exploring alveolar recovery and angiogenesis after lung injury. After the implantation procedure, a collagen scaffold lost 30% of its size by the 14th day and had almost completely degraded by the 90th day *in vivo* [94]. In other research, a 3D collagen model has been used to deliver epithelial cells and fibroblasts to rabbit trachea *in vivo* [95]. Thirdly, the ability to modify gel stiffness

or pore size (the distance between fibers) by changing the number of cross-links and / or collagen concentration makes this model interesting for studying conditions which alter the biomechanical properties of surrounding tissue [96]. The stiffness of collagen substrates can be regulated from one hundred Pa up to several kPa, which mimics the biomechanical conditions of fibrotic, normal or emphysematous lungs. Finally, collagen models are compatible with using standard commercially available kits for endpoint measurements such as RNA, DNA, protein isolation and immunokits. All these advantages make collagen gels a good model for studying lung diseases, metastatic growth, wound repair and fibrosis [55, 66, 90, 97].

Collagen models have several limitations that should be recognized. Fibroblasts, and other mesenchymal cells, will contract/rearrange the hydrogel [98]. The structure of a collagen hydrogel, particularly the fiber arrangement within the hydrogel, can be altered by pH, ionic concentration, and temperature through effects on collagen polymerization [96]. In the end, collagen models are limited by their simplicity: cells only interact with one type of matrix protein, there is a lack of broad tunability, and the cells embedded within these hydrogels can elicit undesirable effects on the structural assembly of the scaffold.

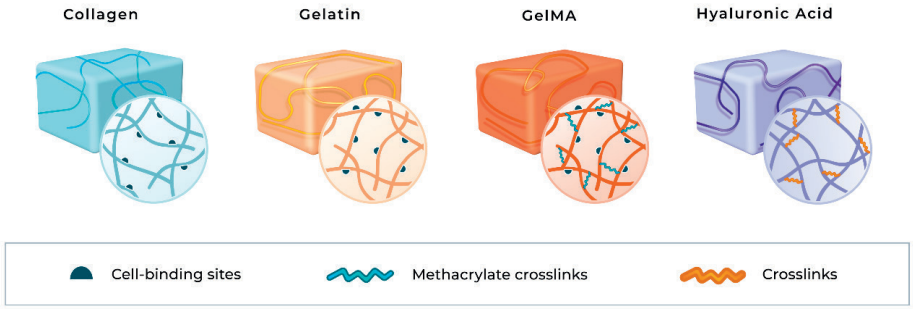

■ **Figure 2: Schematic representation of different types of hydrogels made with single ECM proteins.** Hydrogels of collagen, gelatin and their derivatives present cell-binding sites that facilitate cell attachment. Hyaluronic acid hydrogels in their native form do not contain any cell-binding sites. GelMA and hyaluronic acid hydrogels usually have crosslinks between the protein chains, reinforcing the overall structure and providing mechanical support.

Gelatin & Methacrylated Gelatin (GelMA)

Gelatin is a naturally occurring, and hydrophilic protein, obtained as a result of permanent hydrolysis of collagen [99]. Depending on the method used for its production, there are two types of gelatin type A and type B. Acidic hydrolysis, which

yields type A gelatin, negligibly affects amide groups. Conversely, alkaline hydrolysis converts glutamine and asparagine to glutamate and aspartate residues respectively, resulting in type B gelatin [99]. Gelatin is less immunogenic compared to collagen due to fewer aromatic groups. Moreover, it retains the RGD sequence and MMP degradation sites of the parent collagen molecule that plays an indispensable role in orchestrating cell-matrix adhesion and enabling migration and cellular remodeling respectively [99, 100]. Gelatin is both biodegradable and a biocompatible material and is economical to produce and abundantly extractable from porcine skin, fish, bovine hides, and porcine and bovine bones [101]. Given the above enticing properties, gelatin is one of the most extensively used polymers in the food, pharmaceutical, cosmetic, and biomedical industry and is a generally regarded as safe material.

Gelatin is thermo-reversible and forms a hydrogel as the temperature decreases below 30-35°C [102]. This occurs as gelatin sustains a conformation change from a random coil to triple helix and rearrangement of the triple helices gives rise to a huge polymer network. However, these non-covalent (hydrogen and van der Waals) interactions are broken as the temperatures rise above 30-35°C. In fact, gelatin dissolves in water at 37°C and as a result, native gelatin hydrogels have low stability and elasticity and poor mechanical properties [102]. These limitations are often assuaged by covalently crosslinking gelatin either in its native form or following functionalization of its side chains [103]. Native gelatin can be crosslinked chemically or enzymatically, while modified gelatin is commonly crosslinked thermally, enzymatically or using photo-initiators [103-106] **(Figure 2)**.

Gelatin has been used for a myriad of biomedical applications such as to produce micro or nanoparticles, polymeric fibers and hydrogels for tissue-engineered scaffolds and bioadhesives [107]. 3D bioprinting has especially proven to be an extremely valuable technique in terms of recreating organs with complex architectures, such as lungs, as it enables layer-by-layer deposition of biomaterials and/or cells [108]. Several studies have used gelatin as a bio-ink to print lung scaffolds. For instance, a sodium alginate-gelatin hydrogel, encapsulating non-small cell lung carcinoma patient-derived xenograft cells and cancer associated lung fibroblasts, was 3D printed to model tumor microenvironment *in vitro* [109]. The printed scaffold supported the development of 3D co-culture spheroids up to 25 days. Additionally, tumor-stromal crosstalk was demonstrated by increased expression of vimentin, α-SMA (smooth muscle actin), and loss of E cadherin in co-culture spheroids [109]. This composite sodium alginate-gelatin hydrogel has also been used to support culture of lung cancer cells (A549 and 95D) for at least 2 weeks. Furthermore, 3D culture of these cancer cells enhanced their migratory properties and invasiveness compared to their 2D cultured counterparts [110].

Interestingly, gelatin has been used to produce microbubble-scaffolds, using specialized microfluidic devices, to mimic alveoli structure [111, 112]. A two-channel fluid jacket microfluidic device yielded 3D gelatin microbubble scaffolds that were seeded with mouse pulmonary stem/progenitor cells (mPSCs) and supported the differentiation of mPSCs into alveolar pneumocytes [111]. Additionally, a four-channel microfluidic device has been used to generate disc-shaped gelatin microbubble scaffolds with a uniform pore size of 100µm resembling the alveoli structure [112]. A549 cells seeded in these scaffolds had higher drug resistance compared to their 2D controls and hence the 3D hydrogels are better models for anticancer drugs screening [112]. Microfluidic devices for *in vitro* modeling of the lung microenvironment have also gained traction. Recently, gelatin methacrylate (GelMA) was used to mimic the lung microenvironment in an airway-on-chip model [113]. In this model, the biological properties of GelMA were further enhanced by resuspending Matrigel particulates and encapsulating lung fibroblasts within the GelMA solution [113]. Furthermore, the alveolar-capillary barrier microenvironment was modeled to study the influence of the ECM structure and mechanics on epithelial cell injury during cyclic airway reopening during mechanical ventilation [114].

Another novel use of gelatin has been in the development of prosthetics for tracheal reconstruction [115, 116]. Recently, it has been demonstrated that gelatin-based scaffolds are compatible with techniques such as electrospinning, micro-molding, and photolithography to produce micro- and nano- patterned topographical features to mimic native ECM [117, 118]. The mucosal folding of the respiratory track was mimicked in cell laden GelMA hydrogels that were bonded to pre-stretched tough hydrogel substrates composed of interpenetrating polymer networks of polyacrylamide and alginate. Relaxation of the substrate induced controlled patterns in the GelMA layer [119]. In another study, the microarchitecture of ECM fibers of healthy and diseased lung tissue was mimicked using PCL-gelatin electrospun fibers [114].

In conclusion, gelatin's ability to support cellular activity, modifiable mechanical properties, and several functional groups for chemical modifications make it a highly desirable biomaterial for the generation of 3D models for cell culture with versatile potential for tissue engineering and regenerative medicine particularly in pulmonary diseases.

Other ECM components

Other ECM components and their derivatives have also been used for generating 3D *in vitro* lung models, although model types and the applications of these systems are limited. One of the most applied ECM components is hyaluronic acid (HA), also called hyaluronan: a linear polysaccharide composed of repeating units of

disaccharides (glucuronic acid and N-acetyl glucosamine) [120]. While most studies focus on drug delivery approaches using HA [121], the use of this flexible biomaterial as an *in vitro* model in hydrogel form has also been explored. In its native form, HA does not form viable hydrogels; however, chemical functionalization (additions of methacrylate [122], thiol [123], furan [124]) of HA, as well as combining HA hydrogels with other biopolymers (gelatin [125, 126], fibronectin [127], methylcellulose [124]) results in hydrogel formation **(Figure 2)**. Varying the concentration of HA and the degree of modification of HA molecules results in great variability in the mechanical properties of the resultant hydrogel: (0.35 ± 0.05 kPa – 1613.0 ± 248.5 kPa) [122, 128] . Considering the high range, it would be possible to use such models in fibrotic lung disease research, where hydrogels with higher stiffness can be used to mimic the fibrotic microenvironment.

Other ECM components have been used to construct 3D ECM-based *in vitro* models. Fibronectin, an important ECM glycoprotein, was modified with the addition of polyethylene glycol (PEG) molecules to form mechanically tunable hydrogels that could support sprouting of human umbilical vein endothelial cells (HUVECs) in an *in vitro* model [129]. Similarly, fibrinogen was used in combination with collagen to formulate *in vitro* models with varying stiffness [130]. Fibrin hydrogels were used to create a 3D *in vitro* model for fibroblast-epithelial cell co-culture to mimic the airway [131, 132], or even a tri-culture model for epithelial cells, fibroblasts and endothelial cells [133]. Just like in collagen, gelatin or HA hydrogels, it is possible to modulate the mechanical properties of fibrin hydrogels within an extensive range (1.1 ± 0.3 kPa – 31 ± 2.8 kPa), which increases the applicability of these hydrogels to a variety of lung diseases as well as representing specific locations within lung tissue [134].

3D MODELS – 2: ECM MODELS WITH COMPLEX ECM MIXTURES

Decellularized lung scaffolds

Decellularization is the process of removing cells from tissue or whole organs while minimizing the damage to and preserving the biological integrity, composition, and mechanical properties of the ECM [135]. This technique has enabled generation of acellular, native, and 3D ECM *in vitro* and *ex vivo* models that are useful to study tissue-specific cell-ECM component interactions in healthy and diseased states, and the dynamic reciprocity between cells and their microenvironment [136-138]. Moreover, decellularization of allogeneic and xenogeneic ECM grafts followed by recellularization can ideally provide an unlimited supply for clinical applications such as tissue reconstruction and transplantation [137-139]. Although this has

been realized for 2D tissues with simpler microstructures (skin, small intestinal submucosa, and pericardium) [140], organs with higher complexity such as lungs have proven to be more challenging. There are several methods that can be used in combination to decellularize tissues and organs including physical, chemical, or enzymatic as depicted in **Figure 3A** [141]. Decellularization of lung tissue is mainly achieved by perfusion of decellularization solutions through the airways or vasculature of the lungs or by immersion of tissue segments in these solutions with or without agitation [142].

To mimic the lung microenvironment and stimulate functional organ regeneration, decellularized tissues have been frequently repopulated with a variety of progenitor and stromal cells [142]. Precision cut lung slices (PCLS) have become popular *ex vivo* experimental models and these can also be used in the decellularized form. A positive feedback loop between IPF ECM and fibroblasts was demonstrated when the diseased ECM stimulated pathological gene expression enriched for ECM proteins in fibroblasts seeded on decellularized IPF PCLS [59]. Recently, ECM deposition by non-diseased lung fibroblasts seeded in acellular non-diseased lung PCLS resembled native lung tissue sections more closely compared to a monolayer of fibroblasts grown on plastic [143]. The influence of the microenvironment on cellular behavior was further demonstrated when non-diseased lung fibroblasts differentially expressed basement membrane proteins when seeded in IPF PCLS compared to non-diseased PCLS [144].

Decellularized lung models have played an indispensable role in unravelling underlying disease mechanisms that promote and enhance pathogenesis. For instance, placental microvascular pericytes sustained phenotypic transition (increased expression of α-SMA) when cultured on decellularized IPF lungs compared to decellularized non-diseased lungs, which facilitated a better understanding of the influence of pericytes in progression of IPF [145]. The crucial role of lysyl oxidase enzymes in increased tissue stiffness was uncovered when its inhibitor, β-Aminoproprionitrile, decreased TGF-β induced thickening of collagen fibers in non-disease decellularized lung scaffolds seeded with non-diseased lung fibroblasts [55].

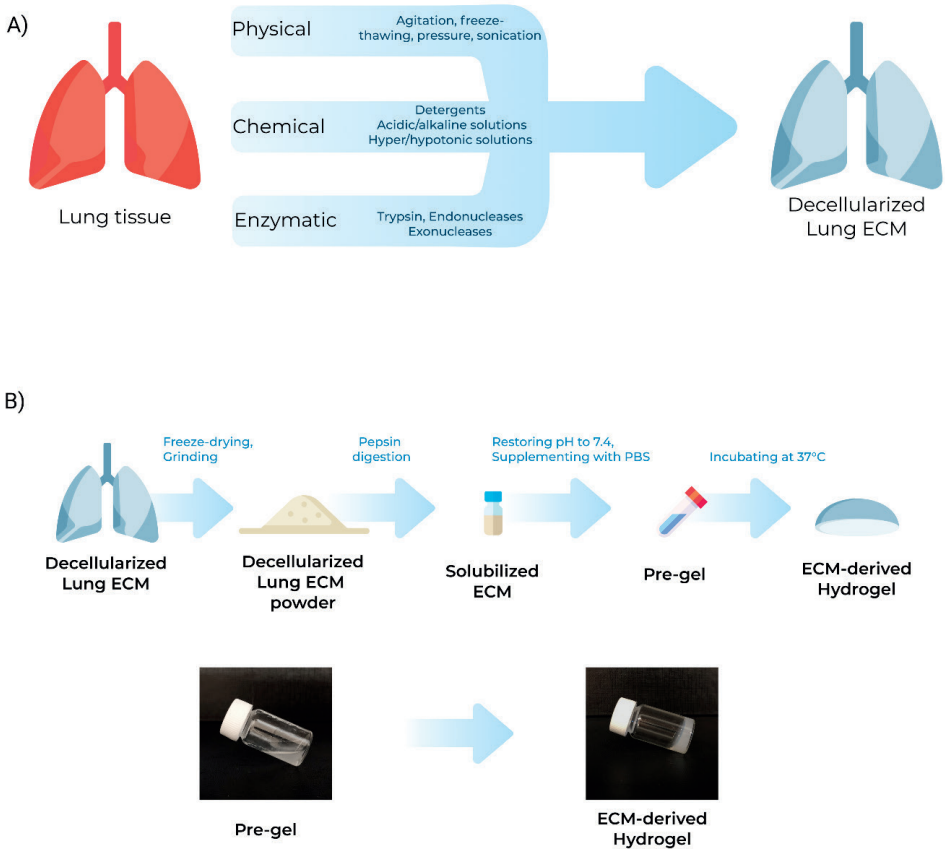

■ **Figure 3: Generation and usage of decellularized lung ECM as a hydrogel.** A) Different methods applied to decellularize lung tissue include physical methods such as freeze thawing or sonication, chemical methods that employ (combination of) detergents and acidic/alkaline solutions and enzymatic methods with endonucleases or exonucleases. Combinations of physical, chemical and enzymatic decellularization methods has also been employed. B) Schematic representation of generation of ECM-derived hydrogels from the decellularized lung ECM. Lung ECM powder, which is obtained after freeze-drying and grinding the decellularized lung scaffold, is digested using pepsin in acidic media. Then, the resulting solution is brought back to pH 7.4 and supplemented with PBS to equilibrate the salt concentration. This solution, also called "pre-gel" can form hydrogels irreversibly once it is incubated at 37°C.

Apart from IPF, acellular scaffolds have also been derived from COPD lung tissue. COPD derived bronchial epithelial cells had enhanced proliferative capacity and maintained basal cell phenotype when seeded on COPD-derived decellularized bronchial constructs compared to non-diseased scaffolds [146]. In contrast, no variation was observed in the differentiation or proliferative potential of emphysematous lung-derived mesenchymal stromal cells grown on decellularized

non-disease and emphysematous decellularized lung tissue, although reduced growth factor production was observed in the latter [147]. These results clearly showed that the state of the ECM largely influences the cellular response and this response varies between different cell types. Another prominent chronic lung disease is asthma. The mechanisms involved in ECM remodeling in asthma have not been as thoroughly investigated using decellularized ECM models as IPF and COPD, reflecting the lack of available tissues from asthmatic donors for decellularization. Preliminary investigations using asthmatic equine models have indicated decreased levels of collagen I and fibronectin levels in bronchi-derived acellular scaffolds [148]. However future investigations of this model are warranted, albeit challenging.

Decellularized lung scaffolds have also been used to model the tumor microenvironment. Decellularized rat lungs repopulated with human cancer cell lines and cultured in customized bioreactors, produced tumor nodules and expressed MMP 9, neither of which was evident in equivalent 2D models [149]. Interestingly, murine decellularized lung matrices supported the invasion and colonization of metastatic breast cancer cells while the majority of non-metastatic cells were unable to survive under the same conditions [150]. These models serve as powerful tools to understand cancer metastasis and in turn will provide platforms for assessing anti-cancer therapies.

Whole lung decellularization for transplantation has been attempted by several research groups. However, these have mainly been restricted to animal models (rodents, porcine, and canine lungs) that have been recolonized for short periods with animal or human lung cells, and in some studies implanted in respective animal models to test compliance and functionality of the engineered lungs [151-160]. Whole human lung or lobe decellularization and recellularization is less frequent for obvious availability and ethical reasons [152, 161]. In addition, there are several recognized limitations that must be overcome to advance this application including the standardization of the patient-derived lung samples and using these scaffolds as *in vitro* models. Moreover, more advanced methods for testing the capacity of the gas exchange in a recellularized *in vitro* model are required to evaluate the efficiency of the recellularization process and subsequent functionality of the engineered lung.

Decellularization presents a potent methodology for the development of *in vitro* models as age and injury induced changes in ECM composition and characteristic anatomical alterations were retained post decellularization of lungs reflective of the original disease state [153, 159, 162]. Extensive information about other factors influencing cellular behavior in response to decellularized scaffolds can be found

elsewhere [140]. Therefore, the use of decellularized tissue for 3D modeling is an advantageous technique in terms of mimicking native tissue structure and composition. However, these models are still a long way from modeling the complexity of lung tissue. The development of long term functional units for gas exchange is of utmost importance. However, this requires both- epithelized airways and endothelialized vessels. Vascularization and innervation of decellularized tissue, seeding, and expanding multiple cell types and lineages together, and developing appropriate methods to measure experimental outcomes are some of the major challenges yet to be overcome.

Decellularized lung ECM-derived hydrogels

Although single protein hydrogels can mimic the mechanical properties and elevate the cell culture model to 3D, they do not represent the full complexity of the matrisome. Next to using decellularized matrices, another approach for incorporating the complexity of the ECM into 3D models has emerged in recent years, lung-derived ECM hydrogels [58, 163]. These hydrogels are generated from solubilized decellularized lung ECM (**Figure 3B**). The decellularized ECM is lyophilized and milled into a fine powder, to increase the surface area of the ECM to aid in the solubilization process. The solubilization of the ECM has most often been performed via pepsin digestion in an acidic buffer [58, 163, 164]. During pepsin digestion, the ECM proteins are enzymatically solubilized into a monomeric suspension, generally under constant agitation for an extended time (24-72h, although this varies for different tissues) at room temperature [164]. After digestion, the pH of the solution is neutralized and buffered with PBS to prepare a thermosensitive ECM pre-gel solution which spontaneously self-assembles into a hydrogel when incubated at 37°C [165]. Recently, it has been shown that ultrasonic cavitation could also be used to solubilize the milled ECM, although the source of ECM was not lung tissue [166]. The whole process disrupts the original complex ultrastructure of the starting tissue ECM and reduces it to a suspension of its multitude of components. The pepsin solubilization process needs to be tailored to the specific organ and the success is dependent upon the pepsin digestion time which affects the mechanical properties such as stiffness and dictates the subsequent effect of the ECM hydrogel on cells [167]. Another important mechanical property for hydrogels is viscoelasticity. Viscoelasticity describes how a material that has both viscous (water, soluble factors) and elastic (ECM proteins) components, distributes forces when a stress is applied [168]. Both stiffness and viscoelasticity have been found to influence cell behavior such as spreading, proliferation and differentiation [169, 170]. For the lung, hydrogel models that incorporate the entirety of the ECM have been made from porcine lungs [163, 171, 172] and human lungs [58]. For now, most cell experiments using

porcine lung ECM hydrogels have seeded cells on top of the hydrogel. Human lung fibroblasts, mesenchymal stromal cells and pulmonary vascular endothelial cells were able to survive and grow on the porcine lung ECM hydrogel [163]. The mechanical properties of human lung ECM hydrogels, both healthy and diseased (IPF and COPD) were compared to those of intact whole lung tissue pieces [58]. The differences in stiffness seen between healthy, COPD and IPF tissues were still present, albeit to a lesser degree, in the corresponding ECM hydrogels. The stiffness of ECM hydrogels resembled that of whole tissue while their viscoelasticity differed. Lung ECM hydrogels are still a very novel tool and there remains a lot to optimize and discover; however, incorporating these in 3D co-culture models will allow researchers to ask and answer more complex questions about the physiology and pathophysiology of the lung and the role of the ECM in disease pathogenesis.

Application of these lung ECM-derived hydrogels in disease-specific models can be further specialized by several different means. While using the pepsin-solubilized ECM as the bulk hydrogel [58, 173] already improves the biomimicry of the 3D ECM-based *in vitro* lung models, using such in combination with other biopolymers could also provide extensive versatility. Although used in a 2D culture model, the combination of solubilized decellularized ECM from control or IPF lungs with polyacrylamide hydrogels with defined stiffness values was shown to form hydrogels with disease-specific compositions [145]. Similarly, reinforcing the solubilized decellularized ECM with alginate resulted in the possibility of fine-tuning the mechanical properties of the resulting hydrogels [171]. The same study also elegantly demonstrated the application of the reinforced ECM hydrogel as a bioink for bioprinting of 3D lung models.

Chemically modifying the solubilized ECM to modulate the biochemical and biomechanical properties provides another alternative to improve the applicability of these hydrogels in 3D models. By functionalizing the solubilized ECM with thiol groups (thiolation) and combining this with methacrylated PEG (PEGMA) molecules, Petrou et al. generated ECM-derived hydrogels with tunable mechanical properties in two separate steps [172]. While the initial stiffness values were adjusted by changing the concentration of the modified ECM in the solution, a second step of stiffening these hydrogels was achieved using photo-crosslinking the PEGMA molecules, resulting in great variability in the stiffness values (soft: 3.63 ± 0.24 kPa, stiff: 13.35 ± 0.83 kPa). The exciting opportunity of utilizing (disease-specific) lung ECM-derived hydrogels brings various levels of innovation to the development of novel 3D *in vitro* models for lung diseases. While alternatives to pepsin digestion have yet to be discovered to prepare solubilized ECM, ECM-derived hydrogels enhance the biomimicry of *in*

vitro models. In addition, the possibility of fine-tuning mechanical properties either by reinforcing the solution with additional biopolymers or functionalization with chemical groups leads the way to de-couple the contribution of biochemical and biomechanical changes in the progression of chronic lung diseases.

Another interesting method to prepare 3D *in vitro* models using solubilized decellularized lung ECM is electrospinning, a versatile scaffold preparation method that allows fine-tuning the size and the alignment of the produced fibers [174]. Utilizing the possibility of modulating the stiffness, fiber alignment and other mechanical properties as well as combinations of them in 3D *in vitro* cultures would enhance the capacity for mimicry of the *in vivo* lung ECM environment of these models.

CHALLENGES

Excitingly, ECM-based 3D culture systems for the *in vitro* modeling of lung diseases have advanced significantly in the last decade. While these 3D culture systems indicated the limitations of 2D culturing, there are many challenges that must be faced before these culture models can become mainstream tools **(Figure 4)**. Single ECM protein models such as collagen or gelatin bring a reductionist approach for research on lung diseases. The possibility of fine-tuning the mechanical properties of such hydrogels allows mimicking many different stages of lung development and disease, yet they lack the complex composition of the native lung ECM. Especially in chronic lung diseases such as asthma, COPD or IPF, the composition of ECM is radically altered, and such changes are not reflected in these models. The altered number and availability of cell binding domains are another limitation of single-protein-based culture systems, mimicking the altered ECM in this aspect is not always possible with these models.

The 3D culture systems derived from the whole lung ECM provide advantages over the single-protein counterparts, especially in providing a more physiological composition and structural arrangement of the ECM in health and disease. Using decellularized matrices in various forms such as tissue pieces or PCLS for disease modeling will advance our understanding of many different disease underlying mechanisms; however, the current procedures for decellularization of lung tissue limit the retention of the total composition of the ECM. Especially GAGs have been recognized to be lost during these harsh processes, and the potential impact of their loss in these culture systems has yet to be fully explored. Using the whole tissue ECM

scaffold in its native form brings the opportunity of utilizing the complex architecture of lung tissue in *in vitro* studies; however, introducing cells back to these samples is not challenge-free. Different strategies of decellularization generate differences between ECM components, structure, and mechanical properties of the obtained scaffold. The impact of these differences on recellularization remains unclear. Ensuring an appropriate 3D distribution of the cells with their correct physiological placement remains a major limitation in using decellularized lung pieces. Additionally, factors such as cell source and seeding density, optimal medium composition, flow rate, and accessibility of the injection site also play a key role in determining the success of recellularization [175]. Long term storage (> 1 year) of decellularized tissue has also proven challenging due to the loss of ECM structure and reduced mechanical and angiogenic properties [176].

Lung ECM-derived hydrogels, on the other hand, can address this problem by providing the control over shape and construction but lack the topographical organization of the ECM present *in vivo*. Since cells can be spatially introduced to the different parts of the hydrogel(s), placing the cells in a physiologically representative manner is possible when using these hydrogels. However, the current methodology to prepare such hydrogels is rather limited: pepsin digestion is currently the most applied method [164]. While the mechanical properties of these hydrogels can resemble the lung tissue in health and diseased states, the implications of the digestion procedure have recently been discussed [58, 167]. Another limitation in the ECM-derived hydrogels for creating 3D models for *in vitro* research is the mechanical tunability. Mechanical properties can be changed by varying the concentration of the initial ECM input, but this variation also changes other properties such as pore size and cell binding site availability. Recent studies have focused on chemically modifying the ECM-hydrogel solutions to introduce a chemical crosslinking for the possibility of tuning mechanical properties [172], while more research is required to understand the potential implications of these modifications other than changing mechanical properties.

CONCLUSIONS

In vitro models for mimicking the lung microenvironment have advanced greatly, especially in the last two decades. While conventional 2D cell and tissue culture models are being routinely used, there is an increasing trend towards research performed using advanced models. One of the most important characteristics of these advanced models is the improved dimensionality. A 3D culture environment

provides improved mimicry due to its resemblance to the physiological conditions, as *in vivo* the cells reside in a 3D network of native ECM proteins. These 3D culture setups can be realized via various means, with one of the well-characterized methods using individual components isolated from ECM. Collagen, gelatin or hyaluronic acid and their derivatives have been extensively studied, and thanks to the advances in the field of biomaterials, they provide great versatility in their applications for modeling lung disease and regeneration. Tunable mechanical properties, pore size, and fiber diameter in these models allow researchers to investigate the connections between the mechanical microenvironment and the cells in lung disease. Decellularized lung ECM, on the other hand, provides the physiologic architecture of the lung tissue, as well as preserving the native composition of the ECM. Using native decellularized lung ECM to understand how disease progresses and the underlying mechanisms has provided valuable information, not only to understand how cells interact with the ECM, but also how the 3D architecture of the lung tissue microenvironment plays a role in such interactions. Recently, processing these matrices to create a hydrogel derived from lung ECM itself has been demonstrated. In addition to keeping the native ECM composition, the biomechanical properties of these hydrogels resembled the biomechanical properties of tissue as well. Using diseased or healthy lung ECM-derived hydrogels alone or in combination with other materials to create advanced *in vitro* models will further improve our knowledge on lung diseases, repair and regeneration mechanisms.

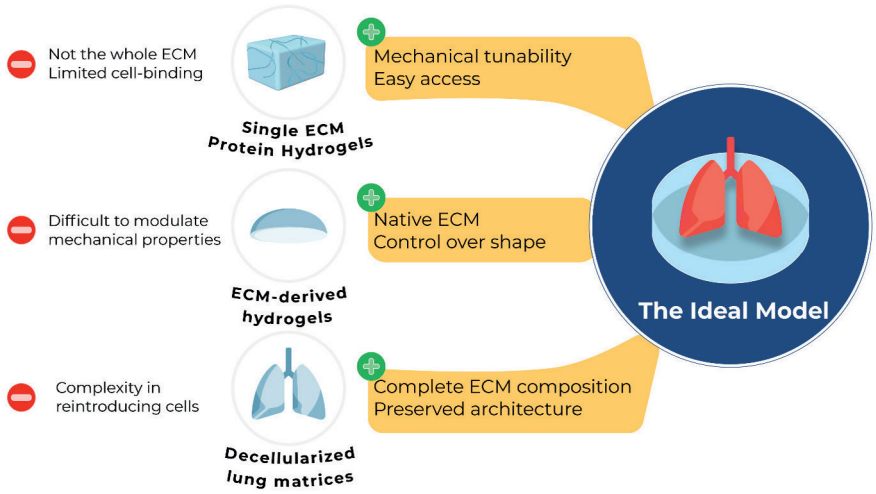

■ **Figure 4: Summary of challenges associated with different types of ECM-based 3D lung models for advanced cell culture and the properties of the ideal model for mimicking lung disease, repair and regeneration.**

As the fields of chemistry, (molecular) biology and biomaterials improve independently, more and more advanced *in vitro* models for 3D modeling of lung diseases, which is one of their intersection points, will be developed. Although there are challenges for each type of material used for such 3D models, as outlined in the previous section and **Figure 4**, combining the strengths of different models for building an ideal 3D *in vitro* lung model based on ECM will be possible in the near future. Such an ideal model would be easily available for both low and high throughput research, in addition to providing the opportunity to alter the mechanical properties without compromising the composition of the model. In concert, using native ECM for such models would enhance the physiological relevance. An ideal 3D model for the lung microenvironment would benefit from the possibility of controlling both the shape and the spatial arrangement of the cells introduced. As lung tissue has very well-defined ECM architecture, resembling this structure in an *in vitro* model would help researchers understand the influence of ECM architecture in disease, repair and regeneration processes.

In summary, ECM-based 3D *in vitro* models for modeling the lung microenvironment is a rapidly-advancing field and using such models will greatly improve our knowledge of lung disease and regeneration mechanisms.

REFERENCES

1. Frantz C, Stewart KM, Weaver VM. The extracellular matrix at a glance. *J Cell Sci* 2010: 123(Pt 24): 4195–4200.
2. Jarvelainen H, Sainio A, Koulu M, Wight TN, Penttinen R. Extracellular matrix molecules: potential targets in pharmacotherapy. *Pharmacol Rev* 2009: 61(2): 198–223.
3. Daley WP, Peters SB, Larsen M. Extracellular matrix dynamics in development and regenerative medicine. *J Cell Sci* 2008: 121(Pt 3): 255–264.
4. Matthes SA, Hadley R, Roman J, White ES. Comparative Biology of the Normal Lung Extracellular Matrix. *In:* Parent RA, ed. Comparative Biology of the Normal Lung. Academic Press, San Diego, 2015; pp. 387–402.
5. White ES. Lung extracellular matrix and fibroblast function. *Ann Am Thorac Soc* 2015: 12 Suppl 1(Suppl 1): S30–33.
6. Upagupta C, Shimbori C, Alsilmi R, Kolb M. Matrix abnormalities in pulmonary fibrosis. *Eur Respir Rev* 2018: 27(148): 180033.
7. McGowan SE. Extracellular matrix and the regulation of lung development and repair. *FASEB J* 1992: 6(11): 2895–2904.
8. Zhou Y, Horowitz JC, Naba A, Ambalavanan N, Atabai K, Balestrini J, Bitterman PB, Corley RA, Ding BS, Engler AJ, Hansen KC, Hagood JS, Kheradmand F, Lin QS, Neptune E, Niklason L, Ortiz LA, Parks WC, Tschumperlin DJ, White ES, Chapman HA, Thannickal VJ. Extracellular matrix in lung development, homeostasis and disease. *Matrix Biol* 2018: 73: 77–104.
9. Brandsma CA, Van den Berge M, Hackett TL, Brusselle G, Timens W. Recent advances in chronic obstructive pulmonary disease pathogenesis: from disease mechanisms to precision medicine. *J Pathol* 2020: 250(5): 624–635.
10. Theocharis AD, Skandalis SS, Gialeli C, Karamanos NK. Extracellular matrix structure. *Adv Drug Deliv Rev* 2016: 97: 4–27.
11. Mecham RP. Elastin in lung development and disease pathogenesis. *Matrix Biol* 2018: 73: 6–20.
12. Starcher BC. Lung elastin and matrix. *Chest* 2000: 117(5 Suppl 1): 229S–234S.
13. Joyce K, Fabra GT, Bozkurt Y, Pandit A. Bioactive potential of natural biomaterials: identification, retention and assessment of biological properties. *Signal Transduct* 2021: 6(1): 122.
14. Souza-Fernandes AB, Pelosi P, Rocco PR. Bench-to-bedside review: the role of glycosaminoglycans in respiratory disease. *Crit Care* 2006: 10(6): 237.
15. Karakioulaki M, Papakonstantinou E, Stolz D. Extracellular matrix remodelling in COPD. *Eur Respir Rev* 2020: 29(158): 190124.
16. Garg HG. Proteoglycans in Lung Disease. CRC Press, 2002.
17. Couchman JR, Pataki CA. An introduction to proteoglycans and their localization. *J Histochem Cytochem* 2012: 60(12): 885–897.
18. Xu J, Mosher D. Fibronectin and Other Adhesive Glycoproteins. *In:* Mecham RP, ed. The Extracellular Matrix: an Overview. Springer Berlin Heidelberg, Berlin, Heidelberg, 2011; pp. 41–75.

19. Saikumar Jayalatha AK, Hesse L, Ketelaar ME, Koppelman GH, Nawijn MC. The central role of IL-33/IL-1RL1 pathway in asthma: From pathogenesis to intervention. *Pharmacol Ther* 2021: 225: 107847.

20. Araujo BB, Dolhnikoff M, Silva LF, Elliot J, Lindeman JH, Ferreira DS, Mulder A, Gomes HA, Fernezlian SM, James A, Mauad T. Extracellular matrix components and regulators in the airway smooth muscle in asthma. *Eur Respir J* 2008: 32(1): 61-69.

21. James AL, Maxwell PS, Pearce-Pinto G, Elliot JG, Carroll NG. The relationship of reticular basement membrane thickness to airway wall remodeling in asthma. *Am J Respir Crit Care Med* 2002: 166(12 Pt 1): 1590-1595.

22. Burgess JK, Mauad T, Tjin G, Karlsson JC, Westergren-Thorsson G. The extracellular matrix - the under-recognized element in lung disease? *J Pathol* 2016: 240(4): 397-409.

23. Burgstaller G, Oehrle B, Gerckens M, White ES, Schiller HB, Eickelberg O. The instructive extracellular matrix of the lung: basic composition and alterations in chronic lung disease. *Eur Respir J* 2017: 50(1).

24. Gu BH, Madison MC, Corry D, Kheradmand F. Matrix remodeling in chronic lung diseases. *Matrix Biol* 2018: 73: 52-63.

25. Wight TN, Frevert CW, Debley JS, Reeves SR, Parks WC, Ziegler SF. Interplay of extracellular matrix and leukocytes in lung inflammation. *Cell Immunol* 2017: 312: 1-14.

26. Ito JT, Lourenco JD, Righetti RF, Tiberio I, Prado CM, Lopes F. Extracellular Matrix Component Remodeling in Respiratory Diseases: What Has Been Found in Clinical and Experimental Studies? *Cells* 2019: 8(4): 342-342.

27. Liu G, Philp AM, Corte T, Travis MA, Schilter H, Hansbro NG, Burns CJ, Eapen MS, Sohal SS, Burgess JK, Hansbro PM. Therapeutic targets in lung tissue remodelling and fibrosis. *Pharmacol Ther* 2021: 225: 107839.

28. Pini L, Hamid Q, Shannon J, Lemelin L, Olivenstein R, Ernst P, Lemiere C, Martin JG, Ludwig MS. Differences in proteoglycan deposition in the airways of moderate and severe asthmatics. *Eur Respir J* 2007: 29(1): 71-77.

29. Bousquet J, Chanez P, Lacoste JY, White R, Vic P, Godard P, Michel FB. Asthma: a disease remodeling the airways. *Allergy* 1992: 47(1): 3-11.

30. Burgess JK, Boustany S, Moir LM, Weckmann M, Lau JY, Grafton K, Baraket M, Hansbro PM, Hansbro NG, Foster PS, Black JL, Oliver BG. Reduction of tumstatin in asthmatic airways contributes to angiogenesis, inflammation, and hyperresponsiveness. *Am J Respir Crit Care Med* 2010: 181(2): 106-115.

31. Mostaco-Guidolin LB, Osei ET, Ullah J, Hajimohammadi S, Fouadi M, Li X, Li V, Shaheen F, Yang CX, Chu F, Cole DJ, Brandsma CA, Heijink IH, Maksym GN, Walker D, Hackett TL. Defective Fibrillar Collagen Organization by Fibroblasts Contributes to Airway Remodeling in Asthma. *Am J Respir Crit Care Med* 2019: 200(4): 431-443.

32. Burgess JK, Jonker MR, Berg M, Ten Hacken NTH, Meyer KB, van den Berge M, Nawijn MC, Heijink IH. Periostin: contributor to abnormal airway epithelial function in asthma? *Eur Respir J* 2021: 57(2): 2001286.

33. Lau JY, Oliver BG, Baraket M, Beckett EL, Hansbro NG, Moir LM, Wilton SD, Williams C, Foster PS, Hansbro PM, Black JL, Burgess JK. Fibulin-1 is increased in asthma--a novel mediator of airway remodeling? *PLoS One* 2010: 5(10): e13360.

34. Liu G, Cooley MA, Nair PM, Donovan C, Hsu AC, Jarnicki AG, Haw TJ, Hansbro NG, Ge Q, Brown AC, Tay H, Foster PS, Wark PA, Horvat JC, Bourke JE, Grainge CL, Argraves WS, Oliver BG, Knight DA, Burgess JK, Hansbro PM. Airway remodelling and inflammation in asthma are dependent on the extracellular matrix protein fibulin-1c. *J Pathol* 2017: 243(4): 510–523.

35. Bidan CM, Veldsink AC, Meurs H, Gosens R. Airway and Extracellular Matrix Mechanics in COPD. *Front Physiol* 2015: 6: 346.

36. Navratilova Z, Kolek V, Petrek M. Matrix Metalloproteinases and Their Inhibitors in Chronic Obstructive Pulmonary Disease. *Arch Immunol Ther Exp (Warsz)* 2016: 64(3): 177–193.

37. Merrilees MJ, Ching PS, Beaumont B, Hinek A, Wight TN, Black PN. Changes in elastin, elastin binding protein and versican in alveoli in chronic obstructive pulmonary disease. *Respir Res* 2008: 9(1): 41.

38. Annoni R, Lancas T, Yukimatsu Tanigawa R, de Medeiros Matsushita M, de Morais Fernezlian S, Bruno A, Fernando Ferraz da Silva L, Roughley PJ, Battaglia S, Dolhnikoff M, Hiemstra PS, Sterk PJ, Rabe KF, Mauad T. Extracellular matrix composition in COPD. *Eur Respir J* 2012: 40(6): 1362–1373.

39. Stone PJ, Gottlieb DJ, O'Connor GT, Ciccolella DE, Breuer R, Bryan-Rhadfi J, Shaw HA, Franzblau C, Snider GL. Elastin and collagen degradation products in urine of smokers with and without chronic obstructive pulmonary disease. *Am J Respir Crit Care Med* 1995: 151(4): 952–959.

40. van Straaten J, Coers W, Noordhoek J, Flipsen J, Kauffman H, Timens W, Postma D. Proteoglycan changes in the extracellular matrix of lung tissue from patients with pulmonary emphysema. *Mod Pathol* 1999: 12(7): 697 - 705.

41. Tjin G, Xu P, Kable SH, Kable EP, Burgess JK. Quantification of collagen I in airway tissues using second harmonic generation. *J Biomed Opt* 2014: 19(3): 36005.

42. Salazar LM, Herrera AM. Fibrotic response of tissue remodeling in COPD. *Lung* 2011: 189(2): 101–109.

43. Suki B, Ito S, Stamenovic D, Lutchen KR, Ingenito EP. Biomechanics of the lung parenchyma: critical roles of collagen and mechanical forces. *J Appl Physiol* 2005: 98(5): 1892–1899.

44. Martinez FJ, Collard HR, Pardo A, Raghu G, Richeldi L, Selman M, Swigris JJ, Taniguchi H, Wells AU. Idiopathic pulmonary fibrosis. *Nat Rev Dis Pri* 2017: 3(1): 17074.

45. Jenkins G. Demystifying pulmonary fibrosis. *Am J Physiol Lung Cell Mol Physiol* 2020: 319(3): L554–L559.

46. Selman M, Pardo A. When things go wrong: exploring possible mechanisms driving the progressive fibrosis phenotype in interstitial lung diseases. *Eur Respir J* 2021: 58(3): 2004507.

47. Blokland KEC, Pouwels SD, Schuliga M, Knight DA, Burgess JK. Regulation of cellular senescence by extracellular matrix during chronic fibrotic diseases. *Clin Sci* 2020: 134(20): 2681–2706.

48. Vasse GF, Nizamoglu M, Heijink IH, Schleputz M, van Rijn P, Thomas MJ, Burgess JK, Melgert BN. Macrophage-stroma interactions in fibrosis: biochemical, biophysical, and cellular perspectives. *J Pathol* 2021: 254(4): 344–357.

49. Haak AJ, Tan Q, Tschumperlin DJ. Matrix biomechanics and dynamics in pulmonary fibrosis. *Matrix Biol* 2018: 73: 64–76.

50. Herrera J, Henke CA, Bitterman PB. Extracellular matrix as a driver of progressive fibrosis. *J Clin Invest* 2018: 128(1): 45–53.

51. Levi N, Papismadov N, Solomonov I, Sagi I, Krizhanovsky V. The ECM path of senescence in aging: components and modifiers. *FEBS J* 2020: 287(13): 2636–2646.

52. Klingberg F, Hinz B, White ES. The myofibroblast matrix: implications for tissue repair and fibrosis. *J Pathol* 2013: 229(2): 298–309.

53. Blaauboer ME, Boeijen FR, Emson CL, Turner SM, Zandieh-Doulabi B, Hanemaaijer R, Smit TH, Stoop R, Everts V. Extracellular matrix proteins: a positive feedback loop in lung fibrosis? *Matrix Biol* 2014: 34: 170–178.

54. Enomoto N, Suda T, Kono M, Kaida Y, Hashimoto D, Fujisawa T, Inui N, Nakamura Y, Imokawa S, Funai K, Chida K. Amount of elastic fibers predicts prognosis of idiopathic pulmonary fibrosis. *Respir Med* 2013: 107(10): 1608–1616.

55. Tjin G, White ES, Faiz A, Sicard D, Tschumperlin DJ, Mahar A, Kable EPW, Burgess JK. Lysyl oxidases regulate fibrillar collagen remodelling in idiopathic pulmonary fibrosis. *Dis Model Mech* 2017: 10(11): 1301–1312.

56. Jones MG, Andriotis OG, Roberts JJ, Lunn K, Tear VJ, Cao L, Ask K, Smart DE, Bonfanti A, Johnson P, Alzetani A, Conforti F, Doherty R, Lai CY, Johnson B, Bourdakos KN, Fletcher SV, Marshall BG, Jogai S, Brereton CJ, Chee SJ, Ottensmeier CH, Sime P, Gauldie J, Kolb M, Mahajan S, Fabre A, Bhaskar A, Jarolimek W, Richeldi L, O'Reilly KM, Monk PD, Thurner PJ, Davies DE. Nanoscale dysregulation of collagen structure-function disrupts mechano-homeostasis and mediates pulmonary fibrosis. *eLife* 2018: 7.

57. Booth AJ, Hadley R, Cornett AM, Dreffs AA, Matthes SA, Tsui JL, Weiss K, Horowitz JC, Fiore VF, Barker TH, Moore BB, Martinez FJ, Niklason LE, White ES. Acellular normal and fibrotic human lung matrices as a culture system for in vitro investigation. *Am J Respir Crit Care Med* 2012: 186(9): 866–876.

58. de Hilster RHJ, Sharma PK, Jonker MR, White ES, Gercama EA, Roobeek M, Timens W, Harmsen MC, Hylkema MN, Burgess JK. Human lung extracellular matrix hydrogels resemble the stiffness and viscoelasticity of native lung tissue. *Am J Physiol Lung Cell Mol Physiol* 2020: 318(4): L698–L704.

59. Parker MW, Rossi D, Peterson M, Smith K, Sikstrom K, White ES, Connett JE, Henke CA, Larsson O, Bitterman PB. Fibrotic extracellular matrix activates a profibrotic positive feedback loop. *J Clin Invest* 2014: 124(4): 1622–1635.

60. Philp CJ, Siebeke I, Clements D, Miller S, Habgood A, John AE, Navaratnam V, Hubbard RB, Jenkins G, Johnson SR. Extracellular Matrix Cross-Linking Enhances Fibroblast Growth and Protects against Matrix Proteolysis in Lung Fibrosis. *Am J Respir Cell Mol Biol* 2018: 58(5): 594–603.

61. Blokland KEC, Habibie H, Borghuis T, Teitsma GJ, Schuliga M, Melgert BN, Knight DA, Brandsma CA, Pouwels SD, Burgess JK. Regulation of Cellular Senescence Is Independent from Profibrotic Fibroblast-Deposited ECM. *Cells* 2021: 10(7): 1628.

62. Jenkins RG, Simpson JK, Saini G, Bentley JH, Russell AM, Braybrooke R, Molyneaux PL, McKeever TM, Wells AU, Flynn A, Hubbard RB, Leeming DJ, Marshall RP, Karsdal MA, Lukey PT, Maher TM. Longitudinal change in collagen degradation biomarkers in idiopathic pulmonary fibrosis: an analysis from the prospective, multicentre PROFILE study. *Lancet Respir Med* 2015: 3(6): 462–472.

63. Lepparanta O, Sens C, Salmenkivi K, Kinnula VL, Keski-Oja J, Myllarniemi M, Koli K. Regulation of TGF-beta storage and activation in the human idiopathic pulmonary fibrosis lung. *Cell Tissue Res* 2012: 348(3): 491–503.

64. Nizamoglu M, Burgess JK. The Multi-Faceted Extracellular Matrix: Unlocking Its Secrets for Understanding the Perpetuation of Lung Fibrosis. *Curr Tissue Microenviron Rep* 2022: 2(4): 53–71.

65. Jaffar J, Unger S, Corte TJ, Keller M, Wolters PJ, Richeldi L, Cerri S, Prele CM, Hansbro PM, Argraves WS, Oliver RA, Oliver BG, Black JL, Burgess JK. Fibulin-1 predicts disease progression in patients with idiopathic pulmonary fibrosis. *Chest* 2014: 146(4): 1055–1063.

66. Olsen KC, Sapinoro RE, Kottmann RM, Kulkarni AA, Iismaa SE, Johnson GV, Thatcher TH, Phipps RP, Sime PJ. Transglutaminase 2 and its role in pulmonary fibrosis. *Am J Respir Crit Care Med* 2011: 184(6): 699–707.

67. Baker BM, Chen CS. Deconstructing the third dimension: how 3D culture microenvironments alter cellular cues. *J Cell Sci* 2012: 125(Pt 13): 3015–3024.

68. Sacchi M, Bansal R, Rouwkema J. Bioengineered 3D Models to Recapitulate Tissue Fibrosis. *Trends Biotechnol* 2020: 38(6): 623–636.

69. Krimmer DI, Oliver BG. What can in vitro models of COPD tell us? *Pulm Pharmacol Ther* 2011: 24(5): 471–477.

70. Weaver VM, Lelievre S, Lakins JN, Chrenek MA, Jones JC, Giancotti F, Werb Z, Bissell MJ. beta4 integrin-dependent formation of polarized three-dimensional architecture confers resistance to apoptosis in normal and malignant mammary epithelium. *Cancer Cell* 2002: 2(3): 205–216.

71. Syed S, Karadaghy A, Zustiak S. Simple polyacrylamide-based multiwell stiffness assay for the study of stiffness-dependent cell responses. *J Vis Exp* 2015(97).

72. Huang X, Yang N, Fiore VF, Barker TH, Sun Y, Morris SW, Ding Q, Thannickal VJ, Zhou Y. Matrix stiffness-induced myofibroblast differentiation is mediated by intrinsic mechanotransduction. *Am J Respir Cell Mol Biol* 2012: 47(3): 340–348.

73. Janmey PA, Fletcher DA, Reinhart-King CA. Stiffness Sensing by Cells. *Physiol Rev* 2020: 100(2): 695–724.

74. Tang X, Ali MY, Saif MT. A Novel Technique for Micro-patterning Proteins and Cells on Polyacrylamide Gels. *Soft Matter* 2012: 8(27): 7197–7206.

75. Kleinman HK, Martin GR. Matrigel: basement membrane matrix with biological activity. *Semin Cancer Biol* 2005: 15(5): 378–386.

76. Muller L, Brighton LE, Carson JL, Fischer WA, 2nd, Jaspers I. Culturing of human nasal epithelial cells at the air liquid interface. *J Vis Exp* 2013(80).

77. Duval K, Grover H, Han LH, Mou Y, Pegoraro AF, Fredberg J, Chen Z. Modeling Physiological Events in 2D vs. 3D Cell Culture. *Physiology (Bethesda)* 2017: 32(4): 266–277.

78. Rozario T, DeSimone DW. The extracellular matrix in development and morphogenesis: a dynamic view. *Dev Biol* 2010: 341(1): 126-140.

79. Schmeichel KL, Bissell MJ. Modeling tissue-specific signaling and organ function in three dimensions. *J Cell Sci* 2003: 116(Pt 12): 2377-2388.

80. Discher DE, Janmey P, Wang YL. Tissue cells feel and respond to the stiffness of their substrate. *Science* 2005: 310(5751): 1139-1143.

81. Liu F, Mih JD, Shea BS, Kho AT, Sharif AS, Tager AM, Tschumperlin DJ. Feedback amplification of fibrosis through matrix stiffening and COX-2 suppression. *J Cell Biol* 2010: 190(4): 693-706.

82. Chiquet M, Gelman L, Lutz R, Maier S. From mechanotransduction to extracellular matrix gene expression in fibroblasts. *Biochim Biophys Acta* 2009: 1793(5): 911-920.

83. Humphrey JD, Dufresne ER, Schwartz MA. Mechanotransduction and extracellular matrix homeostasis. *Nat Rev Mol Cell Biol* 2014: 15(12): 802-812.

84. Huveneers S, Danen EH. Adhesion signaling - crosstalk between integrins, Src and Rho. *J Cell Sci* 2009: 122(Pt 8): 1059-1069.

85. Ingber DE. Tensegrity-based mechanosensing from macro to micro. *Prog Biophys Mol Biol* 2008: 97(2-3): 163-179.

86. Tschumperlin DJ. Matrix, mesenchyme, and mechanotransduction. *Ann Am Thorac Soc* 2015: 12 Suppl 1(Suppl 1): S24-29.

87. Hynes RO. The extracellular matrix: not just pretty fibrils. *Science* 2009: 326(5957): 1216-1219.

88. Rilla K, Mustonen AM, Arasu UT, Härkönen K, Matilainen J, Nieminen P. Extracellular vesicles are integral and functional components of the extracellular matrix. *Matrix Biol* 2019: 75-76: 201-219.

89. Pampaloni F, Reynaud EG, Stelzer EH. The third dimension bridges the gap between cell culture and live tissue. *Nat Rev Mol Cell Biol* 2007: 8(10): 839-845.

90. Ghodbane SA, Dunn MG. Physical and mechanical properties of cross-linked type I collagen scaffolds derived from bovine, porcine, and ovine tendons. *J Biomed Mater Res A* 2016: 104(11): 2685-2692.

91. Patil PP, Reagan MR, Bohara RA. Silk fibroin and silk-based biomaterial derivatives for ideal wound dressings. *Int J Biol Macromol* 2020: 164: 4613-4627.

92. Kanta J. Collagen matrix as a tool in studying fibroblastic cell behavior. *Cell Adh Migr* 2015: 9(4): 308-316.

93. Castillo-Briceno P, Bihan D, Nilges M, Hamaia S, Meseguer J, Garcia-Ayala A, Farndale RW, Mulero V. A role for specific collagen motifs during wound healing and inflammatory response of fibroblasts in the teleost fish gilthead seabream. *Mol Immunol* 2011: 48(6-7): 826-834.

94. Wang L, Zhao Y, Yang F, Feng M, Zhao Y, Chen X, Mi J, Yao Y, Guan D, Xiao Z, Chen B, Dai J. Biomimetic collagen biomaterial induces in situ lung regeneration by forming functional alveolar. *Biomaterials* 2020: 236: 119825.

95. Hamilton NJI, Hynds RE, Gowers KHC, Tait A, Butler CR, Hopper C, Burns AJ, Birchall MA, Lowdell M, Janes SM. Using a Three-Dimensional Collagen Matrix to Deliver Respiratory Progenitor Cells to Decellularized Trachea In Vivo. *Tissue Eng Part C Methods* 2019: 25(2): 93-102.

96. Doyle AD. Generation of 3D Collagen Gels with Controlled Diverse Architectures. *Curr Protoc Stem Cell Biol* 2016: 72: 10 20 11–10 20 16.

97. Joannes A, Brayer S, Besnard V, Marchal-Somme J, Jaillet M, Mordant P, Mal H, Borie R, Crestani B, Mailleux AA. FGF9 and FGF18 in idiopathic pulmonary fibrosis promote survival and migration and inhibit myofibroblast differentiation of human lung fibroblasts in vitro. *Am J Physiol Lung Cell Mol Physiol* 2016: 310(7): L615–629.

98. Bourke JE, Li X, Foster SR, Wee E, Dagher H, Ziogas J, Harris T, Bonacci JV, Stewart AG. Collagen remodelling by airway smooth muscle is resistant to steroids and beta(2)-agonists. *Eur Respir J* 2011: 37(1): 173–182.

99. Su K, Wang C. Recent advances in the use of gelatin in biomedical research. *Biotechnol Lett* 2015: 37(11): 2139–2145.

100. Xiao S, Zhao T, Wang J, Wang C, Du J, Ying L, Lin J, Zhang C, Hu W, Wang L, Xu K. Gelatin Methacrylate (GelMA)-Based Hydrogels for Cell Transplantation: an Effective Strategy for Tissue Engineering. *Stem Cell Rev Rep* 2019: 15(5): 664–679.

101. Rodríguez-Rodríguez R, Espinosa-Andrews H, Velasquillo-Martínez C, García-Carvajal ZY. Composite hydrogels based on gelatin, chitosan and polyvinyl alcohol to biomedical applications: a review. *Int J Polym Mater* 2019: 69(1): 1–20.

102. Xing Q, Yates K, Vogt C, Qian Z, Frost MC, Zhao F. Increasing mechanical strength of gelatin hydrogels by divalent metal ion removal. *Sci Rep* 2014: 4(1): 4706.

103. Klotz BJ, Gawlitta D, Rosenberg AJWP, Malda J, Melchels FPW. Gelatin-Methacryloyl Hydrogels: Towards Biofabrication-Based Tissue Repair. *Trends Biotechnol* 2016: 34(5): 394–407.

104. Melchels F, Blokland K, Ruijter MD, Malda J. A dual crosslinking strategy for reinforcing gelatine-methacrylamide hydrogels for tissue repair. In: 10th World Biomaterials Congress; 2016: Frontiers in Bioengineering and Biotechnology; 2016.

105. Bello AB, Kim D, Kim D, Park H, Lee SH. Engineering and Functionalization of Gelatin Biomaterials: From Cell Culture to Medical Applications. *Tissue Eng Part B Rev* 2020: 26(2): 164–180.

106. Jaipan P, Nguyen A, Narayan RJ. Gelatin-based hydrogels for biomedical applications. *MRS Commun* 2017: 7(3): 416–426.

107. Foox M, Zilberman M. Drug delivery from gelatin-based systems. *Expert Opin Drug Deliv* 2015: 12(9): 1547–1563.

108. Galliger Z, Vogt CD, Panoskaltsis-Mortari A. 3D bioprinting for lungs and hollow organs. *Transl Res* 2019: 211: 19–34.

109. Mondal A, Gebeyehu A, Miranda M, Bahadur D, Patel N, Ramakrishnan S, Rishi AK, Singh M. Characterization and printability of Sodium alginate -Gelatin hydrogel for bioprinting NSCLC co-culture. *Sci Rep* 2019: 9(1): 19914.

110. Wang X, Zhang X, Dai X, Wang X, Li X, Diao J, Xu T. Tumor-like lung cancer model based on 3D bioprinting. *3 Biotech* 2018: 8(12): 501–501.

111. Ling T-Y, Liu Y-L, Huang Y-K, Gu S-Y, Chen H-K, Ho C-C, Tsao P-N, Tung Y-C, Chen H-W, Cheng C-H, Lin K-H, Lin F-H. Differentiation of lung stem/progenitor cells into alveolar pneumocytes and induction of angiogenesis within a 3D gelatin – Microbubble scaffold. *Biomaterials* 2014: 35(22): 5660–5669.

112. Sun Y-J, Hsu C-H, Ling T-Y, Liu L, Lin T-C, Jakfar S, Young I-C, Lin F-H. The preparation of cell-containing microbubble scaffolds to mimic alveoli structure as a 3D drug-screening system for lung cancer. *Biofabrication* 2020: 12(2): 25031-25031.

113. Bennet TJ, Shen B, Siwik J, Pan S, Yang CWT, Sin DD, Hackett TL, Cheung KC. Airway-on-a-Chip: Development and in Vitro Validation of a Microfluidic Cell Culture Model for Chronic Obstructive Pulmonary Disease. In: 2020. p. 440-443.

114. Higuita-Castro N, Nelson MT, Shukla V, Agudelo-Garcia PA, Zhang W, Duarte-Sanmiguel SM, Englert JA, Lannutti JJ, Hansford DJ, Ghadiali SN. Using a Novel Microfabricated Model of the Alveolar-Capillary Barrier to Investigate the Effect of Matrix Structure on Atelectrauma. *Sci Rep* 2017: 7(1): 11623.

115. Lin C-H, Hsu S-h, Su J-M, Chen C-W. Surface modification of poly(ε-caprolactone) porous scaffolds using gelatin hydrogel as the tracheal replacement. *J Tissue Eng Regen Med* 2011: 5(2): 156-162.

116. Park JH, Hong JM, Ju YM, Jung JW, Kang H-W, Lee SJ, Yoo JJ, Kim SW, Kim SH, Cho D-W. A novel tissue-engineered trachea with a mechanical behavior similar to native trachea. *Biomaterials* 2015: 62: 106-115.

117. Aldana AA, Malatto L, Rehman MAU, Boccaccini AR, Abraham GA. Fabrication of Gelatin Methacrylate (GelMA) Scaffolds with Nano- and Micro-Topographical and Morphological Features. *Nanomaterials* 2019: 9(1).

118. Erben A, Horning M, Hartmann B, Becke T, Eisler SA, Southan A, Cranz S, Hayden O, Kneidinger N, Konigshoff M, Lindner M, Tovar GEM, Burgstaller G, Clausen-Schaumann H, Sudhop S, Heymann M. Precision 3D-Printed Cell Scaffolds Mimicking Native Tissue Composition and Mechanics. *Adv Healthc Mater* 2020: 9(24): e2000918.

119. Chan HF, Zhao R, Parada GA, Meng H, Leong KW, Griffith LG, Zhao X. Folding artificial mucosa with cell-laden hydrogels guided by mechanics models. *Proc Natl Acad Sci USA* 2018: 115(29): 7503-7508.

120. Amorim S, Reis CA, Reis RL, Pires RA. Extracellular Matrix Mimics Using Hyaluronan-Based Biomaterials. *Trends Biotechnol* 2021: 39(1): 90-104.

121. Trombino S, Servidio C, Curcio F, Cassano R. Strategies for Hyaluronic Acid-Based Hydrogel Design in Drug Delivery. *Pharmaceutics* 2019: 11(8): 407.

122. Spearman BS, Agrawal NK, Rubiano A, Simmons CS, Mobini S, Schmidt CE. Tunable methacrylated hyaluronic acid-based hydrogels as scaffolds for soft tissue engineering applications. *J Biomed Mater Res A* 2020: 108(2): 279-291.

123. Bermejo-Velasco D, Azemar A, Oommen OP, Hilborn J, Varghese OP. Modulating Thiol p K(a) Promotes Disulfide Formation at Physiological pH: An Elegant Strategy To Design Disulfide Cross-Linked Hyaluronic Acid Hydrogels. *Biomacromolecules* 2019: 20(3): 1412-1420.

124. Tam RY, Yockell-Lelievre J, Smith LJ, Julian LM, Baker AEG, Choey C, Hasim MS, Dimitroulakos J, Stanford WL, Shoichet MS. Rationally Designed 3D Hydrogels Model Invasive Lung Diseases Enabling High-Content Drug Screening. *Adv Mater* 2019: 31(7): e1806214.

125. Kumar P, Ciftci S, Barthes J, Knopf-Marques H, Muller CB, Debry C, Vrana NE, Ghaemmaghami AM. A composite Gelatin/hyaluronic acid hydrogel as an ECM mimic for developing mesenchymal stem cell-derived epithelial tissue patches. *J Tissue Eng Regen Med* 2020: 14(1): 45–57.

126. Bahlmann LC, Baker AEG, Xue C, Liu S, Meier-Merziger M, Karakas D, Zhu L, Co I, Zhao S, Chin A, McGuigan A, Kuruvilla J, Laister RC, Shoichet MS. Gelatin-Hyaluronan Click-Crosslinked Cryogels Elucidate Human Macrophage Invasion Behavior. *Adv Funct Mater* 2021: 2008400.

127. Seidlits SK, Drinnan CT, Petersen RR, Shear JB, Suggs LJ, Schmidt CE. Fibronectin-hyaluronic acid composite hydrogels for three-dimensional endothelial cell culture. *Acta Biomater* 2011: 7(6): 2401–2409.

128. Ondeck MG, Engler AJ. Mechanical Characterization of a Dynamic and Tunable Methacrylated Hyaluronic Acid Hydrogel. *J Biomech Eng* 2016: 138(2): 021003.

129. Trujillo S, Gonzalez-Garcia C, Rico P, Reid A, Windmill J, Dalby MJ, Salmeron-Sanchez M. Engineered 3D hydrogels with full-length fibronectin that sequester and present growth factors. *Biomaterials* 2020: 252(November 2019): 120104.

130. Calitz C, Pavlovic N, Rosenquist J, Zagami C, Samanta A, Heindryckx F. A Biomimetic Model for Liver Cancer to Study Tumor-Stroma Interactions in a 3D Environment with Tunable Bio-Physical Properties. *J Vis Exp* 2020(162).

131. Albers S, Thiebes AL, Gessenich KL, Jockenhoevel S, Cornelissen CG. Differentiation of respiratory epithelium in a 3-dimensional co-culture with fibroblasts embedded in fibrin gel. *Multidiscip Respir Med* 2015: 11(1): 6.

132. Kreimendahl F, Kopf M, Thiebes AL, Duarte Campos DF, Blaeser A, Schmitz-Rode T, Apel C, Jockenhoevel S, Fischer H. Three-Dimensional Printing and Angiogenesis: Tailored Agarose-Type I Collagen Blends Comprise Three-Dimensional Printability and Angiogenesis Potential for Tissue-Engineered Substitutes. *Tissue Eng Part C Methods* 2017: 23(10): 604–615.

133. Kreimendahl F, Ossenbrink S, Kopf M, Westhofen M, Schmitz-Rode T, Fischer H, Jockenhoevel S, Thiebes AL. Combination of vascularization and cilia formation for three-dimensional airway tissue engineering. *J Biomed Mater Res A* 2019: 107(9): 2053–2062.

134. Bachmann B, Spitz S, Schadl B, Teuschl AH, Redl H, Nurnberger S, Ertl P. Stiffness Matters: Fine-Tuned Hydrogel Elasticity Alters Chondrogenic Redifferentiation. *Front Bioeng Biotechnol* 2020: 8(April): 373.

135. Garreta E, Oria R, Tarantino C, Pla-Roca M, Prado P, Fernandez-Aviles F, Campistol JM, Samitier J, Montserrat N. Tissue engineering by decellularization and 3D bioprinting. *Mater Today* 2017: 20(4): 166–178.

136. Badylak SF, Taylor D, Uygun K. Whole-organ tissue engineering: decellularization and recellularization of three-dimensional matrix scaffolds. *Annu Rev Biomed Eng* 2011: 13: 27–53.

137. Gilbert TW. Strategies for tissue and organ decellularization. *J Cell Biochem* 2012: 113(7): 2217–2222.

138. Song JJ, Ott HC. Organ engineering based on decellularized matrix scaffolds. *Trends Mol Med* 2011: 17(8): 424–432.

139. Badylak SF. The extracellular matrix as a biologic scaffold material. *Biomaterials* 2007: 28(25): 3587–3593.

140. Cramer MC, Badylak SF. Extracellular Matrix-Based Biomaterials and Their Influence Upon Cell Behavior. *Ann Biomed Eng* 2020: 48(7): 2132-2153.

141. Keane TJ, Swinehart IT, Badylak SF. Methods of tissue decellularization used for preparation of biologic scaffolds and in vivo relevance. *Methods* 2015: 84: 25-34.

142. Gilpin SE, Wagner DE. Acellular human lung scaffolds to model lung disease and tissue regeneration. *Eur Respir Rev* 2018: 27(148).

143. Rosmark O, Åhrman E, Müller C, Elowsson Rendin L, Eriksson L, Malmström A, Hallgren O, Larsson-Callerfelt A-K, Westergren-Thorsson G, Malmström J. Quantifying extracellular matrix turnover in human lung scaffold cultures. *Sci Rep* 2018: 8(1): 5409-5409.

144. Elowsson Rendin L, Lofdahl A, Ahrman E, Muller C, Notermans T, Michalikova B, Rosmark O, Zhou XH, Dellgren G, Silverborn M, Bjermer L, Malmstrom A, Larsson-Callerfelt AK, Isaksson H, Malmstrom J, Westergren-Thorsson G. Matrisome Properties of Scaffolds Direct Fibroblasts in Idiopathic Pulmonary Fibrosis. *Int J Mol Sci* 2019: 20(16).

145. Sava P, Ramanathan A, Dobronyi A, Peng X, Sun H, Ledesma-Mendoza A, Herzog EL, Gonzalez AL. Human pericytes adopt myofibroblast properties in the microenvironment of the IPF lung. *JCI Insight* 2017: 2(24).

146. Hedstrom U, Oberg L, Vaarala O, Dellgren G, Silverborn M, Bjermer L, Westergren-Thorsson G, Hallgren O, Zhou X. Impaired Differentiation of Chronic Obstructive Pulmonary Disease Bronchial Epithelial Cells Grown on Bronchial Scaffolds. *Am J Respir Cell Mol Biol* 2021: 65(2): 201-213.

147. Kruk DMLW, Wisman M, Bruin HG, Lodewijk ME, Hof DJ, Borghuis T, Daamen WF, van Kuppevelt TH, Timens W, Burgess JK, Ten Hacken NHT, Heijink IH. Abnormalities in reparative function of lung-derived mesenchymal stromal cells in emphysema. *Am J Physiol Lung Cell Mol Physiol* 2021: 320(5): L832-L844.

148. Palma R, Cereta A, Guimaraes L, Da Anunciacao ARD, Delgado AL, Paulino JCD, Oliveira LV, Miglino MA. Characterization of acellular lung scaffolds derived from equine asthma model. *Eur Respir J* 2019: 54(suppl 63): PA599-PA599.

149. Mishra DK, Sakamoto JH, Thrall MJ, Baird BN, Blackmon SH, Ferrari M, Kurie JM, Kim MP. Human lung cancer cells grown in an ex vivo 3D lung model produce matrix metalloproteinases not produced in 2D culture. *PloS one* 2012: 7(9): e45308-e45308.

150. Xiong G, Flynn TJ, Chen J, Trinkle C, Xu R. Development of an ex vivo breast cancer lung colonization model utilizing a decellularized lung matrix. *Integr Biol (Camb)* 2015: 7(12): 1518-1525.

151. Gilpin SE, Charest JM, Ren X, Tapias LF, Wu T, Evangelista-Leite D, Mathisen DJ, Ott HC. Regenerative potential of human airway stem cells in lung epithelial engineering. *Biomaterials* 2016: 108: 111-119.

152. Gilpin SE, Guyette JP, Gonzalez G, Ren X, Asara JM, Mathisen DJ, Vacanti JP, Ott HC. Perfusion decellularization of human and porcine lungs: bringing the matrix to clinical scale. *J Heart Lung Transplant* 2014: 33(3): 298-308.

153. Godin LM, Sandri BJ, Wagner DE, Meyer CM, Price AP, Akinnola I, Weiss DJ, Panoskaltsis-Mortari A. Decreased Laminin Expression by Human Lung Epithelial Cells and Fibroblasts Cultured in Acellular Lung Scaffolds from Aged Mice. *PLoS One* 2016: 11(3): e0150966.

154. Kitano K, Ohata K, Economopoulos KP, Gorman DE, Gilpin SE, Becerra DC, Ott HC. Orthotopic Transplantation of Human Bioartificial Lung Grafts in a Porcine Model: A Feasibility Study. *Semin Thorac Cardiovasc Surg* 2021.

155. Moser PT, Gerli M, Diercks GR, Evangelista-Leite D, Charest JM, Gershlak JR, Ren X, Gilpin SE, Jank BJ, Gaudette GR, Hartnick CJ, Ott HC. Creation of Laryngeal Grafts from Primary Human Cells and Decellularized Laryngeal Scaffolds. *Tissue Eng Part A* 2020: 26(9-10): 543-555.

156. Ott HC, Clippinger B, Conrad C, Schuetz C, Pomerantseva I, Ikonomou L, Kotton D, Vacanti JP. Regeneration and orthotopic transplantation of a bioartificial lung. *Nat Med* 2010: 16(8): 927-933.

157. Petersen TH, Calle EA, Zhao L, Lee EJ, Gui L, Raredon MB, Gavrilov K, Yi T, Zhuang ZW, Breuer C, Herzog E, Niklason LE. Tissue-engineered lungs for in vivo implantation. *Science* 2010: 329(5991): 538-541.

158. Price AP, England KA, Matson AM, Blazar BR, Panoskaltsis-Mortari A. Development of a decellularized lung bioreactor system for bioengineering the lung: the matrix reloaded. *Tissue Eng Part A* 2010: 16(8): 2581-2591.

159. Sokocevic D, Bonenfant NR, Wagner DE, Borg ZD, Lathrop MJ, Lam YW, Deng B, Desarno MJ, Ashikaga T, Loi R, Hoffman AM, Weiss DJ. The effect of age and emphysematous and fibrotic injury on the re-cellularization of de-cellularized lungs. *Biomaterials* 2013: 34(13): 3256-3269.

160. Zhou H, Kitano K, Ren X, Rajab TK, Wu M, Gilpin SE, Wu T, Baugh L, Black LD, Mathisen DJ, Ott HC. Bioengineering Human Lung Grafts on Porcine Matrix. *Ann Surg* 2018: 267(3): 590-598.

161. Nichols JE, Niles J, Riddle M, Vargas G, Schilagard T, Ma L, Edward K, La Francesca S, Sakamoto J, Vega S, Ogadegbe M, Mlcak R, Deyo D, Woodson L, McQuitty C, Lick S, Beckles D, Melo E, Cortiella J. Production and assessment of decellularized pig and human lung scaffolds. *Tissue Eng Part A* 2013: 19(17-18): 2045-2062.

162. Wagner DE, Bonenfant NR, Parsons CS, Sokocevic D, Brooks EM, Borg ZD, Lathrop MJ, Wallis JD, Daly AB, Lam YW, Deng B, DeSarno MJ, Ashikaga T, Loi R, Weiss DJ. Comparative decellularization and recellularization of normal versus emphysematous human lungs. *Biomaterials* 2014: 35(10): 3281-3297.

163. Pouliot RA, Link PA, Mikhaiel NS, Schneck MB, Valentine MS, Kamga Gninzeko FJ, Herbert JA, Sakagami M, Heise RL. Development and characterization of a naturally derived lung extracellular matrix hydrogel. *J Biomed Mater Res A* 2016: 104(8): 1922-1935.

164. Saldin LT, Cramer MC, Velankar SS, White LJ, Badylak SF. Extracellular matrix hydrogels from decellularized tissues: Structure and function. *Acta Biomater* 2017: 49: 1-15.

165. Brightman AO, Rajwa BP, Sturgis JE, McCallister ME, Robinson JP, Voytik-Harbin SL. Time-lapse confocal reflection microscopy of collagen fibrillogenesis and extracellular matrix assembly in vitro. *Biopolymers* 2000: 54(3): 222-234.

166. Hussey GS, Nascari DG, Saldin LT, Kolich B, Lee YC, Crum RJ, El-Mossier SO, D'Angelo W, Dziki JL, Badylak SF. Ultrasonic cavitation to prepare ECM hydrogels. *Acta Biomater* 2020: 108: 77-86.

167. Pouliot RA, Young BM, Link PA, Park HE, Kahn AR, Shankar K, Schneck MB, Weiss DJ, Heise RL. Porcine Lung-Derived Extracellular Matrix Hydrogel Properties Are Dependent on Pepsin Digestion Time. *Tissue Eng Part C Methods* 2020: 26(6): 332-346.

168. Chaudhuri O. Viscoelastic hydrogels for 3D cell culture. *Biomater Sci* 2017: 5(8): 1480-1490.

169. Chaudhuri O, Gu L, Darnell M, Klumpers D, Bencherif SA, Weaver JC, Huebsch N, Mooney DJ. Substrate stress relaxation regulates cell spreading. *Nat Commun* 2015: 6: 6364.

170. Chaudhuri O, Gu L, Klumpers D, Darnell M, Bencherif SA, Weaver JC, Huebsch N, Lee HP, Lippens E, Duda GN, Mooney DJ. Hydrogels with tunable stress relaxation regulate stem cell fate and activity. *Nat Mater* 2016: 15(3): 326-334.

171. De Santis MM, Alsafadi HN, Tas S, Bolukbas DA, Prithiviraj S, Da Silva IAN, Mittendorfer M, Ota C, Stegmayr J, Daoud F, Konigshoff M, Sward K, Wood JA, Tassieri M, Bourgine PE, Lindstedt S, Mohlin S, Wagner DE. Extracellular-Matrix-Reinforced Bioinks for 3D Bioprinting Human Tissue. *Adv Mater* 2021: 33(3): e2005476.

172. Petrou CL, D'Ovidio TJ, Bolukbas DA, Tas S, Brown RD, Allawzi A, Lindstedt S, Nozik-Grayck E, Stenmark KR, Wagner DE, Magin CM. Clickable decellularized extracellular matrix as a new tool for building hybrid-hydrogels to model chronic fibrotic diseases in vitro. *J Mater Chem B* 2020: 8(31): 6814-6826.

173. Zhou J, Wu P, Sun H, Zhou H, Zhang Y, Xiao Z. Lung tissue extracellular matrix-derived hydrogels protect against radiation-induced lung injury by suppressing epithelial-mesenchymal transition. *J Cell Physiol* 2020: 235(3): 2377-2388.

174. Young BM, Shankar K, Allen BP, Pouliot RA, Schneck MB, Mikhaiel NS, Heise RL. Electrospun Decellularized Lung Matrix Scaffold for Airway Smooth Muscle Culture. *ACS Biomater Sci Eng* 2017: 3(12): 3480-3492.

175. Hillebrandt KH, Everwien H, Haep N, Keshi E, Pratschke J, Sauer IM. Strategies based on organ decellularization and recellularization. *Transplant International* 2019: 32(6): 571-585.

176. Baiguera S, Del Gaudio C, Jaus MO, Polizzi L, Gonfiotti A, Comin CE, Bianco A, Ribatti D, Taylor DA, Macchiarini P. Long-term changes to in vitro preserved bioengineered human trachea and their implications for decellularized tissues. *Biomaterials* 2012: 33(14): 3662-3672.

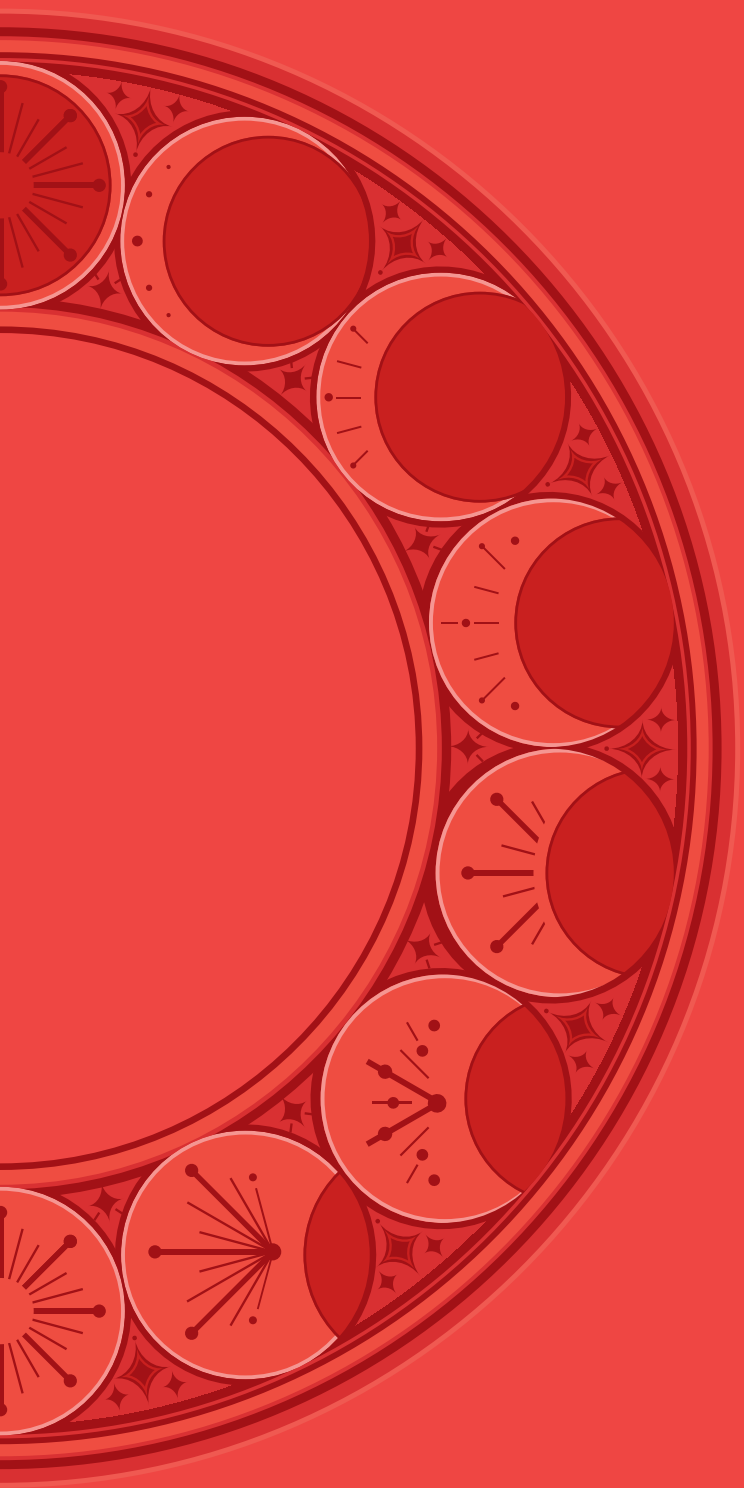

CHAPTER 7

Current possibilities and future opportunities with three-dimensional lung ECM-derived hydrogels

Mehmet Nizamoglu & Janette K. Burgess

Published in *Frontiers in Pharmacology* under a CC BY 4.0 license as:
Nizamoglu, M. & Burgess, J. K. (2023). Current possibilities and future opportunities provided by three-dimensional lung ECM-derived hydrogels. *Frontiers in Pharmacology*, 14.
https://doi.org/10.3389/fphar.2023.1154193

ABSTRACT

Disruption of the complex interplay between cells and extracellular matrix (ECM), the scaffold that provides support, biochemical and biomechanical cues, is emerging as a key element underlying lung diseases. We readily acknowledge that the lung is a flexible, relatively soft tissue that is three dimensional (3D) in structure, hence a need exists to develop *in vitro* model systems that reflect these properties. Lung ECM-derived hydrogels have recently emerged as a model system that mimics native lung physiology; they contain most of the plethora of biochemical components in native lung, as well as reflecting the biomechanics of native tissue. Research investigating the contribution of cell:matrix interactions to acute and chronic lung diseases has begun adopting these models but has yet to harness their full potential. This perspective article provides insight about the latest advances in the development, modification, characterization and utilization of lung ECM-derived hydrogels. We highlight some opportunities for expanding research incorporating lung ECM-derived hydrogels and potential improvements for the current approaches. Expanding the capabilities of investigations using lung ECM-derived hydrogels is positioned at a cross roads of disciplines, the path to new and innovative strategies for unravelling disease underlying mechanisms will benefit greatly from interdisciplinary approaches. While challenges need to be addressed before the maximum potential can be unlocked, with the rapid pace at which this field is evolving, we are close to a future where faster, more efficient and safer drug development targeting the disrupted 3D microenvironment is possible using lung ECM-derived hydrogels.

INTRODUCTION

The human body is a complex, dynamic environment, consisting of many different cell types that reside in or traverse through defined microenvironments, which is tightly regulated to maintain a healthy state. When elements within this system become disrupted, this can lead to the development of disease. In the lung, disruption of the complex interplay between cells and the extracellular matrix (ECM), the scaffold that provides support and biochemical and biomechanical cues, is emerging as a key element for deciphering the mechanism underlying diseases.

WHY SHOULD WE THINK ABOUT 3D IN *IN VITRO* MODEL SYSTEMS?

When we think about the lung *in vivo*, we readily acknowledge that it is a flexible, relatively soft tissue that is three dimensional (3D) in structure. However, in general, when we work with model systems *in vitro*, to try to elucidate processes that underlie homeostasis and disease, we mostly work with two dimensional (2D) systems. In the lung cells are surrounded by a specialised ECM, that is appropriate for their location. Mesenchymal cells are located within a 3D ECM structure, while epithelial and endothelial cells are usually attached to a basement membrane on their basal side and their apical side is subjected to flow of epithelial lining fluid or blood respectively. The stiffness of the lung tissue, in health is usually between 1-5 kilo-pascals (kPa), and in fibrotic disease this can increase up to 100 kPa although the pattern of stiffness can be very heterogeneous [1, 2]. 2D systems are frequently based on a tissue culture plastic or glass surface, with a stiffness in the gigapascal range, and all cells are grown with polarity. While a lot has been gained from working in 2D systems there is now an opportunity to move forward with our models to establish cells in an environment that reflects the physiological conditions in the lung.

The literature builds a strong body of evidence that the microenvironment in which a cell resides dictates its responses. From simple single ECM component studies [3-12], through to more complex cell deposited ECM studies [13-15], the influence of the ECM components on lung cell proliferation, migration, factor output and response to treatment is evident. However, this information has been collated from cells exposed to ECM components in 2D. It is recognised that cells in a 3D environment have differential responses compared to those in 2D [16, 17]. Therefore, developing systems where the influence of the ECM and the microenvironment in 3D can be explored will represent a next step forward for understanding disease underlying mechanisms in the lung.

Hydrogels from Synthetic vs Natural materials

When considering the possibilities for generating 3D microenvironments in which lung cells can prosper there are many different options available. Within the tissue engineering field much work has concentrated on the development of polymers from which soft or stiff hydrogels can be cast or 3D printed [18–21]. These synthetic polymers (including poly acrylamide [22] and dextran [23]) offer many opportunities for tuning biomechanical and structural properties of the microenvironment but are generally inhospitable environments for cells, requiring the addition of cell binding epitopes, such as RGD motifs, to enable cellular attachment [24–26]. Alternatively, natural ECM components have also been used to generate single component hydrogels that readily support cell attachment, but are more limited in the possibilities for tuning their biomechanical properties. Examples of such hydrogels include collagen type I, fibrin, gelatin (methacrylate)and hyaluronan [27–34]. Such hydrogels provide the 3D environment for cells, modelling the dimensionality and possibly the biomechanical mimicry of the *in vivo* situation, but they are not reflective of the complexity of the ECM components within the tissue microenvironment. Hydrogels developed from the solubilized basement membrane matrix secreted by Engelbreth-Holm-Swarm (EHS) mouse sarcoma cells (marketed as Matrigel or Geltrex) have been used for more than 35 years to support cell growth for specific assays, particularly focussing on stem cell expansion assays [35–38]. However, not all cells thrive in such an environment and there are limited possibilities to manipulate the composition and biomechanical environment herein.

A recent advance for the lung field has been the development of hydrogels generated from ECM derived from decellularized lungs. Porcine lung ECM-derived hydrogels were initially reported [39], while human lung ECM-derived hydrogels have recently been established [2]. This perspective article presents the latest advances in lung ECM-derived hydrogels with respect to their development, modification, characterization and utilization. Moreover, it explores opportunities and challenges for the field, highlighting where future research should focus to improve the comparability of data generated with different measurement systems using lung ECM-derived hydrogels. Finally, we discuss the multi-disciplinary nature of the research required to move these model systems forward.

THE POSSIBILITIES WITH LUNG ECM-DERIVED HYDROGELS

Lung ECM-derived hydrogels for mimicking *in vivo* ECM biochemical composition

The ECM, including in the lung, is a complex structure of proteins, glycoproteins, matricellular proteins and many other regulatory proteins and enzymes that keep this dynamic structure in balance during tissue homeostasis [40]. Mimicking such a complex structure when generating an *in vitro* 3D environment in which to culture cells to study cell:matrix interactions is impossible when starting with individual components. Sourcing the ECM from decellularized lungs has provided an opportunity to develop hydrogels that reflect a major proportion of the elements within this complex mixture. The process of decellularization requires treating the tissue with a range of detergents and/or salt solutions [1, 41, 42] that do remove some of the elements that are part of the matrisome, particularly growth factors bound to the ECM and some glycoproteins, but the major structural fibres are retained during this process.

Early proteomic studies [1, 43] illustrated the retention of many components of the lung matrisome in decellularised scaffolds from control and diseased lung samples. A recent study from the team in the Weiss lab [44], has elegantly shown that the components of the ECM are specific for different compartments within the lung (airways, alveolus, blood vessels), and that these change during chronic lung disease. These decellularized scaffolds from lung tissues have now been used as a source of ECM for the generation of hydrogels. The processing of the scaffolds to generate the solution that will gel when brought to physiological conditions is not thought to lead to further loss of ECM components, making this an ideal method for developing a 3D *in vitro* model system in which cells can be cultured in the presence of this complex mixture of the lung ECM microenvironment.

It remains to be seen if the absence of the elements of the matrisome that are lost during the decellularisation process impose a limitation in the interpretation of data generated when cells are seeded in such hydrogels (**Figure 1**). The absence of growth factors anchored in the ECM scaffolds, and therefore the ECM-derived hydrogels, after the decellularization process may be considered a limitation, although it is evident that the growth factor retentive properties of the ECM are retained as growth factors supplied in growth media or as part of the secretome from other cells are rapidly absorbed and then subsequently released from the ECM hydrogels [45]. In addition, ECM-derived hydrogels are a source of extracellular vesicles [46], adding another aspect to the regulatory processes induced by these cell support structures.

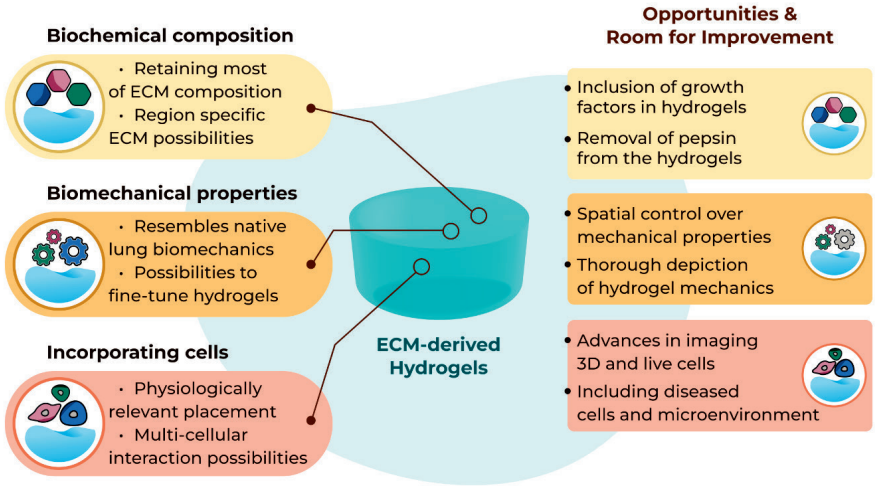

■ **Figure 1: Summary of current possibilities and future opportunities with three-dimensional lung ECM-derived hydrogels.**

Lung ECM-derived Hydrogels for mimicking tissue biomechanical environments

The structural environment provided for cells by lung ECM-derived hydrogels is another advantage when aiming to develop *in vivo* mimicking model systems. Although the adoption of the method for generating lung ECM-derived hydrogels was only recently reported [2, 39], the field is advancing rapidly with innovative approaches exploring how different properties can be measured and modified. Among these properties, mechanical properties and topography are two important characteristics of the hydrogels.

When considering mechanical properties of the hydrogels stiffness, Young's modulus, viscosity or viscoelastic stress relaxation are the usual parameters measured [47]. To date, a number of different strategies for measuring mechanical properties of lung ECM-derived hydrogels have been described, although it is important to highlight the challenge when it comes to comparing different studies performed using different measurement approaches for the mechanical properties [48]. **Rheometry** is one of the most commonly applied methods for measuring mechanical properties of hydrogels [49]. So far, characterization using rheometry has been applied to measure storage (G') and loss (G'') moduli of porcine [39] and human lung ECM-derived hydrogels [42]. In addition, viscosity and Young's modulus

of porcine-sourced lung hydrogels were reported using parallel plate rheometry [50]. Other studies have utilized this method on alginate-porcine ECM [51], poly(ethylene glycol)(PEG)-murine ECM [52], and PEG-porcine ECM [53] hybrid hydrogels. **Low-Load compression testing (LLCT)** is another compression-based method [54] that has been used with lung ECM-derived hydrogels. Stiffness and viscoelastic stress relaxation capacity of human non-disease control, chronic obstructive pulmonary disease (COPD) and idiopathic pulmonary fibrosis (IPF) lung ECM-derived hydrogels have been reported; moreover, the mechanical properties of the hydrogels derived from these diseased lungs resembled such properties of the native tissues from which the ECMs were sourced [2]. Similarly, LLCT-measured stiffness and stress relaxation parameters of both native and chemically crosslinked porcine lung ECM-derived hydrogels were also reported [55, 56]. Lastly, **atomic force microscopy (AFM)**, which is a more micro-level mechanical measurement based on indentation, was recently used to characterize Young's modulus values of porcine lung ECM hydrogels [50].

Measuring the mechanical properties is not only useful for diseased environment characterization, but also for verification of the success of methodologies designed to alter such properties. While it is clear that the use of different concentrations of the starting ECM material (powder) [39] and adjusting the pepsin digestion duration (the essential step in generation of a pre-gel ECM-derived substrate) [57] influences the mechanical properties, one of the initial attempts to specifically modulate the mechanical properties of lung ECM-derived hydrogels was treating the porcine lung ECM with genipin to increase the stiffness [58]. This approach has been extended with thiol-functionalization [52, 53], alginate-reinforcing [51] or fibre crosslinking [56] to allow greater control over mechanical parameters in the lung ECM-derived hydrogels.

The concepts of altering the mechanical properties, measuring and reporting these changes triggered in the lung ECM-derived hydrogels have been evolving as more novel tools are developed (**Figure 1**). However, mechanical characterization of lung ECM-derived hydrogels is far from completed. As of today, tensile testing or fatigue testing on such hydrogels have yet to be performed, although using polyacrylamide-ECM hybrid hydrogels these properties were characterized in an early study [59]. A thorough mechanical and cross-platform characterization of lung ECM-derived hydrogels has not been reported yet. Providing (the comparison of) such characterizations would help the field regarding the interpretation and comparison of different studies using different methods to measure similar parameters. As the field is new, establishing different methods and discussing their advantages and limitations will be important for being able to understand the

emerging knowledge about ECM mechanical properties and the functional impacts of these microenvironment parameters.

Another important property which goes hand-in-hand with mechanics is topography, reflecting the fibrous landscape within the ECM-derived hydrogels. In chronic lung diseases like COPD or lung fibrosis, the ECM topography is altered next to the mechanical properties of ECM [28, 60–63]. Using lung ECM sourced from diseased human lungs, for the generation of the hydrogels, would inherently convey (most of) the biochemical composition and resemble the mechanical properties; however, the native architecture of the lung ECM assembly is lost during the process of preparing ECM-derived hydrogels. Recently, preparing porcine lung ECM hydrogels with micropatterned surfaces was described as a method to prepare arrays for drug screening [64]. This study demonstrates the preparation of spherical patterns on the hydrogel surface with different diameters, although the aspects of altering the hydrogel surface to guide cell fate, behaviour or differentiation remain unexplored. Alternatively, electrospinning could provide another opportunity to alter the structural organization of the fibres [65]. While electrospun Poly(L-lactic acid)(PLLA)/porcine lung ECM hybrid scaffolds have been previously established [66], there is no report of electrospinning of pure decellularized lung ECM. Developing novel tools to modify the topography of the ECM fibres within the hydrogels and the regulation of the structural arrangements within these hydrogels requires more attention. Surface modifications on non-ECM-derived hydrogels is not a novel concept [67, 68], yet little is known about applying such modifications to the locations within the hydrogels in different planes in order to mimic the architecture of the native lung tissue.

The details of measuring, reporting and altering the properties of lung ECM-derived hydrogels gain more importance as the field progresses. Unfortunately to date, attempts at modifying properties of lung ECM-derived hydrogels remain rather limited. While the latest studies have focused on altering mechanical properties at a global level, new and innovative methodologies that will allow us to initiate more targeted modifications in such properties are required. Especially considering the heterogeneity of lung tissue and its architecture, having more control over spatial distribution of alterations in mechanical properties would enhance the *in vivo* mimicking capacity of our models.

LUNG ECM-DERIVED HYDROGELS FOR MIMICKING CELL:MATRIX INTERACTIONS

The *in vivo* mimicry of the composition and mechanics of the cellular microenvironment present in the lung ECM-derived hydrogels creates an ideal setting for culturing cells within a 3D spatial location. As soon as cells are seeded in hydrogels they begin to remodel their microenvironment [28, 31, 34]. Early reports of cells in lung ECM-derived hydrogels reflect findings in single component ECM hydrogels [28], indicating that cells remodel the ECM in which they are embedded, and the nature of the ECM that they encounter directs these remodelling events [69, 70]. This fact makes the use of lung ECM-derived hydrogels sourced from diseased lungs an ideal model to understand cellular responses within such a diseased microenvironment and to provide greater knowledge of the influence of the microenvironment to treatment effects.

Initial studies using porcine lung ECM-derived hydrogels reported successful growth of human and rat mesenchymal stromal (stem) cells (MSCs) in 2016 [39]. Link et al then described successful culture of mouse MSCs, human alveolar epithelial cells (the cell line A549), human primary microvascular endothelial cells (HpuVECs), and human umbilical vein endothelial cells (HUVECs) in porcine lung ECM-derived hydrogels [58]. The field is now rapidly expanding with additional cells types including murine fibroblasts [53], Rat lung MSCs [50] and rat primary alveolar epithelial cells [71] being grown in porcine lung ECM-derived hydrogels. The use of human lung ECM-derived hydrogels is now also possible, with human fibroblasts and airway smooth muscle cells being grown both within and on top of these hydrogels [51, 56, 69].

The field is now moving forward with the cellular systems that are being explored, taking advantage of the values of lung ECM-derived hydrogels. Multi-cellular culture systems are being developed to enable cellular cross-talk in a 3D microenvironment to be examined [72], and lung ECM-derived hydrogels are being incorporated into other experimental systems (for example lung on chip or stretching/mechanical force setups) to bring the cell microenvironment in those systems also [73, 74]. The possibilities for 3D printing lung ECM-derived hydrogels are also being examined, suggesting greater scope for spatial arrangement of cells within their 3D microenvironment will be possible in the future [50, 51].

While the 3D model systems made possible with the use of lung ECM-derived hydrogels are rapidly advancing, the readouts that can be used to investigate end points within these systems are presenting some limitations (**Figure 1**). Traditional

imaging setups are excellent for capturing images in 2D but moving into the third dimension proves challenging to visualise. Lung ECM-derived hydrogels are not translucent, like many of the single ECM or synthetic hydrogels, and this opacity challenges the optical depth of field. The autofluorescence of the lung ECM generates a very noisy image when using many traditional fluorescent reporters. Finally, tracking cell behaviours over time in 3D is extremely difficult to automate when the cells continuously move out of the plane of focus. Advances in imaging and capturing information from cells when they are interacting within their microenvironment is urgently needed to facilitate the full capacity of lung ECM-derived hydrogels.

DISCUSSION AND FUTURE REMARKS:

Studies in lung ECM-derived hydrogels will help to inform us of the optimal microenvironment for different cell types, as the cells continuously remodel their environment in, what appears to be, a programmed response. Whether there is temporal regulation of the remodelling, in particular in response to injury, is an outstanding question for the field. How these processes are altered in chronic lung diseases, and whether the progression of such processes can be reversed is knowledge that can be informed through the use of lung ECM-derived hydrogels. The approaches described above, including modulating mechanical properties of ECM-derived hydrogels without changing the ECM composition and the application of mechanical forces to cells within a 3D microenvironment, are attractive as they will facilitate research enabling the field to begin separating influences of the mechanical changes from those of the biochemical changes in the ECM in lung diseases. Such elucidation may open the door for development of mechanosensitive therapeutic targets for lung diseases.

To fully leverage the advantages offered by lung ECM-derived hydrogels multi-disciplinary teams who bring together expertise from the diverse fields needed to advance such systems will be necessary (**Figure 2**). Innovative researchers from pulmonology, cell and molecular biology, polymer chemistry, biomedical engineering, imaging and physics backgrounds are all needed to maximise opportunities and ensure the current challenges quickly become advantages for this exciting, emerging area of lung disease research.

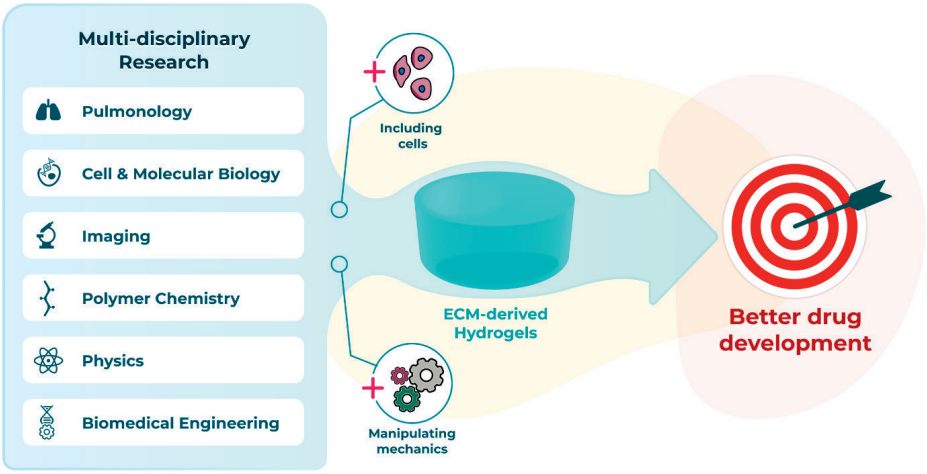

■ **Figure 2: Interdisciplinary advances to progress towards a better preclinical model using hydrogels**

ACKNOWLEDGEMENTS

Authors thank Mr. Albano Tosato for the assistance with figure preparation.

FUNDING

MN and JKB receive unrestricted research funds from Boehringer Ingelheim. JKB also acknowledges support from the NWO (Aspasia 015.013.010).

REFERENCES

1. Booth AJ, Hadley R, Cornett AM, Dreffs AA, Matthes SA, Tsui JL, Weiss K, Horowitz JC, Fiore VF, Barker TH, Moore BB, Martinez FJ, Niklason LE, White ES. Acellular normal and fibrotic human lung matrices as a culture system for in vitro investigation. Am J Respir Crit Care Med 2012: 186(9): 866–876.

2. de Hilster RHJ, Sharma PK, Jonker MR, White ES, Gercama EA, Roobeek M, Timens W, Harmsen MC, Hylkema MN, Burgess JK. Human lung extracellular matrix hydrogels resemble the stiffness and viscoelasticity of native lung tissue. Am J Physiol Lung Cell Mol Physiol 2020: 318(4): L698–L704.

3. Hirst SJ, Twort CH, Lee TH. Differential effects of extracellular matrix proteins on human airway smooth muscle cell proliferation and phenotype. Am J Respir Cell Mol Biol 2000: 23(3): 335–344.

4. Freyer AM, Johnson SR, Hall IP. Effects of growth factors and extracellular matrix on survival of human airway smooth muscle cells. Am J Physiol Lung Cell Mol Physiol 2001: 25(5): 569–576.

5. Bonacci JV, Harris T, Stewart AG. Impact of extracellular matrix and strain on proliferation of bovine airway smooth muscle. Clin Exp Pharmacol Physiol 2003: 30(5–6): 324–328.

6. Parameswaran K, Radford K, Zuo J, Janssen LJ, O'Byrne PM, Cox PG. Extracellular matrix regulates human airway smooth muscle cell migration. Eur Respir J 2004: 24(4): 545–551.

7. Peng Q, Lai D, Nguyen TT, Chan V, Matsuda T, Hirst SJ. Multiple beta 1 integrins mediate enhancement of human airway smooth muscle cytokine secretion by fibronectin and type I collagen. J Immunol 2005: 174(4): 2258–2264.

8. Nguyen TT, Ward JP, Hirst SJ. beta1-Integrins mediate enhancement of airway smooth muscle proliferation by collagen and fibronectin. Am J Respir Crit Care Med 2005: 171(3): 217–223.

9. Bonacci JV, Schuliga M, Harris T, Stewart AG. Collagen impairs glucocorticoid actions in airway smooth muscle through integrin signalling. Br J Pharmacol 2006: 149(4): 365–373.

10. Dekkers BG, Schaafsma D, Nelemans SA, Zaagsma J, Meurs H. Extracellular matrix proteins differentially regulate airway smooth muscle phenotype and function. Am J Physiol Lung Cell Mol Physiol 2007: 292(6): L1405–1413.

11. Reddel CJ, Cultrone D, Rnjak-Kovacina J, Weiss AS, Burgess JK. Tropoelastin modulates TGF-beta1-induced expression of VEGF and CTGF in airway smooth muscle cells. Matrix Biol 2013: 32(7–8): 407–413.

12. Morris GE, Bridge JC, Eltboli OM, Lewis MP, Knox AJ, Aylott JW, Brightling CE, Ghaemmaghami AM, Rose FR. Human airway smooth muscle maintain in situ cell orientation and phenotype when cultured on aligned electrospun scaffolds. Am J Physiol Lung Cell Mol Physiol 2014: 307(1): L38–47.

13. Johnson PR, Burgess JK, Underwood PA, Au W, Poniris MH, Tamm M, Ge Q, Roth M, Black JL. Extracellular matrix proteins modulate asthmatic airway smooth muscle cell proliferation via an autocrine mechanism. J Allergy Clin Immunol 2004: 113(4): 690-696.

14. Chan V, Burgess JK, Ratoff JC, O'Connor B J, Greenough A, Lee TH, Hirst SJ. Extracellular matrix regulates enhanced eotaxin expression in asthmatic airway smooth muscle cells. Am J Respir Crit Care Med 2006: 174(4): 379-385.

15. Harkness LM, Weckmann M, Kopp M, Becker T, Ashton AW, Burgess JK. Tumstatin regulates the angiogenic and inflammatory potential of airway smooth muscle extracellular matrix. J Cell Mol Med 2017.

16. Duval K, Grover H, Han LH, Mou Y, Pegoraro AF, Fredberg J, Chen Z. Modeling Physiological Events in 2D vs. 3D Cell Culture. Physiology (Bethesda) 2017: 32(4): 266-277.

17. Jensen C, Teng Y. Is It Time to Start Transitioning From 2D to 3D Cell Culture? Front Mol Biosci 2020: 7: 33.

18. Tibbitt MW, Anseth KS. Hydrogels as extracellular matrix mimics for 3D cell culture. Biotechnol Bioeng 2009: 103(4): 655-663.

19. Melchels FPW, Domingos MAN, Klein TJ, Malda J, Bartolo PJ, Hutmacher DW. Additive manufacturing of tissues and organs. Prog Polym Sci 2012: 37(8): 1079-1104.

20. Hospodiuk M, Dey M, Sosnoski D, Ozbolat IT. The bioink: A comprehensive review on bioprintable materials. Biotechnol Adv 2017: 35(2): 217-239.

21. Gungor-Ozkerim PS, Inci I, Zhang YS, Khademhosseini A, Dokmeci MR. Bioinks for 3D bioprinting: an overview. Biomater Sci 2018: 6(5): 915-946.

22. Marinkovic A, Liu F, Tschumperlin DJ. Matrices of physiologic stiffness potently inactivate idiopathic pulmonary fibrosis fibroblasts. Am J Respir Cell Mol Biol 2013: 48(4): 422-430.

23. Matera DL, DiLillo KM, Smith MR, Davidson CD, Parikh R, Said M, Wilke CA, Lombaert IM, Arnold KB, Moore BB, Baker BM. Microengineered 3D pulmonary interstitial mimetics highlight a critical role for matrix degradation in myofibroblast differentiation. Sci Adv 2020: 6(37).

24. Lutolf MP, Hubbell JA. Synthetic biomaterials as instructive extracellular microenvironments for morphogenesis in tissue engineering. Nat Biotechnol 2005: 23(1): 47-55.

25. Caracena T, Blomberg R, Hewawasam RS, Fry ZE, Riches DWH, Magin CM. Alveolar epithelial cells and microenvironmental stiffness synergistically drive fibroblast activation in three-dimensional hydrogel lung models. Biomater Sci 2022: 10(24): 7133-7148.

26. Reddy MSB, Ponnamma D, Choudhary R, Sadasivuni KK. A Comparative Review of Natural and Synthetic Biopolymer Composite Scaffolds. Polymers 2021: 13(7): 1105.

27. Bourke JE, Li X, Foster SR, Wee E, Dagher H, Ziogas J, Harris T, Bonacci JV, Stewart AG. Collagen remodelling by airway smooth muscle is resistant to steroids and beta(2)-agonists. Eur Respir J 2011: 37(1): 173-182.

28. Tjin G, White ES, Faiz A, Sicard D, Tschumperlin DJ, Mahar A, Kable EPW, Burgess JK. Lysyl oxidases regulate fibrillar collagen remodelling in idiopathic pulmonary fibrosis. Dis Model Mech 2017: 10(11): 1301-1312.

29. Sun YJ, Hsu CH, Ling TY, Liu L, Lin TC, Jakfar S, Young IC, Lin FH. The preparation of cell-containing microbubble scaffolds to mimic alveoli structure as a 3D drug-screening system for lung cancer. Biofabrication 2020: 12(2): 025031.

30. Hui E, Moretti L, Barker TH, Caliari SR. The Combined Influence of Viscoelastic and Adhesive Cues on Fibroblast Spreading and Focal Adhesion Organization. Cell Mol Bioeng 2021: 14(5): 427-440.

31. Martinez-Garcia FD, Valk MM, Sharma PK, Burgess JK, Harmsen MC. Adipose Tissue-Derived Stromal Cells Alter the Mechanical Stability and Viscoelastic Properties of Gelatine Methacryloyl Hydrogels. Int J Mol Sci 2021: 22(18): 10153.

32. Blokland KEC, Nizamoglu M, Habibie H, Borghuis T, Schuliga M, Melgert BN, Knight DA, Brandsma CA, Pouwels SD, Burgess JK. Substrate stiffness engineered to replicate disease conditions influence senescence and fibrotic responses in primary lung fibroblasts. Front Pharmacol 2022: 13: 989169.

33. Loebel C, Weiner AI, Eiken MK, Katzen JB, Morley MP, Bala V, Cardenas-Diaz FL, Davidson MD, Shiraishi K, Basil MC, Ferguson LT, Spence JR, Ochs M, Beers MF, Morrisey EE, Vaughan AE, Burdick JA. Microstructured Hydrogels to Guide Self-Assembly and Function of Lung Alveolospheres. Adv Mater 2022: 34(28): e2202992.

34. Martinez-Garcia FD, van Dongen JA, Burgess JK, Harmsen MC. Matrix Metalloproteases from Adipose Tissue-Derived Stromal Cells Are Spatiotemporally Regulated by Hydrogel Mechanics in a 3D Microenvironment. Bioengineering 2022: 9(8): 340.

35. Kleinman HK, McGarvey ML, Liotta LA, Robey PG, Tryggvason K, Martin GR. Isolation and characterization of type IV procollagen, laminin, and heparan sulfate proteoglycan from the EHS sarcoma. Biochemistry 1982: 21(24): 6188-6193.

36. Kleinman HK, Martin GR. Matrigel: basement membrane matrix with biological activity. Semin Cancer Biol 2005: 15(5): 378-386.

37. Benton G, George J, Kleinman HK, Arnaoutova IP. Advancing science and technology via 3D culture on basement membrane matrix. J Cell Physiol 2009: 221(1): 18-25.

38. Hughes CS, Postovit LM, Lajoie GA. Matrigel: a complex protein mixture required for optimal growth of cell culture. Proteomics 2010: 10(9): 1886-1890.

39. Pouliot RA, Link PA, Mikhaiel NS, Schneck MB, Valentine MS, Kamga Gninzeko FJ, Herbert JA, Sakagami M, Heise RL. Development and characterization of a naturally derived lung extracellular matrix hydrogel. J Biomed Mater Res A 2016: 104(8): 1922-1935.

40. Hynes RO, Naba A. Overview of the matrisome--an inventory of extracellular matrix constituents and functions. Cold Spring Harb Perspect Biol 2012: 4(1): a004903.

41. Wagner DE, Bonenfant NR, Parsons CS, Sokocevic D, Brooks EM, Borg ZD, Lathrop MJ, Wallis JD, Daly AB, Lam YW, Deng B, DeSarno MJ, Ashikaga T, Loi R, Weiss DJ. Comparative decellularization and recellularization of normal versus emphysematous human lungs. Biomaterials 2014: 35(10): 3281-3297.

42. Dabaghi M, Saraei N, Carpio MB, Nanduri V, Ungureanu J, Babi M, Chandiramohan A, Noble A, Revill SD, Zhang B, Ask K, Kolb M, Shargall Y, Moran-Mirabal J, Hirota JA. A Robust Protocol for Decellularized Human Lung Bioink Generation Amenable to 2D and 3D Lung Cell Culture. Cells 2021: 10(6): 1538.

43. Uhl F, Zvarova B, Ahlers B, Hood C, Deng B, Lam Y, Beatman E, Schweitzer K, Petrache I, Weiss D, Wagner D. Characterization of decellularized COPD lung matrices using mass spectrometry proteomics. Eur Respir J 2018: 52(suppl 62): LSC-1085.

44. Hoffman ET, Uhl FE, Asarian L, Deng B, Becker C, Uriarte JJ, Downs I, Young B, Weiss DJ. Regional and disease specific human lung extracellular matrix composition. Biomaterials 2023: 293: 121960.

45. van Dongen JA, Getova V, Brouwer LA, Liguori GR, Sharma PK, Stevens HP, van der Lei B, Harmsen MC. Adipose tissue-derived extracellular matrix hydrogels as a release platform for secreted paracrine factors. J Tissue Eng Regen Med 2019: 13(6): 973-985.

46. Ulldemolins A, Jurado A, Herranz-Diez C, Gavara N, Otero J, Farre R, Almendros I. Lung Extracellular Matrix Hydrogels-Derived Vesicles Contribute to Epithelial Lung Repair. Polymers 2022: 14(22): 4907.

47. Vedadghavami A, Minooei F, Mohammadi MH, Khetani S, Rezaei Kolahchi A, Mashayekhan S, Sanati-Nezhad A. Manufacturing of hydrogel biomaterials with controlled mechanical properties for tissue engineering applications. Acta Biomater 2017: 62: 42-63.

48. Polio SR, Kundu AN, Dougan CE, Birch NP, Aurian-Blajeni DE, Schiffman JD, Crosby AJ, Peyton SR. Cross-platform mechanical characterization of lung tissue. PLoS One 2018: 13(10): e0204765.

49. Stojkov G, Niyazov Z, Picchioni F, Bose RK. Relationship between Structure and Rheology of Hydrogels for Various Applications. Gels 2021: 7(4): 255.

50. Falcones B, Sanz-Fraile H, Marhuenda E, Mendizabal I, Cabrera-Aguilera I, Malandain N, Uriarte JJ, Almendros I, Navajas D, Weiss DJ, Farre R, Otero J. Bioprintable Lung Extracellular Matrix Hydrogel Scaffolds for 3D Culture of Mesenchymal Stromal Cells. Polymers 2021: 13(14): 2350.

51. De Santis MM, Alsafadi HN, Tas S, Bolukbas DA, Prithiviraj S, Da Silva IAN, Mittendorfer M, Ota C, Stegmayr J, Daoud F, Konigshoff M, Sward K, Wood JA, Tassieri M, Bourgine PE, Lindstedt S, Mohlin S, Wagner DE. Extracellular-Matrix-Reinforced Bioinks for 3D Bioprinting Human Tissue. Adv Mater 2021: 33(3): e2005476.

52. Saleh KS, Hewawasam R, Serbedzija P, Blomberg R, Noreldeen SE, Edelman B, Smith BJ, Riches DWH, Magin CM. Engineering Hybrid-Hydrogels Comprised of Healthy or Diseased Decellularized Extracellular Matrix to Study Pulmonary Fibrosis. Cell Mol Bioeng 2022: 15(5): 505-519.

53. Petrou CL, D'Ovidio TJ, Bolukbas DA, Tas S, Brown RD, Allawzi A, Lindstedt S, Nozik-Grayck E, Stenmark KR, Wagner DE, Magin CM. Clickable decellularized extracellular matrix as a new tool for building hybrid-hydrogels to model chronic fibrotic diseases in vitro. J Mater Chem B 2020: 8(31): 6814-6826.

54. Sharma PK, Busscher HJ, Terwee T, Koopmans SA, van Kooten TG. A comparative study on the viscoelastic properties of human and animal lenses. Exp Eye Res 2011: 93(5): 681-688.

55. Martinez-Garcia FD, de Hilster RHJ, Sharma PK, Borghuis T, Hylkema MN, Burgess JK, Harmsen MC. Architecture and Composition Dictate Viscoelastic Properties of Organ-Derived Extracellular Matrix Hydrogels. Polymers 2021: 13(18): 3113.

56. Nizamoglu M, de Hilster RHJ, Zhao F, Sharma PK, Borghuis T, Harmsen MC, Burgess JK. An in vitro model of fibrosis using crosslinked native extracellular matrix-derived hydrogels to modulate biomechanics without changing composition. Acta Biomater 2022: 147: 50-62.

57. Pouliot RA, Young BM, Link PA, Park HE, Kahn AR, Shankar K, Schneck MB, Weiss DJ, Heise RL. Porcine Lung-Derived Extracellular Matrix Hydrogel Properties Are Dependent on Pepsin Digestion Time. Tissue Eng Part C Methods 2020: 26(6): 332-346.

58. Link PA, Pouliot RA, Mikhaiel NS, Young BM, Heise RL. Tunable Hydrogels from Pulmonary Extracellular Matrix for 3D Cell Culture. J Vis Exp 2017(119).

59. Sava P, Ramanathan A, Dobronyi A, Peng X, Sun H, Ledesma-Mendoza A, Herzog EL, Gonzalez AL. Human pericytes adopt myofibroblast properties in the microenvironment of the IPF lung. JCI Insight 2017: 2(24).

60. Abraham T, Hogg J. Extracellular matrix remodeling of lung alveolar walls in three dimensional space identified using second harmonic generation and multiphoton excitation fluorescence. J Struct Biol 2010: 171(2): 189-196.

61. Tjin G, Xu P, Kable SH, Kable EP, Burgess JK. Quantification of collagen I in airway tissues using second harmonic generation. J Biomed Opt 2014: 19(3): 36005.

62. Burgess JK, Harmsen MC. Chronic lung diseases: entangled in extracellular matrix. Eur Respir Rev 2022: 31(163): 210202.

63. Nizamoglu M, Burgess JK. The Multi-Faceted Extracellular Matrix: Unlocking Its Secrets for Understanding the Perpetuation of Lung Fibrosis. Curr Tissue Microenviron Rep 2022: 2(4): 53-71.

64. Zhu X, Li Y, Yang Y, He Y, Gao M, Peng W, Wu Q, Zhang G, Zhou Y, Chen F, Bao J, Li W. Ordered micropattern arrays fabricated by lung-derived dECM hydrogels for chemotherapeutic drug screening. Materials Today Bio 2022: 15: 100274.

65. Hasirci V, Hasirci N. Nano- and Microarchitecture of Biomaterial Surfaces. Fundamentals of Biomaterials. Springer New York, 2018; pp. 303-329.

66. Young BM, Shankar K, Allen BP, Pouliot RA, Schneck MB, Mikhaiel NS, Heise RL. Electrospun Decellularized Lung Matrix Scaffold for Airway Smooth Muscle Culture. ACS Biomater Sci Eng 2017: 3(12): 3480-3492.

67. Richbourg NR, Peppas NA, Sikavitsas VI. Tuning the biomimetic behavior of scaffolds for regenerative medicine through surface modifications. J Tissue Eng Regen Med 2019: 13(8): 1275-1293.

68. Cai SX, Wu CX, Yang WG, Liang WF, Yu HB, Liu LQ. Recent advance in surface modification for regulating cell adhesion and behaviors. Nanotechnol Rev 2020: 9(1): 971-989.

69. Nizamoglu M, Koster T, Thomas M, Timens W, Koss CK, El Kasmi KC, Melgert BN, Heijink IH, Burgess JK. 3D Fibrotic Lung Extracellular Matrix Hydrogels Trigger Pro-Fibrotic Responses in Primary Lung Fibroblasts. American Thoracic Society 20232. American Thoracic Society, 2022; pp. A5245-A5245.

70. Falcones B, Soderlund Z, Ibanez-Fonseca A, Almendros I, Otero J, Farre R, Rolandsson Enes S, Elowsson Rendin L, Westergren-Thorsson G. hLMSC Secretome Affects Macrophage Activity Differentially Depending on Lung-Mimetic Environments. Cells 2022: 11(12): 1866.

71. Marhuenda E, Villarino A, Narciso ML, Camprubi-Rimblas M, Farre R, Gavara N, Artigas A, Almendros I, Otero J. Lung Extracellular Matrix Hydrogels Enhance Preservation of Type II Phenotype in Primary Alveolar Epithelial Cells. Int J Mol Sci 2022: 23(9): 4888.

72. Park J, Wetzel I, Dreau D, Cho H. 3D Miniaturization of Human Organs for Drug Discovery. Adv Healthc Mater 2018: 7(2): 1700551.

73. Park S, Kim TH, Kim SH, You S, Jung Y. Three-Dimensional Vascularized Lung Cancer-on-a-Chip with Lung Extracellular Matrix Hydrogels for In Vitro Screening. Cancers (Basel) 2021: 13(16): 3930.

74. Marhuenda E, Villarino A, Narciso M, Elowsson L, Almendros I, Westergren-Thorsson G, Farre R, Gavara N, Otero J. Development of a physiomimetic model of acute respiratory distress syndrome by using ECM hydrogels and organ-on-a-chip devices. Front Pharmacol 2022: 13: 945134.

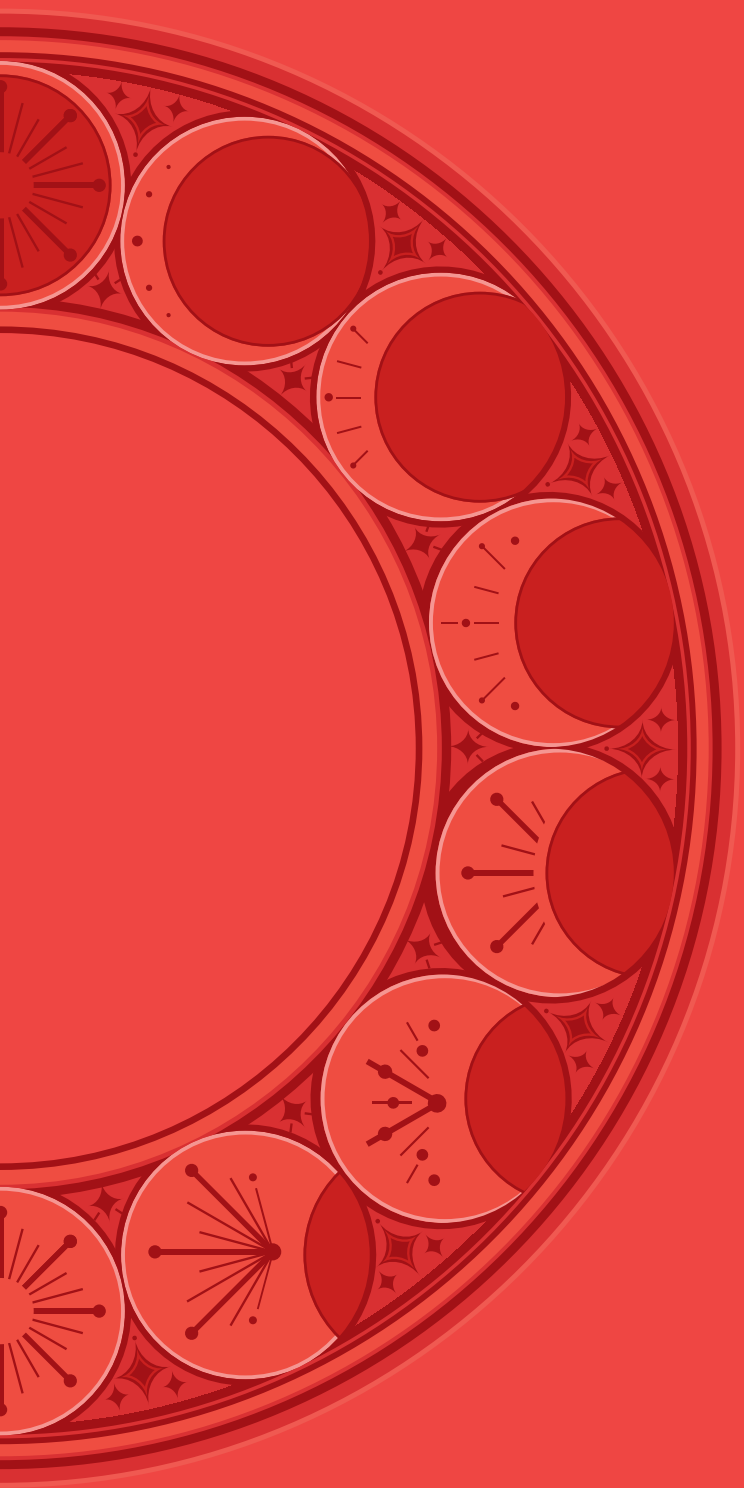

CHAPTER 8

An *in vitro* model of fibrosis using crosslinked native extracellular matrix-derived hydrogels to modulate biomechanics without changing composition

Mehmet Nizamoglu †, Roderick H.J de Hilster † *, Fenghua Zhao, Prashant K. Sharma, Theo Borghuis, Martin C. Harmsen, Janette K. Burgess

† These authors contributed equally

Published in *Acta Biomaterialia* under a CC BY-NC-ND 4.0 license as:
Nizamoglu, M., de Hilster, R. H. J., Zhao, F., Sharma, P. K., Borghuis, T., Harmsen, M. C., & Burgess, J. K. (2022). An in vitro model of fibrosis using crosslinked native extracellular matrix-derived hydrogels to modulate biomechanics without changing composition. *Acta Biomaterialia*, 147, 50–62.
https://doi.org/10.1016/j.actbio.2022.05.031

ABSTRACT

Extracellular matrix (ECM) is a dynamic network of proteins, proteoglycans and glycosaminoglycans, providing structure to the tissue and biochemical and biomechanical instructions to the resident cells. In fibrosis, the composition and the organization of the ECM are altered, and these changes influence cellular behaviour. Biochemical (i. e. protein composition) and biomechanical changes in ECM take place simultaneously *in vivo*. Investigating these changes individually *in vitro* to examine their (patho)physiological effects has been difficult. In this study, we generated an *in vitro* model to reflect the altered mechanics of a fibrotic microenvironment through applying fibre crosslinking via ruthenium/sodium persulfate crosslinking on native lung ECM-derived hydrogels. Crosslinking of the hydrogels without changing the biochemical composition of the ECM resulted in increased stiffness and decreased viscoelastic stress relaxation. The altered stress relaxation behaviour was explained using a generalized Maxwell model. Fibre analysis of the hydrogels showed that crosslinked hydrogels had a higher percentage of matrix with a high density and a shorter average fibre length. Fibroblasts seeded on ruthenium-crosslinked lung ECM-derived hydrogels showed myofibroblastic differentiation with a loss of spindle-like morphology together with greater α-smooth muscle actin (α-SMA) expression, increased nuclear area and circularity without any decrease in the viability, compared with the fibroblasts seeded on the native lung-derived ECM hydrogels. In summary, ruthenium crosslinking of native ECM-derived hydrogels provides an exciting opportunity to alter the biomechanical properties of the ECM-derived hydrogels while maintaining the protein composition of the ECM to study the influence of mechanics during fibrotic lung diseases.

INTRODUCTION

Extracellular matrix (ECM) is the structural component of every tissue, formed by a complex network of proteins, glycosaminoglycans and proteoglycans [1]. The highly tissue-specific nature of the ECM is dictated by the presence of a defined grouping of matrisome elements, incorporating demarcated ratios of ECM proteins [2]. These distinctions also result in different mechanical properties of the ECM, depending on the origin of the tissue [3]. Next to being structural support for the cells, the ECM provides biochemical and biomechanical cues to cells *in vivo* [4]. As such, it has proven challenging to mimic and incorporate the ECM structure and mechanics into (*in vitro)* studies regarding the structure and function of the ECM in health and disease. In fibrotic lung diseases, not only is the ECM composition altered but also its mechanical properties, resulting in higher stiffness and decreases in stress relaxation [5, 6]. All the changes that are evident within a fibrotic ECM have been revealed to instruct cells and influence their responses to contribute to the progression of fibrosis, as reported and reviewed elsewhere [7-13].

To investigate the mechanical properties of (fibrotic) ECM *in vitro*, the ECM is often mimicked using hydrogels. ECM-derived hydrogels, which have been introduced to the field in the last decade, are a promising alternative to other types of hydrogels such as collagen, gelatine, or hyaluronic acid [14]. ECM hydrogels which are developed from native decellularized tissue, retain most of the native ECM composition and, in general, resemble the mechanical properties of the parent tissue [6]. The most common method to produce hydrogels from ECM is to digest decellularized ECM powder with porcine pepsin at low pH with constant agitation [14]. Our recent study illustrated the preparation of ECM-derived hydrogels from human decellularized lung ECM, and established that the mechanical properties of the diseased (fibrotic) lung ECM-derived hydrogels resembled the mechanics of the decellularized fibrotic lung ECM [6]. Fibrotic lung ECM (both in native and hydrogel form) showed decreased viscoelastic stress relaxation compared to control lung ECM [6]. The stiffness of fibrotic lung tissue was ~10 times higher than its hydrogel counterpart, possibly due to the absence of chemical crosslinks and lung-resident cells in the ECM hydrogel. Previous studies showed that the composition of fibrotic lung ECM is different to that seen in control lung due to dysregulation of the ECM degradation/deposition processes resulting in an aberrant ECM [15]. To investigate the separate influences on the cells of the altered mechanical properties or ECM composition in the fibrotic microenvironment, advanced and innovative *in vitro* models are needed. Recently, altering the mechanical properties of methacrylate or thiol functionalized ECM-derived hydrogels using click-chemistry has been shown [16, 17]. Given that these

processes rely on interactions with amine groups of lysine or arginine amino acids, which are known to be parts of cell binding domains including GFOGER, IKVAV or RGD. The implications of methacrylation or thiolation of ECM proteins on cellular functions still need to be explored [16, 18-20]. Alternatively, chemical crosslinking has been applied to ECM-derived hydrogels using harsh chemicals such as glutaraldehyde or genipin, but cytotoxicity limits their use when cells are present in the hydrogel [21]. Another option is using near visible light UV-induced ruthenium/sodium persulfate (SPS) crosslinking, which has been employed on several other types of hydrogels (gelatine or fibrin) with and without cells present in the hydrogels [22, 23]. The higher wavelength (405 nm) of the crosslinking light, which decreases the cytotoxicity, and the lack of requirement for any additional functionalization on the target material are the main advantages of this crosslinking method [24]. Using ruthenium/SPS crosslinking to reinforce the mechanical stability of the ECM-derived hydrogels has recently been reported by Kim et al. [25]; however, the implications of altering the mechanical properties of the hydrogels without changing the (bio)chemical composition have yet to be explored in terms of fibrosis and for developing *in vitro* models for fibrosis research.

In this study, we aimed to develop an *in vitro* model for examining the influence of mechanical properties of the fibrotic microenvironment by using native lung-derived ECM hydrogels (LdECM), which were generated using ruthenium/SPS crosslinking. We hypothesized that the ruthenium crosslinking would increase the stiffness of lung-derived ECM hydrogels (Ru-LdECM), while the viscoelastic relaxation would decrease, to then trigger pro-fibrotic activation of lung fibroblasts.

MATERIALS AND METHODS

Porcine Lung Decellularization

Porcine lungs (~6-month, female) were purchased from a local slaughterhouse (Kroon Vlees, Groningen, the Netherlands). The lung was dissected, cartilaginous airways and large blood vessels removed, before cutting into ~1cm^3 cubes that were homogenized in a kitchen blender prior to decellularization. The lung homogenate was decellularized as previously described [26, 27]. In short, the homogenate was repeatedly washed with Milli-Q® water and centrifuged at 3,000 x g until the supernatant was completely clear. The sedimented material went through two rounds of sequential treatment with 0.1 % Triton X-100 (Sigma-Aldrich, St. Louis, MO, USA), 2 % sodium deoxycholate (Sigma-Aldrich), 1 M NaCl solution and 30 µg/mL DNase (Sigma-Aldrich) in $MgSO_4$ (Sigma-Aldrich) 1.3 mM and $CaCl_2$ (Sigma-Aldrich) 2 mM,

10 mM Tris pH8 (Sigma-Aldrich) solution each for 24 h at 4°C with constant shaking, except for the DNAse treatments, which were at 37°C with shaking. The volume ratio of tissue homogenate to decellularization/washing solution was always 1:10. Between treatments, the homogenate was washed three times with Milli-Q® water, with centrifugation at 3,000 x g between washes. After two cycles of decellularization, the tissue homogenate was sterilised by adding 0.18 % peracetic acid and 4.8 % ethanol, and left shaking at 4 °C for 24 h. After tissue sterilization the resultant decellularized ECM was washed three times with sterile Dulbecco's phosphate-buffered saline (DPBS) and stored in sterile DPBS containing 1 % penicillin-streptomycin (Gibco Invitrogen, Carlsbad, CA, USA) at 4 °C (**Figure 1A**).

Hydrogel preparation

The decellularized lung ECM was snap-frozen in liquid nitrogen and lyophilized with a FreeZone Plus lyophilizer (Labconco, Kansas City, USA), before being ground into a powder with an A11 Analytical mill (IKA, Staufen, Germany). For solubilization, 20 mg/mL of ECM powder was digested with 2 mg/mL porcine pepsin (Sigma-Aldrich) in 0.01 M HCl under constant agitation at RT for 48 h [28]. Digestion was stopped by neutralising the pH with 0.1 M NaOH and the solution was brought to 1X PBS with one-tenth volume 10X PBS to generate the lung ECM pre-gel solution which was stored at 4°C indefinitely.

A ruthenium Visible Light Photo initiator (400-450nm) kit (Advanced BioMatrix, San Diego, California, US) containing pentamethyl cyclopentadienyl bis(triphenylphosphine) ruthenium(II) chloride (CAS Number: 92361-49-4, hereafter referred as ruthenium) and sodium persulfate (CAS: 7775-27-1) was used to crosslink the LdECM hydrogels (**Figure 1B**). 20 µL of each ruthenium. (37.4 mg/mL) and sodium persulfate (119 mg/mL) solutions were added per 1 mL of ECM hydrogel. The control gel received the same volume of sterile ddH_2O water. In the dark, both the ruthenium-containing gel and the control gel without ruthenium were pipetted (200 µL) into a 48-well plate and incubated at 37°C for 1 h. After the hydrogels had settled, crosslinking of the ECM by photoinitiated ruthenium was triggered by exposing the samples to UV/Visible light from 4.5 cm distance using 2 x 9W UV lamps (405 nm) (20 mW/cm^2 light intensity) for 5 min to generate Ru-LdECM hydrogel (**Figure 1B**). Finally, the gels were immersed in 400 µL of Dulbecco's Modified Eagle Medium (DMEM) Low Glucose growth media (Lonza) supplemented with 10% foetal bovine serum (FBS), 1% penicillin-streptomycin and 1% GlutaMAX (Gibco) (hereafter referred as complete growth medium), and were washed 3X with media before cell seeding in order to remove excess (both reacted and unreacted) ruthenium and sodium persulfate.

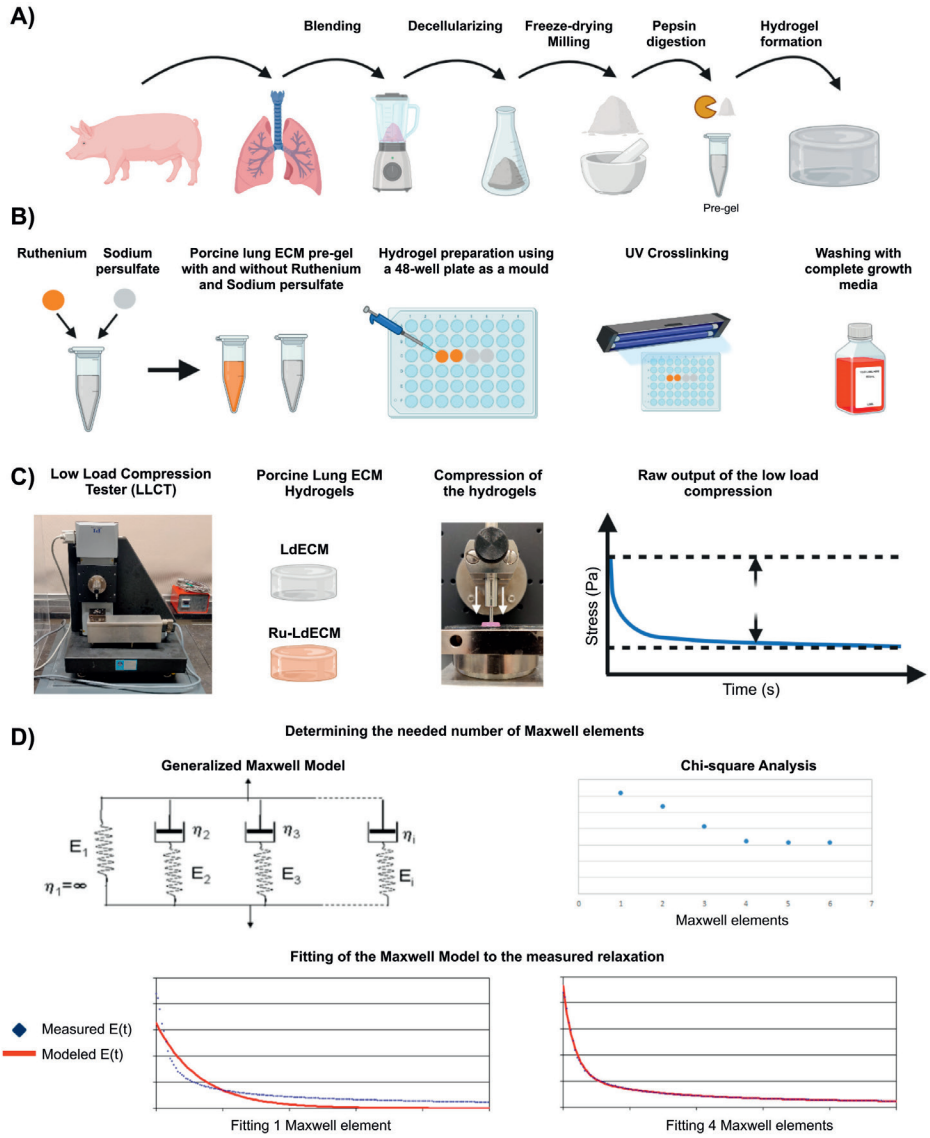

■ **Figure 1: Schematic representation of the methodology. A) Porcine lung ECM hydrogel preparation.** Porcine lungs were blended, decellularized and freeze-dried before grinding to a fine powder. Afterwards, the ECM powder was pepsin digested to prepare the pre-gel solution which can form hydrogels after incubating at 37°C. B) Fibre crosslinking of porcine lung ECM hydrogels. Lung derived-ECM (LdECM) hydrogels were used as is or mixed with ruthenium and sodium persulfate solutions before casting to 48-well plates. Afterwards, the pre-gel solutions were incubated at 37°C and UV-crosslinked. C) Mechanical characterization of the uncrosslinked and ruthenium crosslinked ECM hydrogels. Low Load Compression Tester (LLCT) was used to determine the stiffness and stress relaxation of LdECM and Ru-LdECM hydrogels. The stress relaxation was modelled with a Maxwell elements system, and a chi^2 analysis was used to determine the number of Maxwell elements to fit the measured relaxation. Figure created with BioRender.

Characterization of the Mechanical properties

Both LdECM and Ru-LdECM hydrogels were made as described in hydrogel preparation. The gels were subjected to uniaxial compression with a 2.5 mm diameter plunger at three different locations, at least 2 mm away from the gel border and ensuring 2 mm or more between each compression site (**Figure 1C**). The stress relaxation test was performed with a low-load compression tester (LLCT) at RT as described previously [6, 26, 29]. The LabVIEW 7.1 program was used for the LLCT load cell and linear positioning for control and data acquisition. The resolution in position, load, and time determination was 0.001 mm, 2 mg, and 25 ms, respectively, and the compression speed was controlled in feedback mode. Samples were compressed to 20% of their original thickness (strain $\varepsilon = 0.2$) at a deformation speed of 20 %/s (strain rate $\dot{\varepsilon} = 0.2\ s^{-1}$). The deformation was held constant for 100 s and the stress continuously monitored. During compression, the required stress was plotted against the strain. In this plot, a linear increase in stress as a function of strain was observed between a strain of 0.04 and 0.1; the slope of the line fit to this region was taken as Young's modulus. Young's modulus essentially describes the stiffness of a material [30]. Since the Young's modulus of the viscoelastic gel depends on the strain rate, values reported here are valid only at a strain rate of $0.2\ s^{-1}$.

After compression, the required stress to maintain a constant strain of $0.2\ s^{-1}$, continuously decreases with time, which is a clear indication of the viscoelastic nature of the hydrogels and called stress relaxation. The shape of the stress relaxation curve was mathematically modelled with a generalized Maxwell model (2) (Fig. 1C). The continuously changing stress [$\sigma(t)$] was converted into continuously changing stiffness [$E(t)$] by dividing with the constant strain of $0.2\ s^{-1}$. Obtained $E(t)$ values were fitted to Eq. 1 to obtain the relaxation time constants (τ_i), and Eq. 2 provided relative importance (R_i) for each Maxwell element.

$$E(t) = E_1 e^{-t/\tau_1} + E_2 e^{-t/\tau_2} + E_3 e^{-t/\tau_3} + \dots E_n e^{-t/\tau_n} \quad (1)$$

$$R_i = 100.\frac{E_i}{\sum_{i=1}^{n} E_i} \quad (2)$$

where i varies from 1 to 4 or from 1 to 3 when necessary. The optimal number of Maxwell elements was determined with the chi-square function expressed by Eq. 3 (typically 3 or 4) and visually matching the modelled stress relaxation curve to the measured curve (Fig. 1C).

$$x^2 = \sum_{j=0}^{100} \left(\frac{E_j - E(t_j)}{\sigma_j} \right) \quad (3)$$

where j varies from 0 to 100 s, E_j is the experimentally measured value at time j, $E(t_j)$ is the fit value at time j calculated with Eq. 1, and σ_j is the standard error that the LLCT makes because of inherent errors in position, time, and load measurements.

Histological characterisation of ECM hydrogel fibre structure

LdECM and Ru-LdECM hydrogels were prepared and washed as described above and fixed with 2% paraformaldehyde in PBS (PFA; Sigma-Aldrich) at RT for 20 min. The gels were then embedded in 1% Ultrapure agarose (Invitrogen, Waltham, MA, USA) before using a graded alcohol series to dehydrate followed by paraffin embedding. Sections (4 µm) were deparaffinised, and stained with 0.1 % Picrosirius Red (PSR) (Sigma-Aldrich) in 1.3% aqueous solution of picric acid to visualize collagens and their network. Slides were mounted with Neo-Mount® Mounting Medium (Merck, Darmstadt, Germany).

Cell culture

MRC-5 foetal lung fibroblasts (n=5) were cultured in complete growth medium. The MRC-5s were washed with Hank's Balanced Salt Solution (HBSS; Gibco), harvested using 0.25% Trypsin-EDTA (Gibco) and centrifuged at 500 x g for 5 minutes. Cells were resuspended in 1 mL complete growth media and counted with a NucleoCounter NC-200™ (Chemometec, Allerod, Denmark). Fibroblasts were seeded on top of pre-prepared and washed LdECM and Ru-LdECM hydrogels in complete growth media with the seeding density 10.000 cells/gel. The cells were cultured on the gels for 1 or 7 days. Gels used for live/dead staining were stained with the live/dead stain and were subsequently harvested. Gels intended for immunofluorescent imaging were fixed in 2% PFA in PBS for 30 minutes. After fixation, hydrogels were washed three times with PBS and stored in PBS containing 1% penicillin-streptomycin at 4°C until analyses.

Live/dead staining

Cell viability of the MRC-5 cells cultured on LdECM and Ru-LdECM hydrogels was assessed after 1 and 7 days using Calcein AM (Thermo Scientific, Breda, the Netherlands) to stain live cells and propidium iodide (PI; Sigma-Aldrich) for staining dead cells, as previously described [31]. The hydrogels were first washed with HBSS and then incubated with serum free media containing 5 µM Calcein AM and 2 µM PI, for 1 hour at 37°C. After incubation, fluorescent images were captured using a EVOS Cell Imaging System (Thermo Scientific) with GFP (509 nm) and Texas Red (615 nm) channels.

Immunofluorescence Staining

The hydrogels were treated with avidin/biotin blocking kit (ThermoFisher) before being incubated with 0.5 µg/mL biotinylated wheat germ agglutinin (Vector Laboratories, Burlingame, USA) for 20 min at 37°C . Then the hydrogels were washed and permeabilized by incubating with 0.5% v/v Triton X-100 in HBSS for 10 min at RT and subsequently blocked in 2.5% v/v BSA + 0.1% Triton-X 100 in HBSS for 30 min at RT. Endogenous peroxidase activity was blocked by 30 min incubation in a 0.3% hydrogen peroxide solution. Afterwards, the hydrogels were incubated overnight with a mouse anti-human α-smooth muscle actin antibody (DAKO, Glostrup, Denmark) at 4°C. A rabbit-anti-mouse antibody conjugated with peroxidase (DAKO) and streptavidin conjugated with Alexa Fluor 555 (ThermoFisher) were used as a second step for 45 minutes at room temperature Staining for α-SMA was then developed by Opal650 tyramide (Akoya Biosciences, Marlborough MA, USA) according to the manufacturer's instructions. After staining with 0.1 µg/mL DAPI solution (Merck), the hydrogels were mounted with Citifluor Mounting Medium (Science Services, Munich, Germany) and fluorescence microscopy was performed to acquire images.

Imaging and image analysis

Fluorescent images of PSR-stained LdECM and Ru-LdECM hydrogel sections were generated with Zeiss LSM 780 CLSM confocal microscope (Carl Zeiss NTS GmbH, Oberkochen, Germany), λ_{ex} 561 nm / λ_{em} 566/670 nm at 40x magnification. TWOMBLI plugin for FIJI ImageJ was used to assess the number of fibres, end points, branching points, total fibre length and alignment, lacunarity, high density matrix (HDM) and curvature of the fibres as previously described (*Supplementary Figure 1*) [26, 32]. Fluorescent images of cell-seeded hydrogels stained for αSMA, wheat germ agglutinin and DAPI were generated with Leica SP8 confocal microscope (Leica, Wetzlar, Germany), using λ_{ex} 627 nm / λ_{em} 650 nm for αSMA, λ_{ex} 555 nm / λ_{em} 580 nm for wheat germ agglutinin and λ_{ex} 359 nm / λ_{em} 457 nm for DAPI at 40X and 63X magnifications. Five separate images per sample (n = 5) were used to calculate the stiffness-induced changes in the expression of α-SMA, nuclei area and eccentricity (which is also described as inverse circularity (Supplementary Figure 2). Expression of α-SMA per nuclei was calculated using built-in functions for measuring area in ImageJ. CellProfiler 4.2.1 software was used to analyse the nuclei characteristics on the DAPI-stained images as previously described [33]. Circularity of the samples were calculated from the eccentricity values using the equation (4).

$$Circularity\ (n) = 1 - Eccentricity\ (n) \quad (4)$$

Statistical analysis

All statistical analyses were performed using GraphPad Prism v9.1.0 (GraphPad Company, San Diego, USA). Data are presented as mean values with standard deviation (SD). All data was tested for outliers using the robust regression and outlier removal (ROUT) test and analysed for normality using Shapiro-Wilk and Q-Q plots (*Supplementary Figure 3*). For the data that were normally distributed, differences between control porcine lung ECM hydrogel and ruthenium crosslinked ECM hydrogels generated from the same batch of LdECM and used in the same experiment were tested by paired t-test to compare the effect of crosslinking between different experiments. For the data that were not normally distributed, Mann-Whitney test was used to compare the effect of crosslinking between different experiments. All data were considered significantly different when $p < 0.05$.

RESULTS

Ruthenium crosslinking increases hydrogel stiffness

Both LdECM and Ru-LdECM solutions were able to form hydrogels after incubating at 37 °C. UV/Visible light crosslinking did not result in a macroscopic change in the LdECM hydrogels. Ru-LdECM hydrogels (and the solution before the crosslinking) had a bright orange colour due to the ruthenium addition.

Stiffness measurements on LdECM and Ru-LdECM hydrogels were performed using a low-load compression tester (LLCT). Ruthenium crosslinking increased the stiffness of the Ru-LdECM 5-10-fold ($p = 0.0026$, paired t-test) (**Figure 2**).

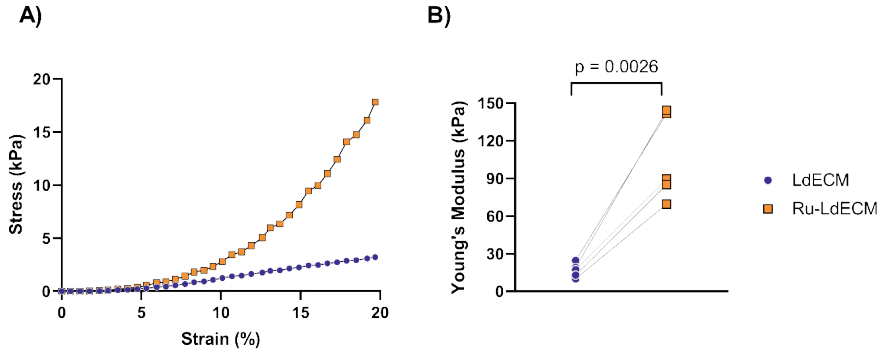

■ **Figure 2: Comparison of stiffness of control and ruthenium-crosslinked hydrogels.** LdECM and Ru-LdECM hydrogels were mechanically tested using Low Load Compression Tester (LLCT) with a fixed 20% strain ratio. A) Representative stress-strain curve for LdECM and Ru-LdECM hydrogels. B) Comparison of stiffness of LdECM and Ru-LdECM hydrogels. Each dot represents the mean of three independent measurements on the same hydrogel for each sample (n = 5). Applied test: Paired t-test to compare the LdECM and Ru-LdECM hydrogels that were generated in the same experimental batch (as indicated by the connecting lines in the graph). LdECM: Lung-derived ECM Hydrogels, Ru-LdECM: Ruthenium-crosslinked Lung-derived ECM Hydrogels

Decreased stress relaxation rate in ruthenium-crosslinked ECM hydrogels

The stress relaxation behaviour of both the LdECM and RU-LdECM hydrogels were measured after applying 20% strain using LLCT measurement. The average stress relaxation profiles of both groups over 100 s are visualized in **Figure 3A.** Ru-LdECM hydrogels did not reach 100% stress relaxation during the 100 s monitored, while some LdECM hydrogels achieved 100% stress relaxation. In addition to the decreased total stress relaxation percentage (in 100s) in the Ru-LdECM hydrogels, the relaxation profile was different. The rate of stress relaxation slowed down earlier in the crosslinked hydrogels. To assess the dynamic differences in the initial stress relaxation behaviour patterns in both groups the time to reach 50% total stress relaxation was compared. LdECM hydrogels reached 50% stress relaxation in significantly shorter time compared to the Ru-LdECM hydrogels. ($p = 0.0054$, paired t-test) (**Figure 3B**).

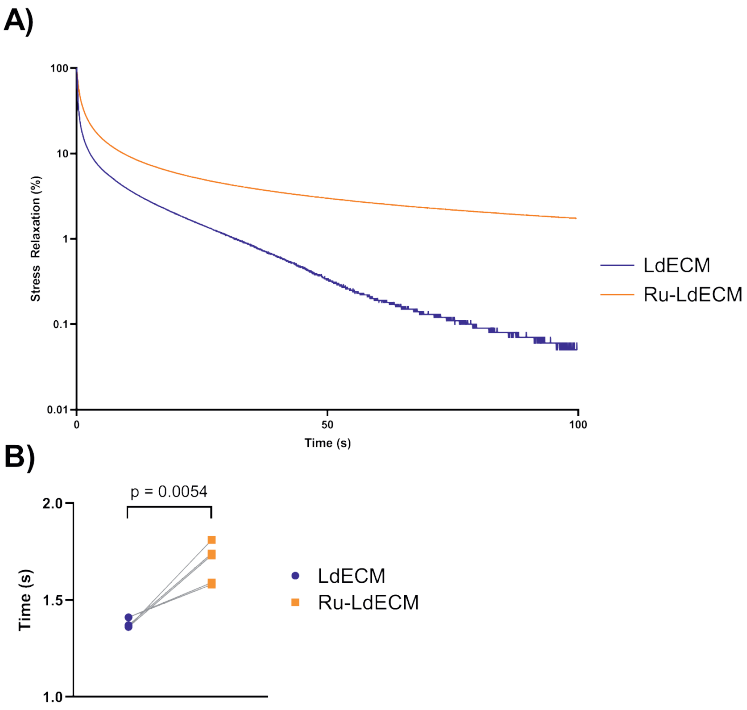

■ **Figure 3: Stress relaxation in control and ruthenium-crosslinked ECM-derived hydrogels.** After compressing the LdECM and Ru-LdECM hydrogels using Low Load Compression Tester (LLCT) with a fixed 20% strain ratio, the stress relaxation behaviour was recorded over 100s period. A) Average stress relaxation behaviour over 100 s duration. B) Time taken to reach 50% stress relaxation. Each dot represents the mean of three independent measurements on the same hydrogel for each sample (n = 5). Applied test: Paired t-test to compare the LdECM and Ru-LdECM hydrogels that were generated in the same experimental batch (as indicated by the connecting lines in the graph). LdECM: Lung-derived Extracellular Matrix Hydrogels, Ru-LdECM: Ruthenium-crosslinked Lung-derived Extracellular Matrix Hydrogels.

Altered relaxation profile in ruthenium-crosslinked ECM hydrogels

Since the ECM hydrogels are a viscoelastic material with various elastic (e.g., ECM proteins) and viscous components (e.g., water, bound water), we mathematically modelled this using a generalized Maxwell model. This approach allowed the total relaxation data to be split into Maxwell elements that can theoretically be attributed to physical components in the hydrogels. Each of these Maxwell elements are responsible for a part of the total relaxation (relative importance), as well as occurring within a specific time window during the relaxation process. The distribution of the time constants of these different elements and their respective relative importance are presented in **Figure 4**. The stress relaxation of the LdECM hydrogels could be

modelled with 3 Maxwell elements while Ru-LdECM hydrogels needed 4 Maxwell elements. Next to the difference in the number of Maxwell elements required to explain the relaxation profiles, the time constants of the elements differed between the two groups: the first element was significantly faster in the LdECM hydrogels ($p = 0.002$, paired t-test) while the third element took longer in the LdECM hydrogels ($p = 0.002$, paired t-test) compared to the Ru-LdECM (**Figure 4A**).

The relative importance of the Maxwell elements was used to assess the individual contribution of each element to the total stress relaxation over the 100 seconds (**Figure 4B).** In both types of hydrogels, the first element made the greatest contribution to the stress relaxation profile, although the percentage contribution was significantly lower in the Ru-LdECM hydrogels compared with the LdECM hydrogels ($p = 0.002$, paired t-test). The contribution of the second Maxwell element was the second largest in both groups while the relaxation profile of the Ru-LdECM hydrogels had a significant increase in the contribution of this element compared to uncrosslinked hydrogels ($p = 0.0002$, paired t-test). The third element had the lowest percentage contribution in LdECM hydrogels, with this contribution being lower than this element in its ruthenium-crosslinked counterpart ($p = 0.002$, paired t-test).

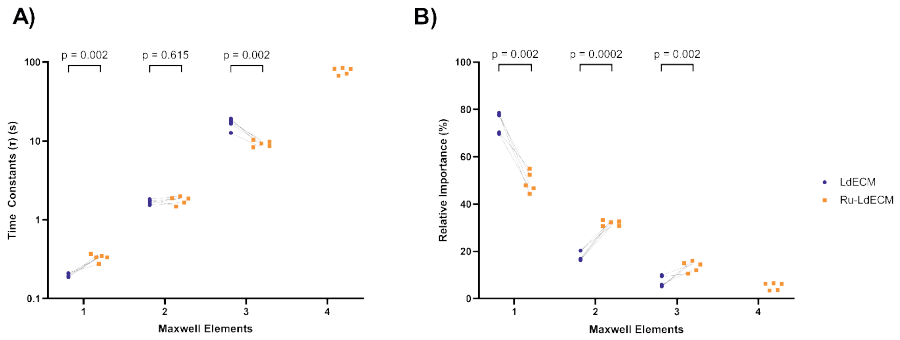

■ **Figure 4: Analysis of the stress relaxation behaviour through the generalized Maxwell model system.** The relaxation profiles of the both types of hydrogels over 100 s period was mathematically modelled using a Maxwell model system and the relative importance values of the Maxwell Elements were determined. A) Time constants for each Maxwell element for LdECM and Ru-LdECM hydrogels. B) Relative importance (%) of the each Maxwell element for LdECM and Ru-LdECM hydrogels. Each dot represents the mean of three independent measurements on the same hydrogel (n = 5). Applied test: Paired t-test to compare the LdECM and Ru-LdECM hydrogels that were generated in the same experimental batch (as indicated by the connecting lines in the graph). LdECM: Lung-derived ECM Hydrogels, Ru-LdECM: Ruthenium-crosslinked Lung-derived ECM Hydrogels

Increased density and decreased alignment of fibres in lung ECM hydrogels after ruthenium crosslinking

Ru-LdECM hydrogels had a denser fibre network compared to LdECM hydrogels (**Figure 5A**). The average fibre length was shorter in Ru-LdECM than LdECM hydrogels ($p = 0.0026$, paired t-test). While the normalized numbers of endpoints and branchpoints did not differ between LdECM and Ru-LdECM hydrogels, the percentage of area with high density matrix (HDM) was greater in Ru-LdECM hydrogels compared with LdECM hydrogels ($p = 0.0146$, paired t-test). Alignment of the fibres in Ru-LdECM hydrogels was lower than LdECM hydrogels ($p = 0.0048$, paired t-test) (**Figure 5B-G**).

The differences in the curvature of the fibres with different length were compared in LdECM and Ru-LdECM hydrogels. Curvature of the fibres with shorter length (< 40 µm) were higher in the crosslinked hydrogels, suggesting that shorter fibres were more bent in Ru-LdECM hydrogels while curvature of the longer fibres was not different between these two groups (**Table 1**).

Ruthenium crosslinking does not affect fibroblast viability but induces altered morphology

After 1 day of culture, no dead cells were observed and the fibroblasts were viable on both types of hydrogels (**Figure 6**). The viability of the fibroblasts did not change over a 7-day culture period (*Supplementary Figure 4*). On both gels the fibroblasts appeared to be lying flat on the surface of the hydrogels; however, the fibroblasts on LdECM hydrogels display a more spindle-shaped morphology, while fibroblasts on Ru-LdECM gels are were more hypertrophic and display more protrusions. Suggesting a more migratory phenotype for fibroblasts on Ru-LdECM hydrogels. At day 7, a fully confluent monolayer was present on both control and crosslinked hydrogels with no differences in viability.

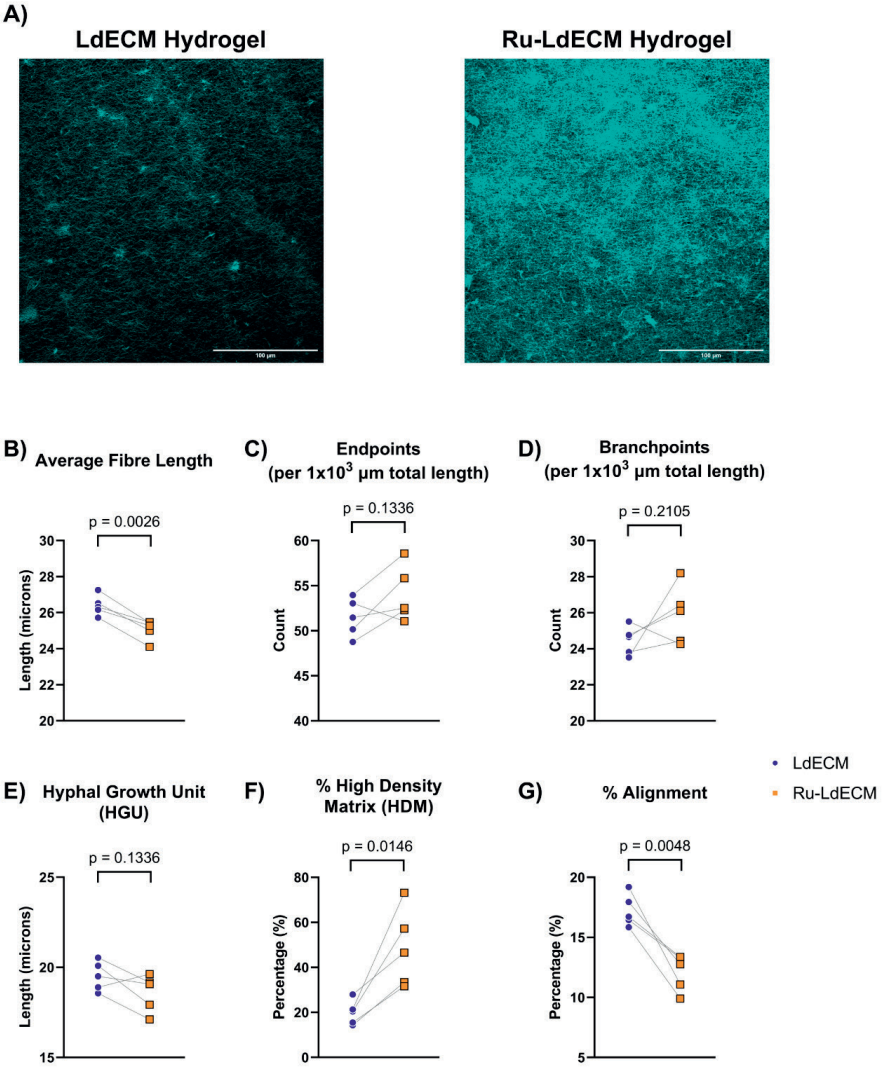

■ **Figure 5: Picrosirius red staining on LdECM and Ru-LdECM and fibre characteristics analysis on the collagen network.** LdECM and Ru-LdECM hydrogels were stained using Picrosirius red staining and generated fluorescent images were analysed using TWOMBLI plugin in FIJI ImageJ. A) Representative images of Picrosirius red staining on LdECM and Ru-LdECM hydrogels, B) Average Fibre Length, C) Endpoints per 1000 µm total length, D) Branchpoints per 1000 µm total length, E) HGU, F) % of High Density Matrix (HDM), G) % fibre Alignment. Each dot represents the mean of measurements of 5 different randomized regions on the fluorescent images of Picrosirius red staining for each sample (n=5). Applied statistical test: paired t-test to compare the LdECM and Ru-LdECM hydrogels that were generated in the same experimental batch (as indicated by the connecting lines in the graph). LdECM: Lung-derived ECM Hydrogels, Ru-LdECM: Ruthenium-crosslinked Lung-derived ECM Hydrogels

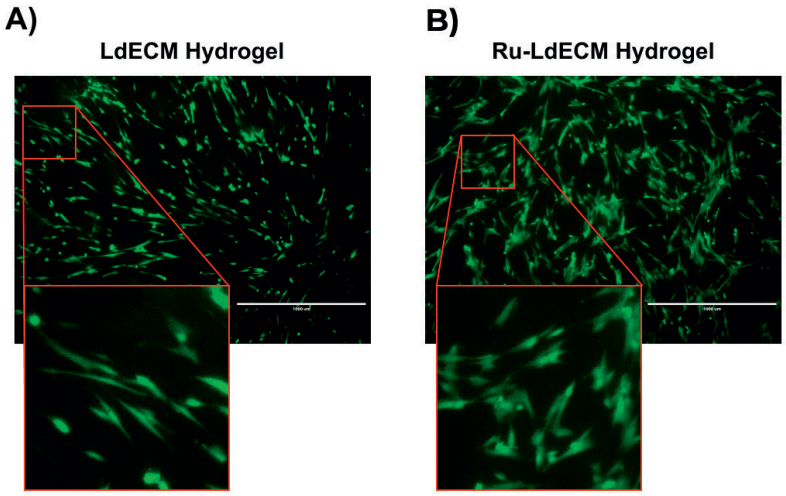

- **Figure 6: Live/dead staining on MRC-5 fibroblasts seeded on LdECM and Ru-LdECM hydrogels on day 1 using Calcein AM (green) and propidium iodide (red).** A) MRC-5 fibroblasts cultured on the LdECM hydrogels, B) MRC-5 fibroblasts cultures on Ru-LdECM hydrogels. Scale bar: 1000 µm. Results are representative for all experiments (n =5). LdECM: Lung-derived ECM Hydrogels, Ru-LdECM: Ruthenium-crosslinked Lung-derived ECM Hydrogels

- **Table 6: TWOMBLI analysis for the curvature of fibres with different lengths.** All results show mean ± standard deviation of n = 5. Each analysis was performed using averages of 5 different randomized regions on the fluorescent images of Picrosirius red staining for each sample. LdECM: Lung-derived ECM Hydrogels, Ru-LdECM: Ruthenium-crosslinked Lung-derived ECM Hydrogels. Applied statistical test: paired-t test to compare the LdECM and Ru-LdECM hydrogels that were generated in the same experimental batch. $P < 0.05$ was considered statistically significant.

	Average Curvature (Δ°)		
Fibre Length	**LdECM**	**Ru-LdECM**	**P values**
10 µm fibres	42.40 ± 0.92	44.98 ± 0.89	0.019
20 µm fibres	53.47 ± 0.98	56.02 ± 0.92	0.022
30 µm fibres	59.12 ± 0.71	60.84 ± 0.86	0.027
40 µm fibres	62.55 ± 0.51	63.29 ± 1.02	0.12
50 µm fibres	64.32 ± 0.79	64.60 ± 0.84	0.58

Ruthenium crosslinking of ECM hydrogel promotes differentiation of fibroblasts to myofibroblasts

Fibroblasts seeded on Ru-LdECM hydrogels had higher expression of α-SMA when compared to LdECM hydrogel-seeded fibroblasts (**Figure 7**). In addition to the stronger expression of α-SMA, the organization of the cytoskeleton was altered in the fibroblasts seeded on the Ru-LdECM hydrogels (**Figure 7B**, lower row). When these images were quantified using ImageJ, fibroblasts seeded on Ru-LdECM hydrogels had significantly higher α-SMA expression per nuclei ($p < 0.0001$) compared with the fibroblasts seeded on LdECM hydrogels (**Figure 8A).** These myofibroblast-like characteristics were also accompanied by a change in the nuclear morphology.

At day 7, the nuclei in the fibroblasts on Ru-LdECM hydrogels had an altered morphology as illustrated by the higher area ($p < 0.0001$, Mann-Whitney test) with an increased circularity ($p < 0.0001$, Mann-Whitney test) compared with the fibroblasts seeded on LdECM hydrogels (**Figure 8, B and C**).

DISCUSSION

In this study we describe a model that enables modulation of the mechanical properties of an ECM without changing the composition. Using this model, we illustrated that by modulating the crosslinks between ECM fibres, the stiffness and stress relaxation properties of the ECM-derived hydrogels were altered. The crosslinking influenced the ECM fibre characteristics with a higher percentage of high density matrix and lower percentage of alignment being evident within the hydrogels treated with ruthenium. Fibroblasts grown on the surface of the crosslinked hydrogels displayed more myofibroblast-like characteristics. The features of this model illustrate that it would provide an innovative research tool for investigating the importance of biomechanical changes in fibrotic diseases.

The increase in stiffness caused by ruthenium crosslinking in the LdECM hydrogels is similar to the increase in stiffness seen in fibrotic lung diseases such as idiopathic pulmonary fibrosis (IPF) [15]. Booth et al. measured the stiffness of whole non-IPF and IPF human lungs before and after decellularization and found that the fibrotic regions of the IPF lung often reached a stiffness of 100 kPa or more, a vast increase compared to that of normal lung which has an average stiffness of 1.96 kPa [15]. The increased stiffness of IPF human lung was still present in hydrogels when compared to hydrogels generated from control human lungs, albeit proportionally reduced when compared to the intact lung tissue [6]. Recreating the (patho)physiological stiffness

is essential to study the corresponding behaviour of cells during fibrotic diseases [34]. Ruthenium crosslinking on ECM-derived hydrogels provides an ideal opportunity to recreate the (patho)physiological stiffness. This is due to the fact that it does not require additional modifications on the ECM itself, enabling the modification of the mechanical properties while keeping the biochemical composition of the ECM constant. Thus these hydrogels mimic only the altered mechanical properties

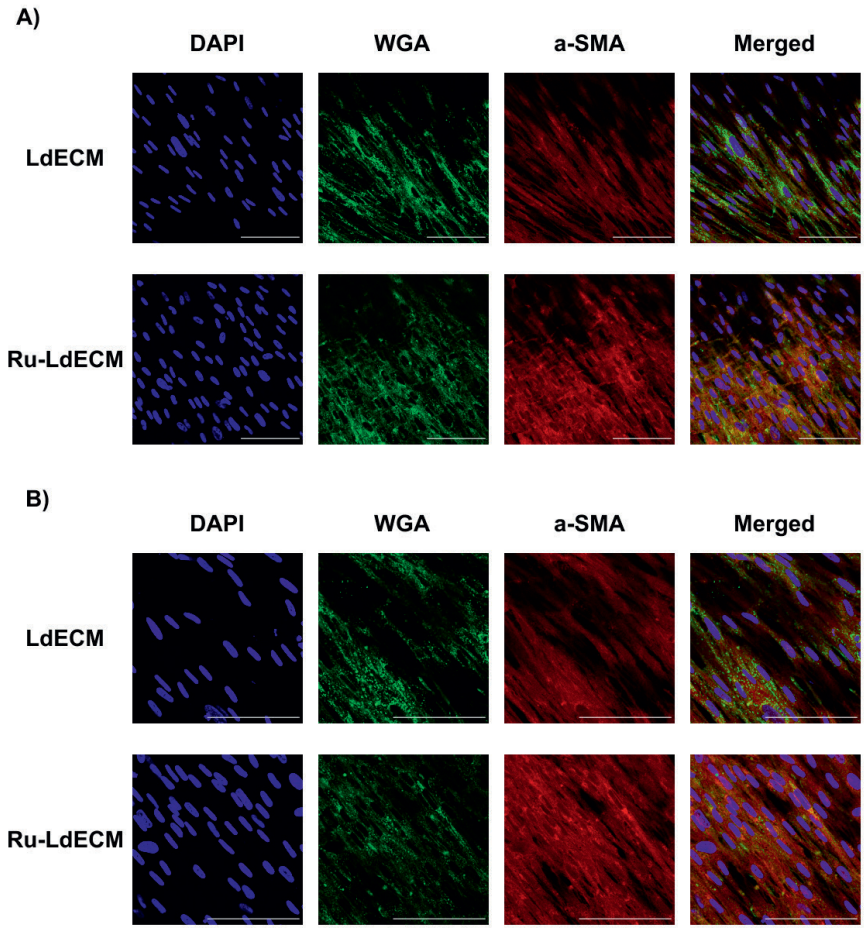

Figure 7: Fluorescence images for the comparison of cell nuclei (DAPI), cell membrane (WGA) and cytoskeleton (α-SMA) on MRC-5 fibroblasts seeded on LdECM and Ru-LdECM hydrogels at day 7. A) Top row: Stained LdECM hydrogels imaged at original objective magnification 40×, bottom row: digitally magnified versions of the respective images B) Stained Ru-LdECM hydrogels imaged at original objective magnification 40×, bottom row: digitally magnified versions of the respective Scale bars: 100 µm. LdECM: Lung-derived ECM Hydrogels, Ru-LdECM: Ruthenium-crosslinked Lung-derived ECM Hydrogels. WGA: Wheat germ agglutinin, α-SMA: alpha smooth muscle actin

observed in fibrotic diseases. Ruthenium crosslinking relies on the crosslinking of the tyrosine amino acids and the potential for employing this strategy on the ECM-derived hydrogels has recently been demonstrated by Kim et al. [25]. The ruthenium crosslinking of the ECM in our model allows us to recreate the (patho)physiological mechanical environment in a fibrotic lung. This method can most likely be adapted to generate tissue specific fibrotic environments that are representative of many organ microenvironments.

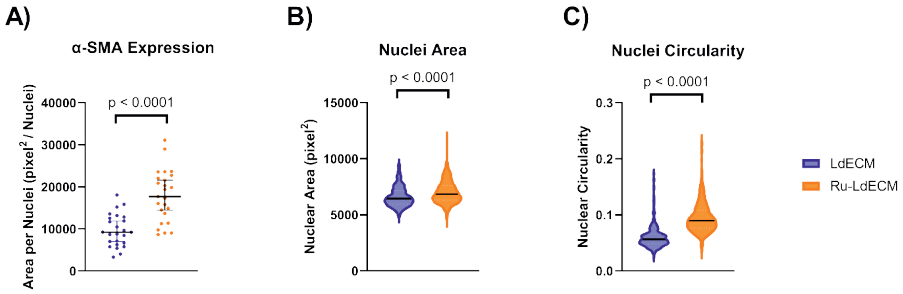

■ **Figure 8: Comparison of the fibroblasts seeded on LdECM and Ru-LdECM hydrogels. α-SMA and DAPI-stained fluorescent images of the fibroblasts were analysed using the ImageJ and CellProfiler software to compare the α-SMA expression per nuclei, the nuclear area and circularity.** A) Quantification of the α-SMA expression per cell nuclei imaged in the fluorescent images. B) Comparison of nuclear area of fibroblasts seeded on LdECM and Ru-LdECM. C) Nuclear circularity of the fibroblasts seeded on LdECM and Ru-LdECM hydrogels. For panel A, each data point represents the quantification of the images generated from different randomized regions (n=5 per hydrogel) from different hydrogels (n=5 total). Applied statistical test: Mann-Whitney test. For panels B and C, each data point represents measurement on an individual nucleus for the respective characteristic, in total from 5 different randomized regions on the fluorescent images of DAPI staining for each sample (n=5). Applied statistical test: Mann-Whitney test. α-SMA: alpha-smooth muscle actin, LdECM: Lung-derived ECM Hydrogels, Ru-LdECM: Ruthenium-crosslinked Lung-derived ECM Hydrogels

Different rheology measuring techniques will yield slightly different results and have specific benefits. A study by Polio et al. used cavitation rheology, micro-indentation, tensile testing and small amplitude oscillatory shear rheometry on porcine lung and found that each technique resulted in a different Young's modulus [35]. A previous study shows the difference in viscoelastic properties of human lung ECM hydrogels and intact (patho)physiological counterparts where the hydrogels had a lower stiffness and higher total relaxation [6]. The first Maxwell element was the main contributor to the stress relaxation in hydrogels whereas with lung tissue this was more equally divided amongst the elements. ECM hydrogels are reconstituted solutions of decellularized and enzyme-digested ECM proteins and therefore they

lack the chemical crosslinks and the cellular components present in intact and native ECM. This is most likely why the stress relaxation and Young's modulus of the hydrogels differs from intact tissue. Introducing the crosslinks back into the hydrogel as well as tissue specific cells who will remodel their local environment over time can possibly be the factor to bridge the gap that still exists between hydrogel models and native tissue.

Stress relaxation has been found to be an important mechanism that can regulate cellular fate and behaviour [36]. Ruthenium crosslinked LdECM hydrogels had a lower and more complex stress relaxation than uncrosslinked LdECM hydrogels, similar to that of IPF human lung compared to normal human lung [6]. To date, attributing individual Maxwell elements to specific components of a hydrogel such as water, small molecules, cells, or type of crosslinks formed in the ECM remains difficult in absence of a dedicated systematic study [37]. However, the fourth Maxwell element (with a relaxation time constant of ~100 s) for Ru-LdECM hydrogels required to describe their relaxation profile can be attributed to the secondary ECM network formed through the ruthenium crosslinking since this is the only difference between the two tested hydrogels. A similar difference in stress relaxation was found between control and fibrotic human lung ECM-derived hydrogels, showing three Maxwell elements in control hydrogels and 4 Maxwell elements in fibrotic hydrogels [6]. While the differences in species might complicate comparisons between porcine and human lung-derived hydrogels with respect to mechanical properties, the presence of a fourth Maxwell element in a Ru-LdECM hydrogels suggests that these hydrogels were able to resemble the stress relaxation behaviour of fibrotic lung ECM-derived hydrogels.

Ruthenium crosslinking of ECM hydrogels led to a more dense ECM network reflective of tissue changes in fibrotic diseases. Crosslinking the ECM fibres together in LdECM hydrogels resulted in lower fibre lengths and more dense matrix packed areas. In fibrotic lung diseases like IPF, topography and organization of the ECM are altered, as recently summarized elsewhere [38]. Through post-translational modifications and crosslinking of the collagen network by the lysyl oxidase (LO) family of enzymes, lung ECM in IPF has been reported to be more mature and organized, compared to non-IPF lung ECM [4, 39]. The denser matrix with a high degree of crosslinking is a key feature of fibrotic lung disease and protects the ECM from proteolysis [40]. The overall organization of the ECM in IPF is decreased when compared to normal lungs, a characteristic which was also present in the Ru-LdECM hydrogels as seen in the lower alignment [41]. Similar values in normalized numbers of endpoints and branchpoints suggest that fibre integrity was not affected during the crosslinking

and existing branches were crosslinked. The shorter fibres in crosslinked hydrogels might be explained with the increased curvature in these samples: the effect of crosslinking on curvature of fibres with respect to the fibre length was prominent in shorter fibres (<40 µm) while longer fibres did not have differences among the two groups. These observations indicate that the ruthenium-crosslinking mainly influences the shorter fibres and decreases the average fibre length. Together with the mechanical characterization data, these results show that the mechanical properties were altered through the changes in the alignment and density of the matrix (HDM) in the crosslinked hydrogels.

One of the most important components of the fibrotic microenvironment is the (myo) fibroblasts and their responses to the altered ECM. In our model, the cells remained viable and the fibroblasts seeded on crosslinked hydrogels lost their spindle-like morphology that we observed on the native LdECM hydrogels. This observation is in parallel with previously reported studies showing the effect of stiffness on human lung fibroblasts [42]. As a response to the altered mechanical properties in Ru-LdECM hydrogels, the fibroblasts have displayed more myofibroblast-like characteristics.. Increased α-SMA expression and altered organization have been previously reported in lung fibroblasts as a response to increasing stiffness of their environment [42, 43]. Parallel to these previous studies, IPF fibroblasts have been reported to have higher levels of α-SMA expression both at gene [44] and protein [45] levels, compared with non-disease control lung-derived fibroblasts. In addition, another study reported that myofibroblast differentiation was not triggered by an isolated increase in the fibre density of synthetic 3D culture while keeping the stiffness of the environment constant [46]. This observation is also in concert with our results as both stiffness and the fibre organization are altered in Ru-LdECM hydrogels. The accompanying changes in the nuclear morphology was also in agreement with the influence of increased stiffness [47]. As reviewed by Wang et al., nuclear mechanotransduction as a response to a stiffer microenvironment (such as in fibrosis) has yet to be completely understood; however, such a change can result in altered gene regulation or nuclear transportation of cytoplasmic factors [48]. Another implication of the altered nuclear morphology due to increased stiffness was shown to influence the differentiation of mesenchymal stromal cells [49]. These demonstrated changes on the seeded fibroblasts in our study suggest that the biomechanical properties of the fibrotic microenvironment were replicated in our model.

Our study utilizes a crosslinking strategy on native ECM-hydrogels using a ruthenium complex and sodium persulfate, as described recently by Kim et al. [25]. While this innovative approach has its advantages, our study has also some limitations. First of

all, assessing the amounts of excess (unreacted) ruthenium and sodium persulfate remaining in the hydrogels was not possible with our current methodology; however, our future research is looking into further optimizing the amount of ruthenium and sodium persulfate in the reaction. In this study, we have seeded the fibroblasts on top of the hydrogels (2D) instead of seeding them within the hydrogel network. Although a 3D environment would represent the physiological situation in the body, a 2D culture system was preferred in this study to ensure proper visualization of the cell viability and morphology. Our study reports a model for examining the influence of biomechanical changes of the fibrotic microenvironment without investigating any gene and protein output from the fibroblasts . Although the influence of a fibrotic biomechanical microenvironment on fibroblasts have been shown to promote a pro-fibrotic phenotype both in gene and protein levels (as reviewed in [5, 50]), such investigations are beyond the scope of this study. Lastly, the power of Maxwell modelling of the stress relaxation profiles of the native and crosslinked ECM hydrogels has not been completely realized and seems to remain as a mathematical exercise. The reason is that unlike other research areas e.g. microbial biofilms where relaxation constants has been linked to the composition [37], for hydrogels this systematic study is not yet available. With that, such modelling still proves useful in terms of analysing the altered stress relaxation behaviour.

CONCLUSION

This study demonstrates the mechanical characterization of an *in vitro* ECM-based fibrosis model for advancement of investigations on effects of a fibrotic microenvironment on the cells. The next step for this model is to investigate how changes in the stiffness or viscoelastic relaxation can instruct the cells for further profibrotic responses, especially in a 3-dimensional setting. In addition, fibre characteristics analysis revealed that the changes in the fibre organization (alignment, density, curvature) accompany the altered pattern in the viscoelastic stress relaxation behaviour. More research on the influence of these altered fibre characteristics on the profibrotic activation of different cells (fibroblasts, macrophages...) have yet to be explored. Overall, this study shows the preparation and the characterization of an *in vitro* fibrosis model. Such advanced *in vitro* models for fibrosis research will improve our understanding on de-coupling the mechanical changes from the biochemical changes taking place in fibrosis.

DECLARATION OF COMPETING INTEREST

RHJH, FZ, TB, PKS, MCH have no conflicts to declare. MN and JKB receive unrestricted research funds from Boehringer Ingelheim.

ACKNOWLEDGEMENTS

The authors thank Albano Tosato for the assistance with graphical abstract preparation. Nederlandse Organisatie voor Wetenschappelijk Onderzoek (NWO) Aspasia-premie grant number 015.013.010 awarded to JKB.

SUPPLEMENTARY FIGURES

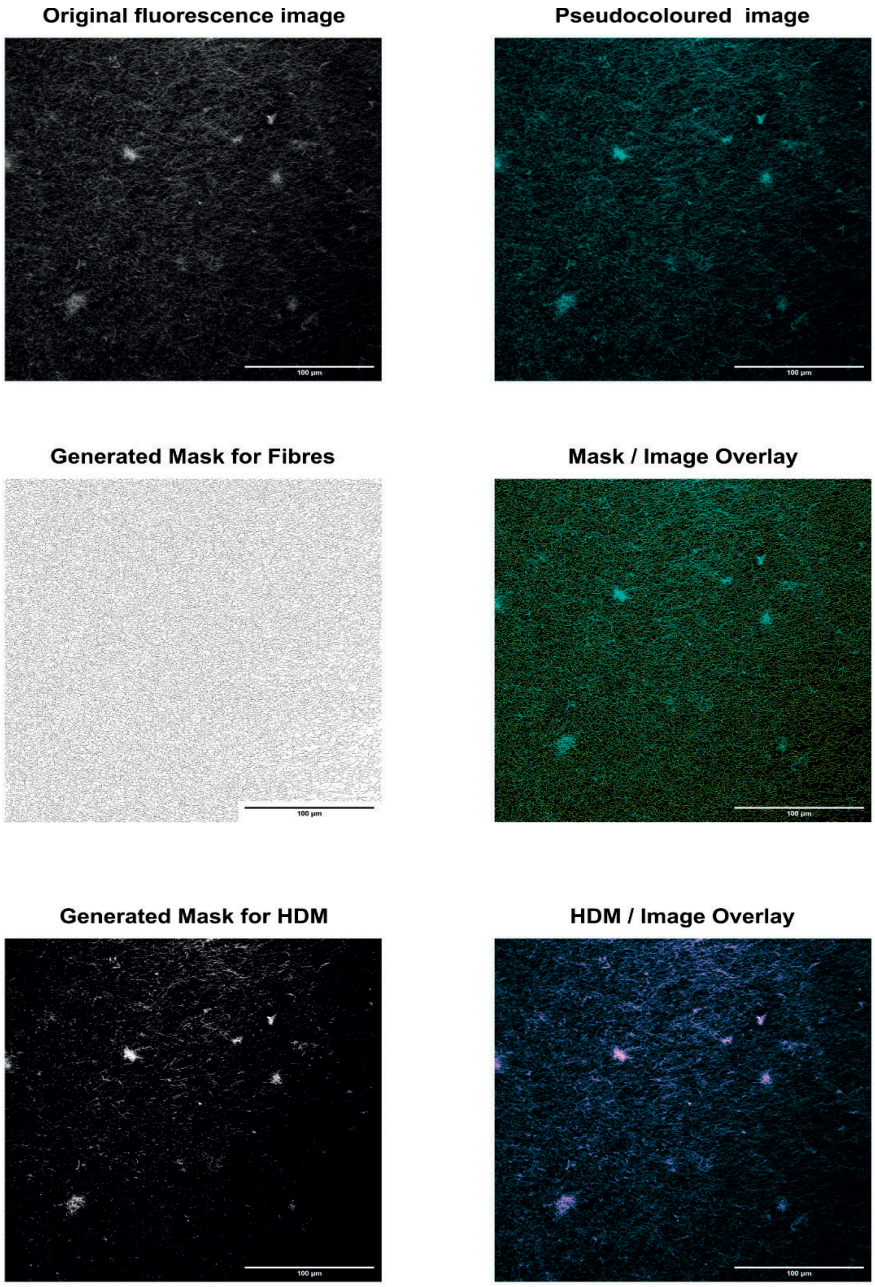

Supplementary Figure 1: Example of the masks and HDM generated through TWOMBLI analysis and their overlays with the original images

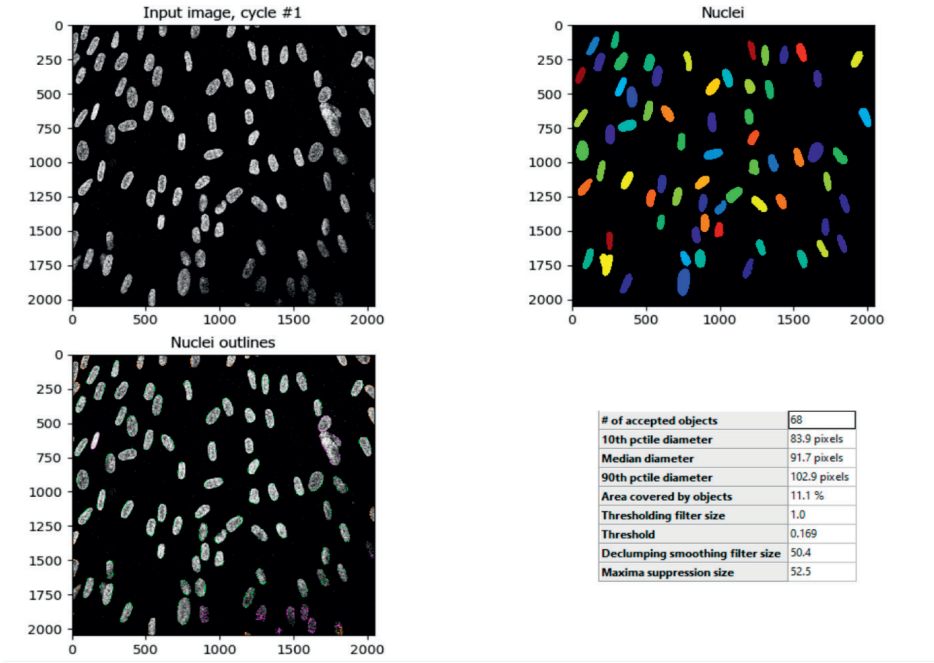

Supplementary Figure 2: Example pipeline of the CellProfiler software for the nuclei analysis.

A)

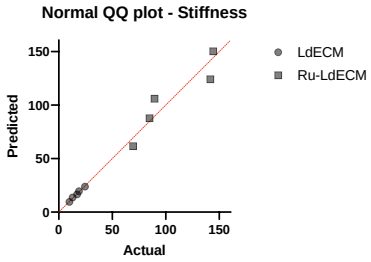
Normal QQ plot - Stiffness
Predicted
Actual
0
50
100
150
LdECM
Ru-LdECM

B)

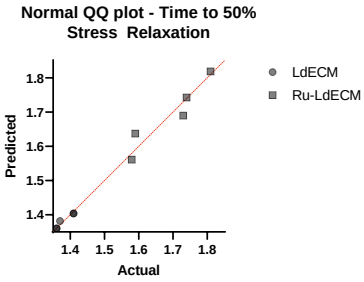
Normal QQ plot - Time to 50% Stress Relaxation
Predicted
Actual
1.4
1.5
1.6
1.7
1.8
LdECM
Ru-LdECM

C)

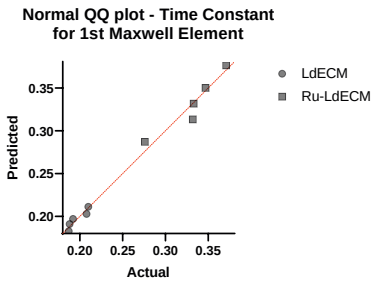
Normal QQ plot - Time Constant for 1st Maxwell Element
Predicted
Actual
0.20
0.25
0.30
0.35
LdECM
Ru-LdECM

D)

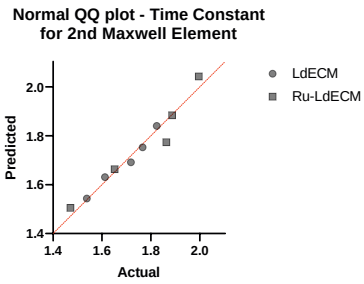
Normal QQ plot - Time Constant for 2nd Maxwell Element
Predicted
Actual
1.4
1.6
1.8
2.0
LdECM
Ru-LdECM

E)

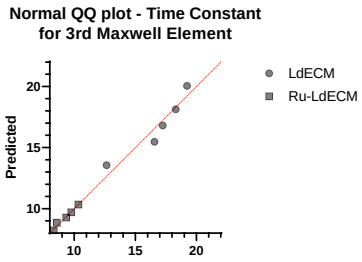
Normal QQ plot - Time Constant for 3rd Maxwell Element
Predicted
10
15
20
LdECM
Ru-LdECM

F)

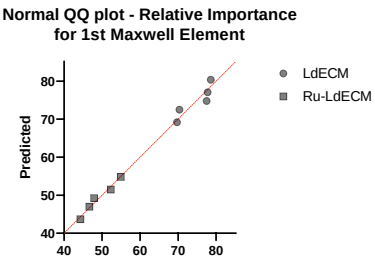
Normal QQ plot - Relative Importance for 1st Maxwell Element
Predicted
40
50
60
70
80
LdECM
Ru-LdECM

G)

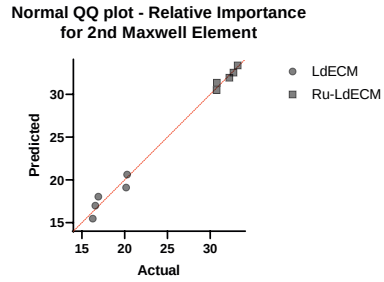
Normal QQ plot - Relative Importance for 2nd Maxwell Element
Predicted
Actual
LdECM
Ru-LdECM

H)

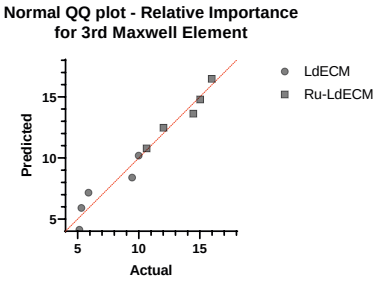
Normal QQ plot - Relative Importance for 3rd Maxwell Element
Predicted
Actual
LdECM
Ru-LdECM

I)

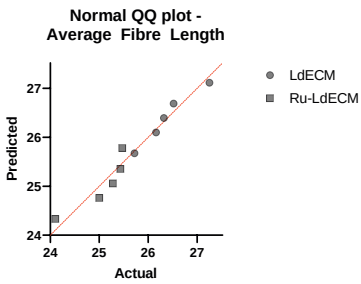
Normal QQ plot - Average Fibre Length
Predicted
Actual
LdECM
Ru-LdECM

J)

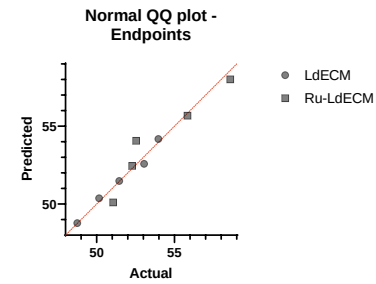
Normal QQ plot - Endpoints
Predicted
Actual
LdECM
Ru-LdECM

K)

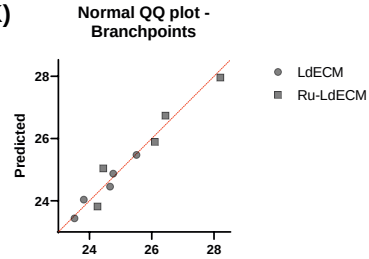
Normal QQ plot - Branchpoints
Predicted
LdECM
Ru-LdECM

L)

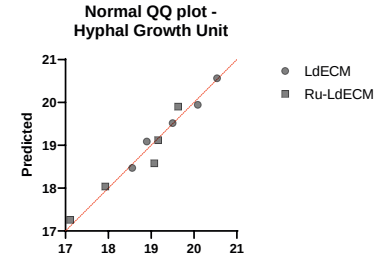
Normal QQ plot - Hyphal Growth Unit
Predicted
LdECM
Ru-LdECM

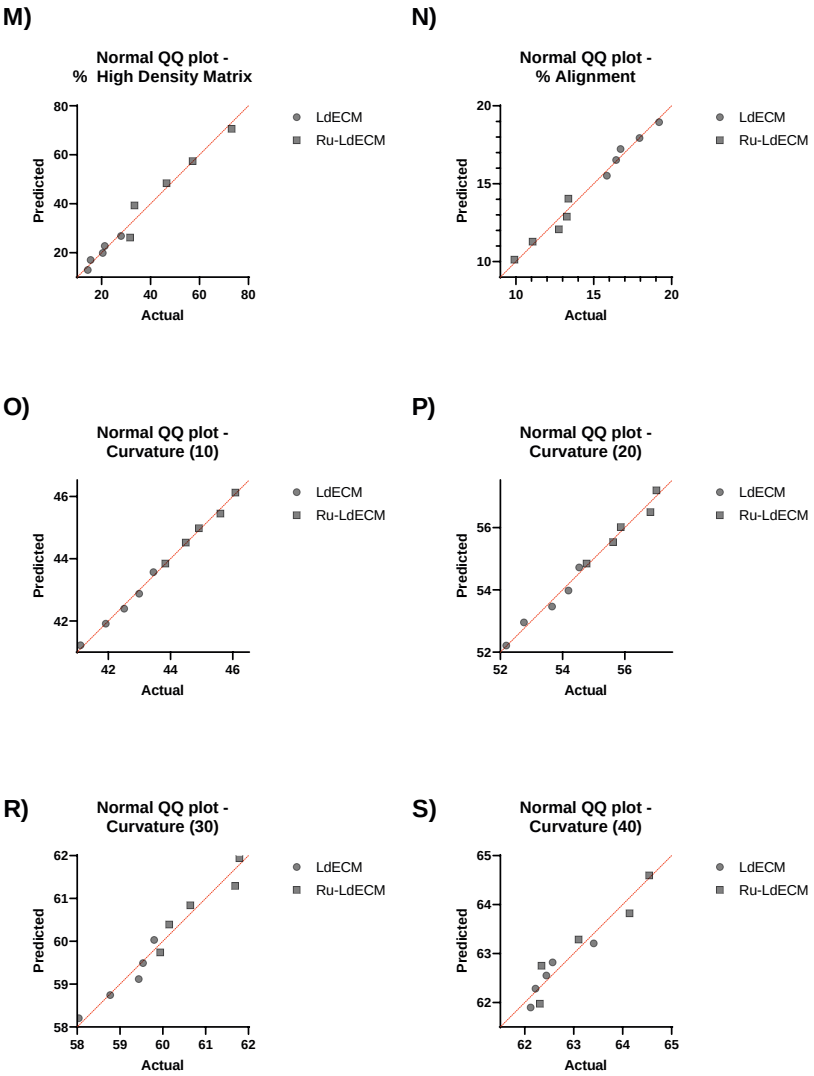

Supplementary Figure 3:Q-Q plots for the normality assessments of the data analyzed using parametric tests. A) Stiffness, B) Time to 50% Stress Relaxation, C) Time Constant for 1st Maxwell Element, D) Time Constant for 2nd Maxwell Element, E) Time Constant for 3rd Maxwell Element, F) Relative Importance for 1st Maxwell Element, G) Relative Importance for 2nd Maxwell Element, H) Relative Importance for 3rd Maxwell Element, I) Average Fibre Length, J) Number of Endpoints, K) Number of Branchpoints, L) Hyphal Growth Unit, M) % High Density Matrix, N) % Alignment, O) Curvature (10 µm fibres), P) Curvature (20 µm fibres), R) Curvature (30 µm fibres), S) Curvature (40 µm fibres), T) Curvature (50 µm fibres).

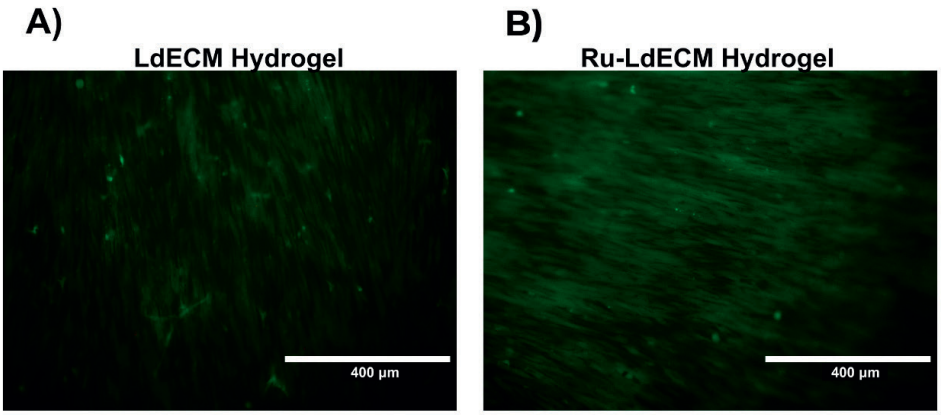

Supplementary Figure 4: Example image of the live/dead staining at day 7.

REFERENCES

1. Theocharis AD, Skandalis SS, Gialeli C, Karamanos NK. Extracellular matrix structure. *Adv Drug Deliv Rev* 2016: 97: 4-27.
2. Frantz C, Stewart KM, Weaver VM. The extracellular matrix at a glance. *J Cell Sci* 2010: 123(Pt 24): 4195-4200.
3. Muiznieks LD, Keeley FW. Molecular assembly and mechanical properties of the extracellular matrix: A fibrous protein perspective. *Biochim Biophys Acta* 2013: 1832(7): 866-875.
4. Burgess JK, Mauad T, Tjin G, Karlsson JC, Westergren-Thorsson G. The extracellular matrix - the under-recognized element in lung disease? *J Pathol* 2016: 240(4): 397-409.
5. Tschumperlin DJ, Ligresti G, Hilscher MB, Shah VH. Mechanosensing and fibrosis. *J Clin Invest* 2018: 128(1): 74-84.
6. de Hilster RHJ, Sharma PK, Jonker MR, White ES, Gercama EA, Roobeek M, Timens W, Harmsen MC, Hylkema MN, Burgess JK. Human lung extracellular matrix hydrogels resemble the stiffness and viscoelasticity of native lung tissue. *Am J Physiol Lung Cell Mol Physiol* 2020: 318(4): L698-L704.
7. Blokland KEC, Pouwels SD, Schuliga M, Knight DA, Burgess JK. Regulation of cellular senescence by extracellular matrix during chronic fibrotic diseases. *Clin Sci* 2020: 134(20): 2681-2706.
8. Vasse GF, Nizamoglu M, Heijink IH, Schleputz M, van Rijn P, Thomas MJ, Burgess JK, Melgert BN. Macrophage-stroma interactions in fibrosis: biochemical, biophysical, and cellular perspectives. *J Pathol* 2021: 254(4): 344-357.
9. Haak AJ, Tan Q, Tschumperlin DJ. Matrix biomechanics and dynamics in pulmonary fibrosis. *Matrix Biol* 2018: 73: 64-76.
10. Herrera J, Henke CA, Bitterman PB. Extracellular matrix as a driver of progressive fibrosis. *J Clin Invest* 2018: 128(1): 45-53.
11. Blaauboer ME, Boeijen FR, Emson CL, Turner SM, Zandieh-Doulabi B, Hanemaaijer R, Smit TH, Stoop R, Everts V. Extracellular matrix proteins: a positive feedback loop in lung fibrosis? *Matrix Biol* 2014: 34: 170-178.
12. Parker MW, Rossi D, Peterson M, Smith K, Sikstrom K, White ES, Connett JE, Henke CA, Larsson O, Bitterman PB. Fibrotic extracellular matrix activates a profibrotic positive feedback loop. *J Clin Invest* 2014: 124(4): 1622-1635.
13. Nizamoglu M, Burgess JK. The Multi-Faceted Extracellular Matrix: Unlocking Its Secrets for Understanding the Perpetuation of Lung Fibrosis. *Curr Tissue Microenviron Rep* 2022: 2(4): 53-71.
14. Saldin LT, Cramer MC, Velankar SS, White LJ, Badylak SF. Extracellular matrix hydrogels from decellularized tissues: Structure and function. *Acta Biomater* 2017: 49: 1-15.
15. Booth AJ, Hadley R, Cornett AM, Dreffs AA, Matthes SA, Tsui JL, Weiss K, Horowitz JC, Fiore VF, Barker TH, Moore BB, Martinez FJ, Niklason LE, White ES. Acellular normal and fibrotic human lung matrices as a culture system for in vitro investigation. *Am J Respir Crit Care Med* 2012: 186(9): 866-876.

16. Petrou CL, D'Ovidio TJ, Bolukbas DA, Tas S, Brown RD, Allawzi A, Lindstedt S, Nozik-Grayck E, Stenmark KR, Wagner DE, Magin CM. Clickable decellularized extracellular matrix as a new tool for building hybrid-hydrogels to model chronic fibrotic diseases in vitro. *J Mater Chem B* 2020: 8(31): 6814-6826.

17. Visscher DO, Lee H, van Zuijlen PPM, Helder MN, Atala A, Yoo JJ, Lee SJ. A photo-crosslinkable cartilage-derived extracellular matrix bioink for auricular cartilage tissue engineering. *Acta Biomater* 2021: 121: 193-203.

18. Nichol JW, Koshy ST, Bae H, Hwang CM, Yamanlar S, Khademhosseini A. Cell-laden microengineered gelatin methacrylate hydrogels. *Biomaterials* 2010: 31(21): 5536-5544.

19. Pupkaite J, Rosenquist J, Hilborn J, Samanta A. Injectable Shape-Holding Collagen Hydrogel for Cell Encapsulation and Delivery Cross-linked Using Thiol-Michael Addition Click Reaction. *Biomacromolecules* 2019: 20(9): 3475-3484.

20. Huettner N, Dargaville TR, Forget A. Discovering Cell-Adhesion Peptides in Tissue Engineering: Beyond RGD. *Trends Biotechnol* 2018: 36(4): 372-383.

21. Vyborny K, Vallova J, Koci Z, Kekulova K, Jirakova K, Jendelova P, Hodan J, Kubinova S. Genipin and EDC crosslinking of extracellular matrix hydrogel derived from human umbilical cord for neural tissue repair. *Sci Rep* 2019: 9(1): 10674.

22. Lim KS, Klotz BJ, Lindberg GCJ, Melchels FPW, Hooper GJ, Malda J, Gawlitta D, Woodfield TBF. Visible Light Cross-Linking of Gelatin Hydrogels Offers an Enhanced Cell Microenvironment with Improved Light Penetration Depth. *Macromol Biosci* 2019: 19(6): e1900098.

23. Hsieh JY, Keating MT, Smith TD, Meli VS, Botvinick EL, Liu WF. Matrix crosslinking enhances macrophage adhesion, migration, and inflammatory activation. *APL Bioeng* 2019: 3(1): 016103.

24. Keating M, Lim M, Hu Q, Botvinick E. Selective stiffening of fibrin hydrogels with micron resolution via photocrosslinking. *Acta Biomater* 2019: 87: 88-96.

25. Kim H, Kang B, Cui XL, Lee SH, Lee K, Cho DW, Hwang W, Woodfield TBF, Lim KS, Jang J. Light-Activated Decellularized Extracellular Matrix-Based Bioinks for Volumetric Tissue Analogs at the Centimeter Scale. *Adv Funct Mater* 2021: 31(32): 2011252.

26. Martinez-Garcia FD, de Hilster RHJ, Sharma PK, Borghuis T, Hylkema MN, Burgess JK, Harmsen MC. Architecture and Composition Dictate Viscoelastic Properties of Organ-Derived Extracellular Matrix Hydrogels. *Polymers (Basel)* 2021: 13(18).

27. Pouliot RA, Link PA, Mikhaiel NS, Schneck MB, Valentine MS, Kamga Gninzeko FJ, Herbert JA, Sakagami M, Heise RL. Development and characterization of a naturally derived lung extracellular matrix hydrogel. *J Biomed Mater Res A* 2016: 104(8): 1922-1935.

28. Pouliot RA, Young BM, Link PA, Park HE, Kahn AR, Shankar K, Schneck MB, Weiss DJ, Heise RL. Porcine Lung-Derived Extracellular Matrix Hydrogel Properties Are Dependent on Pepsin Digestion Time. *Tissue Eng Part C Methods* 2020: 26(6): 332-346.

29. Sharma PK, Busscher HJ, Terwee T, Koopmans SA, van Kooten TG. A comparative study on the viscoelastic properties of human and animal lenses. *Exp Eye Res* 2011: 93(5): 681-688.

30. Callister WD, Jr., Rethwisch DG. Materials science and engineering : an introduction. 9th ed. John Wiley & Sons, New York, 2017.

31. Martinez-Garcia FD, Valk MM, Sharma PK, Burgess JK, Harmsen MC. Adipose Tissue-Derived Stromal Cells Alter the Mechanical Stability and Viscoelastic Properties of Gelatine Methacryloyl Hydrogels. *Int J Mol Sci* 2021: 22(18): 10153.

32. Wershof E, Park D, Barry DJ, Jenkins RP, Rullan A, Wilkins A, Schlegelmilch K, Roxanis I, Anderson KI, Bates PA, Sahai E. A FIJI macro for quantifying pattern in extracellular matrix. *Life Sci Alliance* 2021: 4(3).

33. McQuin C, Goodman A, Chernyshev V, Kamentsky L, Cimini BA, Karhohs KW, Doan M, Ding L, Rafelski SM, Thirstrup D, Wiegraebe W, Singh S, Becker T, Caicedo JC, Carpenter AE. CellProfiler 3.0: Next-generation image processing for biology. *PLoS Biol* 2018: 16(7): e2005970.

34. Marinkovic A, Liu F, Tschumperlin DJ. Matrices of physiologic stiffness potently inactivate idiopathic pulmonary fibrosis fibroblasts. *Am J Respir Cell Mol Biol* 2013: 48(4): 422-430.

35. Polio SR, Kundu AN, Dougan CE, Birch NP, Aurian-Blajeni DE, Schiffman JD, Crosby AJ, Peyton SR. Cross-platform mechanical characterization of lung tissue. *PLoS One* 2018: 13(10): e0204765.

36. Chaudhuri O, Gu L, Klumpers D, Darnell M, Bencherif SA, Weaver JC, Huebsch N, Lee HP, Lippens E, Duda GN, Mooney DJ. Hydrogels with tunable stress relaxation regulate stem cell fate and activity. *Nat Mater* 2016: 15(3): 326-334.

37. Peterson BW, van der Mei HC, Sjollema J, Busscher HJ, Sharma PK. A distinguishable role of eDNA in the viscoelastic relaxation of biofilms. *mBio* 2013: 4(5): e00497-00413.

38. Burgess JK, Harmsen MC. Chronic lung diseases: entangled in extracellular matrix. *Eur Respir Rev* 2022: 31(163): 210202.

39. Tjin G, White ES, Faiz A, Sicard D, Tschumperlin DJ, Mahar A, Kable EPW, Burgess JK. Lysyl oxidases regulate fibrillar collagen remodelling in idiopathic pulmonary fibrosis. *Dis Model Mech* 2017: 10(11): 1301-1312.

40. Philp CJ, Siebeke I, Clements D, Miller S, Habgood A, John AE, Navaratnam V, Hubbard RB, Jenkins G, Johnson SR. Extracellular Matrix Cross-Linking Enhances Fibroblast Growth and Protects against Matrix Proteolysis in Lung Fibrosis. *Am J Respir Cell Mol Biol* 2018: 58(5): 594-603.

41. James DS, Jambor AN, Chang HY, Alden Z, Tilbury KB, Sandbo NK, Campagnola PJ. Probing ECM remodeling in idiopathic pulmonary fibrosis via second harmonic generation microscopy analysis of macro/supramolecular collagen structure. *J Biomed Opt* 2019: 25(1): 1-13.

42. Asano S, Ito S, Takahashi K, Furuya K, Kondo M, Sokabe M, Hasegawa Y. Matrix stiffness regulates migration of human lung fibroblasts. *Physiol Rep* 2017: 5(9).

43. Liu F, Mih JD, Shea BS, Kho AT, Sharif AS, Tager AM, Tschumperlin DJ. Feedback amplification of fibrosis through matrix stiffening and COX-2 suppression. *J Cell Biol* 2010: 190(4): 693-706.

44. Jaffar J, Yang SH, Kim SY, Kim HW, Faiz A, Chrzanowski W, Burgess JK. Greater cellular stiffness in fibroblasts from patients with idiopathic pulmonary fibrosis. *Am J Physiol Lung Cell Mol Physiol* 2018: 315(1): L59-L65.

45. Roach KM, Wulff H, Feghali-Bostwick C, Amrani Y, Bradding P. Increased constitutive alphaSMA and Smad2/3 expression in idiopathic pulmonary fibrosis myofibroblasts is KCa3.1-dependent. *Respir Res* 2014: 15(1): 155.

46. Matera DL, DiLillo KM, Smith MR, Davidson CD, Parikh R, Said M, Wilke CA, Lombaert IM, Arnold KB, Moore BB, Baker BM. Microengineered 3D pulmonary interstitial mimetics highlight a critical role for matrix degradation in myofibroblast differentiation. *Sci Adv* 2020: 6(37).

47. Galarza Torre A, Shaw JE, Wood A, Gilbert HTJ, Dobre O, Genever P, Brennan K, Richardson SM, Swift J. An immortalised mesenchymal stem cell line maintains mechano-responsive behaviour and can be used as a reporter of substrate stiffness. *Sci Rep* 2018: 8(1): 8981.

48. Wang N, Tytell JD, Ingber DE. Mechanotransduction at a distance: mechanically coupling the extracellular matrix with the nucleus. *Nat Rev Mol Cell Biol* 2009: 10(1): 75-82.

49. Swift J, Ivanovska IL, Buxboim A, Harada T, Dingal PC, Pinter J, Pajerowski JD, Spinler KR, Shin JW, Tewari M, Rehfeldt F, Speicher DW, Discher DE. Nuclear lamin-A scales with tissue stiffness and enhances matrix-directed differentiation. *Science* 2013: 341(6149): 1240104.

50. Freeberg MAT, Perelas A, Rebman JK, Phipps RP, Thatcher TH, Sime PJ. Mechanical Feed-Forward Loops Contribute to Idiopathic Pulmonary Fibrosis. *Am J Pathol* 2021: 191(1): 18-25.

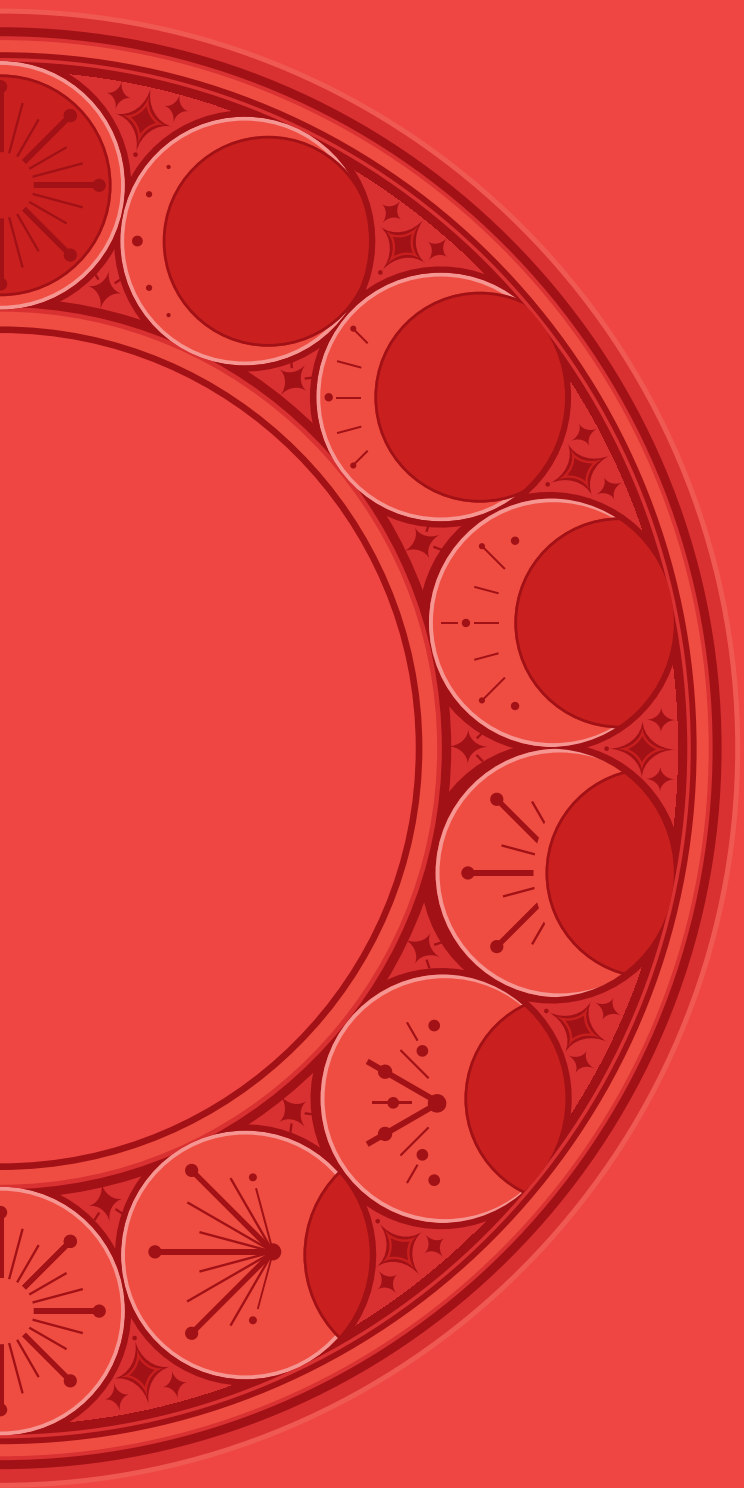

CHAPTER 9

Fibroblast remodeling of extracellular matrix is directed by the fibrotic nature of the three-dimensional microenvironment

Mehmet Nizamoglu, Frederique Alleblas, Taco Koster, Theo Borghuis, Judith M. Vonk, Matthew J. Thomas Eric S. White Carolin K. Watson , Wim Timens, Karim C. El Kasmi, Barbro N. Melgert, Irene H. Heijink, Janette K. Burgess

Submitted

ABSTRACT

Idiopathic pulmonary fibrosis (IPF), for which effective treatments are limited, results in excessive and disorganized deposition of an aberrant extracellular matrix (ECM). An altered ECM microenvironment is postulated to contribute to disease perpetuation in a feed-forward manner through inducing profibrotic behavior by lung fibroblasts, the main producers and regulators of ECM. Here, we examined this hypothesis in a 3D *in vitro* model system by growing primary lung fibroblasts in ECM-derived hydrogels from non-fibrotic (control) or IPF lung tissue. Culture of fibroblasts in fibrotic hydrogels did not trigger a change in the overall amount of collagen or glycosaminoglycans but did cause a drastic change in fiber organization compared to culture in control hydrogels. Mechanical properties of fibrotic hydrogels were modified by fibroblasts while control hydrogels were not. These results illustrate how the 3D microenvironment plays a crucial role in directing cells to exhibit pro-fibrotic responses by providing biochemical and/or biomechanical cues.

INTRODUCTION

Tissue fibrosis results from an increase in fibroblasts with an aberrant deposition of extracellular matrix (ECM) and abnormal alterations of the ECM structure and composition [1]. While fibrosis is recognized as a coinciding phenomenon in some diseases, such as in inflammatory diseases or several cancers, organ fibrosis itself is one of the leading causes of death worldwide each year [2]. Among these diseases, idiopathic pulmonary fibrosis (IPF) has a worse prognosis than most cancers and remains incurable to date [3]. Currently, IPF is thought to originate from repeating (micro)injuries to the lung epithelium resulting in an aberrant tissue repair response [4]. During this aberrant tissue repair response, fibroblasts emerge as key players that deposit ECM in an abnormal manner, resulting in scarring of lung interstitium that impairs gas exchange in lungs of patients with IPF [5]. Although there is an urgent unmet need for developing novel treatment strategies, lack of appropriate animal models that recapitulate this human disease hinders this process [6]. For new and improved therapeutics against IPF, our understanding of how fibrotic responses are perpetuated and how IPF progresses needs to be advanced.

ECM is drastically altered in fibrotic lung diseases both biochemically and biomechanically [7]. While collagen deposition in the alveolar septa is considered one of the hallmarks of fibrotic scar development, numerous other ECM components such as fibronectin, hyaluronic acid, periostin and fibulin-1 are also present to a greater extent in fibrotic lung ECM [8]. In addition to altered ECM composition, fiber structure in fibrotic ECM is also substantially different compared to healthy ECM: fibrotic lungs having a higher percentage of disorganized collagen [9, 10]. Such changes in the fiber organization and content are also postulated to translate into the well-documented changes in the mechanical properties of fibrotic tissue: IPF lungs are many-fold stiffer than control counterparts [11]. Recently, decreased stress relaxation properties of fibrotic lungs were also described, illustrating not only stiffness but also additional mechanical parameters accompany lung fibrosis [12]. Although initially thought of as an inert structure that only provided a physical scaffold, ECM has now been shown to instruct behavior of resident and transmigratory cells [13]. ECM deposited by fibroblasts in fibrosis resulted in activation of naïve fibroblasts seeded onto this ECM [14]. In addition to the origin of the microenvironment, the dimensionality of the environment (two-dimensional (2D) vs. three-dimensional (3D)) has been shown to influence how fibroblasts respond to their microenvironment [15]. While these pioneering studies illustrate that a fibrotic microenvironment instructs cellular behavior, the influence of a 3D fibrotic microenvironment on fibroblasts remains unexplored.

Hydrogels, which are water-swollen polymeric networks, have been used as an *in vitro* tool to mimic the 3D organ microenvironment. Synthetic hydrogels, such as those based on dextran [15], and natural hydrogels based on collagen type I [9] have been used for *in vitro* studies. While synthetic hydrogels provide opportunities to fine-tune the structural arrangement of the fibers and mechanical properties, they lack the biological implications of the altered biochemical microenvironment as found in IPF lungs [16]. Natural hydrogels can provide bioactive cues to cells seeded in them; however, mechanically tuning these hydrogels to mimic a diseased microenvironment is rather limited [17]. Hydrogels made of decellularized organ-derived ECM can provide an ideal background for addressing these concerns [18]. Decellularized ECMs (dECMs) retain most of the biochemical composition of the native organs and tissues [19], and hydrogels derived from these dECMs have been shown to recapitulate the mechanical properties of their native tissues [18]. Specifically, ECM-derived hydrogels prepared from lung tissue from patients with IPF show the increased stiffness characteristics of native tissue, making these hydrogels an ideal candidate for recapitulating the (fibrotic) microenvironment *in vitro [12]*. The unexplored interaction between the 3D fibrotic ECM and fibroblasts can therefore be mimicked using such hydrogels to improve our understanding of how the fibrotic response is perpetuated by the feedback from the fibrotic microenvironment itself during IPF.

In this study, we hypothesized that an altered microenvironment in fibrotic lungs contributes to perpetuation of fibrosis by inducing profibrotic behavior of lung fibroblasts. To address this, we used an *in vitro* model using IPF and control lung ECM-derived hydrogels cultured with either IPF or control lung-derived primary fibroblasts in a combined fashion for 7 and 14 days. We investigated the influence of the fibrotic microenvironment on both IPF and control fibroblasts by comparing the ECM remodeling responses of the fibroblasts seeded in IPF and control ECM in 3D. We characterized fibroblast induced changes to the microenvironment with respect to modulation of collagen and glycosaminoglycan (GAG) content, collagen fiber organization and mechanical properties by comparing the fibroblast-originated responses with empty hydrogels.

RESULTS

Collagen presence in control and IPF hydrogels is similar and does not change upon seeding with either control or IPF fibroblasts

We first assessed interactions between a fibrotic microenvironment and fibroblasts on collagen presence in the lung ECM-derived hydrogels by analyzing the collagen content at day 7 and 14. PicroSirius Red (PSR)-stained sections of empty or fibroblast-seeded control and IPF hydrogels were analyzed using an automated image analysis that compared three different levels of staining strength: weak, moderate and strong staining (**Figure 1A**). In all three categories, we did not detect intrinsic differences in the percentage of PSR-stained area between control and IPF hydrogels without fibroblasts (*Supplementary Tables 1-6*, also shown as the dotted line in Figure **1B-G** for each separate analysis). When fibroblasts were seeded in these hydrogels, we found no differences in percentage area positive for collagen content induced by either control or IPF fibroblasts at day 7 or 14 (**Figure 1B-G**). Similarly, the mean intensities of staining within the weak, moderate and strong PSR-staining was comparable in all groups (*Supplementary Figure 1, Supplementary Tables 7-12*). We also examined the distribution of (GAG) in all groups by staining adjacent sections with Alcian Blue. Comparable to collagen content, pecentage area of GAG content was similar in control and IPF empty hydrogels, and this did not change in hydrogels seeded with control or IPF fibroblasts (*Supplementary Figure 2, Supplementary Tables 13-18*).

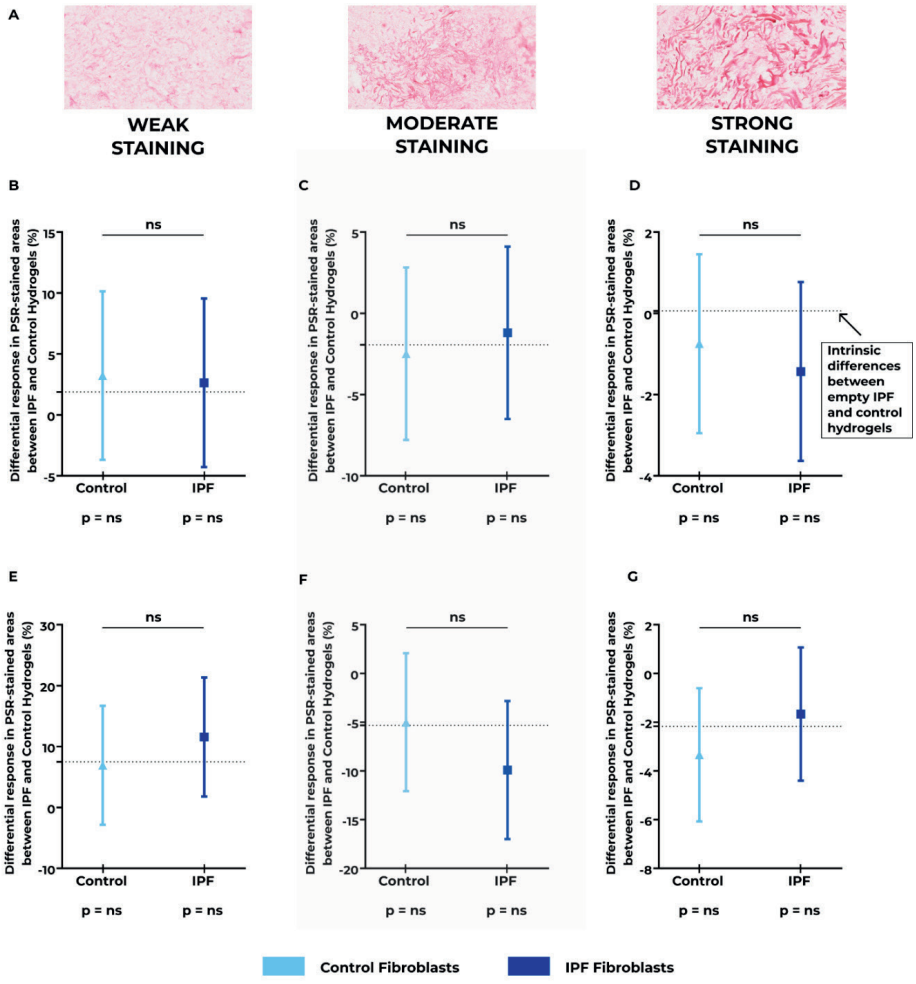

■ **Figure 1: Deposited collagen amounts in empty and fibroblast-seeded lung ECM-derived hydrogels.** Control or IPF primary lung fibroblasts were seeded in control or IPF lung ECM-derived hydrogels and cultured for 7 or 14 days. Collagens were visualized using PicroSirius Red (PSR) staining on sections of paraffin-embedded fibroblast-seeded hydrogels and staining levels were compared with their corresponding empty hydrogel samples. A) Example images for the three levels of the strength of PSR staining. Day 7 responses with respect to B) weak C) moderate and D) strong PSR-stained areas (% area). Day 14 responses with respect to E) weak F) moderate and G) strong PSR-stained areas (% area). The dotted line shows the intrinsic difference between the IPF and control empty hydrogels. The estimate (± 95% confidence interval) shows the difference in PSR-staining between the IPF and control hydrogels seeded with control (light blue, triangle) or IPF (dark blue, square) fibroblasts. P values below each fibroblast group represent the differences induced by fibroblasts in IPF versus control hydrogels compared to the intrinsic difference between empty IPF and control hydrogels. P-values above the estimates indicate the differences between the responses of IPF and control fibroblasts in the different hydrogels. Applied statistical test: mixed-model analysis. ns: not significant, IPF: Idiopathic pulmonary fibrosis. n=6 for fibroblast donors, 1 image per sample was analyzed.

Fibroblasts change collagen organization only in IPF hydrogels

We then investigated whether fibroblasts induced changes in collagen organization and whether this was different in fibrotic versus control hydrogels using TWOMBLI. This analysis revealed the changes triggered in fibrotic ECM (**Figure 2**). The first parameter we studied was the percentage area occupied by high density matrix, which describes the collagen fiber organization at a global level (**Figure 2A**). Intrinsic differences between control and IPF hydrogels were not detected on day 7, but were clearly visible on day 14 with IPF hydrogels having more high density matrix than control hydrogels (*Supplementary Tables 19&20*, also denoted as the dotted lines in **Figure 2B-C)**. When we seeded fibroblasts in these hydrogels, we found that control fibroblasts further decreased the percentage of high density matrix in IPF hydrogels compared to control hydrogels below the already existing differences, both on day 7 and day 14 (**Figure 2B and 2C**, respectively). On the other hand, IPF fibroblasts decreased the percentage of high density matrix of IPF hydrogels only on day 14 (**Figure 2C**). The differential modulation of the hydrogels by control and IPF fibroblasts was significantly different ($p = 5.12 \times 10^{-6}$ for day 7 and $p = 0.027$ for day 14), indicating that not only hydrogel type but also the fibroblast origin contributes to dysregulated collagen organization in IPF.

We then characterized the degree of fiber alignment within the hydrogels (**Figure 2D**). We did not detect any intrinsic differences between control and IPF hydrogels with respect to fiber alignment (*Supplementary Tables 21&22*). When control fibroblasts were seeded in each type of hydrogel, they did not change the percentage fiber alignment in IPF hydrogels compared to control hydrogels at any time point (**Figure 2E** and **2F**). However, when seeding IPF fibroblasts, we found fiber alignment was greater in IPF hydrogels compared to control hydrogels on both day 7 and day 14 (**Figure 2E** and **2F,** $p = 4.00 \times 10^{-3}$ for day 7 and $p = 2.57 \times 10^{-6}$ for day 14). The differential modulation of the fiber alignment by control and IPF fibroblasts was significantly different on both days ($p = 5.00 \times 10^{-3}$ for day 7, $p = 7.64 \times 10^{-4}$ for day 14).

Fibroblasts modify individual collagen fibers differently in fibrotic compared to control ECM

In addition to global fiber organization, individual fiber structure could also be altered by the seeded fibroblasts. Individual fiber structure was therefore assessed using TWOMBLI. Three individual fiber structural parameters were analyzed: average fiber length (AFL, µm), number of endpoints per 1000 µm fiber total length, and number of branchpoints per 1000 µm fiber total length (**Figure 3**).

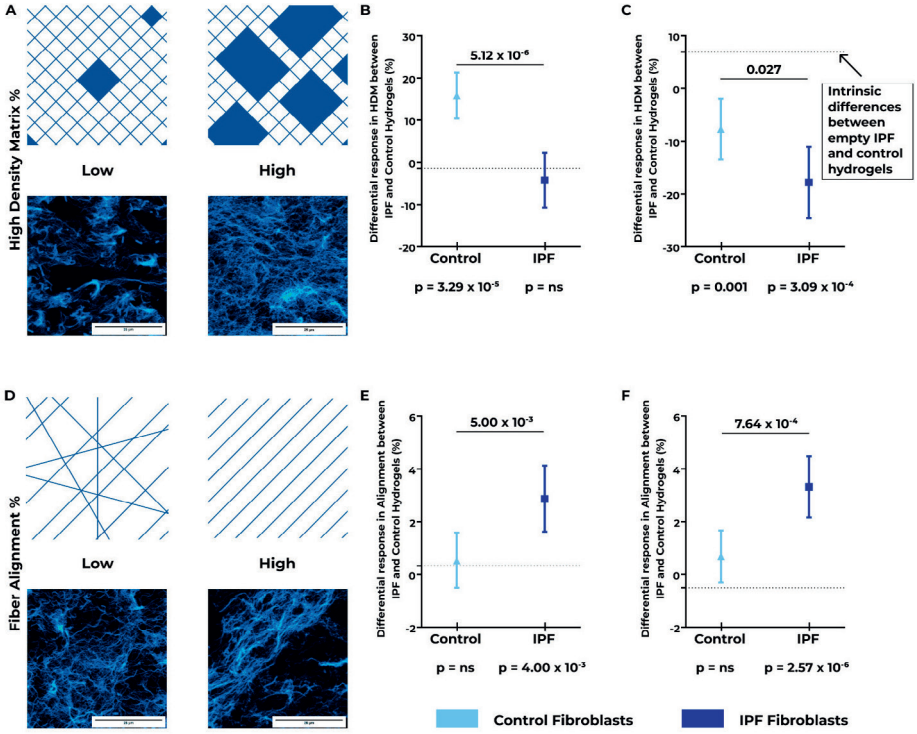

■ **Figure 2: Changes in the global fiber organization in empty and fibroblast-seeded control and IPF lung ECM-derived hydrogels.** Control and IPF primary lung fibroblasts were seeded in control or IPF lung ECM-derived hydrogels and cultured for 7 or 14 days. Fluorescence images of Picro-Sirius Red (PSR) stained sections of paraffin-embedded hydrogels were analyzed for global fiber characteristics and compared with their corresponding empty hydrogel samples. A) Schematic representation and example fluorescence images of high and low percentages of high-density matrix (HDM). B) Day 7 response analysis for HDM (% area), C) Day 14 response analysis for HDM (% area), D) Schematic representation and example fluorescence images of high and low percentages of fiber alignment. E) Day 7 response analysis for fiber alignment (% fibers), F) Day 14 response analysis for fiber alignment (% fibers). The dotted line shows the intrinsic difference between the empty IPF and control hydrogels. The estimate (± 95% confidence interval) shows the difference between the IPF and control hydrogels seeded with control (light blue, triangle) or IPF (dark blue, square) fibroblasts. P values below each fibroblast group represent the differences induced by fibroblasts in IPF versus control hydrogels compared to the intrinsic difference between IPF and control empty hydrogels. P-values above the estimates indicate the differences between the responses of IPF and control fibroblasts in the different hydrogels. Applied statistical test: mixed-model analysis. ns: not significant, IPF: Idiopathic pulmonary fibrosis. n=6 for fibroblast donors, 6 images per sample were captured and analyzed.

The analysis of average fiber length illustrated that, intrinsically, IPF hydrogels had shorter fibers on average, compared to control hydrogels (*Supplementary Tables 23&24*, also shown as the dotted line in **Figure 3A** and **3D** for day 7 and 14, respectively). When control fibroblasts were seeded in IPF hydrogels, the average fiber length was further decreased in IPF hydrogels on day 7 (**Figure 3A**, $p = 7.44 \times 10^{-5}$), while this modulation was not detected on day 14 (**Figure 3D**). IPF fibroblasts, on the other hand, increased the average fiber length in IPF hydrogels compared to control hydrogels only on day 14 (**Figure 3D**, $p = 1.26 \times 10^{-4}$). These modulations by control and IPF fibroblasts were significantly different from each other both on day 7 ($p = 6.30 \times 10^{-5}$) and day 14 ($p = 2.00 \times 10^{-5}$).

The number of individual fibers (number of endpoints) was higher in IPF hydrogels compared with control hydrogels on day 7, but this difference was not detected on day 14 (*Supplementary Tables 25&26*, also shown as the dotted line in **Figure 3B** and **3E** for day 7 and 14, respectively). When control fibroblasts were seeded into these hydrogels, we found more endpoints in IPF hydrogels compared to control hydrogels on day 7, above the existing intrinsic difference between these two hydrogels (**Figure 3B**). This modulation, however, was not observed on day 14 (**Figure 3E**). In contrast, IPF fibroblasts did not change the number of endpoints in IPF hydrogels compared to control hydrogels on either day 7 or day 14. These differential responses between control and IPF fibroblasts, differed significantly on both day 7 ($p = 0.005$) and day 14 ($p = 5.56 \times 10^{-4}$) (**Figure 3B** and **3E**, respectively).

We also investigated the number of branchpoints as a measure of the number of fibers that had connections with other fibers. IPF hydrogels had more branchpoints than control hydrogels on day 7 ($p = 0.007$) while this intrinsic difference was not detectable on day 14 (*Supplementary Tables 27&28*, also shown as the dotted line in **Figure 3C** and **3F** for day 7 and 14, respectively). When either control or IPF fibroblasts were seeded in these hydrogels, no additional changes in the number of branchpoints induced by fibroblasts were detected in either control or IPF hydrogels on day 7 (**Figure 3C**). However, on day 14 both control ($p = 5.57 \times 10^{-6}$) and IPF fibroblasts ($p = 2.13 \times 10^{-5}$) strongly decreased the number of branchpoints in IPF hydrogels but not in control hydrogels (**Figure 3F**).

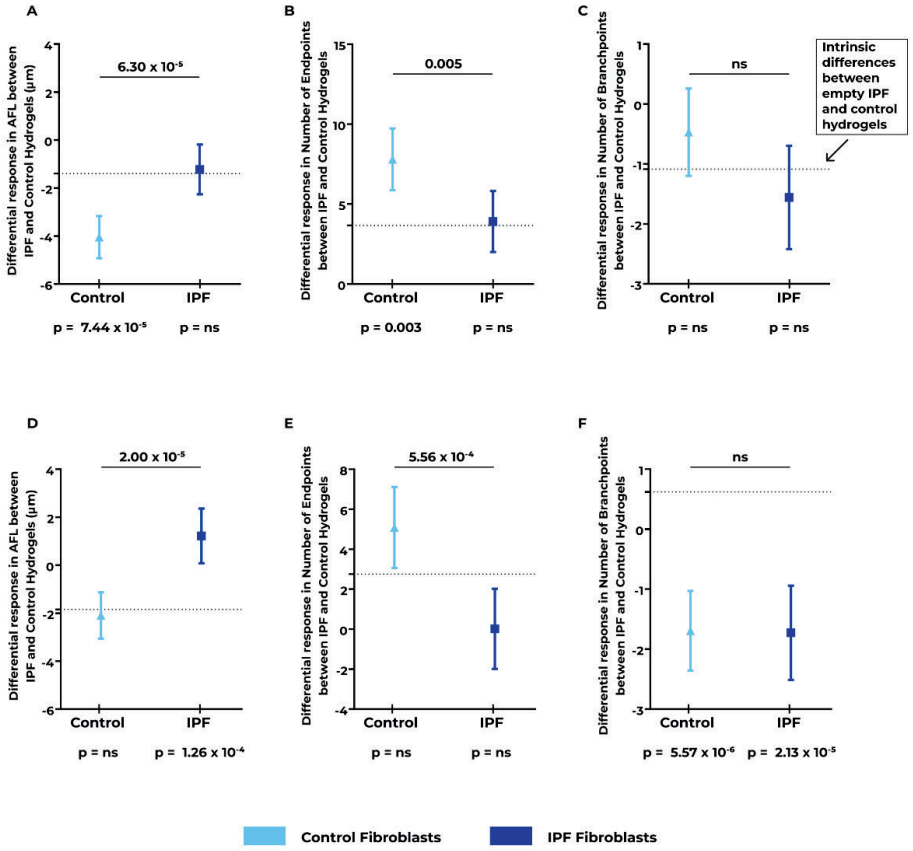

■ **Figure 3: Individual collagen fiber structure in empty and fibroblast-seeded control and IPF lung ECM-derived hydrogels.** Control and IPF primary lung fibroblasts were seeded in control or IPF lung ECM-derived hydrogels and cultured for 7 or 14 days. Fluorescence images of PicroSirius Red (PSR) stained sections of paraffin-embedded hydrogels were analyzed for individual fiber characteristics and compared with their corresponding empty hydrogel samples. Day 7 responses with respect to A) average fiber length (AFL) (µm), B) number of endpoints per 1000 µm fiber total length, C) number of branchpoints per 1000 µm fiber total length. Day 14 responses with respect to D) average fiber length (AFL) (µm), E) number of endpoints per 1000 µm fiber total length, F) number of branchpoints per 1000 µm fiber total length. The dotted line shows the intrinsic difference between empty IPF and control hydrogels. The estimate (± 95% confidence interval) shows the difference between the IPF and control hydrogels seeded with control (light blue, triangle) or IPF (dark blue, square) fibroblasts. P values below each fibroblast group represent the differences induced by fibroblasts in IPF versus control hydrogels compared to the intrinsic difference between IPF and control empty hydrogels. P-values above the estimates indicate the differences between the responses of IPF and control fibroblasts in the different hydrogels. Applied statistical test: mixed-model analysis. ns: not significant. IPF: Idiopathic pulmonary fibrosis. n=6 for fibroblast donors, 6 images per sample were captured and analyzed.

Fibrotic microenvironment triggered differential regulation of fiber curvature by fibroblasts

We then moved on to characterize changes in the curvature of the collagen fibers in empty and fibroblast-seeded ECM-derived hydrogels as another parameter for comparing responses of control and IPF fibroblasts to their microenvironment. The curvature of fibers was analyzed with respect to low and high curvature windows (**Figure 4A**). Low curvature windows capture the individual waviness (periodicity) of the fibers (more micro-scale) while higher curvature windows detect the global changes in the fiber shapes (changes in the peak height of the curves). These parameters are useful for describing the topographical arrangement of the fibers within the ECM hydrogel. Intrinsic differences between IPF and control hydrogels in the low curvature window were present in day 7 samples ($p = 0.004$), while they were not apparent for the high curvature windows (*Supplementary Tables 29&30*, respectively, also shown as the dotted lines in **Figure 4B**). Control fibroblasts seeded in IPF hydrogels increased the fiber periodicity in low curvature windows ($p = 0.001$, **Figure 4B**) while they did not change the curvature heights in the higher curvature windows. IPF fibroblasts did not induce any periodicity changes (as measured in the low curvature windows); however, these fibroblasts reduced the peak heights of the fiber curves (as measured in the high curvature windows) in IPF hydrogels beyond the existing differences between IPF and empty hydrogels ($p = 0.049$, **Figure 4B**). Both low and high curvature window responses of control and IPF fibroblasts to fibrotic hydrogels differed from each other ($p = 3.2 \times 10^{-4}$ for low and $p = 0.006$ for high curvature windows). Empty hydrogels analyzed on day 14 revealed intrinsic differences between IPF and control hydrogels in low ($p = 1.15 \times 10^{-11}$), and high ($p = 0.026$) curvature window samples (*Supplementary Tables 31&32*, respectively, also shown as dotted line in **Figure 4C**). The existing differences between the IPF and control hydrogels were decreased by both control ($p = 3.57 \times 10^{-4}$) and IPF (3.01×10^{-10}) fibroblasts in low curvature window. While both groups of fibroblasts decreased the fiber curvature periodicity in IPF hydrogels compared to control hydrogels, their responses significantly differed from each other as well ($p = 7.74 \times 10^{-4}$). On the other hand, only IPF fibroblasts responded to fibrotic hydrogels in measurements in the high curvature window ($p = 0.002$). Even though only IPF fibroblasts altered the fiber curvature height, there were no apparent differences in the responses of IPF and control fibroblasts in this setting. These data indicate that IPF fibroblasts altered the topographical arrangement of the collagen fibers within their 3D microenvironment to a greater extent than the control fibroblasts.

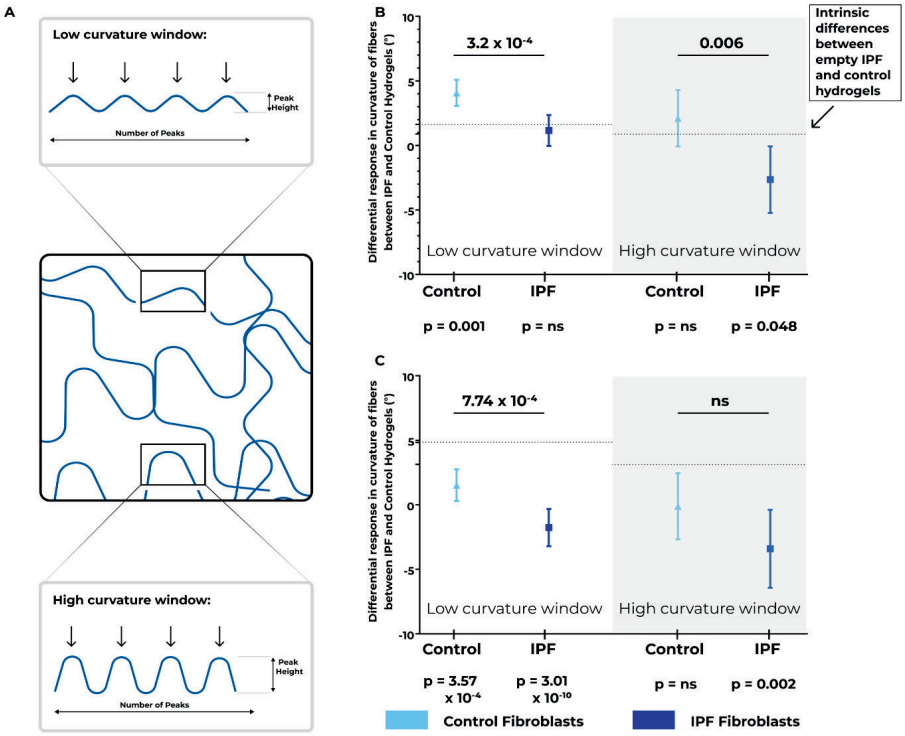

■ **Figure 4: Investigation of collagen fiber curvature in empty and fibroblast-seeded control and IPF lung ECM-derived hydrogels.** Control and IPF primary lung fibroblasts were seeded in control or IPF lung ECM-derived hydrogels and cultured for 7 or 14 days. Fluorescence images of PicroSirius Red (PSR) stained sections of paraffin-embedded hydrogels were analyzed for the differences in collagen fiber curvature and compared with their corresponding empty hydrogel samples. A) Schematic representation of low and high curvature windows with respect to periodicity of peaks and peak height, B) Day 7 response analysis for fiber curvature with respect to number of peaks and peak height, C) Day 14 response analysis for fiber curvature with respect to number of peaks and peak height. The dotted line shows the intrinsic difference between empty IPF and control hydrogels. The estimate (± 95% confidence interval) shows the difference between the IPF and control hydrogels seeded with control (light blue, triangle) or IPF (dark blue, square) fibroblasts. P values below each fibroblast group represent the differences induced by fibroblasts in IPF versus control hydrogels compared to the intrinsic difference between IPF and control empty hydrogels. P-values above the estimates indicate the differences between the responses of IPF and control fibroblasts in the different hydrogels. Applied statistical test: mixed-model analysis. ns: not significant, IPF: Idiopathic pulmonary fibrosis. n=6 for fibroblast donors, 6 images per sample were captured and analyzed.

Stiffness increased but stress relaxation remained comparable when fibroblasts were in fibrotic hydrogels

Lastly, we characterized mechanical properties of both empty and fibroblast-seeded control and IPF hydrogels after 7 or 14 days of culture. Stiffness (**Figure 5A and 5B**) and viscoelastic stress relaxation (**Figure 5E and 5F**) behavior of hydrogels were measured using a Low-Load Compression Tester (LLCT). Empty IPF hydrogels were stiffer than empty control hydrogels on both day 7 ($p = 5.57 \times 10^{-6}$) and day 14 ($p = 4.93 \times 10^{-22}$) (*Supplementary Tables 33&34*, also shown as the dotted line in **Figure 5C** and **5D** for day 7 and 14, respectively), reflecting previous reports [12]. When control fibroblasts were seeded in IPF hydrogels, they stiffened the hydrogels significantly more than they stiffened control hydrogels on day 7 (**Figure 5C**, $p = 0.002$). Similar to control fibroblasts, IPF fibroblasts also increased stiffness of IPF hydrogels more than they stiffened control hydrogels (**Figure 5D**, $p = 0.002$). The responses of control and IPF fibroblasts in IPF hydrogels compared to control hydrogels were comparable. However, on day 14 only control fibroblasts increased the stiffness of IPF hydrogels compared to control hydrogels beyond the already existing stiffness differences (**Figure 5D**, $p = 9.22 \times 10^{-5}$). Modulation of IPF hydrogels compared to control hydrogels by control fibroblasts on day 14 was significantly different from how IPF fibroblasts modulated the two types of hydrogels ($p = 0.027$).

Viscoelastic stress relaxation was the other mechanical parameter analyzed after 7 and 14 days of culture of control and IPF fibroblasts in control and IPF hydrogels. The time to reach 50% stress relaxation was measured in seconds and compared between the groups (**Figure 5E**). IPF hydrogels relaxed significantly slower than control hydrogels both on day 7 ($p = 1.47 \times 10^{-12}$) and day 14 ($p = 5.82 \times 10^{-14}$) (*Supplementary Tables 35&36*, also shown as the dotted line in **Figure 5G** and **5H** for day 7 and 14, respectively). Seeding of either control or IPF fibroblasts into the hydrogels did not significantly change stress relaxation beyond the intrinsic differences that were already present on day 7 (**Figure 5G**). On day 14, however, only control fibroblasts caused a slower relaxation of IPF hydrogels compared to control hydrogels, in addition to the existing differences (**Figure 5H**, $p = 0.033$). IPF fibroblasts did not change the relaxation properties of the hydrogels beyond the existing differences between control and IPF.

DISCUSSION

In this study, we used a 3D *in vitro* model composed of human lung ECM and human primary lung fibroblasts to assess the influence of the microenvironment on fibroblast responses. We showed that while collagen content and GAG content were unchanged by the fibroblast groups, fiber organization directed by the fibroblasts differed substantially due to influence of the ECM microenvironment. When examining individual collagen fiber characteristics the fibrotic microenvironment did not induce significant changes. However, the global structure of the ECM arrangement, as illustrated by fiber alignment and high density matric proportion was impacted by the nature of the microenvironment. Control fibroblasts did not alter the fiber alignment, while fibrotic fibroblasts increased fiber alignment and this happened to a greater extent in the fibrotic microenvironment. In contrast, control fibroblasts modulated the percentage of high density matrix in a temporal manner in the fibrotic microenvironment, while the IPF fibroblasts reduced the percentage of high density matrix. In addition, control fibroblasts altered the topographical arrangement of the collagen fibers, giving them a greater degree of curvature than that seen with the IPF fibroblasts. The mechanical characteristics of the fibrotic microenvironment were increased by fibroblasts from both control and IPF donors, whereas this change was not seen in the control hydrogels. These findings illustrate that the fibrotic microenvironment imparts a powerful message that drives cellular responses. Overall, our results illustrate that the fibroblast-seeded lung ECM-derived hydrogel model is a powerful *in vitro* tool for understanding cell interactions with the local microenvironment, and divulging greater knowledge of feedback by the fibrotic ECM and how fibroblasts remodel the microenvironment during this response.

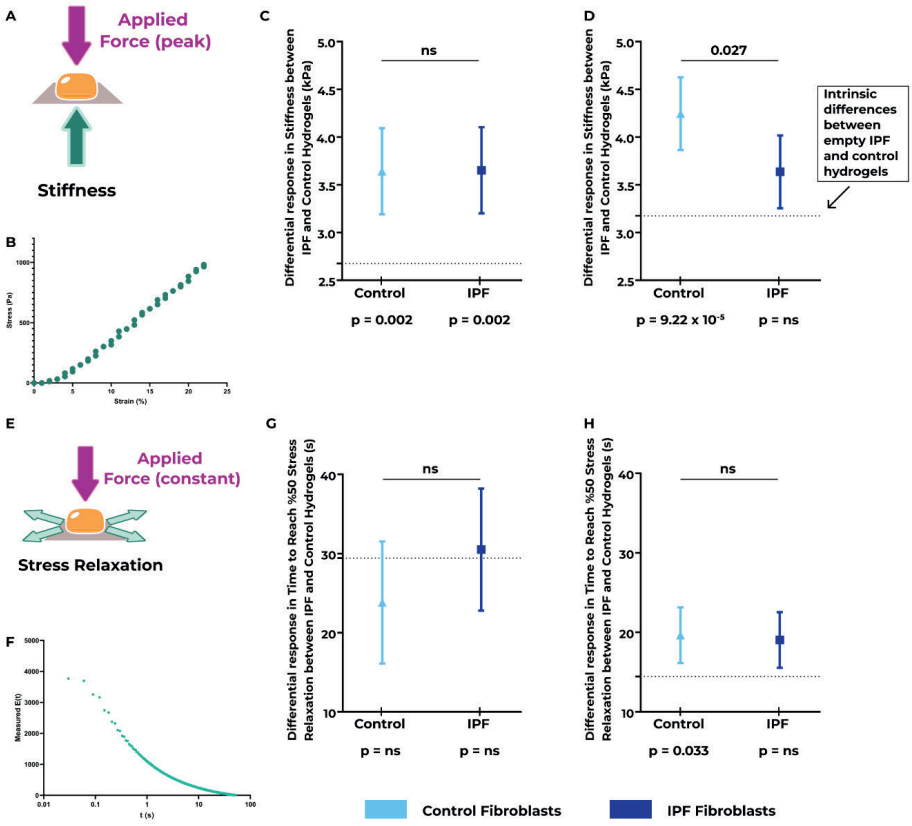

■ **Figure 5: Mechanical properties in empty and fibroblast-seeded control and IPF lung ECM-derived hydrogels.** Control and IPF primary lung fibroblasts were seeded in control or IPF lung ECM-derived hydrogels and cultured for 7 or 14 days. Fibroblast-seeded hydrogels were mechanically tested using low load compression testing (LLCT) and compared with their corresponding empty hydrogels. A) Schematic representation of the stiffness analysis performed using compression. B) An example stress-strain curve obtained using LLCT, C) Day 7 response analysis for stiffness of the hydrogels (kPa), D) Day 14 response analysis for stiffness of the hydrogels (kPa), E) Schematic representation of the stress relaxation analysis performed using compression. F) An example relaxation profile obtained using LLCT, G) Day 7 response analysis for time to reach 50% stress relaxation (s), H) Day 14 response analysis for time to reach 50% stress relaxation (s). The dotted line shows the intrinsic difference between empty IPF and control hydrogels. The estimate (± 95% confidence interval) shows the difference between the IPF and control hydrogels seeded with control (light blue, triangle) or IPF (dark blue, square) fibroblasts. P values below each fibroblast group represent the differences induced by fibroblasts in IPF versus control hydrogels compared to the intrinsic difference between IPF and control empty hydrogels. P-values above the estimates indicate the differences between the responses of IPF and control fibroblasts in the different hydrogels. Applied statistical test: mixed-model analysis. All measurements were performed at 20% strain rate. Applied statistical test: mixed-model analysis. ns: not significant, IPF: Idiopathic pulmonary fibrosis. n=6 for fibroblast donors, 3 independent locations per sample were measured.

Collagen amount and organization are known to be drastically altered in IPF; higher amounts of collagen with an increased disorganization of the fiber structure have been consistently documented [8, 11, 13]. In our hydrogel system, fibroblasts did not induce changes in collagen amount between empty and fibroblast-seeded hydrogels, suggesting that these fibroblasts did not deposit detectable new collagen in this model and timeframe. A recent study reported an increase in protein levels of collagen types VII, X and XIV, detected using mass spectrometry, by control fibroblasts cultured in spheroid form with presence of IPF lung ECM, compared to non-IPF ECM [20]. These data provide further evidence, supporting prior reports [11, 14, 21, 22] that the IPF ECM provides a pro-fibrotic signal for fibroblasts. While our data appear to contrast the previous studies, the use of mass spectrometry may provide additional sensitivity that would enable a more penetrating investigation of the collagen changes. In our model system, the fibroblast-induced differences in high density matrix and collagen fiber alignment as directed by the type of environment (hydrogel) in which the cells were grown, implies that the lack of detectable changes in total collagen amount does not necessarily reflect a lack in pro-fibrotic responses by fibroblasts.

Increased fiber density was previously proposed as a mechanism for triggering activation of fibroblasts [15]. Therefore, in a fibrotic microenvironment, with higher amounts of dense fibers [23, 24], greater fibroblast responses would be expected. Interestingly, control fibroblasts appeared to have opposite responses at different time points, with an initial increase in high density matrix after 7 days but a subsequent decrease after 14 days. These differences in time might reflect how naïve fibroblasts are imprinted by a fibrotic microenvironment as time passes so their responses to fibrotic environment are changed. In IPF fibroblasts, the decrease in high density matrix with a concomitant increase in fiber alignment, points at exaggerated responses of these fibroblasts, when confronted with fibrotic ECM. These specific responses of IPF fibroblasts suggest that the origin of both microenvironment and fibroblasts play a crucial role in determining the organizational changes of collagen fibers.

Enhanced collagen crosslinking is recognized to be enhanced in IPF lung tissues [9, 25]. Our results showing decreased amounts of high density matrix in fibrotic ECM modulated by both types of fibroblasts in day 14 samples do not initially seem to be in concert with previous reports showing enhanced fibroblast activation by increased ECM crosslinking in IPF [25]. Further research is required to examine if the high density matrix in this hydrogel model is composed of crosslinked collagen fibers or if it is non-covalent aggregations of fibers. The latter may have different cellular signaling implications than the highly cross-linked ECM in IPF tissue, parallel to the previous reports showing different levels of myofibroblast activation in chemically crosslinked

hydrogels compared with physically crosslinked hydrogels [26]. While it was out of the scope of this study, it is important to recognize that a role of proteoglycans in collagen crosslinking and fiber organization has been previously reported [27], and their presence might also play a role in the collagen organization measured in this model.

The organization of individual collagen fibers is also an important element for determining cellular responses to the microenvironment in which they reside [11]. With respect to the individual fiber organization parameters that were analyzed in our study, control and IPF fibroblasts responded differently from each other, with the exception of the alterations to the number of branchpoints. The opposite responses elicited by the fibroblasts to fibrotic and control hydrogels highlights that not only the origin of the microenvironment but also the origin of fibroblasts plays a role in dictating the collagen organization. Fiber curvature (collagen topographical arrangement), as both an individual and global fiber parameter, was differentially regulated by control and IPF fibroblasts seeded in fibrotic hydrogels compared to control hydrogels. It is intriguing that these changes coincided with the changes in the mechanical parameters initiated by the fibroblasts. In particular, control fibroblasts had an exaggerated response to the fibrotic microenvironment, resulting in an increased stiffness compared to control hydrogels. While the decrease in high density matrix and increase in stiffness do not seem to go hand-in-hand, fibroblasts might be realigning the fibers that are dissociated from the high density matrix in a manner that leads to the increased stiffness. The lack of changes in the peak height of the collagen fiber curves in control fibroblast-seeded hydrogels could also be one of the key factors playing a role in increased stiffness in these hydrogels. Together with previous reports showing the influence of fiber curvature amplitude and wavelength on fibroblast migration and polarization [28], investigating the influence of fibrotic ECM curvature on fibroblasts might reveal new insights into how fibroblast-ECM interactions are regulated by the physical state of the matrix structure. The stress relaxation behavior of the empty and fibroblast-seeded hydrogels showed that the changes in high density matrix and stiffness do not strongly influence the stress relaxation capacity of the fibers. It would be of interest to further investigate the altered stress relaxation of the fibers with respect to activation of the fibroblasts, as previously pre-stress in ECM fibers has been shown to release stored TGF-β from the ECM [29, 30]. Regardless, a recent report indicates that a microenvironment with slow stress capacity hinders cellular migration of mesenchymal spheroids [31]. How cellular migration plays a role in the profibrotic activation of fibroblasts with respect to organization of ECM requires further studies.

While our study establishes the interplay between the native microenvironment and the fibroblast responses in 3D, it has a few limitations. Human lung ECM (both

control and IPF) hydrogels were variable between experimental runs. Although we generated a combined batch of ECM derived from 7 different donors to minimize this variation, sample-to-sample variation was still present in our results. Empty hydrogels harvested at each of the assessment time points also reflected this variation. However, we accounted for this variation during our analyses and only compared empty hydrogels to fibroblast-seeded hydrogels within the same time point and the same experimental run. Even with this comparison, it is not possible to rule out the fact that spontaneous fiber reorganization still continues during the course of 14 day cell culture in empty and fibroblast-seeded hydrogels. Another potential limitation of the study is related to collagen detection: as the starting weights of control and IPF lung ECM powders were the same, and as the majority of the remaining proteins within the dECMs were collagens, detecting small changes that might have been induced by the fibroblasts may not have been possible with the methodologies used in this study. While investigating changes in different collagens individually and also other ECM proteins was outside of the scope of this project, it is not possible to rule out that specific collagens may have been altered by the fibroblasts more than the others, or that other ECM proteins including proteoglycans may have been involved. Lastly, viscoelastic stress relaxation of the control and IPF lung ECM-derived hydrogels is difficult, if at all possible, to resemble native tissue (a recognized limitation of this model [12, 32]), as opposed to the stiffness values that do recapitulate the patterns seen in lung tissues.

The model described in this study also provides opportunities for further research. Although our current model is based on fibroblast-ECM interactions, introducing other cell types such as epithelial cells, circulating immune cells or other mesenchymal cells would help mimicking the complex interplay between these cells and ECM during IPF or other fibrotic lung diseases. Moreover, this model system can greatly advance investigating cell responses following treatment with Nintedanib or Pirfenidone, which were initially performed on cell-derived matrices [33]. While our study focused on IPF, it has important implications for understanding the interplay between cells and their fibrotic environment in many other fibrotic diseases and even cancer, reflecting the remodeled ECM associated with tumors. Understanding how activation of fibroblasts occurs in a fibrotic microenvironment has the potential to reveal additional intervention possibilities for the treatment of diseases involving fibrotic responses. Future studies utilizing this model could investigate if the fibroblast responses differ in the presence of antifibrotic treatments that are currently approved for pulmonary fibrosis.

In summary, we examined how a 3D fibrotic microenvironment is interacting with fibroblast remodeling of this environment by both control and IPF fibroblasts using native lung ECM-derived hydrogels and primary lung fibroblasts. Through employing native ECM from control and IPF lungs, most biochemical and biomechanical properties of control and IPF lungs were mimicked in these hydrogels, thereby presenting an improved model system for investigating the interplay between the microenvironment and fibroblasts during the fibrotic process. Considering the lack of physiologically replicative models available for basic and translational research on generating treatment strategies targeting fibrosis, employing *in vitro* models derived from human-sourced materials can pave the way towards better understanding of fibrosis and better drug discovery processes.

MATERIALS AND METHODS

Experimental Design

The experimental approach adopted in this study is described in **Figure 6**. The specific details of the methods are described below.

Lung decellularization

Decellularized control (macroscopically normal tissue, referred to as control throughout the manuscript) and lung tissue from patients with IPF were kindly provided by Dr. Steven Huang, University of Michigan, USA. De-identified control and IPF human lung tissue were provided by the University of Michigan; as the tissues were de-identified and coming from deceased donors, the University of Michigan Institutional Review Board deemed this work exempt from oversight. The decellularization procedure was performed as described previously [11]. Briefly, the fresh lung tissue samples were washed with 1X PBS (Gibco, Waltham, MA, United States). The tissue sample was washed for 24 hours per step at 4°C (unless otherwise stated) with the series of different solutions under constant agitation conditions: 1% (v/v) Triton X-100 (Sigma Aldrich, St. Louis, MO, USA), 2% (wt/v) sodium deoxycholate (Sigma Aldrich), 1 M NaCl (Sigma Aldrich), 30 mg/L DNase (Sigma Aldrich) with 1.3 mM $MgSO_4.7H_2O$ (Sigma Aldrich) and 2 mM $CaCl_2$ (Sigma Aldrich) at 37°C. The washing series was performed twice with three times PBS washes between every different solution. Afterwards, the ECM samples were treated with 0.18 % peracetic acid solution (32% w/w; Merck, Darmstadt, Germany) in 4.8% ethanol (Fresenius Kabi, Bad Homburg vor der Höhe, Germany) solution for 24 hours at 4°C with constant shaking. Lastly, the ECM samples were washed using PBS and kept in PBS (+1% Penicillin-Streptomycin (Gibco)) at 4°C until the next step.

Lyophilization and grinding of decellularized lung samples

Decellularized lung samples were lyophilized in order to remove excess water. Briefly, the samples were snap-frozen using liquid nitrogen, then freeze-dried using a Labconco Freezone 2.5 Liter Benchtop Lyophilizer (Labconco, Kansas City, MO, USA) until the samples reached complete dryness. Once the lung scaffold samples were dry, they were brought to room temperature for the grinding process. An IKA A11 Basic Analytical Mill (IKA, Germany) was used to grind the lung scaffold pieces to a fine powder. Lung ECM powders were kept at room temperature with desiccant until use.

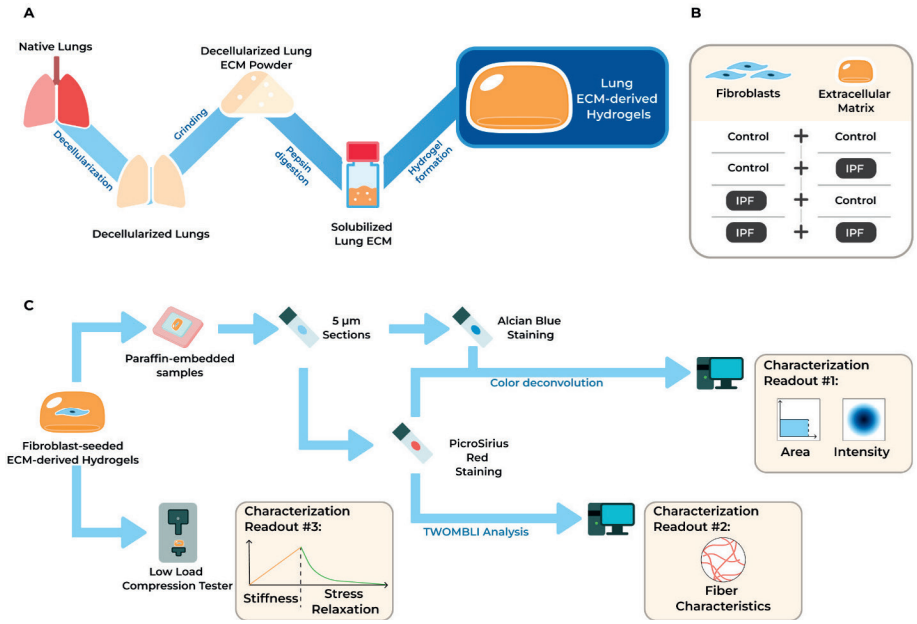

■ **Figure 6: Overview of the experimental design and readouts measured in this study.** A) Control and IPF lungs were decellularized, ground to a fine powder and digested using pepsin in acidic medium. The solubilized lung ECM was used to prepare lung ECM-derived hydrogels. B) Combinatorial approach used in the experiments. Fibroblasts and ECM groups were cross-combined to have combinations of control and IPF originated samples in every experimental batch. C) The readout applied in this study: PicroSirius Red and Alcian Blue stained sections of empty and fibroblast-seeded control and IPF lung ECM-derived hydrogels were scanned and digitally analyzed for area only or area and intensity (Characterization Readout #1). Fluorescence images of PicroSirius Red stained sections of empty and fibroblast-seeded control and IPF lung ECM-derived hydrogels were analyzed using TWOMBLI plugin in ImageJ to analyze the fiber characteristics (Characterization Readout #2). The mechanical properties (stiffness and stress relaxation) of empty and fibroblast-seeded control and IPF lung ECM-derived hydrogels were measured using low load compression tester (Characterization Readout #3).

Preparation of lung ECM-derived hydrogels

Decellularized lung ECM powders were pooled (n = 7 each for both control and IPF lung ECM samples) with equal amounts of powder dry weight per donor in order to minimize the patient-to-patient variation. Using this powder, pepsin digestion was performed using 2 mL of 2 mg/mL pepsin (Sigma-Aldrich) solution in 0.01 M HCl for 40 mg dry ECM powder in a 7.5 mL glass vial as previously described [34]. The digestion was performed for 72 hours with constant stirring at room temperature. After the incubation, the pH was brought back to physiological conditions (pH = 7.4) using 0.1 M NaOH (Sigma-Aldrich) solution before being mixed with 10X PBS (Gibco) solution to supplement the solution (will be referred to as pre-gel from here on) with physiological salts and ions. Resulting control and IPF pre-gels were cast into the wells of a 48-well plate or in a 1.5 mL Eppendorf tube and incubated for 1-2 hours to allow gelation and after the incubation, the hydrogel formation was checked.

Primary lung fibroblast isolation and cell culture

Control and IPF primary human lung fibroblasts were isolated from lung tissue of patients undergoing surgery for tumor resection or lung transplantation at the University Medical Center Groningen (UMCG) as previously described [35]. Control tissue was obtained from macroscopically normal looking tissue from tumor excision surgery, as far as possible from the tumor. IPF primary human lung fibroblasts were isolated from the peripheral lung tissue of explanted lung tissue of patients who underwent lung transplantation as previously described. This study protocol was consistent with the Research Code of the University Medical Center Groningen ((https://www.umcg.nl/documents/770534/2183586/umcg-research-code-2018-en.pdf/9680a460-3feb-543d-7d58-bc9d4f7277de?t=1614951313016, last accessed 12/01/2023) and the national ethical and professional guidelines ("Code of conduct for Health Research (only in Dutch):Gedragscode-Gezondheidsonderzoek-2022.pdf (https://www.coreon.org/gedragscode-gezondheidsonderzoek, last accessed 12/01/2023). Lung tissues used in this study were derived from leftover lung material after lung surgery from archival materials that are exempt from consent in compliance with applicable laws and regulations (Dutch laws: Medical Treatment Agreement Act (WGBO) art 458 / GDPR art 9/ UAVG art 24). This material was not subject to the Medical Research Human Subjects Act in the Netherlands, and, therefore, an ethics waiver was provided by the Medical Ethical Committee of the University Medical Center Groningen.

The characteristics of the patients are presented in **Table 1**. The fibroblast cultures were maintained in complete growth media (DMEM Low Glucose (Gibco), supplemented with 10% FBS (Sigma-Aldrich), 1% Penicillin-Streptomycin (Gibco) and 1% GlutaMAX (Gibco)) and only used when tested negative against *mycoplasma* infection using a PCR screening. Fibroblasts were used at passage 5.

Table 7: Patient characteristics of the fibroblasts donors used in this study. *: tested with Mann-Whitney test. †: tested with Fisher's exact test. ES: Ex-smoker, F: Female, IPF: Idiopathic pulmonary fibrosis, M: Male, NS: Non-smoker,

	Control	IPF	P value
Age (median, (min-max))	65, (59-72)	63.5, (61-68)	0.688 *
Sex (M/F)	6/0	6/0	>0.999†
Smoking status	5 EX, 1 NS	4 EX, 2 NS	>0.999†

Seeding primary lung fibroblasts in lung ECM-derived hydrogels

Primary human lung fibroblasts (n = 6 for both control and IPF, all at passage 5) were harvested using 0.25% Trypsin-EDTA (Gibco) and centrifuged at 500 x *g* for 5 minutes. Afterwards, the supernatant was discarded and the pellet resuspended using 10 mL full complete growth media to count the cells using an automated cell counter NC-200 (Chemometec, Denmark). Then, the cell suspension was transferred to new tubes at a concentration of 2.5×10^6 cells per tube and centrifuged again. The supernatants were discarded and the pellets were resuspended using 2.5 mL pre-gel of each type. After ensuring the proper dispersal of the cell pellet in the pre-gel solution, 200 µL cell suspension was cast per well of 48-well plates and incubated for 2 hours. For each experimental set, empty hydrogels from control or IPF pre-gels were also cast and used as fibroblast-free controls. After observing hydrogel formation, the empty and fibroblast-seeded hydrogels were supplemented with 400 µL complete growth media for the culture period. The gels were incubated for 7 and 14 days with complete growth media in a CO_2 incubator (5% CO_2, 37°C), with half change of growth media at days 4, 7 and 11.

Paraffin Embedding, Sectioning, and Deparaffinization

ECM-derived hydrogels (both fibroblast-seeded and empty) were fixed using 500 µL 2% paraformaldehyde (PFA; Sigma-Aldrich) for 30 minutes at room temperature after removing the growth media from the wells at the end of 7- or 14-day culture period. Afterwards, they were embedded in 1% agarose (Invitrogen, Waltham, MA, USA) solution to prevent dehydration. Agarose-embedded hydrogels then were fixed with 4% formalin and embedded in paraffin. Five µm sections from the paraffin-embedded samples were cut and placed on Star Frost (Knittel Glass, Braunschweig, Germany) glass slides and incubated at 65°C for 1 hour to ensure retention of the sections on the slides. Then, the slides were deparaffinized using serial ten minute incubations in xylene (Klinipath BV, Duiven, Netherlands) solution, 100% ethanol (Fresenius Kabi), 96% ethanol, 70% ethanol and distilled water.

Picrosirius Red Staining for visualization of collagens

PicroSirius Red (PSR) solution was prepared using 0.5 g Sirius red F3B (Sigma) in 500 mL saturated aqueous picric acid solution. Deparaffinized slides were washed with distilled water and then incubated with the PSR solution for an hour. Afterwards, the slides were washed with acidified water (5 mL glacial acetic acid (Merck) in 11 mL distilled water) twice and dehydrated through 75%, 96%, 100% ethanol (Fresenius Kabi) and xylene (Klinipath BV) solutions. After airdrying the slides, they were mounted using a non-aqueous mounting medium and kept in dark until imaging.

Alcian Blue Staining for visualization of glycosaminoglycans

Alcian blue solution was prepared using 1 g Alcian blue (Sigma-Aldrich) powder in 100 mL 3% acetic acid solution. Nuclear fast red solution was prepared using 0.1 g nuclear fast red powder in 100 mL distilled water with 5 g $Al_2(SO4)_3$ (Sigma-Aldrich). Deparaffinized slides were washed with distilled water and then incubated with the Alcian blue solution for 30 minutes at room temperature. Afterwards, the slides were washed with running tap water for 2 minutes and rinsed in distilled water. Counter-staining was performed through incubation with nuclear fast red solution for 5 minutes and the slides were washed in running tap water for 1 minute. The slides then were dehydrated through 75%, 96%, 100% ethanol (Fresenius Kabi) and xylene (Klinipath BV) solutions. After airdrying the slides, they were mounted using a non-aqueous mounting medium and kept in dark until imaging.

Imaging

Immunohistochemical staining results were imaged using a Hamamatsu scanner (Hamamatsu Photonics K.K., Herrsching, Germany) at 40X magnification. Fluorescent microscopy images of the PSR stained hydrogels were captured with Leica SP8X white light laser confocal microscope (Leica, Wetzlar, Germany) with UV-vis absorption (λ_{ex}) 561 nm and emission (λ_{em}) 566 / 670 nm using 63x/1.40 Oil immersion lens with a digital zoom 2X.

Image Analysis

Analysis of Light Microscopy Images

Specific image areas with stained gel were extracted into TIF (LZW) files using Aperio ImageScope V12.4.0.5043 (Leica Biosystems, Amsterdam, Netherlands). These TIF files were opened in Adobe Photoshop CS6 Extended (San Jose, California, USA) and artifacts, such as obvious background staining, hairs or other contaminations and folded areas of gels, were removed. Ten areas from ten distinct regions per image (1 image per gel) were randomly selected and saved as separate image files to enable

calculation of the average lowest threshold for identifiable specific staining for all images. These 10 images were opened in FIJI 1.53F51 (LOCI, University of Wisconsin) [36] as 8-bit images and split into different channels that captured the different staining colors, using the appropriate vector for the thresholds of the staining using color deconvolution. An in-house built macro (*Supplementary Document 1* for PSR Images and *Supplementary Document 2* for AB Images) was used along with the FIJI SlideJ plugin (tile size: 20000) to calculate the outputs from all images. Results were saved as a text to tab file and opened in R studio 4.1.1 (Boston, MA, USA) to sort the percentage area of positively stained pixels and the average intensity of the positively stained pixels data of the different staining levels (Supplementary Figure 39) using an in-house built macro as previously described [37]. Briefly, the strength of the signal from each pixel was determined and categorized as "weak", "moderate" or "strong" based on the level of the strength. The pixels that belong to each of these categories were then combined per image and used in the following steps. Area percentage and intensity values for each category per image were calculated in Microsoft Excel 2016 (Microsoft, Resmond, WA, USA). For these calculations, the sorted rows Area_Colour (area) and RawIntDen_Colour (intensity) were used. Stained area (%) and intensity values (arbitrary units) of each category was calculated using equation (i) and equation (ii), respectively, as shown below.

(i) $$\text{Area (\%)} = \frac{\text{Number of pixels meeting category criteria}}{\text{Total number of pixels}} \times 100\%$$

(ii) $$\text{Intensity (au)} = 255 - \frac{\text{Sum of intensity values in pixels meeting category criteria}}{\text{Total number of pixels}}$$

Analysis of Fluorescence Microscopy Images

For every sample, images were generated of 6 randomly selected areas and saved as TIF (LZW) files. Each image was analyzed using the TWOMBLI-plugin in FIJI 1.53F51 (LOCI), and the following parameters were examined: the area, total fiber length, end points, branchpoints, curvature (with curvature windows 20 and 50), percentage of high density matrix and alignment of fibers [38].

Mechanical testing with Low Load Compression Testing (LLCT)

Stiffness values and viscoelastic relaxation properties of the hydrogels at day 7 and 14 were measured using a Low Load Compression Tester as previously described [32, 39]. The LLCT analysis was performed on three different randomly selected locations on each hydrogel using 20% fixed strain rate. The measurement locations had at least 1.5 mm distance between them and 0.5 mm from the edges to ensure robustness and representativeness of the measurements. The stress ((Equation (iii)) and strain (Equation (iv)) values were calculated as described below and the slope of the line

was used to calculate Young's modulus (E, stiffness) (Equation (v)) until the peak point for the highest measurement observed). Relaxation values were calculated starting from the time point at which highest stiffness was observed by using the formula (Equation (vi)). Time duration for reaching 100% relaxation was recorded as 'Relaxation time'. Time duration for reaching 50% of the total relaxation was recorded as 'Time to Reach 50% Stress Relaxation'. All calculations were performed using Microsoft Excel 2016.

(iii) $$Stress = \frac{Load\ x\ g}{Area}$$

(iv) $$Strain = \frac{Deformation}{Thickness}$$

(v) $$E(t) = \frac{Stress}{Strain}$$

(vi) $$Relaxation\ (t) = \frac{E(t_0) - E(t)}{E(t_0)}$$

Statistical Analysis

Statistical analyses of the measured parameters were performed using an interaction analysis in a mixed model analysis in IBM SPSS Statistics 26 (IBM, Armonk, New York, USA). For each parameter analyzed, the interactions between the disease status of the hydrogels and disease status of the fibroblasts, as well as fibroblast seeding status of the hydrogels were used. For all analyses presented, a random effect was used for the intercept per experimental batch (i.e. same combination of control or IPF fibroblasts and control or IPF hydrogel for the 6 experimental conditions (n=6 batches)). TWOMBLI results were analyzed using 6 different images generated per sample to address the sample heterogeneity. Mechanical characterization results were analyzed using triplicated measurements performed on the same sample to tackle the heterogeneity within samples. Presented results show estimate ± 95% confidence interval for all results.

ACKNOWLEDGMENTS

Authors thank Mr. Albano Tosato for assistance in preparation of visuals. **Funding:** MN, TK, BNM, IHH and JKB receive unrestricted research funds from Boehringer Ingelheim. JKB also acknowledges support from the Nederlandse Organisatie voor Wetenschappelijk Onderzoek (NWO) (Aspasia 015.013.010). This collaboration project is co-financed by the Ministry of Economic Affairs and Climate Policy, the Netherlands, by means of the PPP-allowance made available by the Top Sector Life

Sciences & Health to stimulate public–private partnerships. **Competing interests:** MN, TK, BNM, IHH and JKB receive unrestricted research funds from Boehringer Ingelheim. MJT, CKW, ESW and KCK are employees of Boehringer Ingelheim. **Data and materials availability:** Estimates used to reach to reach the presented conclusions in this manuscript are included within the manuscript and/or added in the Supplementary Materials (*Supplementary Figures 3–38* for graphs with individual estimate points and statistical analyses of these individual points in *Supplementary Tables 1–36* are included in *Supplementary Document 3*). The raw data that support the findings of this study are available from the corresponding author upon reasonable request.

SUPPLEMENTARY FIGURES AND TABLES

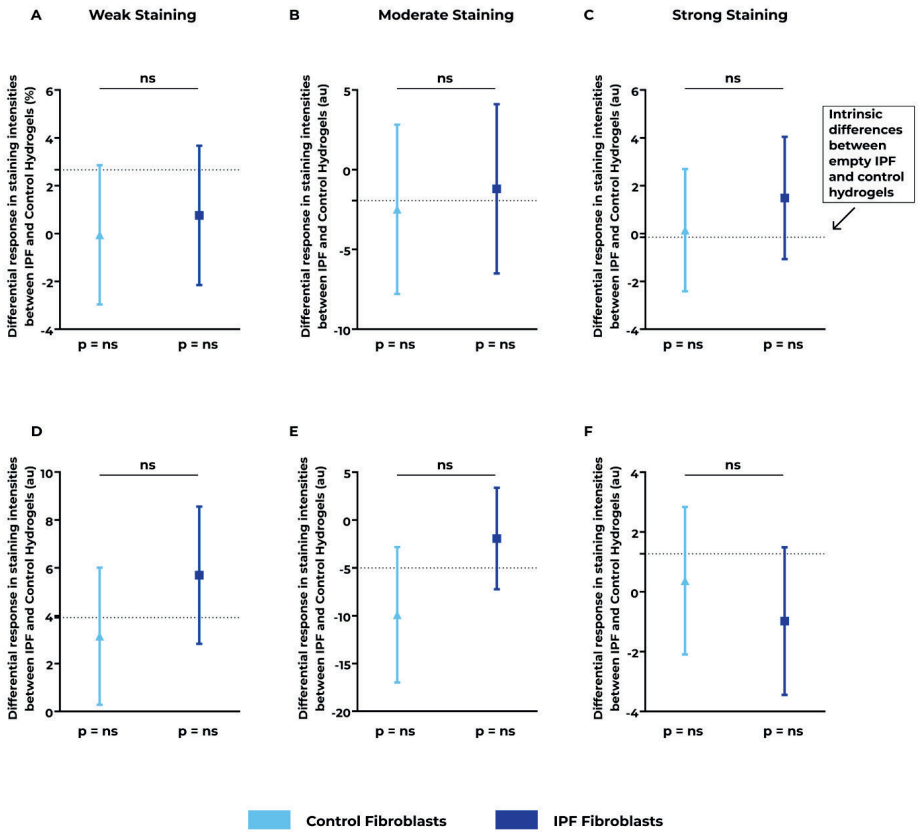

Supplementary Figure 1: Deposited collagen intensities in empty and fibroblast-seeded lung ECM-derived hydrogels. Control or IPF primary lung fibroblasts were seeded in control or IPF lung ECM-derived hydrogels and cultured for 7 or 14 days. Collagens were visualized using PicroSirius Red (PSR) staining on sections of paraffin-embedded fibroblast-seeded hydrogels and staining intensities were compared with their corresponding empty hydrogel samples. Day 7 responses with respect to A) weak B) moderate and C) strong PSR-stained intensities (arbitrary unit (au)). Day 14 responses with respect to D) weak E) moderate and F) strong PSR-stained areas (au). The dotted line shows the intrinsic difference between the empty IPF and control hydrogels. The estimate (± 95% confidence interval) shows the difference in the intensity of PSR-staining between the IPF and control hydrogels seeded with control (light blue, triangle) or IPF (dark blue, square) fibroblasts. P values below each fibroblast group represent the differences induced by fibroblasts in IPF versus control hydrogels compared to the intrinsic difference between empty IPF and control hydrogels. P-values above the estimates indicate the differences between the responses of IPF and control fibroblasts in the different hydrogels. Applied statistical test: mixed-model analysis. ns: not significant, IPF: Idiopathic pulmonary fibrosis. n=6 for fibroblast donors, 1 image per sample was analyzed.

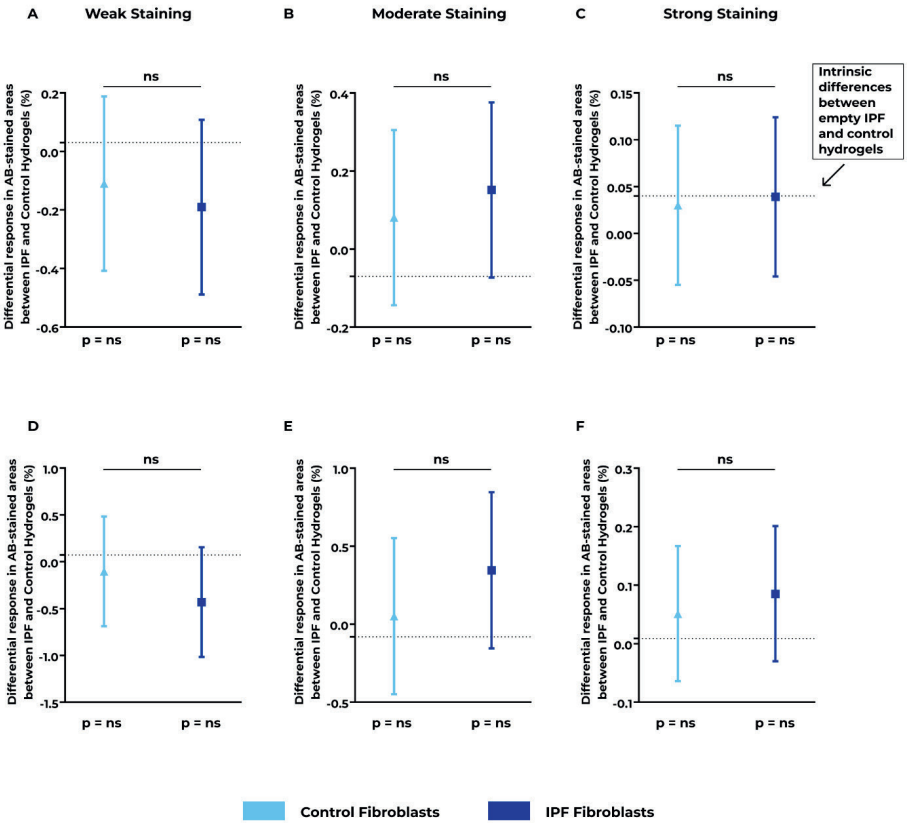

Supplementary Figure 2: Deposited glycosaminoglycan amounts in empty and fibroblast-seeded lung ECM-derived hydrogels. Control or IPF primary lung fibroblasts were seeded in control or IPF lung ECM-derived hydrogels and cultured for 7 or 14 days. Glycosaminoglycans were visualized using Alcian Blue (AB) staining on sections of paraffin-embedded fibroblast-seeded hydrogels and staining levels were compared with their corresponding empty hydrogel samples. Day 7 responses with respect to A) weak B) moderate and C) strong AB-stained areas (% area). Day 14 responses with respect to D) weak E) moderate and F) strong AB-stained areas (% area). The dotted line shows the intrinsic difference between the empty IPF and control hydrogels. The estimate (± 95% confidence interval) shows the difference in AB-staining between the IPF and control hydrogels seeded with control (light blue, triangle) or IPF (dark blue, square) fibroblasts. P values below each fibroblast group represent the differences induced by fibroblasts in IPF versus control hydrogels compared to the intrinsic difference between empty IPF and control hydrogels. P-values above the estimates indicate the differences between the responses of IPF and control fibroblasts in the different hydrogels. Applied statistical test: mixed-model analysis. ns: not significant, IPF: Idiopathic pulmonary fibrosis. n=6 for fibroblast donors, 1 image per sample was analyzed.

Supplementary Table 1: Individual comparisons between the different groups of empty and fibroblast-seeded control and IPF hydrogels for weakly stained PicroSirius Red area on day 7 samples

		Control Hydrogels			IPF Hydrogels		
		Empty	Control Fb	IPF Fb	Empty	Control Fb	IPF Fb
Control Hydrogels	Empty		0.478	0.364	0.583		
	Control Fb	0.478		0.111			
	IPF Fb	0.364	0.111				
IPF Hydrogels	Empty	0.583				0.273	0.489
	Control Fb				0.273		0.079
	IPF Fb				0.489	0.079	

Not significant
Significant
Comparison not applicable

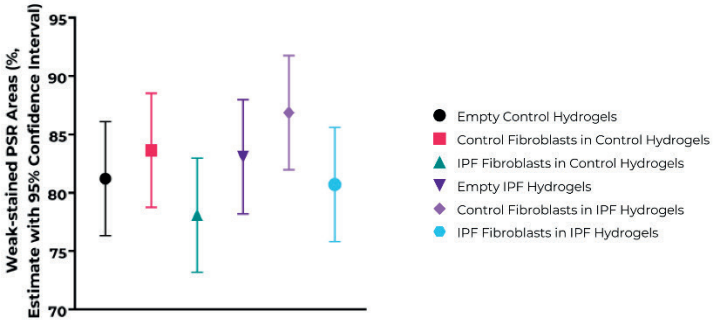

Supplementary Figure 3: Individual comparisons between the different groups of empty and fibroblast-seeded control and IPF hydrogels for the estimates of weakly stained PicroSirius Red (PSR) area (%) for day 7 samples.

Supplementary Table 2: Individual comparisons between the different groups of empty and fibroblast-seeded control and IPF hydrogels for weakly stained PicroSirius Red area on day 14 samples

		Control Hydrogels			IPF Hydrogels		
		Empty	Control Fb	IPF Fb	Empty	Control Fb	IPF Fb
Control Hydrogels	Empty		0.371	0.941	0.126		
	Control Fb	0.371		0.334			
	IPF Fb	0.941	0.334				
IPF Hydrogels	Empty	0.126				0.435	0.439
	Control Fb				0.435		0.995
	IPF Fb				0.439	0.995	

Not significant
Significant
Comparison not applicable

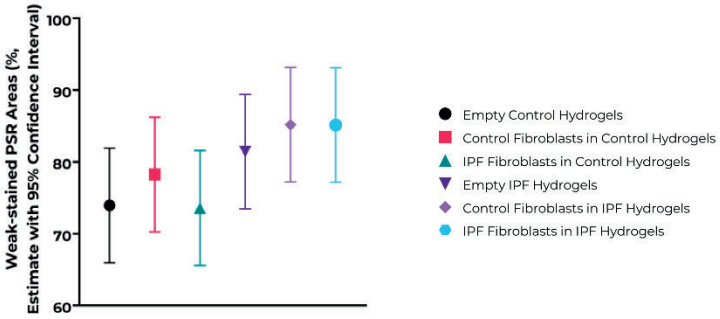

Supplementary Figure 4: Individual comparisons between the different groups of empty and fibroblast-seeded control and IPF hydrogels for the estimates of weakly stained PicroSirius Red (PSR) area (%) for day 14 samples.

Supplementary Table 3: Individual comparisons between the different groups of empty and fibroblast-seeded control and IPF hydrogels for moderately stained PicroSirius Red area on day 7 samples

		Control Hydrogels			IPF Hydrogels		
		Empty	Control Fb	IPF Fb	Empty	Control Fb	IPF Fb
Control Hydrogels	Empty		0.465	0.398	0.462		
	Control Fb	0.639		0.121			
	IPF Fb	0.412	0.201				
IPF Hydrogels	Empty	0.955				0.350	0.263
	Control Fb				0.230		0.045
	IPF Fb				0.584	0.045	

Not significant
Significant
Comparison not applicable

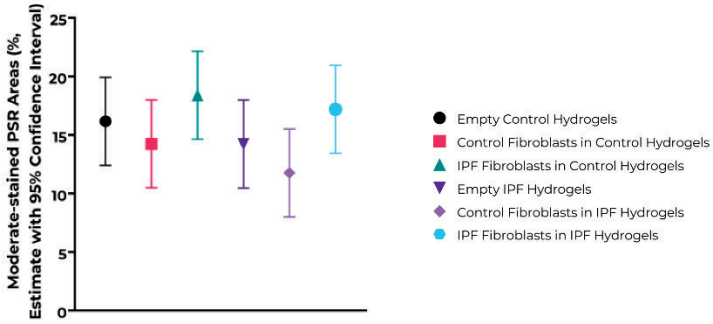

Supplementary Figure 5: Individual comparisons between the different groups of empty and fibroblast-seeded control and IPF hydrogels for the estimates of moderately stained PicroSirius Red (PSR) area (%) for day 7 samples.

Supplementary Table 4: Individual comparisons between the different groups of empty and fibroblast-seeded control and IPF hydrogels for moderately stained PicroSirius Red area on day 14 samples

		Control Hydrogels			IPF Hydrogels		
		Empty	Control Fb	IPF Fb	Empty	Control Fb	IPF Fb
Control Hydrogels	Empty		0.405	0.638	0.134		
	Control Fb	0.405		0.198			
	IPF Fb	0.638	0.198				
IPF Hydrogels	Empty	0.134				0.458	0.399
	Control Fb				0.458		0.919
	IPF Fb				0.399	0.919	

Not significant
Significant
Comparison not applicable

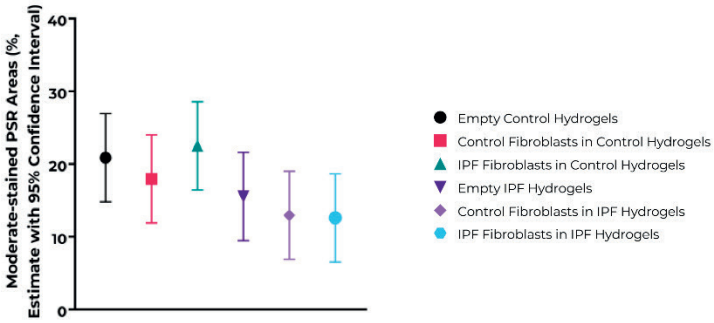

Supplementary Figure 6: Individual comparisons between the different groups of empty and fibroblast-seeded control and IPF hydrogels for the estimates of moderately stained PicroSirius Red (PSR) area (%) for day 14 samples.

Supplementary Table 5: Individual comparisons between the different groups of empty and fibroblast-seeded control and IPF hydrogels for strongly stained PicroSirius Red area on day 7 samples

		Control Hydrogels			IPF Hydrogels		
		Empty	**Control Fb**	**IPF Fb**	**Empty**	**Control Fb**	**IPF Fb**
Control Hydrogels	Empty		0.639	0.412	0.955		
	Control Fb	0.639		0.201			
	IPF Fb	0.412	0.201				
IPF Hydrogels	Empty	0.955				0.230	0.584
	Control Fb				0.230		0.507
	IPF Fb				0.584	0.507	

Not significant
Significant
Comparison not applicable

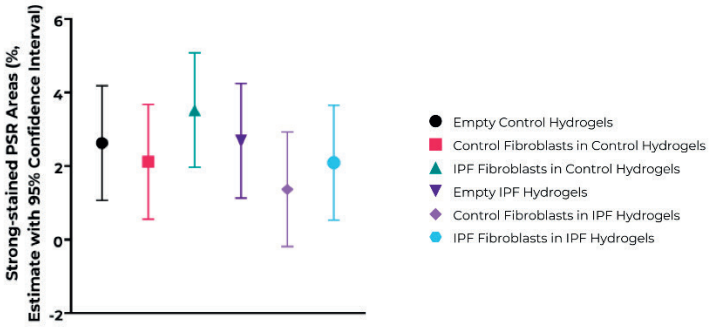

Supplementary Figure 7: Individual comparisons between the different groups of empty and fibroblast-seeded control and IPF hydrogels for the estimates of strongly stained PicroSirius Red (PSR) area (%) for day 7 samples.

Supplementary Table 6: Individual comparisons between the different groups of empty and fibroblast-seeded control and IPF hydrogels for strongly stained PicroSirius Red area on day 14 samples

		Control Hydrogels			IPF Hydrogels		
		Empty	Control Fb	IPF Fb	Empty	Control Fb	IPF Fb
Control Hydrogels	Empty		1.000	0.343	0.115		
	Control Fb	1.000		0.343			
	IPF Fb	0.343	0.343				
IPF Hydrogels	Empty	0.115				0.387	0.563
	Control Fb				0.387		0.771
	IPF Fb				0.563	0.771	

Not significant
Significant
Comparison not applicable

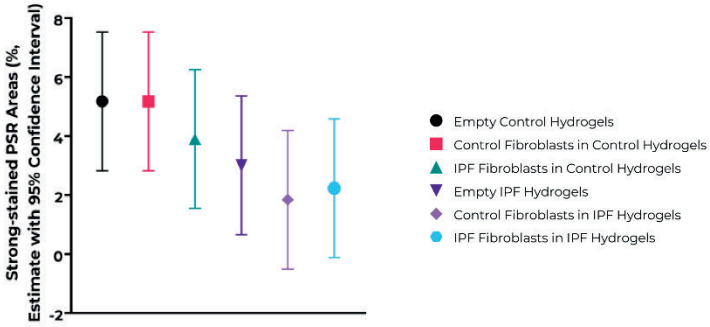

Supplementary Figure 8: Individual comparisons between the different groups of empty and fibroblast-seeded control and IPF hydrogels for the estimates of strongly stained PicroSirius Red (PSR) area (%) for day 14 samples.

Supplementary Table 7: Individual comparisons between the different groups of empty and fibroblast-seeded control and IPF hydrogels for mean intensity of weakly stained PicroSirius Red on day 7 samples

		Control Hydrogels			IPF Hydrogels		
		Empty	Control Fb	IPF Fb	Empty	Control Fb	IPF Fb
Control Hydrogels	Empty		0.600	0.663	0.071		
	Control Fb	0.600		0.181			
	IPF Fb	0.663	0.181				
IPF Hydrogels	Empty	0.071				0.682	0.026
	Control Fb				0.682		0.062
	IPF Fb				0.026	0.062	

Not significant
Significant
Comparison not applicable

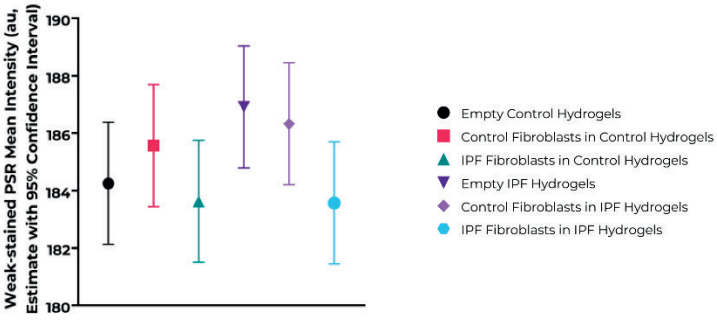

Supplementary Figure 9: Individual comparisons between the different groups of empty and fibroblast-seeded control and IPF hydrogels for the estimates of mean intensity of weakly stained PicroSirius Red (PSR) area (au) for day 7 samples.

Supplementary Table 8: Individual comparisons between the different groups of empty and fibroblast-seeded control and IPF hydrogels for mean intensity of weakly stained PicroSirius Red on day 14 samples

		Control Hydrogels			IPF Hydrogels		
		Empty	Control Fb	IPF Fb	Empty	Control Fb	IPF Fb
Control Hydrogels	Empty		0.403	0.057	0.009		
	Control Fb	0.403		0.165			
	IPF Fb	0.057	0.165				
IPF Hydrogels	Empty	0.009				0.720	0.493
	Control Fb				0.720		0.691
	IPF Fb				0.493	0.691	

Not significant
Significant
Comparison not applicable

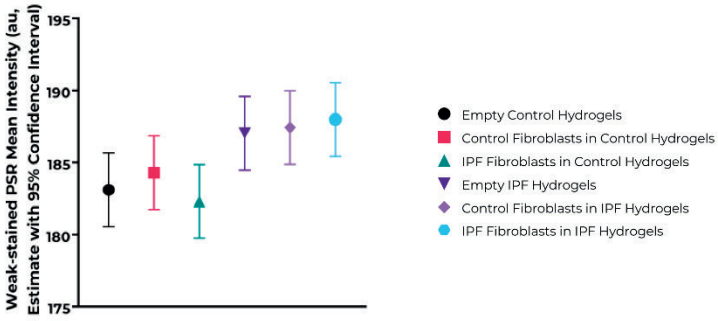

Supplementary Figure 10: Individual comparisons between the different groups of empty and fibroblast-seeded control and IPF hydrogels for the estimates of mean intensity of weakly stained PicroSirius Red (PSR) area (au) for day 14 samples.

Supplementary Table 9: Individual comparisons between the different groups of empty and fibroblast-seeded control and IPF hydrogels for mean intensity of moderately stained PicroSirius Red on day 7 samples

		Control Hydrogels			IPF Hydrogels		
		Empty	Control Fb	IPF Fb	Empty	Control Fb	IPF Fb
Control Hydrogels	Empty		0.465	0.398	0.462		
	Control Fb	0.465		0.121			
	IPF Fb	0.398	0.121				
IPF Hydrogels	Empty	0.462				0.350	0.263
	Control Fb				0.350		0.045
	IPF Fb				0.263	0.045	

Not significant
Significant
Comparison not applicable

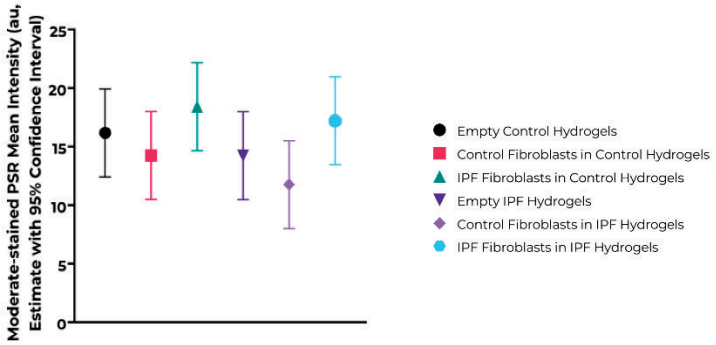

Supplementary Figure 11: Individual comparisons between the different groups of empty and fibroblast-seeded control and IPF hydrogels for the estimates of mean intensity of moderately stained PicroSirius Red (PSR) area (au) for day 7 samples.

Supplementary Table 10: Individual comparisons between the different groups of empty and fibroblast-seeded control and IPF hydrogels for mean intensity of moderately stained PicroSirius Red on day 14 samples

		Control Hydrogels			IPF Hydrogels		
		Empty	Control Fb	IPF Fb	Empty	Control Fb	IPF Fb
Control Hydrogels	Empty		0.405	0.198	0.158		
	Control Fb	0.405		0.198			
	IPF Fb	0.198	0.198				
IPF Hydrogels	Empty	0.158				0.458	0.399
	Control Fb				0.458		0.919
	IPF Fb				0.399	0.919	

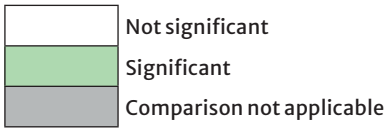

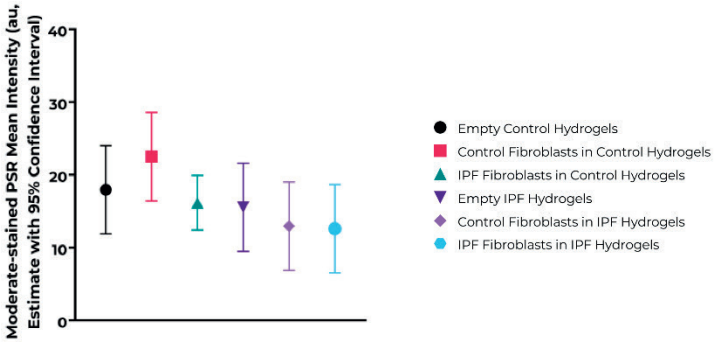

Supplementary Figure 12: Individual comparisons between the different groups of empty and fibroblast-seeded control and IPF hydrogels for the estimates of mean intensity of moderately stained PicroSirius Red (PSR) area (au) for day 14 samples.

Supplementary Table 11: Individual comparisons between the different groups of empty and fibroblast-seeded control and IPF hydrogels for mean intensity of strongly stained PicroSirius Red on day 7 samples

		Control Hydrogels			IPF Hydrogels		
		Empty	Control Fb	IPF Fb	Empty	Control Fb	IPF Fb
Control Hydrogels	Empty		0.702	0.431	0.903		
	Control Fb	0.702		0.246			
	IPF Fb	0.431	0.246				
IPF Hydrogels	Empty	0.903				0.538	0.612
	Control Fb				0.538		0.914
	IPF Fb				0.612	0.914	

Not significant
Significant
Comparison not applicable

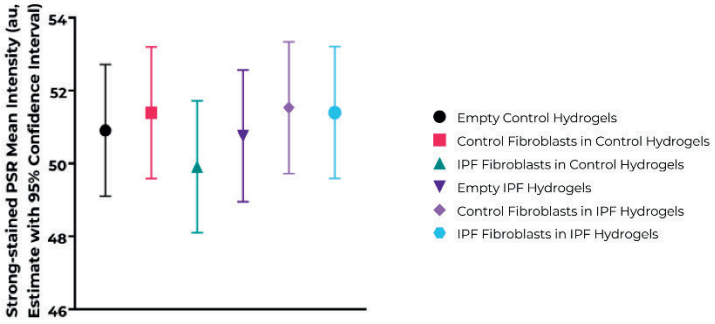

Supplementary Figure 13: Individual comparisons between the different groups of empty and fibroblast-seeded control and IPF hydrogels for the estimates of mean intensity of strongly stained PicroSirius Red (PSR) area (au) for day 7 samples.

Supplementary Table 12: Individual comparisons between the different groups of empty and fibroblast-seeded control and IPF hydrogels for mean intensity of strongly stained PicroSirius Red on day 14 samples

		Control Hydrogels			IPF Hydrogels		
		Empty	Control Fb	IPF Fb	Empty	Control Fb	IPF Fb
Control Hydrogels	Empty		0.701	0.296	0.298		
	Control Fb	0.701		0.503			
	IPF Fb	0.296	0.503				
IPF Hydrogels	Empty	0.298				0.719	0.425
	Control Fb				0.719		0.659
	IPF Fb				0.425	0.659	

Not significant
Significant
Comparison not applicable

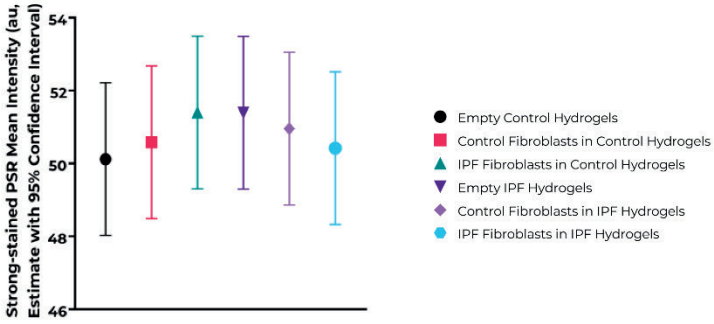

Supplementary Figure 14: Individual comparisons between the different groups of empty and fibroblast-seeded control and IPF hydrogels for the estimates of mean intensity of strongly stained PicroSirius Red (PSR) area (au) for day 14 samples.

Supplementary Table 13: Individual comparisons between the different groups of empty and fibroblast-seeded control and IPF hydrogels for weakly stained Alcian Blue area on day 7 samples

		Control Hydrogels			IPF Hydrogels		
		Empty	Control Fb	IPF Fb	Empty	Control Fb	IPF Fb
Control Hydrogels	Empty		0.281	0.080	0.696		
	Control Fb	0.281		0.453			
	IPF Fb	0.080	0.453				
IPF Hydrogels	Empty	0.696				1.000	0.827
	Control Fb				1.000		0.827
	IPF Fb				0.827	0.827	

Not significant
Significant
Comparison not applicable

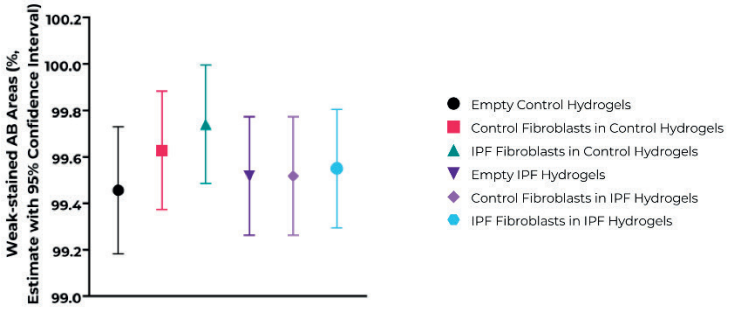

Supplementary Figure 15: Individual comparisons between the different groups of empty and fibroblast-seeded control and IPF hydrogels for the estimates of weakly stained Alcian blue (AB) area (%) for day 7 samples.

Supplementary Table 14: Individual comparisons between the different groups of empty and fibroblast-seeded control and IPF hydrogels for weakly stained Alcian Blue area on day 14 samples

		Control Hydrogels			IPF Hydrogels		
		Empty	Control Fb	IPF Fb	Empty	Control Fb	IPF Fb
Control Hydrogels	Empty		0.634	0.487	0.749		
	Control Fb	0.634		0.224			
	IPF Fb	0.487	0.224				
IPF Hydrogels	Empty	0.749				0.241	0.289
	Control Fb				0.241		0.908
	IPF Fb				0.289	0.908	

Not significant
Significant
Comparison not applicable

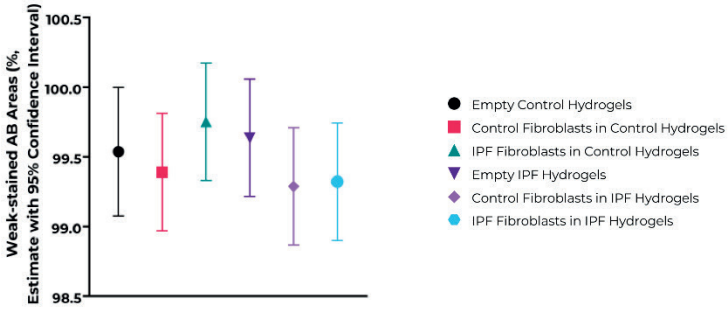

Supplementary Figure 16: Individual comparisons between the different groups of empty and fibroblast-seeded control and IPF hydrogels for the estimates of weakly stained Alcian blue (AB) area (%) for day 14 samples.

Supplementary Table 15: Individual comparisons between the different groups of empty and fibroblast-seeded control and IPF hydrogels for moderately stained Alcian Blue area on day 7 samples

		Control Hydrogels			IPF Hydrogels		
		Empty	Control Fb	IPF Fb	Empty	Control Fb	IPF Fb
Control Hydrogels	Empty		0.234	0.064	0.430		
	Control Fb	0.234		0.456			
	IPF Fb	0.064	0.456				
IPF Hydrogels	Empty	0.430				0.780	0.871
	Control Fb				0.780		0.906
	IPF Fb				0.871	0.906	

Not significant
Significant
Comparison not applicable

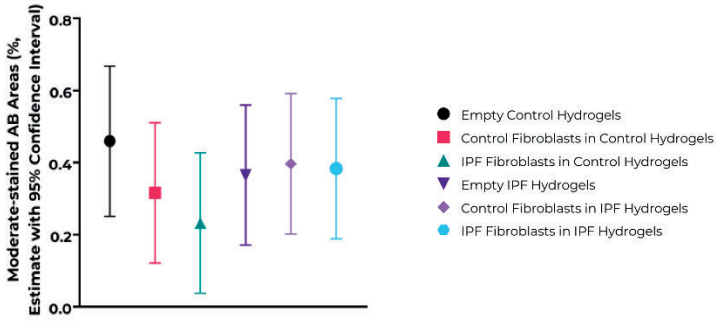

Supplementary Figure 17: Individual comparisons between the different groups of empty and fibroblast-seeded control and IPF hydrogels for the estimates of moderately stained Alcian blue (AB) area (%) for day 7 samples.

Supplementary Table 16: Individual comparisons between the different groups of empty and fibroblast-seeded control and IPF hydrogels for moderately stained Alcian Blue area on day 14 samples

		Control Hydrogels			IPF Hydrogels		
		Empty	Control Fb	IPF Fb	Empty	Control Fb	IPF Fb
Control Hydrogels	Empty		0.642	0.467	0.683		
	Control Fb	0.642		0.215			
	IPF Fb	0.467	0.215				
IPF Hydrogels	Empty	0.683				0.267	0.303
	Control Fb				0.267		0.934
	IPF Fb				0.303	0.934	

Not significant
Significant
Comparison not applicable

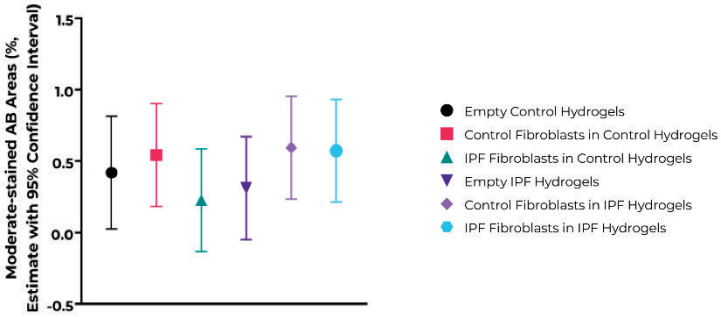

Supplementary Figure 18: Individual comparisons between the different groups of empty and fibroblast-seeded control and IPF hydrogels for the estimates of moderately stained Alcian blue (AB) area (%) for day 14 samples.

Supplementary Table 17: Individual comparisons between the different groups of empty and fibroblast-seeded control and IPF hydrogels for strongly stained Alcian Blue area on day 7 samples

		Control Hydrogels			IPF Hydrogels		
		Empty	Control Fb	IPF Fb	Empty	Control Fb	IPF Fb
Control Hydrogels	Empty		0.507	0.201	0.488		
	Control Fb	0.507		0.505			
	IPF Fb	0.201	0.505				
IPF Hydrogels	Empty	0.488				0.463	0.240
	Control Fb				0.463		0.650
	IPF Fb				0.240	0.650	

Not significant
Significant
Comparison not applicable

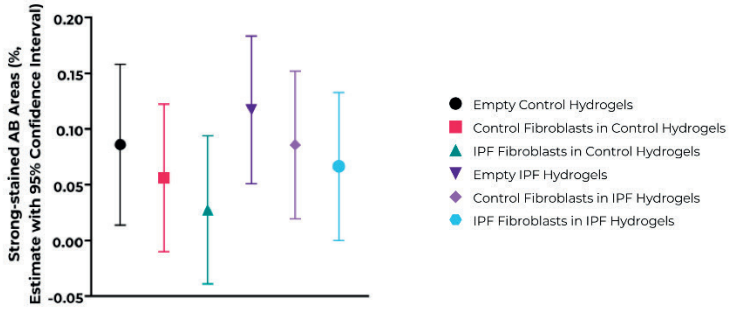

Supplementary Figure 19: Individual comparisons between the different groups of empty and fibroblast-seeded control and IPF hydrogels for the estimates of strongly stained Alcian blue (AB) area (%) for day 7 samples.

Supplementary Table 18: Individual comparisons between the different groups of empty and fibroblast-seeded control and IPF hydrogels for strongly stained Alcian Blue area on day 14 samples

		Control Hydrogels			IPF Hydrogels		
		Empty	Control Fb	IPF Fb	Empty	Control Fb	IPF Fb
Control Hydrogels	Empty		0.686	0.711	0.883		
	Control Fb	0.686		0.419			
	IPF Fb	0.711	0.419				
IPF Hydrogels	Empty	0.883				0.253	0.358
	Control Fb				0.253		0.818
	IPF Fb				0.358	0.818	

Not significant
Significant
Comparison not applicable

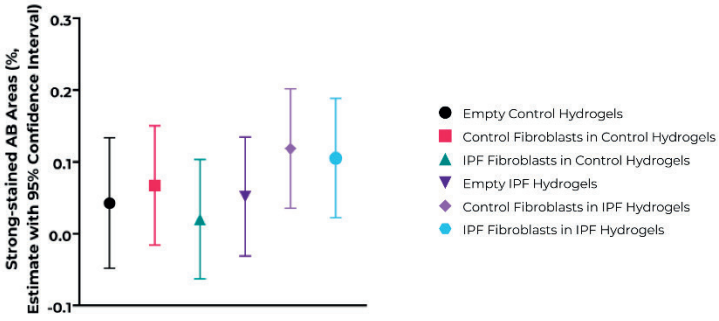

Supplementary Figure 20: Individual comparisons between the different groups of empty and fibroblast-seeded control and IPF hydrogels for the estimates of strongly stained Alcian blue (AB) area (%) for day 14 samples.

Supplementary Table 19: Individual comparisons between the different groups of empty and fibroblast-seeded control and IPF hydrogels for high-density matrix on day 7 samples

		Control Hydrogels			IPF Hydrogels		
		Empty	**Control Fb**	**IPF Fb**	**Empty**	**Control Fb**	**IPF Fb**
Control Hydrogels	Empty		0.400	0.412	0.630		
	Control Fb	0.400		0.109			
	IPF Fb	0.412	0.109				
IPF Hydrogels	Empty	0.630				0.147	0.631
	Control Fb				0.147		0.362
	IPF Fb				0.631	0.362	

Not significant
Significant
Comparison not applicable

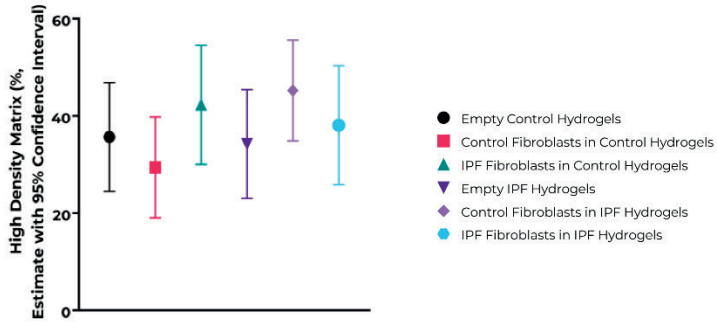

Supplementary Figure 21: Individual comparisons between the different groups of empty and fibroblast-seeded control and IPF hydrogels for the estimates of percentages of high-density matrix (%) for day 7 samples.

Supplementary Table 20: Individual comparisons between the different groups of empty and fibroblast-seeded control and IPF hydrogels for high-density matrix on day 14 samples

		Control Hydrogels			IPF Hydrogels		
		Empty	Control Fb	IPF Fb	Empty	Control Fb	IPF Fb
Control Hydrogels	Empty		0.512	0.056	0.029		
	Control Fb	0.512		0.160			
	IPF Fb	0.056	0.160				
IPF Hydrogels	Empty	0.029				0.043	0.029
	Control Fb				0.043		0.705
	IPF Fb				0.029	0.705	

Not significant
Significant
Comparison not applicable

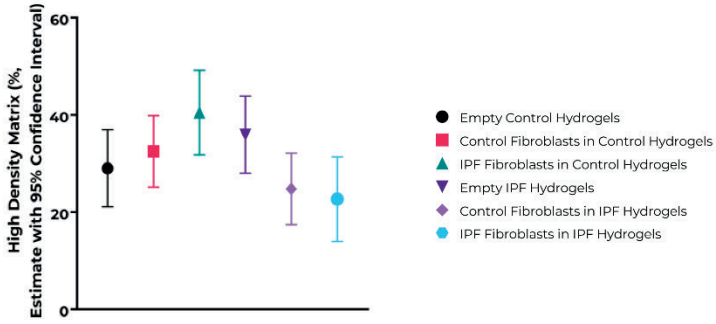

Supplementary Figure 22: Individual comparisons between the different groups of empty and fibroblast-seeded control and IPF hydrogels for the estimates of percentages of high-density matrix (%) for day 14 samples.

Supplementary Table 21: Individual comparisons between the different groups of empty and fibroblast-seeded control and IPF hydrogels for fiber alignment on day 7 samples

		Control Hydrogels			IPF Hydrogels		
		Empty	**Control Fb**	**IPF Fb**	**Empty**	**Control Fb**	**IPF Fb**
Control Hydrogels	Empty		0.266	0.401	0.572		
	Control Fb	0.266		0.844			
	IPF Fb	0.401	0.844				
IPF Hydrogels	Empty	0.572				0.366	0.094
	Control Fb				0.366		0.013
	IPF Fb				0.094	0.013	

Not significant
Significant
Comparison not applicable

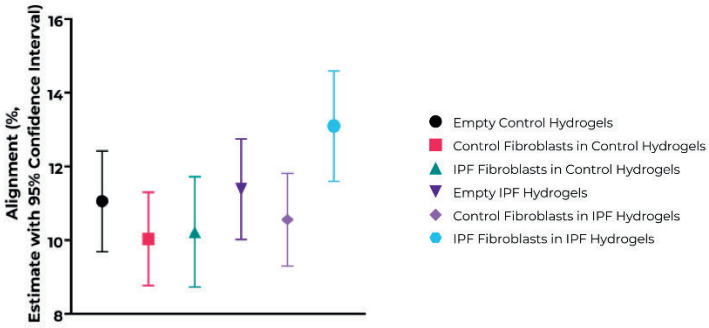

Supplementary Figure 23: Individual comparisons between the different groups of empty and fibroblast-seeded control and IPF hydrogels for the estimates of percentages of alignment (%) for day 7 samples.

Supplementary Table 22: Individual comparisons between the different groups of empty and fibroblast-seeded control and IPF hydrogels for fiber alignment on day 14 samples

		Control Hydrogels			IPF Hydrogels		
		Empty	**Control Fb**	**IPF Fb**	**Empty**	**Control Fb**	**IPF Fb**
Control Hydrogels	Empty		0.392	0.999	0.317		
	Control Fb	0.392		0.416			
	IPF Fb	0.999	0.416				
IPF Hydrogels	Empty	0.317				0.094	0.019
	Control Fb				0.094		0.335
	IPF Fb				0.019	0.335	

Not significant
Significant
Comparison not applicable

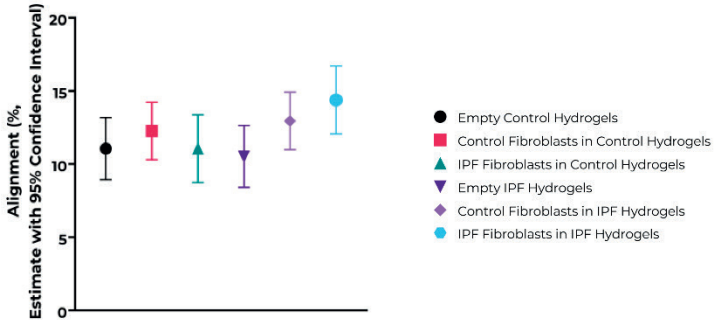

Supplementary Figure 24: Individual comparisons between the different groups of empty and fibroblast-seeded control and IPF hydrogels for the estimates of percentages of alignment (%) for day 14 samples.

Supplementary Table 23: Individual comparisons between the different groups of empty and fibroblast-seeded control and IPF hydrogels for average fiber length on day 7 samples

		Control Hydrogels			IPF Hydrogels		
		Empty	Control Fb	IPF Fb	Empty	Control Fb	IPF Fb
Control Hydrogels	Empty		0.311	0.689	0.004		
	Control Fb	0.311		0.175			
	IPF Fb	0.689	0.175				
IPF Hydrogels	Empty	0.004				0.137	0.802
	Control Fb				0.137		0.240
	IPF Fb				0.802	0.240	

Not significant
Significant
Comparison not applicable

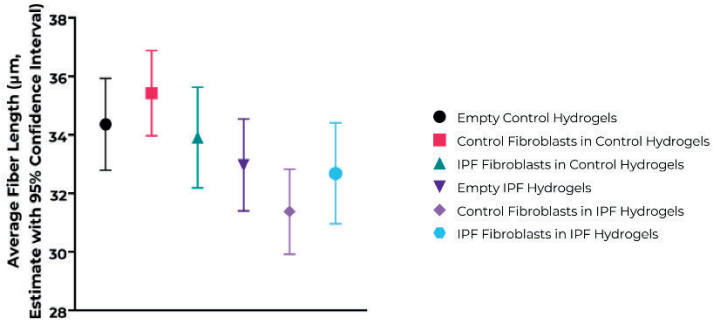

Supplementary Figure 25: Individual comparisons between the different groups of empty and fibroblast-seeded control and IPF hydrogels for the estimates of average fiber length (µm) for day 7 samples.

Supplementary Table 24: Individual comparisons between the different groups of empty and fibroblast-seeded control and IPF hydrogels for average fiber length on day 14 samples

		Control Hydrogels			IPF Hydrogels		
		Empty	Control Fb	IPF Fb	Empty	Control Fb	IPF Fb
Control Hydrogels	Empty		0.181	0.295	5.87×10^{-4}		
	Control Fb	0.181		0.025			
	IPF Fb	0.295	0.025				
IPF Hydrogels	Empty	5.87×10^{-4}				0.263	0.123
	Control Fb				0.263		0.571
	IPF Fb				0.123	0.571	

Not significant
Significant
Comparison not applicable

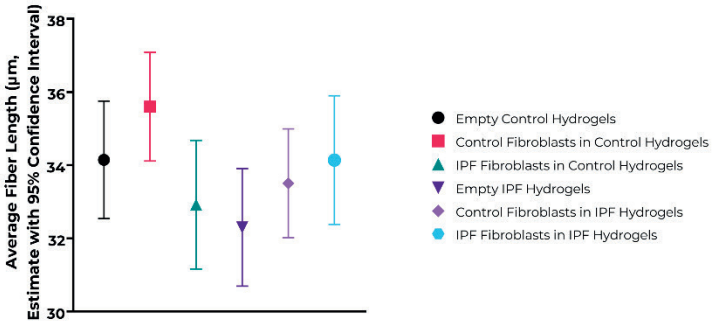

Supplementary Figure 26: Individual comparisons between the different groups of empty and fibroblast-seeded control and IPF hydrogels for the estimates of average fiber length (µm) for day 14 samples.

Supplementary Table 25: Individual comparisons between the different groups of empty and fibroblast-seeded control and IPF hydrogels for number of endpoints on day 7 samples

		Control Hydrogels			IPF Hydrogels		
		Empty	**Control Fb**	**IPF Fb**	**Empty**	**Control Fb**	**IPF Fb**
Control Hydrogels	Empty		0.259	0.155	1.68×10^{-4}		
	Control Fb	0.259		0.033			
	IPF Fb	0.155	0.033				
IPF Hydrogels	Empty	1.68×10^{-4}				0.216	0.111
	Control Fb				0.216		0.931
	IPF Fb				0.111	0.931	

Not significant
Significant
Comparison not applicable

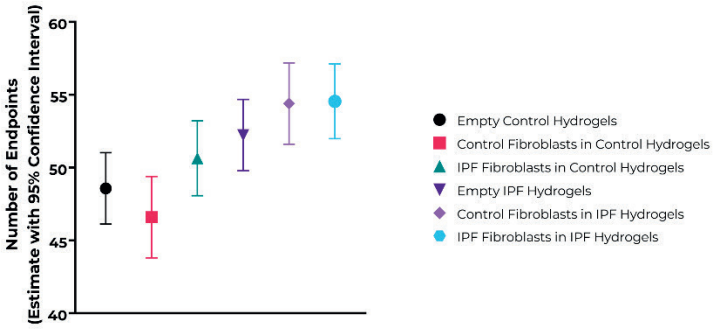

Supplementary Figure 27: Individual comparisons between the different groups of empty and fibroblast-seeded control and IPF hydrogels for the estimates of number of endpoints for day 7 samples.

Supplementary Table 26: Individual comparisons between the different groups of empty and fibroblast-seeded control and IPF hydrogels for number of endpoints on day 14 samples

		Control Hydrogels			IPF Hydrogels		
		Empty	Control Fb	IPF Fb	Empty	Control Fb	IPF Fb
Control Hydrogels	Empty		0.110	0.470	0.006		
	Control Fb	0.110		0.039			
	IPF Fb	0.470	0.039				
IPF Hydrogels	Empty	0.006				0.790	0.260
	Control Fb				0.790		0.505
	IPF Fb				0.260	0.505	

Not significant
Significant
Comparison not applicable

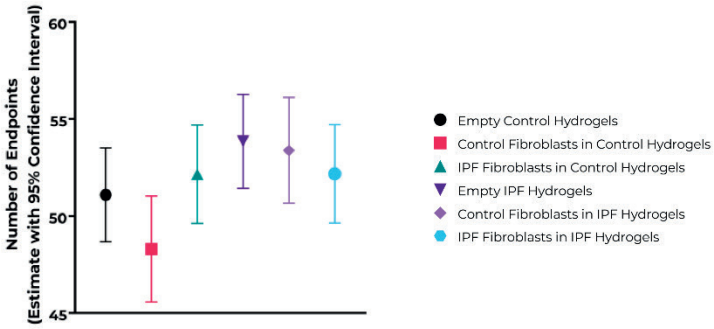

Supplementary Figure 28: Individual comparisons between the different groups of empty and fibroblast-seeded control and IPF hydrogels for the estimates of number of endpoints for day 14 samples.

Supplementary Table 27: Individual comparisons between the different groups of empty and fibroblast-seeded control and IPF hydrogels for number of branchpoints on day 7 samples

		Control Hydrogels			IPF Hydrogels		
		Empty	Control Fb	IPF Fb	Empty	Control Fb	IPF Fb
Control Hydrogels	Empty		0.719	0.895	0.007		
	Control Fb	0.719		0.633			
	IPF Fb	0.895	0.633				
IPF Hydrogels	Empty	0.007				0.769	0.742
	Control Fb				0.769		0.537
	IPF Fb				0.742	0.537	

Not significant
Significant
Comparison not applicable

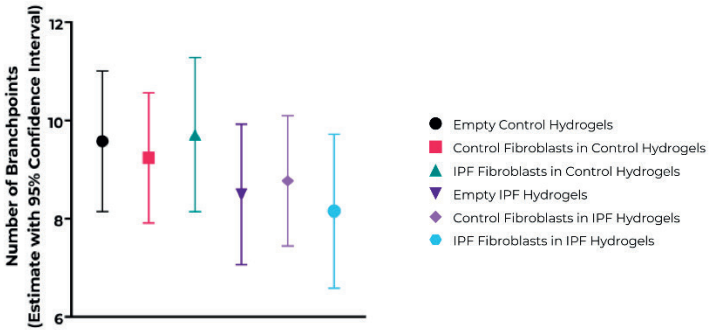

Supplementary Figure 29: Individual comparisons between the different groups of empty and fibroblast-seeded control and IPF hydrogels for the estimates of number of branchpoints for day 7 samples.

Supplementary Table 28: Individual comparisons between the different groups of empty and fibroblast-seeded control and IPF hydrogels for number of branchpoints on day 14 samples

		Control Hydrogels			IPF Hydrogels		
		Empty	**Control Fb**	**IPF Fb**	**Empty**	**Control Fb**	**IPF Fb**
Control Hydrogels	Empty		0.337	0.247	0.090		
	Control Fb	0.337		0.767			
	IPF Fb	0.247	0.767				
IPF Hydrogels	Empty	0.090				0.071	0.148
	Control Fb				0.071		0.798
	IPF Fb				0.148	0.798	

Not significant
Significant
Comparison not applicable

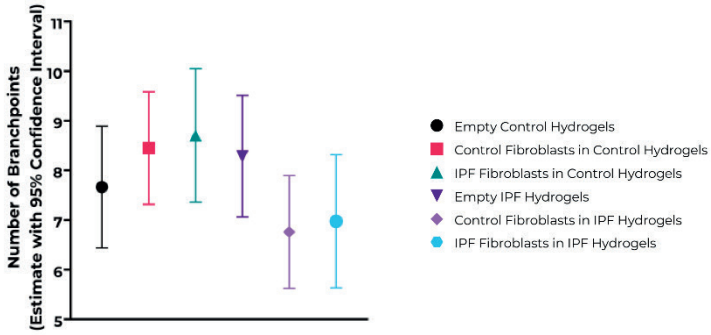

Supplementary Figure 30: Individual comparisons between the different groups of empty and fibroblast-seeded control and IPF hydrogels for the estimates of number of branchpoints for day 14 samples.

Supplementary Table 29: Individual comparisons between the different groups of empty and fibroblast-seeded control and IPF hydrogels for low curvature window on day 7 samples

		Control Hydrogels			IPF Hydrogels		
		Empty	Control Fb	IPF Fb	Empty	Control Fb	IPF Fb
Control Hydrogels	Empty		0.973	0.586	0.004		
	Control Fb	0.973		0.552			
	IPF Fb	0.586	0.552				
IPF Hydrogels	Empty	0.004				0.043	0.871
	Control Fb				0.043		0.074
	IPF Fb				0.871	0.074	

Not significant
Significant
Comparison not applicable

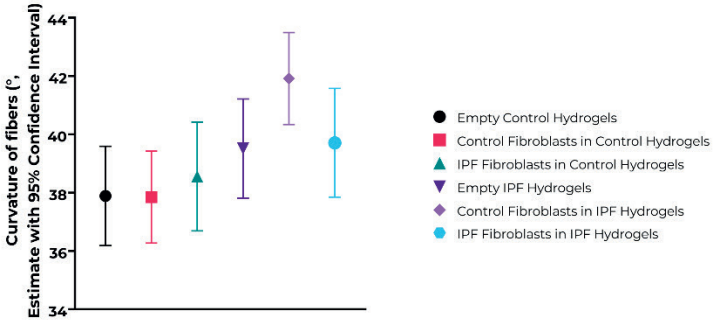

Supplementary Figure 31: Individual comparisons between the different groups of empty and fibroblast-seeded control and IPF hydrogels for the estimates of curvature of fibers in low curvature windows (°) for day 7 samples.

Supplementary Table 30: Individual comparisons between the different groups of empty and fibroblast-seeded control and IPF hydrogels for low curvature window on day 14 samples

		Control Hydrogels			IPF Hydrogels		
		Empty	Control Fb	IPF Fb	Empty	Control Fb	IPF Fb
Control Hydrogels	Empty		0.586	0.010	1.14×10^{-11}		
	Control Fb	0.586		0.027			
	IPF Fb	0.010	0.027				
IPF Hydrogels	Empty	1.14×10^{-11}				0.018	0.009
	Control Fb				0.018		0.593
	IPF Fb				0.009	0.593	

Not significant
Significant
Comparison not applicable

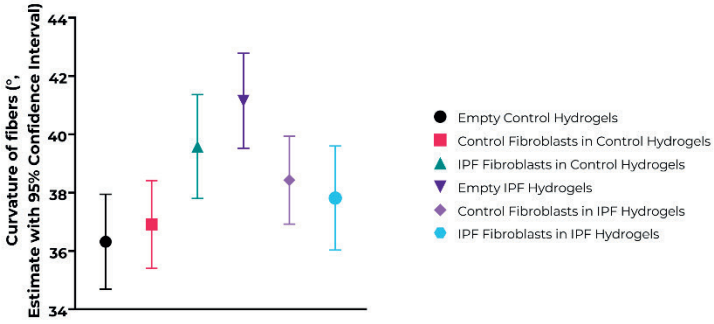

Supplementary Figure 32: Individual comparisons between the different groups of empty and fibroblast-seeded control and IPF hydrogels for the estimates of curvature of fibers in low curvature windows (°) for day 14 samples.

Supplementary Table 31: Individual comparisons between the different groups of empty and fibroblast-seeded control and IPF hydrogels for high curvature window on day 7 samples

		Control Hydrogels			IPF Hydrogels		
		Empty	**Control Fb**	**IPF Fb**	**Empty**	**Control Fb**	**IPF Fb**
Control Hydrogels	Empty		0.857	0.511	0.460		
	Control Fb	0.857		0.610			
	IPF Fb	0.511	0.610				
IPF Hydrogels	Empty	0.460				0.345	0.171
	Control Fb				0.345		0.025
	IPF Fb				0.171	0.025	

Not significant
Significant
Comparison not applicable

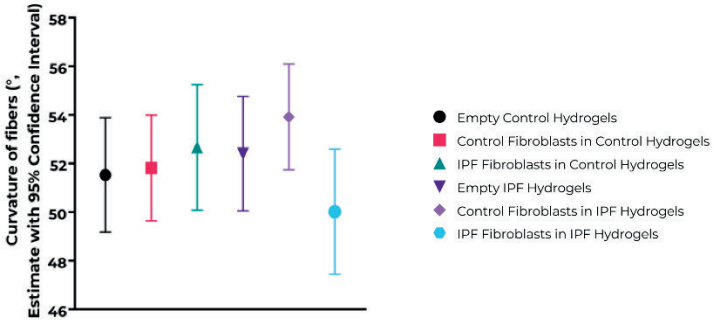

Supplementary Figure 33: Individual comparisons between the different groups of empty and fibroblast-seeded control and IPF hydrogels for the estimates of curvature of fibers in high curvature windows (°) for day 7 samples.

Supplementary Table 32: Individual comparisons between the different groups of empty and fibroblast-seeded control and IPF hydrogels for high curvature window on day 14 samples

		Control Hydrogels			IPF Hydrogels		
		Empty	Control Fb	IPF Fb	Empty	Control Fb	IPF Fb
Control Hydrogels	Empty		0.863	0.093	0.026		
	Control Fb	0.863		0.114			
	IPF Fb	0.093	0.114				
IPF Hydrogels	Empty	0.026				0.780	0.058
	Control Fb				0.780		0.766
	IPF Fb				0.058	0.766	

Not significant
Significant
Comparison not applicable

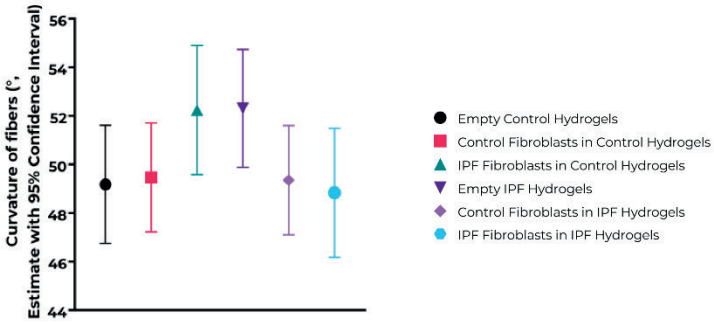

Supplementary Figure 34: Individual comparisons between the different groups of empty and fibroblast-seeded control and IPF hydrogels for the estimates of curvature of fibers in high curvature windows (°) for day 14 samples.

Supplementary Table 33: Individual comparisons between the different groups of empty and fibroblast-seeded control and IPF hydrogels for stiffness on day 7 samples

		Control Hydrogels			IPF Hydrogels		
		Empty	**Control Fb**	**IPF Fb**	**Empty**	**Control Fb**	**IPF Fb**
Control Hydrogels	Empty		0.497	0.846	4.93×10^{-22}		
	Control Fb	0.497		0.639			
	IPF Fb	0.846	0.639				
IPF Hydrogels	Empty	4.93×10^{-22}				0.002	0.006
	Control Fb				0.002		0.658
	IPF Fb				0.006	0.658	

Not significant
Significant
Comparison not applicable

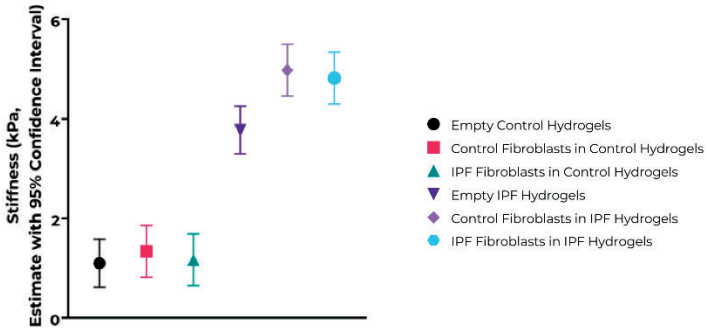

Supplementary Figure 35: Individual comparisons between the different groups of empty and fibroblast-seeded control and IPF hydrogels for the estimates of stiffness of hydrogels (kPa) for day 7 samples.

Supplementary Table 34: Individual comparisons between the different groups of empty and fibroblast-seeded control and IPF hydrogels for stiffness on day 14 samples

		Control Hydrogels			IPF Hydrogels		
		Empty	Control Fb	IPF Fb	Empty	Control Fb	IPF Fb
Control Hydrogels	Empty		0.958	0.653	1.15×10^{-31}		
	Control Fb	0.958		0.629			
	IPF Fb	0.653	0.629				
IPF Hydrogels	Empty	1.15×10^{-31}				1.70×10^{-4}	0.027
	Control Fb				1.70×10^{-4}		0.068
	IPF Fb				0.027	0.068	

Not significant
Significant
Comparison not applicable

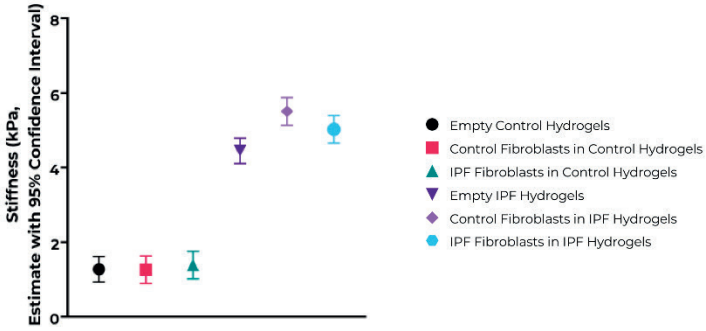

Supplementary Figure 36: Individual comparisons between the different groups of empty and fibroblast-seeded control and IPF hydrogels for the estimates of stiffness of hydrogels (kPa) for day 14 samples.

Supplementary Table 35: Individual comparisons between the different groups of empty and fibroblast-seeded control and IPF hydrogels for time to reach 50% stress relaxation on day 7 samples

		Control Hydrogels			IPF Hydrogels		
		Empty	Control Fb	IPF Fb	Empty	Control Fb	IPF Fb
Control Hydrogels	Empty		0.745	0.821	1.47×10^{-12}		
	Control Fb	0.745		0.924			
	IPF Fb	0.821	0.924				
IPF Hydrogels	Empty	1.47×10^{-12}				0.573	0.691
	Control Fb				0.573		0.358
	IPF Fb				0.691	0.358	

Not significant
Significant
Comparison not applicable

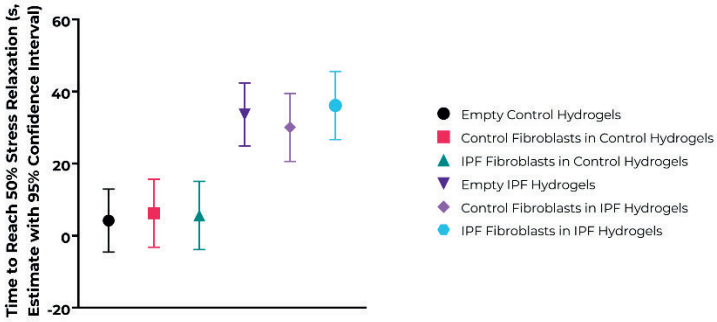

Supplementary Figure 37: Individual comparisons between the different groups of empty and fibroblast-seeded control and IPF hydrogels for the estimates of time to reach 50% stress relaxation (s) for day 7 samples.

Supplementary Table 36: Individual comparisons between the different groups of empty and fibroblast-seeded control and IPF hydrogels for time to reach 50% stress relaxation on day 14 samples

		Control Hydrogels			IPF Hydrogels		
		Empty	Control Fb	IPF Fb	Empty	Control Fb	IPF Fb
Control Hydrogels	Empty		0.719	0.515	5.82×10^{-14}		
	Control Fb	0.719		0.778			
	IPF Fb	0.515	0.778				
IPF Hydrogels	Empty	5.82×10^{-14}				0.023	0.020
	Control Fb				0.023		0.953
	IPF Fb				0.020	0.953	

Not significant
Significant
Comparison not applicable

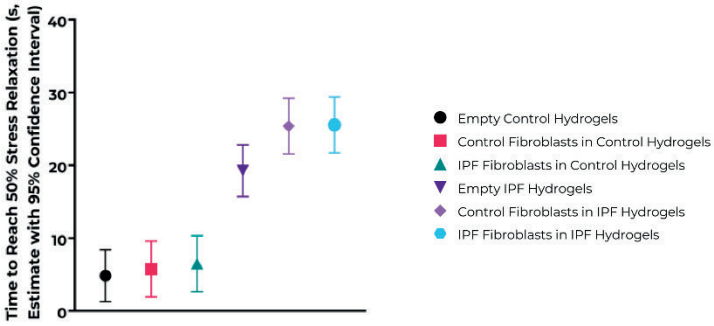

Supplementary Figure 38: Individual comparisons between the different groups of empty and fibroblast-seeded control and IPF hydrogels for the estimates of time to reach 50% stress relaxation (s) for day 14 samples.

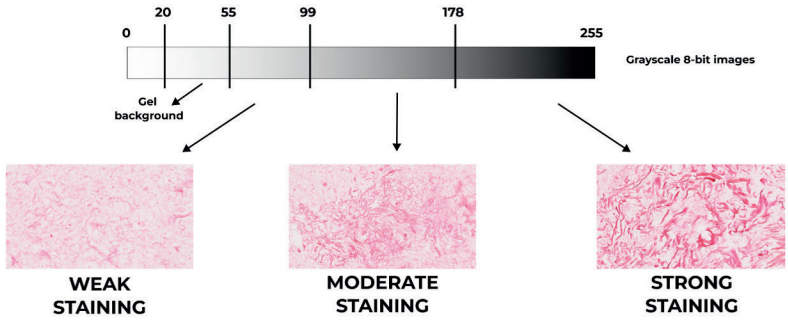

Supplementary Figure 39: Image analysis strategy used to analyze images of PicroSirius Red stained-slides. 8-bit images were converted to grayscale images and each pixel was assigned a strength between 0-255. Based on the strength values, the gel background was detected between 20 - 55 pixel strengths, and the remaining values (55 - 255) were divided into three categories to compare: weak staining (left), moderate staining (middle) and strong staining (right).

Supplementary Document 1: ImageJ Macro used to analyze the images of PicroSirius Red-stained slides

```
name=getTitle();
print(name);
display=getTitle();
   run("Set Measurements...", "area mean modal integrated median skewness kurtosis area_
fraction limit display redirect=None decimal=6");

run("Colour Deconvolution", "vectors=[ Picro_Sirius_Red]");
// Vector Picro_Sirius_Red = // Picro_Sirius_Red, 0.650,0.700,0.450, 0.150,0.750,0.400,
0.200,0.500,0.800

selectWindow(name+"-(Colour_1)");
            setAutoThreshold("Default");
                        setThreshold(195, 200);
                                    run("Measure");
                        setThreshold(156, 194);
                                    run("Measure");
                        setThreshold(117, 155);
                                    run("Measure");
                        setThreshold(78, 116);
                                    run("Measure");
                        setThreshold(39, 77);
                                    run("Measure");
                        setThreshold(0, 38);
                                    run("Measure");
   run("Close All");
```

Supplementary Document 2: ImageJ Macro used to analyze the images of Alcian blue-stained slides

```
name=getTitle();
print(name);
display=getTitle();
   run("Set Measurements...", "area mean modal integrated median skewness kurtosis area_
fraction limit display redirect=None decimal=6");
run("Duplicate...", " ");
run("8-bit");
name1=getTitle();
   rename(name1+"-(Colour_0)");
            setAutoThreshold("Default");
            setThreshold(0, 220);
            run("Measure");
   close();
run("Colour Deconvolution", "vectors=[ AlcianBlue]");
// AlcianBlue vector: AlcianBlue, 0.300,0.850,0.400, 0.800,0.550,0.250,
0.00000000,0.00000000,0.0000000

// Fill in below the thresholds for Colour2 image
selectWindow(name+"-(Colour_2)");
            setAutoThreshold("Default");
                        setThreshold(0, 220);
                                    run("Measure");
                        setThreshold(188, 220);
                                    run("Measure");
                        setThreshold(150, 187);
                                    run("Measure");
                        setThreshold(113, 149);
                                    run("Measure");
                        setThreshold(75, 112);
                                    run("Measure");
                        setThreshold(38, 74);
                                    run("Measure");
                        setThreshold(0, 37);
                                    run("Measure");
   run("Close All");
```

REFERENCES

1. Wynn TA. Cellular and molecular mechanisms of fibrosis. *J Pathol* 2008: 214(2): 199-210.
2. Henderson NC, Rieder F, Wynn TA. Fibrosis: from mechanisms to medicines. *Nature* 2020: 587(7835): 555-566.
3. Vancheri C, Failla M, Crimi N, Raghu G. Idiopathic pulmonary fibrosis: a disease with similarities and links to cancer biology. *Eur Respir J* 2010: 35(3): 496-504.
4. Lederer DJ, Martinez FJ. Idiopathic Pulmonary Fibrosis. *N Engl J Med* 2018: 378(19): 1811-1823.
5. Martinez FJ, Collard HR, Pardo A, Raghu G, Richeldi L, Selman M, Swigris JJ, Taniguchi H, Wells AU. Idiopathic pulmonary fibrosis. *Nat Rev Dis Pri* 2017: 3(1): 17074.
6. Jenkins RG, Moore BB, Chambers RC, Eickelberg O, Konigshoff M, Kolb M, Laurent GJ, Nanthakumar CB, Olman MA, Pardo A, Selman M, Sheppard D, Sime PJ, Tager AM, Tatler AL, Thannickal VJ, White ES, Cell ATSAoR, Molecular B. An Official American Thoracic Society Workshop Report: Use of Animal Models for the Preclinical Assessment of Potential Therapies for Pulmonary Fibrosis. *Am J Respir Cell Mol Biol* 2017: 56(5): 667-679.
7. Nizamoglu M, Burgess JK. The Multi-Faceted Extracellular Matrix: Unlocking Its Secrets for Understanding the Perpetuation of Lung Fibrosis. *Curr Tissue Microenviron Rep* 2022: 2(4): 53-71.
8. Burgess JK, Mauad T, Tjin G, Karlsson JC, Westergren-Thorsson G. The extracellular matrix - the under-recognized element in lung disease? *J Pathol* 2016: 240(4): 397-409.
9. Tjin G, White ES, Faiz A, Sicard D, Tschumperlin DJ, Mahar A, Kable EPW, Burgess JK. Lysyl oxidases regulate fibrillar collagen remodelling in idiopathic pulmonary fibrosis. *Dis Model Mech* 2017: 10(11): 1301-1312.
10. Jones MG, Andriotis OG, Roberts JJ, Lunn K, Tear VJ, Cao L, Ask K, Smart DE, Bonfanti A, Johnson P, Alzetani A, Conforti F, Doherty R, Lai CY, Johnson B, Bourdakos KN, Fletcher SV, Marshall BG, Jogai S, Brereton CJ, Chee SJ, Ottensmeier CH, Sime P, Gauldie J, Kolb M, Mahajan S, Fabre A, Bhaskar A, Jarolimek W, Richeldi L, O'Reilly KM, Monk PD, Thurner PJ, Davies DE. Nanoscale dysregulation of collagen structure-function disrupts mechano-homeostasis and mediates pulmonary fibrosis. *eLife* 2018: 7.
11. Booth AJ, Hadley R, Cornett AM, Dreffs AA, Matthes SA, Tsui JL, Weiss K, Horowitz JC, Fiore VF, Barker TH, Moore BB, Martinez FJ, Niklason LE, White ES. Acellular normal and fibrotic human lung matrices as a culture system for in vitro investigation. *Am J Respir Crit Care Med* 2012: 186(9): 866-876.
12. de Hilster RHJ, Sharma PK, Jonker MR, White ES, Gercama EA, Roobeek M, Timens W, Harmsen MC, Hylkema MN, Burgess JK. Human lung extracellular matrix hydrogels resemble the stiffness and viscoelasticity of native lung tissue. *Am J Physiol Lung Cell Mol Physiol* 2020: 318(4): L698-L704.
13. Burgstaller G, Oehrle B, Gerckens M, White ES, Schiller HB, Eickelberg O. The instructive extracellular matrix of the lung: basic composition and alterations in chronic lung disease. *Eur Respir J* 2017: 50(1).

14. Parker MW, Rossi D, Peterson M, Smith K, Sikstrom K, White ES, Connett JE, Henke CA, Larsson O, Bitterman PB. Fibrotic extracellular matrix activates a profibrotic positive feedback loop. *J Clin Invest* 2014: 124(4): 1622-1635.

15. Matera DL, DiLillo KM, Smith MR, Davidson CD, Parikh R, Said M, Wilke CA, Lombaert IM, Arnold KB, Moore BB, Baker BM. Microengineered 3D pulmonary interstitial mimetics highlight a critical role for matrix degradation in myofibroblast differentiation. *Sci Adv* 2020: 6(37).

16. Campbell DR, Jr., Senger CN, Ryan AL, Magin CM. Engineering Tissue-Informed Biomaterials to Advance Pulmonary Regenerative Medicine. *Front Med* 2021: 8: 647834.

17. Bailey KE, Floren ML, D'Ovidio TJ, Lammers SR, Stenmark KR, Magin CM. Tissue-informed engineering strategies for modeling human pulmonary diseases. *Am J Physiol Lung Cell Mol Physiol* 2019: 316(2): L303-L320.

18. Saldin LT, Cramer MC, Velankar SS, White LJ, Badylak SF. Extracellular matrix hydrogels from decellularized tissues: Structure and function. *Acta Biomater* 2017: 49: 1-15.

19. Wagner DE, Bonvillain RW, Jensen T, Girard ED, Bunnell BA, Finck CM, Hoffman AM, Weiss DJ. Can stem cells be used to generate new lungs? Ex vivo lung bioengineering with decellularized whole lung scaffolds. *Respirology* 2013: 18(6): 895-911.

20. Radwanska A, Cottage CT, Piras A, Overed-Sayer C, Sihlbom C, Budida R, Wrench C, Connor J, Monkley S, Hazon P, Schluter H, Thomas MJ, Hogaboam CM, Murray LA. Increased expression and accumulation of GDF15 in IPF extracellular matrix contribute to fibrosis. *JCI Insight* 2022: 7(16).

21. Vasse GF, Van Os L, De Jager M, Jonker MR, Borghuis T, Van Den Toorn LT, Jellema P, White ES, Van Rijn P, Harmsen MC, Heijink IH, Melgert BN, Burgess JK. Adipose Stromal Cell-Secretome Counteracts Profibrotic Signals From IPF Lung Matrices. *Front Pharmacol* 2021: 12: 669037.

22. Blokland KEC, Habibie H, Borghuis T, Teitsma GJ, Schuliga M, Melgert BN, Knight DA, Brandsma C-A, Pouwels SD, Burgess JK. Regulation of Cellular Senescence Is Independent from Profibrotic Fibroblast-Deposited ECM. *Cells* 2021: 10(7): 1628.

23. Tilbury K, Hocker J, Wen BL, Sandbo N, Singh V, Campagnola PJ. Second harmonic generation microscopy analysis of extracellular matrix changes in human idiopathic pulmonary fibrosis. *J Biomed Opt* 2014: 19(8): 086014.

24. Tisler M, Alkmin S, Chang HY, Leet J, Bernau K, Sandbo N, Campagnola PJ. Analysis of fibroblast migration dynamics in idiopathic pulmonary fibrosis using image-based scaffolds of the lung extracellular matrix. *Am J Physiol Lung Cell Mol Physiol* 2020: 318(2): L276-L286.

25. Philp CJ, Siebeke I, Clements D, Miller S, Habgood A, John AE, Navaratnam V, Hubbard RB, Jenkins G, Johnson SR. Extracellular Matrix Cross-Linking Enhances Fibroblast Growth and Protects against Matrix Proteolysis in Lung Fibrosis. *Am J Respir Cell Mol Biol* 2018: 58(5): 594-603.

26. Grønlien KG, Pedersen ME, Rønning SB, Solberg NT, Tønnesen HH. Tuning of 2D cultured human fibroblast behavior using lumichrome photocrosslinked collagen hydrogels. *Mater Today Commun* 2022: 31: 103635.

27. Douglas T, Heinemann S, Bierbaum S, Scharnweber D, Worch H. Fibrillogenesis of collagen types I, II, and III with small leucine-rich proteoglycans decorin and biglycan. *Biomacromolecules* 2006: 7(8): 2388-2393.

28. Fischer RS, Sun X, Baird MA, Hourwitz MJ, Seo BR, Pasapera AM, Mehta SB, Losert W, Fischbach C, Fourkas JT, Waterman CM. Contractility, focal adhesion orientation, and stress fiber orientation drive cancer cell polarity and migration along wavy ECM substrates. *Proc Natl Acad Sci USA* 2021: 118(22): e2021135118.

29. Wipff PJ, Rifkin DB, Meister JJ, Hinz B. Myofibroblast contraction activates latent TGF-beta1 from the extracellular matrix. *J Cell Biol* 2007: 179(6): 1311-1323.

30. Klingberg F, Chow ML, Koehler A, Boo S, Buscemi L, Quinn TM, Costell M, Alman BA, Genot E, Hinz B. Prestress in the extracellular matrix sensitizes latent TGF-beta1 for activation. *J Cell Biol* 2014: 207(2): 283-297.

31. Wu DT, Diba M, Yang S, Freedman BR, Elosegui-Artola A, Mooney DJ. Hydrogel viscoelasticity modulates migration and fusion of mesenchymal stem cell spheroids. *Bioeng Transl Med* 2023: 8(3): e10464.

32. Martinez-Garcia FD, de Hilster RHJ, Sharma PK, Borghuis T, Hylkema MN, Burgess JK, Harmsen MC. Architecture and Composition Dictate Viscoelastic Properties of Organ-Derived Extracellular Matrix Hydrogels. *Polymers* 2021: 13(18): 3113.

33. Epstein Shochet G, Wollin L, Shitrit D. Fibroblast-matrix interplay: Nintedanib and pirfenidone modulate the effect of IPF fibroblast-conditioned matrix on normal fibroblast phenotype. *Respirology* 2018: 23(8): 756-763.

34. Pouliot RA, Link PA, Mikhaiel NS, Schneck MB, Valentine MS, Kamga Gninzeko FJ, Herbert JA, Sakagami M, Heise RL. Development and characterization of a naturally derived lung extracellular matrix hydrogel. *J Biomed Mater Res A* 2016: 104(8): 1922-1935.

35. Noordhoek JA, Postma DS, Chong LL, Menkema L, Kauffman HF, Timens W, van Straaten JF, van der Geld YM. Different modulation of decorin production by lung fibroblasts from patients with mild and severe emphysema. *COPD* 2005: 2(1): 17-25.

36. Schindelin J, Arganda-Carreras I, Frise E, Kaynig V, Longair M, Pietzsch T, Preibisch S, Rueden C, Saalfeld S, Schmid B, Tinevez JY, White DJ, Hartenstein V, Eliceiri K, Tomancak P, Cardona A. Fiji: an open-source platform for biological-image analysis. *Nat Methods* 2012: 9(7): 676-682.

37. Koloko Ngassie ML, De Vries M, Borghuis T, Timens W, Sin DD, Nickle D, Joubert P, Horvatovich P, Marko-Varga G, Teske JJ, Vonk JM, Gosens R, Prakash YS, Burgess JK, Brandsma CA. Age-associated differences in the human lung extracellular matrix. *Am J Physiol Lung Cell Mol Physiol* 2023: 324(6): L799-L814.

38. Wershof E, Park D, Barry DJ, Jenkins RP, Rullan A, Wilkins A, Schlegelmilch K, Roxanis I, Anderson KI, Bates PA, Sahai E. A FIJI macro for quantifying pattern in extracellular matrix. *Life Sci Alliance* 2021: 4(3).

39. Nizamoglu M, de Hilster RHJ, Zhao F, Sharma PK, Borghuis T, Harmsen MC, Burgess JK. An in vitro model of fibrosis using crosslinked native extracellular matrix-derived hydrogels to modulate biomechanics without changing composition. *Acta Biomater* 2022: 147: 50-62.

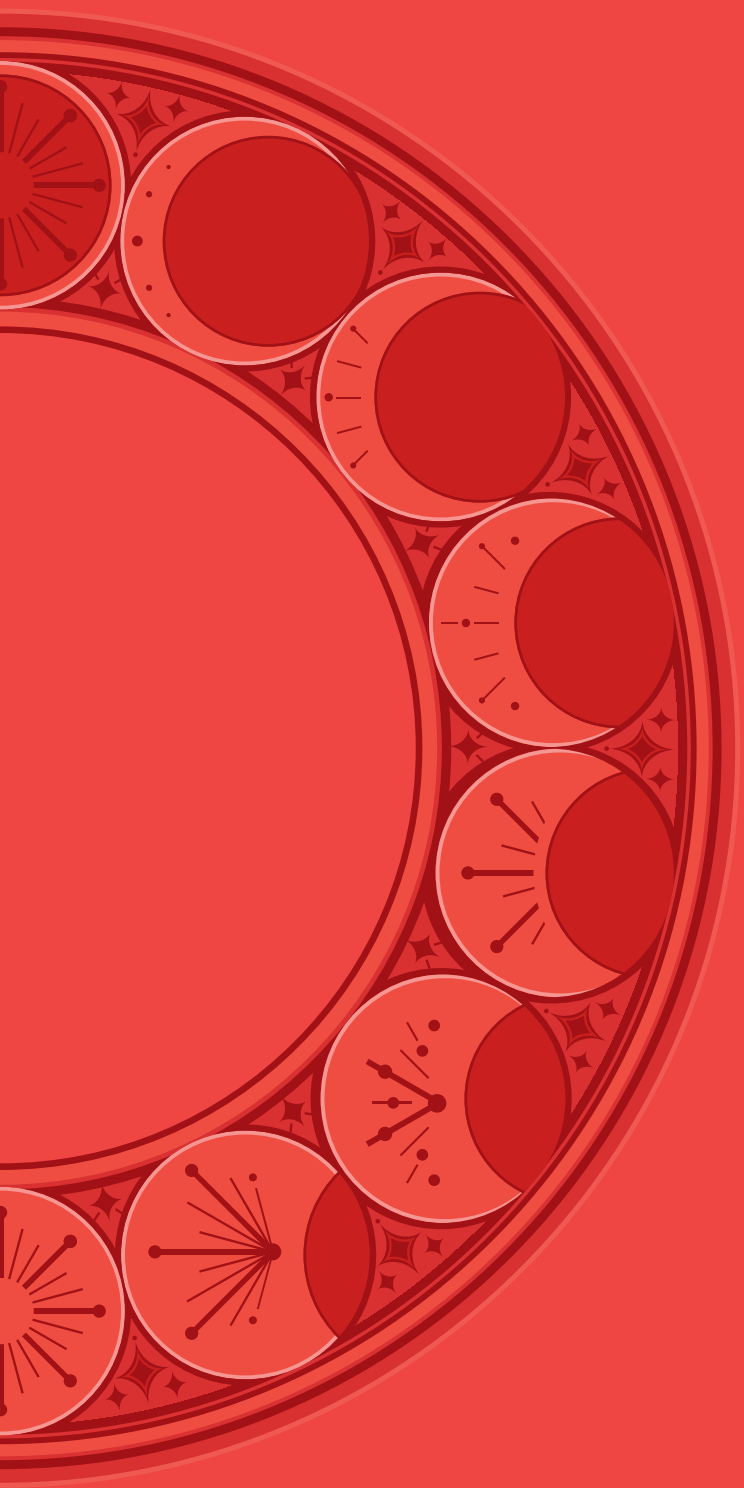

CHAPTER 10

General discussion and future perspectives

Idiopathic pulmonary fibrosis (IPF) is a devastating lung disease with poor prognosis, high mortality rate and no cure available [1]. In IPF, the extracellular matrix (ECM), a dynamic and biologically active network of molecules that provides structural support to organs and tissues, is replaced with a disorganized and abnormal ECM structure. The deposition of this aberrant ECM in alveolar septa in the form of scar tissue is hypothesized to originate from abnormal wound repair responses to (micro) injuries in lung epithelium and resulting in recruitment of activated fibroblasts, the main producers of ECM, in a positive feedback cycle that results in generation of more fibrotic ECM for fibroblasts to respond [2]. How we look at the disease processes is changing: modifications in ECM are not just a silent byproduct of disease progression but an active contributor to this process [3]. We now know that (fibrotic) lung ECM does not only hold the tissue together but can provide cues to both resident and transmigrating cells [4, 5]. The details of these cell-ECM interactions in the context of IPF have not been thoroughly explored previously. This thesis aimed to investigate fibrotic ECM-cell interactions and how the fibrotic ECM stimulates profibrotic response in cells within this microenvironment.

Lung ECM in IPF is drastically altered compared to control (non-IPF) lung ECM. Increased amounts of ECM components, higher amounts of crosslinking of collagens, altered topography and biomechanics in IPF lung ECM have been well-described (as reviewed in **Chapter 2**). Among these changes, collagen production, organization and crosslinking have been the main focuses: collagen synthesis biomarkers have been shown to predict disease progression in IPF [6, 7], increased levels of collagen maturity have been described in IPF lungs compared with control lungs [8], and collagen crosslinking has been shown to enhance fibroblast proliferation in IPF [9]. One of the important aspects in collagen organization is the presence of FACIT (Fibril Associated Collagens with Interrupted Triple helices) [10]. Collagen types IX, XII and XIV belong to this category of collagens, which provide support in the organization of collagen fibrils during fibril assembly in tissue [11]. However, their involvement in IPF, which is now known to include altered collagen organization, has not been described in detail. In **Chapter 3**, I describe the occurrence and distribution of collagen type XIV (COL14) in the lungs of patients with IPF, compared with control donor lungs. I found proportionally lower amounts of collagen type XIV in IPF lungs. These proportionally lower amounts point at possible mechanisms of decreased synthesis or increased degradation of collagen type XIV compared to other ECM components, which paves the way to a potential biomarker for IPF. Currently, it is not possible to discern whether rate of production of collagen type XIV does not match the production rate of other ECM components in IPF or whether this particular collagen is degraded more in IPF lungs. However, the consistently lower proportion of collagen type XIV in IPF

can lead to possibilities of detecting (the absence of) production or degradation biomarkers of collagen type XIV for instance in blood. If these biomarkers can be detected, a next step would be investigating their change throughout the disease prognosis in patients with IPF. A recent proteomics study highlighted differences between IPF and control lung ECM samples but collagen type XIV was not found to be different between IPF and control samples [12]. This is particularly interesting as an earlier mass spectrometry-based proteomics study revealed a 10 times increase in the counts of collagen type XIV in IPF lung tissue compared to control tissue [13]. While my observations and the earlier proteomics study reported by Booth et al. [12] do not fit with proteomics analysis reported by Hoffman et al. [13], the discrepancies between these studies can be explained by different sensitivities of the methods applied. Regardless, these initial observations I made require further mechanistic *in vitro* and *in vivo* studies on involvement of collagen type XIV in IPF to understand the role of these lower proportions of collagen type XIV in the altered collagen organization and composition in fibrotic ECM.

Investigating fibrotic lung diseases, such as IPF, *in vivo* and *in vitro* requires appropriate models that can (partially) mimic the complex nature of these chronic diseases. While *in vivo* models of fibrosis induced through bleomycin have been frequently used [14], the spontaneous resolution of fibrosis in these models does not properly represent the human disease [15]. Innovative *in vitro* models derived from patient materials are emerging as an alternative for modeling these diseases: precision lung cut slices, organoids, cell-seeded lung ECM-derived hydrogels and lung-on-chip systems provide a wide range of applications with strengths and limitations within each model system (as reviewed in **Chapter 4**). Among these models, organoid cultures derived from alveolar epithelial cells isolated from the lungs of patients with IPF was a gap in the literature. In **Chapter 5**, I described such organoid culture systems for the first time for IPF and compared IPF lung-derived cells to control lung-derived counterparts. I showed that epithelial cells isolated from the lungs of patients with IPF had lower organoid forming capacity compared with those isolated from control donors when supporting cells, which include stromal cells, endothelial cells and macrophages, were present (unfractionated suspensions); however, not in their absence. While the alveolar epithelial cells in IPF have been suggested to become senescent and have reduced regenerative capacity [16], my results showing comparable regenerative capacity of IPF and control lung-derived epithelial cells alone were not in concert with these previous reports. On the other hand, when the supporting cells were present, there were differences in the regenerative capacity of IPF epithelial cells compared to control-derived epithelial cells in the organoid cultures. This implies that the reduced regenerative capacity

results from the interactions between the cells rather than an intrinsic defect in the alveolar epithelial cells. There are several potential reasons for why unfractionated organoids had lowered regenerative capacity, one of which being other cells in the supporting cell populations. Although there were no significant differences detected in the proportions of supporting cells, the screened cellular markers might have missed some of the other less common cell types that might have impact on epithelial cell regeneration. The potential differences in the survival of these cells in the organoid cultures can also contribute to the results generated. Another potential explanation for why the unfractionated cell population resulted in reduced regenerative capacity could be the differences between paracrine factors secreted from the supporting cells isolated from IPF lungs and control lungs, which was out of the scope of these initial observations. Lastly, the influence of potential imprinting of the native fibrotic ECM on the supporting cell populations could result in the reduced regenerative capacity in the unfractionated cultures. The supporting cell populations in lung parenchyma have been previously implied to be responsive to instructions coming from the fibrotic ECM [17]. While the ECM-mimicking substance used in this study during organoid culture was the same for both control and IPF groups, investigating how fibrotic ECM is involved in the interactions between the stromal cells and epithelial cells in IPF may reveal additional mechanisms of how epithelial repair is impaired in IPF. Considering the recent reports of transcriptomic profiling of epithelial cells which showed an ECM-producing gene signature in the epithelial cells [18], this newly produced ECM could be responsible for the feedback provided to the supporting cells, which in turn may reduce regenerative capacity of epithelial cells. In addition to the fibroblasts, which are well documented to contribute to the fibrotic microenvironment seen in IPF lungs [19], a certain subpopulation of endothelial cells has been found to be in close proximity to fibroblastic foci in IPF lungs and could thus also contribute [20] [21]. Similarly, profibrotic macrophages contribute to a more fibrotic microenvironment [22], which subsequently gives further feedback towards both epithelial cells and supporting cell populations. The overruling capacity of (fibrotic) ECM on delicate interactions between lung resident cells requires further attention to reveal its complete potential.

In the last decade, the importance of the influence of lung microenvironment has been also reflected in the methods developed to mimic ECM in *in vitro* models. Generation of appropriate substitutes for ECM to be used in these models started with relatively simple models composed of one type of material. Models prepared with synthetic polymers provide greater control over properties such as stiffness, fiber organization and degradability natural polymers , while those models employing natural polymers have advantages in availability of bioactive cues and cell-binding

domains [23]. Using individual ECM components such as collagen type I or hyaluronic acid as ECM substitutes in *in vitro* models have advanced our understanding of the influence dictated by the choice of material in such models (as outlined in **Chapter 6**). More recently, generating hydrogels from the decellularized lung ECM itself has been described and has paved the way for a multitude of opportunities for mimicking *in vivo* complexity of ECM in *in vitro* conditions (as reviewed in **Chapter 6** and discussed in **Chapter 7).** Lung ECM-derived hydrogels provide both most of the diversity of ECM biochemical composition as seen *in vivo* and some of the mechanical properties of the native lung tissue [24, 25]. While these properties are important, modifying them in a controlled and cell-friendly manner was not previously explored. In **Chapter 8**, I addressed this unmet need in the field and applied UV-visible light triggered crosslinking of fibers through Ruthenium crosslinking in porcine lung ECM-derived hydrogels. By doing so, I successfully kept the biochemical composition intact while altering mechanical properties to be able to study the influence of altered mechanics in chronic lung diseases such as IPF. I verified the successful application of fiber crosslinking in our model by showing fibrotic mechanical properties such as stiffness and stress relaxation as well as altered fiber characteristics, which include fiber curvature, fiber alignment and percentage area covered by dense fibers. As a result of such changes in the fiber organization in the hydrogels, fibroblasts seeded on crosslinked lung ECM-derived hydrogels responded in a manner similar to the responses of pro-fibrotic fibroblasts isolated from IPF lungs, demonstrated through increased alpha-smooth muscle actin (αSMA) expression and increased nuclear area. These characterizations are in concert with previously published studies examining the role of altered stiffness in fibroblast responses [26-29]. While my initial setup was two-dimensional for proof-of-principle purposes, applying the same methodology in three-dimensional cultures with the presence of cells can also be performed while retaining cell viability [30], although responses of different cells types (such as lung epithelial or endothelial cells) have yet to be characterized. The applied fiber crosslinking in my study was through linking tyrosine amino acids, [31] while the natural fiber crosslinking in collagens in ECM takes place through lysyl oxidases and transglutaminases acting on lysine and glutamine amino acids [32]. Involvement of both of these enzymes for fiber crosslinking in the context of IPF has been previously shown. The comparison of how the enzymatic crosslinking differs from the Ruthenium-induced crosslinking, and how their potential differences influence cellular responses remains unexplored. In addition to the enzymatic crosslinking for the arrangement of fibers, the collagen organization is also regulated through other ECM components such as proteoglycans and FACITs. Inclusion of collagen type XIV that I described in **Chapter 3** in the development of improved models of fibrotic mechanics generated in **Chapter 8** would certainly be worthy of investigation.

Another intriguing application of my method described in **Chapter 8** would be using it in organoid culture systems, such as organoids derived from IPF lungs (as described in **Chapter 5**) to investigate how stiffer ECM influences the interplay between epithelial cells and supporting cell populations. Investigating the cross-section of fibrotic mechanics and fibrotic ECM-imprinted cells in the context of alveolar epithelium regeneration would reveal additional dynamics and interactions that the current limit of our knowledge has not even reached. Another implication of the findings in my thesis translates to organoid culture using mesenchymal cells embedded in Matrigel; the potential pathological instructions delivered from Matrigel, being derived from sarcoma ECM [33], towards fibroblasts may have consequences for how these fibroblasts remodel the environment and hence signal to epithelial cells. Examining the interaction between biomechanics of fibrotic ECM and resident cells during lung fibrosis in *in vitro* models with multiple cells types will advance our understanding on the perpetuation of the fibrotic response.

The opportunities provided by 3D *in vitro* models can be further strengthened by using materials of human origin. One of the initial reports using such material was by Booth et al., in which they reported the use of decellularized ECM derived from fibrotic human lungs as an ideal system to be used in *in vitro* culture [13]. In the same study, they have also observed fibrotic ECM-triggered changes in lung fibroblasts [13]. Our understanding of cell-matrix interactions in fibrosis was furthered by Parker et al., who demonstrated a positive pro-fibrotic feedback loop between fibrotic ECM and fibroblasts [34]. While these pioneering studies have advanced the possibilities of recapitulating the lung microenvironment *in vitro*, the challenges in recellularization of intact decellularized matrices with respect to size and shape of the matrices remained as a roadblock [35-37]. Lung ECM-derived hydrogels provide a unique opportunity to bypass the limitations of intact matrices in size and shape, as well as facilitating the (re)introduction of cells (as discussed in **Chapter 7**). Based on this, in **Chapter 9**, I have mimicked fibroblast-ECM interactions in the context of IPF by comparing the responses of primary lung fibroblasts isolated from control and IPF lungs and seeded in either IPF or control lung ECM-derived hydrogels. I characterized these fibroblast-seeded ECM-derived hydrogels with respect to collagen and GAG content, collagen fiber organization and mechanical properties, and compared them to their empty counterparts. I showed that control fibroblasts and IPF fibroblasts responded differently to fibrotic microenvironment: for most parameters, the responses of control fibroblasts in fibrotic microenvironment were towards making the environment even more fibrotic as shown by decreased high-density matrix, increased fiber curvature, increased stiffness of the hydrogels, compared to the empty hydrogels, while IPF-derived fibroblasts exerted less pronounced effects.

This combined approach to understand fibroblast responses that were dictated by the microenvironment to which they were exposed reflected the existing literature with respect to the instructiveness of the ECM in lung fibrosis [9, 13, 29, 34], and advanced it by providing an *in vitro* model system that recapitulated the biochemical and biomechanical complexity of lung ECM *in vivo*. The exaggerated responses of control fibroblasts might be explained by these fibroblasts being naïve and ready to be instructed by the microenvironment, while the IPF fibroblasts being already imprinted and less sensitive to the additional feedback coming from the hydrogels. In addition, I have shown how the fibroblasts responses differed with respect to parameters related to collagen fiber organization and mechanical properties of the hydrogels. While the initial efforts in understanding fibrotic ECM focused solely on the (accumulation of) collagens, there is now a growing body of evidence investigating the fiber organization, fiber crosslinking or ECM topography report how cells are able respond to structural arrangement of ECM alone [38–42]. These emerging studies could prove important especially for guiding new efforts to find novel therapeutic targets and develop new strategies to treat lung fibrosis by targeting not only fibrotic cells but fibrotic ECM characteristics.

Building on the reports by Booth et al. [13] and Parker et al. [34], my results illustrate the capacity of fibrotic ECM-driven instructions through complex dynamics between the ECM and fibroblasts. An interesting observation from this study was that control fibroblasts changed the microenvironment even in control hydrogels, with respect to several parameters, which might indicate that these cells have an optimal set of conditions associated with their ideal environment and work towards establishing them. By understanding the *de facto* states of different cells within their microenvironment, future therapeutic strategies against lung fibrosis can be developed to target mechanisms that imbalance these default states.

The mimicking capacity of the abovementioned model for capturing the lung microenvironment *in vitro* could be further bolstered by introducing another cell type such as epithelial cells to investigate interactions between different cell types and ECM (as reported in **Chapter 5).** Applying additional fiber crosslinking to separately investigate the influence of mechanical properties (as developed in **Chapter 8**) with the presence of fibrotic ECM composition could also advance the mimicry achieved in this model. Cell-seeded hydrogels derived from native human lung ECM brings a cutting edge to both basic and translational research.

In conclusion, the findings of this thesis break new grounds in the field of fibrotic lung diseases. The new results and methods originating from this thesis provide new

horizons in the uncharted skies of the complex nature of these devastating diseases. As introduced in **Chapter 1**, this thesis aimed to investigate how ECM rules them all; and why the fibrotic ECM has such a strong influence of in fibrotic processes has become more unclouded with findings of my thesis (**Figure 1**).

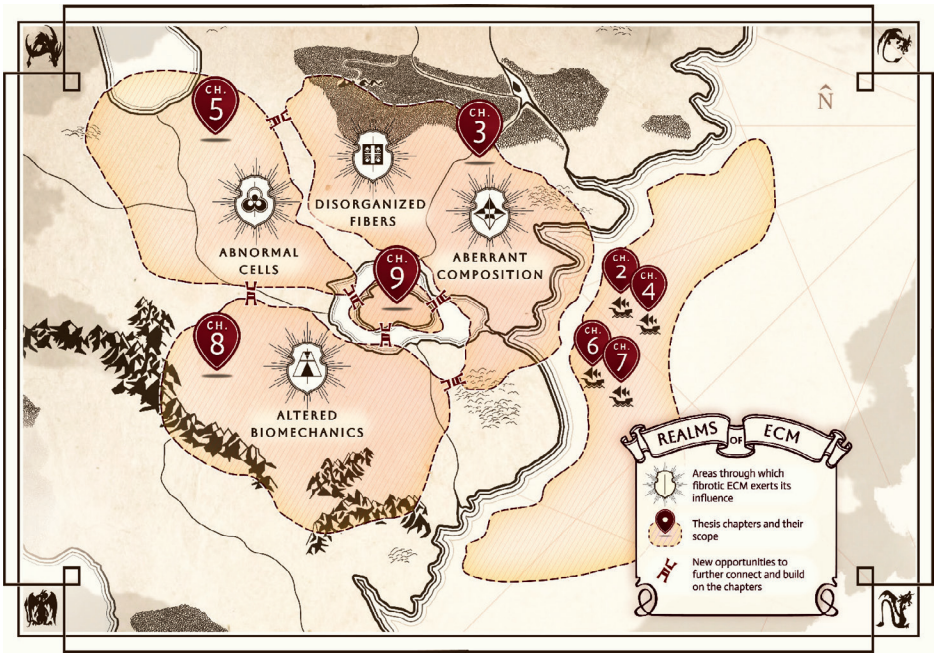

Figure 1: The landscape and influence of the Realms of Extracellular Matrix (ECM) unclouded by the findings of thesis. The experimental chapters of this thesis (Chapters 3, 5, 8 & 9) encompass the landscape of the (combinations of) four areas through which fibrotic ECM exerts its influence: aberrant composition, disorganized fibers, altered biomechanics and (direction of) abnormal cells. These areas are bound by the theoretical chapters of this thesis (Chapters 2, 4, 6 & 7) which provide conceptual context. New opportunities for further exploration have been discovered through connecting the individual chapters and building on the findings made herein. While new fields have been unclouded by these chapters and are ready to be explored, they only mark the beginning of the new adventures.

FUTURE PERSPECTIVES

The findings and methodologies generated in this thesis enable a wide repertoire of future applications for both *in vitro* disease modeling and improving our understanding of disease mechanisms. In addition to the points highlighted in the section above, one of the future steps would be further characterization of the *in vitro*

models. The differences between the ECM components with respect to content and amount in different regions of lung ECM in health and disease were described in a recent study using mass spectrometry by Hoffman et al [12]. An intriguing question that remains is to what extent lung ECM-derived hydrogels can recapitulate this protein content and composition. Analyzing lung ECM-derived hydrogels using similar approaches can strengthen arguments regarding the capacity of lung ECM-derived hydrogels to recapitulate the biochemical composition of lung ECM. Moreover, comparing the changes in proteomic profiles of the stroma through such analysis can generate novel findings. Another question that requires future research is whether cell-seeded lung ECM-derived hydrogels can re-capture, and expand upon, previous observations with respect to the applicability of ECM fragments as biomarkers of fibrotic lung diseases.

Furthermore, approach to identify novel mechanisms of cell:ECM interactions in fibrosis using *in vitro* models developed in this thesis, could be through transcriptomics analysis. Profiling of healthy and IPF lungs using single-cell RNA-sequencing (scRNAseq) has been extensively demonstrated in the last decade [18, 20, 22, 43-48]. By investigating the gene profiles of cells seeded in control or diseased lung ECM-derived hydrogels and comparing these gene signatures to the existing fibrotic RNA signatures, the potential applicability of the model to reflect gene changes that take place in the lung tissue could be revealed. After this initial validation, the utilization of the model can be expanded for assessing possible treatment preclinically. However, isolating RNA from cells, especially fibroblasts, from (human) lung ECM-derived hydrogels remains challenging due to poor quality and/or quantity of isolated RNA that is achievable to date. Although recovering cells via enzymatic digestion is an alternative, the cells might change their transcriptomic profile during the recovery process. Together with advances in the field of spatial transcriptomics, these challenges will need to be bypassed for a thorough gene-level characterization of cells embedded in lung ECM (diseased) microenvironment.

Advanced imaging methodologies can also be applied to the *in vitro* models described in this thesis in order to promote our understanding on fibrotic ECM. Although the current field of clinical imaging is still limited to investigate the changes in ECM during lung fibrosis, novel methods such as optical coherence tomography (OCT), confocal laser endomicroscopy (CLE) or high resolution computed tomography (HRCT) to investigate ECM structure *in vivo* are being developed thanks to the advances in the fields of physics and imaging [49]. Some of the other methods such as photoacoustic or ultrasound imaging can also provide additional information about the tissue architecture [50]. Most of the deep tissue imaging methods so

far target cells and cellular components [51], but a recent study illustrated the possibility of targeting the ECM itself [52]. It remains undiscovered whether these methods, alone or in combination, can be used to monitor the changes in the ECM organization and topography, especially during clinical assessments. It is intriguing to speculate on possibilities of utilization of some of the specific parameters regarding ECM organization investigated in this thesis for the assessment of the disease progression. Assessment of more micro-scale changes in ECM structure and organization during lung fibrosis before it translates to macro-scale changes in the whole lung tissue can bring an advantage for monitoring disease progression, both alone and in combination with other clinical parameters. Realigning our perspectives for considering (the changes in) the ECM more than just collagens and structural support and realizing its potential for being monitored for disease progression and for being targeted for treatment strategies may bring new possibilities for patients

Further developing innovative models, described in this thesis, is possible through several different paths, all of which have their own forests and mountains to conquer. Recapitulating physiological ECM composition in (alveolar) organoid cultures derived from primary human cells remains still challenging, even with the use of lung ECM-derived hydrogels. The same hydrogels also have limitations in capturing the complex biomechanical nature of native tissue; specifically, stress relaxation behavior of the tissue is currently missing in lung ECM-derived hydrogels. Lastly, introducing perfusion and breathing dynamics to these *in vitro* models also needs more attention, as the primary function of lungs is providing gas exchange through intricate blood vessels surrounding alveolar structure. Together with the recent encouraging changes in the legislations with respect to *in vitro* studies being considered enough for taking pre-clinical studies to clinical trials [53], future opportunities for using such models can only go further.

CLOSING REMARKS

"Not all those who wander are lost." – J.R.R. Tolkien.

Understanding the complex interactions between the dynamic ECM and resident cells in lung fibrosis is the essence of understanding the disease mechanisms. Even though there still remains a whole different world of possibilities to discover, it is now high time to wander along the edges of knowledge. Only through these steps, we can hope to first uncloud, then conquer the whole realm of influence of ECM in lung fibrosis, which *rules them all.*

REFERENCES

1. Lederer DJ, Martinez FJ. Idiopathic Pulmonary Fibrosis. *N Engl J Med* 2018: 378(19): 1811-1823.
2. Martinez FJ, Collard HR, Pardo A, Raghu G, Richeldi L, Selman M, Swigris JJ, Taniguchi H, Wells AU. Idiopathic pulmonary fibrosis. *Nat Rev Dis Primers* 2017: 3(1): 17074.
3. Burgess JK, Mauad T, Tjin G, Karlsson JC, Westergren-Thorsson G. The extracellular matrix - the under-recognized element in lung disease? *J Pathol* 2016: 240(4): 397-409.
4. Burgstaller G, Oehrle B, Gerckens M, White ES, Schiller HB, Eickelberg O. The instructive extracellular matrix of the lung: basic composition and alterations in chronic lung disease. *Eur Respir J* 2017: 50(1).
5. Burgess JK, Harmsen MC. Chronic lung diseases: entangled in extracellular matrix. *Eur Respir Rev* 2022: 31(163): 210202.
6. Organ LA, Duggan A-MR, Oballa E, Taggart SC, Simpson JK, Kang'Ombe AR, Braybrooke R, Molyneaux PL, North B, Karkera Y, Leeming DJ, Karsdal MA, Nanthakumar CB, Fahy WA, Marshall RP, Jenkins RG, Maher TM. Biomarkers of collagen synthesis predict progression in the PROFILE idiopathic pulmonary fibrosis cohort. *Respir Res* 2019: 20(1).
7. Jessen H, Hoyer N, Prior TS, Frederiksen P, Karsdal MA, Leeming DJ, Bendstrup E, Sand JMB, Shaker SB. Turnover of type I and III collagen predicts progression of idiopathic pulmonary fibrosis. *Respir Res* 2021: 22(1): 205.
8. Tjin G, White ES, Faiz A, Sicard D, Tschumperlin DJ, Mahar A, Kable EPW, Burgess JK. Lysyl oxidases regulate fibrillar collagen remodelling in idiopathic pulmonary fibrosis. *Dis Model Mech* 2017: 10(11): 1301-1312.
9. Philp CJ, Siebeke I, Clements D, Miller S, Habgood A, John AE, Navaratnam V, Hubbard RB, Jenkins G, Johnson SR. Extracellular Matrix Cross-Linking Enhances Fibroblast Growth and Protects against Matrix Proteolysis in Lung Fibrosis. *Am J Respir Cell Mol Biol* 2018: 58(5): 594-603.
10. Onursal C, Dick E, Angelidis I, Schiller HB, Staab-Weijnitz CA. Collagen Biosynthesis, Processing, and Maturation in Lung Ageing. *Frontiers in Medicine* 2021: 8.
11. Karsdal MA, Nielsen SH, Leeming DJ, Langholm LL, Nielsen MJ, Manon-Jensen T, Siebuhr A, Gudmann NS, Ronnow S, Sand JM, Daniels SJ, Mortensen JH, Schuppan D. The good and the bad collagens of fibrosis - Their role in signaling and organ function. *Adv Drug Deliv Rev* 2017: 121: 43-56.
12. Hoffman ET, Uhl FE, Asarian L, Deng B, Becker C, Uriarte JJ, Downs I, Young B, Weiss DJ. Regional and disease specific human lung extracellular matrix composition. *Biomaterials* 2023: 293: 121960.
13. Booth AJ, Hadley R, Cornett AM, Dreffs AA, Matthes SA, Tsui JL, Weiss K, Horowitz JC, Fiore VF, Barker TH, Moore BB, Martinez FJ, Niklason LE, White ES. Acellular normal and fibrotic human lung matrices as a culture system for in vitro investigation. *Am J Respir Crit Care Med* 2012: 186(9): 866-876.

14. Miles T, Hoyne GF, Knight DA, Fear MW, Mutsaers SE, Prêle CM. The contribution of animal models to understanding the role of the immune system in human idiopathic pulmonary fibrosis. *Clinical & Translational Immunology* 2020: 9(7).

15. Kolb P, Upagupta C, Vierhout M, Ayaub E, Bellaye PS, Gauldie J, Shimbori C, Inman M, Ask K, Kolb MRJ. The importance of interventional timing in the bleomycin model of pulmonary fibrosis. *Eur Respir J* 2020: 55(6): 1901105.

16. Meiners S, Lehmann M. Senescent Cells in IPF: Locked in Repair? *Frontiers in Medicine* 2020: 7.

17. Herrera J, Henke CA, Bitterman PB. Extracellular matrix as a driver of progressive fibrosis. *J Clin Invest* 2018: 128(1): 45–53.

18. Habermann AC, Gutierrez AJ, Bui LT, Yahn SL, Winters NI, Calvi CL, Peter L, Chung MI, Taylor CJ, Jetter C, Raju L, Roberson J, Ding G, Wood L, Sucre JMS, Richmond BW, Serezani AP, McDonnell WJ, Mallal SB, Bacchetta MJ, Loyd JE, Shaver CM, Ware LB, Bremner R, Walia R, Blackwell TS, Banovich NE, Kropski JA. Single-cell RNA sequencing reveals profibrotic roles of distinct epithelial and mesenchymal lineages in pulmonary fibrosis. *Sci Adv* 2020: 6(28): eaba1972.

19. Liu X, Dai K, Zhang X, Huang G, Lynn H, Rabata A, Liang J, Noble PW, Jiang D. Multiple Fibroblast Subtypes Contribute to Matrix Deposition in Pulmonary Fibrosis. *Am J Respir Cell Mol Biol* 2023: 0(ja): null.

20. Adams TS, Schupp JC, Poli S, Ayaub EA, Neumark N, Ahangari F, Chu SG, Raby BA, DeIuliis G, Januszyk M, Duan Q, Arnett HA, Siddiqui A, Washko GR, Homer R, Yan X, Rosas IO, Kaminski N. Single-cell RNA-seq reveals ectopic and aberrant lung-resident cell populations in idiopathic pulmonary fibrosis. *Sci Adv* 2020: 6(28): eaba1983.

21. Moss BJ, Ryter SW, Rosas IO. Pathogenic Mechanisms Underlying Idiopathic Pulmonary Fibrosis. *Annu Rev Pathol* 2022: 17(1): 515–546.

22. Morse C, Tabib T, Sembrat J, Buschur KL, Bittar HT, Valenzi E, Jiang Y, Kass DJ, Gibson K, Chen W, Mora A, Benos PV, Rojas M, Lafyatis R. Proliferating SPP1/MERTK-expressing macrophages in idiopathic pulmonary fibrosis. *Eur Respir J* 2019: 54(2): 1802441–1802441.

23. Caliari SR, Burdick JA. A practical guide to hydrogels for cell culture. *Nat Methods* 2016: 13(5): 405–414.

24. de Hilster RHJ, Sharma PK, Jonker MR, White ES, Gercama EA, Roobeek M, Timens W, Harmsen MC, Hylkema MN, Burgess JK. Human lung extracellular matrix hydrogels resemble the stiffness and viscoelasticity of native lung tissue. *Am J Physiol Lung Cell Mol Physiol* 2020: 318(4): L698–L704.

25. Saldin LT, Cramer MC, Velankar SS, White LJ, Badylak SF. Extracellular matrix hydrogels from decellularized tissues: Structure and function. *Acta Biomater* 2017: 49: 1–15.

26. Asano S, Ito S, Takahashi K, Furuya K, Kondo M, Sokabe M, Hasegawa Y. Matrix stiffness regulates migration of human lung fibroblasts. *Physiol Rep* 2017: 5(9).

27. Blokland KEC, Nizamoglu M, Habibie H, Borghuis T, Schuliga M, Melgert BN, Knight DA, Brandsma CA, Pouwels SD, Burgess JK. Substrate stiffness engineered to replicate disease conditions influence senescence and fibrotic responses in primary lung fibroblasts. *Front Pharmacol* 2022: 13: 989169.

28. Swift J, Ivanovska IL, Buxboim A, Harada T, Dingal PC, Pinter J, Pajerowski JD, Spinler KR, Shin JW, Tewari M, Rehfeldt F, Speicher DW, Discher DE. Nuclear lamin-A scales with tissue stiffness and enhances matrix-directed differentiation. *Science* 2013: 341(6149): 1240104.

29. Liu F, Mih JD, Shea BS, Kho AT, Sharif AS, Tager AM, Tschumperlin DJ. Feedback amplification of fibrosis through matrix stiffening and COX-2 suppression. *J Cell Biol* 2010: 190(4): 693-706.

30. Kim H, Kang B, Cui X, Lee SH, Lee K, Cho DW, Hwang W, Woodfield TB, Lim KS, Jang J. Light-Activated Decellularized Extracellular Matrix-Based Bioinks for Volumetric Tissue Analogs at the Centimeter Scale. *Advanced Functional Materials* 2021: 2011252.

31. Bjork JW, Johnson SL, Tranquillo RT. Ruthenium-catalyzed photo cross-linking of fibrin-based engineered tissue. *Biomaterials* 2011: 32(10): 2479-2488.

32. Sorushanova A, Delgado LM, Wu Z, Shologu N, Kshirsagar A, Raghunath R, Mullen AM, Bayon Y, Pandit A, Raghunath M, Zeugolis DI. The Collagen Suprafamily: From Biosynthesis to Advanced Biomaterial Development. *Adv Mater* 2019: 31(1): e1801651.

33. Kozlowski MT, Crook CJ, Ku HT. Towards organoid culture without Matrigel. *Communications Biology* 2021: 4(1).

34. Parker MW, Rossi D, Peterson M, Smith K, Sikstrom K, White ES, Connett JE, Henke CA, Larsson O, Bitterman PB. Fibrotic extracellular matrix activates a profibrotic positive feedback loop. *J Clin Invest* 2014: 124(4): 1622-1635.

35. Prakash YS, Tschumperlin DJ, Stenmark KR. Coming to terms with tissue engineering and regenerative medicine in the lung. *American Journal of Physiology-Lung Cellular and Molecular Physiology* 2015: 309(7): L625-L638.

36. Carragher N, Piccinini F, Tesei A, Jr OJT, Bickle M, Horvath P. Concerns, challenges and promises of high-content analysis of 3D cellular models. *Nature Reviews Drug Discovery* 2018: 17(8): 606-606.

37. Shakir S, Hackett TL, Mostaço-Guidolin LB. Bioengineering lungs: An overview of current methods, requirements, and challenges for constructing scaffolds. *Frontiers in Bioengineering and Biotechnology* 2022: 10.

38. Seo BR, Chen X, Ling L, Song YH, Shimpi AA, Choi S, Gonzalez J, Sapudom J, Wang K, Andresen Eguiluz RC, Gourdon D, Shenoy VB, Fischbach C. Collagen microarchitecture mechanically controls myofibroblast differentiation. *Proc Natl Acad Sci U S A* 2020: 117(21): 11387-11398.

39. Davidson CD, Jayco DKP, Matera DL, DePalma SJ, Hiraki HL, Wang WY, Baker BM. Myofibroblast activation in synthetic fibrous matrices composed of dextran vinyl sulfone. *Acta Biomater* 2020: 105: 78-86.

40. Matera DL, DiLillo KM, Smith MR, Davidson CD, Parikh R, Said M, Wilke CA, Lombaert IM, Arnold KB, Moore BB, Baker BM. Microengineered 3D pulmonary interstitial mimetics highlight a critical role for matrix degradation in myofibroblast differentiation. *Sci Adv* 2020: 6(37).

41. Matera DL, Wang WY, Smith MR, Shikanov A, Baker BM. Fiber Density Modulates Cell Spreading in 3D Interstitial Matrix Mimetics. *ACS Biomater Sci Eng* 2019: 5(6): 2965-2975.

42. Baker BM, Trappmann B, Wang WY, Sakar MS, Kim IL, Shenoy VB, Burdick JA, Chen CS. Cell-mediated fibre recruitment drives extracellular matrix mechanosensing in engineered fibrillar microenvironments. *Nat Mater* 2015: 14(12): 1262-1268.

43. Joshi N, Watanabe S, Verma R, Jablonski RP, Chen CI, Cheresh P, Markov NS, Reyfman PA, McQuattie-Pimentel AC, Sichizya L, Lu Z, Piseaux-Aillon R, Kirchenbuechler D, Flozak AS, Gottardi CJ, Cuda CM, Perlman H, Jain M, Kamp DW, Budinger GRS, Misharin AV. A spatially restricted fibrotic niche in pulmonary fibrosis is sustained by M-CSF/M-CSFR signalling in monocyte-derived alveolar macrophages. *Eur Respir J* 2020: 55(1).

44. Reyfman PA, Walter JM, Joshi N, Anekalla KR, McQuattie-Pimentel AC, Chiu S, Fernandez R, Akbarpour M, Chen CI, Ren Z, Verma R, Abdala-Valencia H, Nam K, Chi M, Han S, Gonzalez-Gonzalez FJ, Soberanes S, Watanabe S, Williams KJN, Flozak AS, Nicholson TT, Morgan VK, Winter DR, Hinchcliff M, Hrusch CL, Guzy RD, Bonham CA, Sperling AI, Bag R, Hamanaka RB, Mutlu GM, Yeldandi AV, Marshall SA, Shilatifard A, Amaral LAN, Perlman H, Sznajder JI, Argento AC, Gillespie CT, Dematte J, Jain M, Singer BD, Ridge KM, Lam AP, Bharat A, Bhorade SM, Gottardi CJ, Budinger GRS, Misharin AV. Single-Cell Transcriptomic Analysis of Human Lung Provides Insights into the Pathobiology of Pulmonary Fibrosis. *Am J Respir Crit Care Med* 2019: 199(12): 1517-1536.

45. Travaglini KJ, Nabhan AN, Penland L, Sinha R, Gillich A, Sit RV, Chang S, Conley SD, Mori Y, Seita J, Berry GJ, Shrager JB, Metzger RJ, Kuo CS, Neff N, Weissman IL, Quake SR, Krasnow MA. A molecular cell atlas of the human lung from single-cell RNA sequencing. *Nature* 2020: 587(7835): 619-625.

46. Tsukui T, Sun KH, Wetter JB, Wilson-Kanamori JR, Hazelwood LA, Henderson NC, Adams TS, Schupp JC, Poli SD, Rosas IO, Kaminski N, Matthay MA, Wolters PJ, Sheppard D. Collagen-producing lung cell atlas identifies multiple subsets with distinct localization and relevance to fibrosis. *Nat Commun* 2020: 11(1): 1920.

47. Mcdonough JE, Ahangari F, Li Q, Jain S, Verleden SE, Herazo-Maya J, Vukmirovic M, Deiuliis G, Tzouvelekis A, Tanabe N, Chu F, Yan X, Verschakelen J, Homer RJ, Manatakis DV, Zhang J, Ding J, Maes K, De Sadeleer L, Vos R, Neyrinck A, Benos PV, Bar-Joseph Z, Tantin D, Hogg JC, Vanaudenaerde BM, Wuyts WA, Kaminski N. Transcriptional regulatory model of fibrosis progression in the human lung. *JCI Insight* 2019: 4(22).

48. Sikkema L, Strobl D, Zappia L, Madissoon E, Markov N, Zaragosi L, Ansari M, Arguel M, Apperloo L, Bécavin C, Berg M, Chichelnitskiy E, Chung M, Collin A, Gay A, Hooshiar Kashani B, Jain M, Kapellos T, Kole T, Mayr C, von Papen M, Peter L, Ramírez-Suástegui C, Schniering J, Taylor C, Walzthoeni T, Xu C, Bui L, de Donno C, Dony L, Guo M, Gutierrez A, Heumos L, Huang N, Ibarra I, Jackson N, Kadur Lakshminarasimha Murthy P, Lotfollahi M, Tabib T, Talavera-Lopez C, Travaglini K, Wilbrey-Clark A, Worlock K, Yoshida M, Desai T, Eickelberg O, Falk C, Kaminski N, Krasnow M, Lafyatis R, Nikolíc M, Powell J, Rajagopal J, Rozenblatt-Rosen O, Seibold M, Sheppard D, Shepherd D, Teichmann S, Tsankov A, Whitsett J, Xu Y, Banovich N, Barbry P, Duong T, Meyer K, Kropski J, Pe'er D, Schiller H, Tata P, Schultze J, Misharin A, Nawijn M, Luecken M, Theis F. An integrated cell atlas of the human lung in health and disease. *bioRxiv* 2022: 2022.2003.2010.483747.

49. Wijsman PC, van Smoorenburg LH, de Bruin DM, Annema JT, Kerstjens HAM, Mets OM, van den Berge M, Bonta PI, Burgess JK. Imaging the pulmonary extracellular matrix. *Current Opinion in Physiology* 2021: 22: 100444.

50. Huang Q, Garrett A, Bose S, Blocker S, Rios AC, Clevers H, Shen X. The frontier of live tissue imaging across space and time. *Cell Stem Cell* 2021: 28(4): 603-622.

51. Yoon S, Cheon SY, Park S, Lee D, Lee Y, Han S, Kim M, Koo H. Recent advances in optical imaging through deep tissue: imaging probes and techniques. *Biomaterials Research* 2022: 26(1).

52. Jailkhani N, Ingram JR, Rashidian M, Rickelt S, Tian C, Mak H, Jiang Z, Ploegh HL, Hynes RO. Noninvasive imaging of tumor progression, metastasis, and fibrosis using a nanobody targeting the extracellular matrix. *Proceedings of the National Academy of Sciences* 2019: 116(28): 14181-14190.

53. 117th Congress (2021-2022). *S.5002 - FDA Modernization Act 2.0*. 2022. https://www.congress.gov/bill/117th-congress/senate-bill/5002.

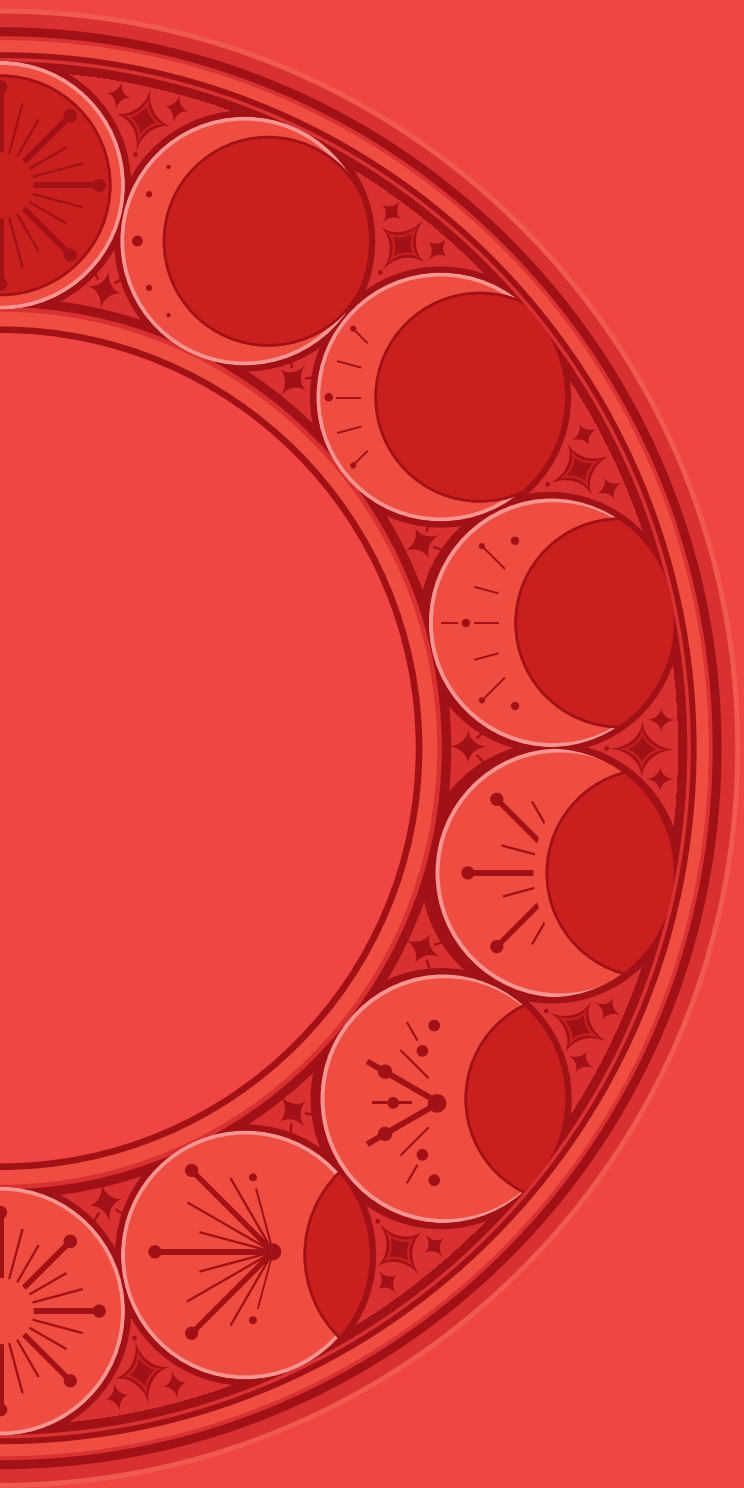

APPENDICES

ENGLISH SUMMARY

Lung fibrosis includes a group of devastating rare diseases with poor prognosis and very low survival rates. Among these, idiopathic pulmonary fibrosis (IPF) is the most common form although its origin is poorly understood. Deposition of the excessive extracellular matrix (ECM) by the recruited (myo)fibroblasts due to an abnormal wound repair mechanism originating from the epithelial cells is currently thought to be central theme of the disease. This fibrotic ECM can exert its influence through its aberrant composition, altered biomechanics or disorganized fibers to guide cells towards abnormal behavior. Therefore, this thesis aimed to investigate the interactions between the fibrotic ECM and the cells in the context of the perpetuation of the (pro-)fibrotic responses.

Chapter 2 outlines the changes in lung ECM in lung fibrosis with respect to its biochemical and biomechanical properties as well as topography. After summarizing how resident cell-driven pro-fibrotic responses can be caused by different properties of the fibrotic ECM, an updated landscape of the involvement of ECM-degrading enzymes and degradation products from ECM proteins is also given. Building on this knowledge, **Chapter 3** explored how one of the less well-investigated collagens, collagen type XIV, is involved in IPF. While it was known that collagen type XIV, supports collagen fibril organization, its status with respect to its amount and localization was not demonstrated before. Transcriptomics analysis on publicly available datasets revealed an increase in *COL14A1* gene, which codes the collagen type XIV protein, in fibroblasts and myofibroblasts. When the stained sections of IPF lungs were analyzed digitally, a lower proportional area for collagen type XIV was found for both whole tissue and specific tissue compartments such as airway wall or parenchyma. These consistently lower proportions of collagen type XIV may have implications for the assembly of the ECM fibers which may contribute to progression of fibrosis.

The importance of different methods of recreating lung microenvironment in three-dimensional (3D) composes of the main message of **Chapter 4**, in which different state-of-the-art *in vitro* models were discussed with respect to their advantages, disadvantages and challenges associated with them. These model systems, namely precision cut lung slices, lung organoids, (cell-seeded) lung ECM-derived hydrogels and lung-on-chip systems, provide exciting opportunities to mimic lung *in vitro*. **Chapter 5** includes one of such models, lung organoids, to explore the regenerative responses of the epithelial cells isolated from lungs of patients with IPF. Comparison of the number and the size of organoids formed by the epithelial cells in the presence

of stromal cells to those formed by epithelial cells alone revealed. These results highlight that the epithelial cells may not be intrinsically defected in IPF, but the negative influence of stromal cells isolated from the fibrotic ECM may be influencing their regenerative capacity in the lungs of patients with IPF.

An important aspect of *in vitro* models is the inclusion of an ECM-mimicking substance. As lung ECM is vital for its functions, these models are required to have proper materials for mimicking the complex composition and/or architecture of lung tissue. **Chapter 6** demonstrates utilization of different materials for *in vitro* models in the context of lung health and disease. The recent advances using such models were summarized as well as the challenges related to using models of different composition and complexity. **Chapter 7** builds on the foundation of **Chapter 6** and provides a perspective to lung ECM-derived hydrogels as an advanced and innovative tool for mimicking lung microenvironment. These hydrogels are derived from the native lung ECM, retains most of the complex biochemical composition and resembles the mechanical properties of the source tissue.

Chapter 8 demonstrates one of the examples for advancing the mimicking capacity of lung ECM-derived hydrogels described in **Chapters 4, 6 and 7**. While mechanical properties were historically determined by the concentration and the composition of the ECM powder, applying external fiber crosslinking to these hydrogels through a UV/visible range light-triggered reaction revealed that stiffer hydrogels could be produced without altering the biochemical composition. This method, namely Ruthenium crosslinking, was also shown to leave no cytotoxicity in the hydrogels. Increased stiffness, accompanied by altered fiber organization, triggered myofibroblast differentiation in the fibroblasts seeded on top of the crosslinked hydrogels when compared to the untouched hydrogels. This methodology provided a new and cell-friendly manner to alter mechanical properties of the ECM-derived hydrogels for mimicking diseased lung microenvironment *in vitro*. Another illustration of employing lung ECM-derived hydrogels for advanced *in vitro* modeling was done in **Chapter 9**. Hydrogels derived from the decellularized ECM of lungs of IPF and non-IPF donors were seeded with fibroblasts derived from either IPF or non-IPF lungs in a combinatorial manner. While these remodeling responses did not include a detectable change in collagen or glycosaminoglycan content in the hydrogels, collagen fiber organization and mechanical properties of the hydrogels were drastically altered by the fibroblasts seeded in IPF hydrogels due to the instructions provided by the fibrotic ECM, which results in a more pro-fibrotic microenvironment altogether. By characterizing the responses of both types of fibroblasts in both types of microenvironment and comparing the ECM remodeling responses of these

fibroblast to the existing differences between the IPF and non-IPF lung ECM-derived hydrogels, it was possible to show that both cell and microenvironment origin play a crucial role in determining the ECM remodeling responses of fibroblasts.

Overall, this thesis furthers our understanding on the complex cell:matrix interactions and demonstrates the overruling capacity of fibrotic ECM in the context of lung fibrosis either by providing new mechanisms by which fibrotic ECM acts or by providing innovative and advanced methodologies to recreate lung microenvironment *in vitro*.

NEDERLANDSE SAMENVATTING

Longfibrose omvat een groep zeldzame ziekten die zeer ernstig zijn met een slechte prognose en zeer lage overlevingspercentages, waarbij er littekenvorming (fibrose) plaatsvindt in de longblaasjes, die verantwoordelijk zijn voor de gaswisseling. Hiervan is idiopathische longfibrose (IPF) de meest voorkomende vorm, hoewel de oorsprong ervan slecht wordt begrepen. Schade aan de bekledende cellen van de longblaasjes (het epitheel) en een abnormaal wondherstelmechanisme wordt momenteel beschouwd als belangrijk onderliggend mechanisme van de ziekte. Hierbij vindt overmatige afzetting plaats van structurele eiwitvezels die de longcellen omgeven (extracellulaire matrix; ECM), zoals collageen. Dit gebeurt door een bepaald celtype in de longen die betrokken is bij weefsel herstel, de (myo)fibroblast, als gevolg van een abnormaal wondherstelmechanisme. Deze overmatige, fibrotische ECM kan invloed uitoefenen op cellen door een afwijkende samenstelling, veranderde mechanische effecten op de cellen en/of ongeorganiseerde vezels, wat kan leiden tot abnormaal gedrag van de cellen. Daarom was dit proefschrift gericht op het onderzoeken van wisselwerking tussen fibrotische ECM en cellen in de context van fibrose.

Hoofdstuk 2 schetst de veranderingen in long-ECM tijdens longfibrose en de specifieke impact ervan op de functie en gedrag van cellen die van nature in de long aanwezig zijn, zoals epitheelcellen, fibroblasten en lokale immuuncellen. Het is nu algemeen geaccepteerd dat de afwijkende samenstelling van ECM met ongeorganiseerde vezels en verstijving bij fibrose cellen instrueert tot pro-fibrotisch gedrag. Daarnaast voegen de veranderde mechanistische effecten op de cellen (biomechanica) en topografie van de long-ECM tijdens longfibrose extra dimensies toe aan het instructievermogen van long-ECM. Een belangrijk aspect in dit hoofdstuk is het bijgewerkte overzicht van ECM-afbrekende enzymen en afbraakproducten van ECM-eiwitten, en hun betrokkenheid bij de progressie van de fibrotische respons. In **Hoofdstuk 3** is onderzocht hoe collageen type XIV, een van de minder bestudeerde collageentypes, tot expressie wordt gebracht in IPF. Hoewel bekend was dat collageen type XIV de organisatie van collageenvezels ondersteunt, was de expressie ervan met betrekking tot de hoeveelheid en lokalisatie niet bekend bij IPF. Beschikbare datasets met analyses omtrent de afschrijving van het erfelijke materiaal, leidend tot de aanmaak van het eiwit onthulden een toename van de expressie van het COL14A1-gen, dat codeert voor collageen type XIV-eiwit, in fibroblasten en myofibroblasten. In IPF-longen zelf werd proportioneel minder collageen type XIV gevonden in IPF voor zowel de hele long als specifieke weefselcompartimenten zoals de luchtwegwand of het parenchym. Deze lagere hoeveelheden collageen type XIV kunnen implicaties

hebben voor het aan elkaar hechten van de ECM-vezels, wat kan bijdragen aan de progressie van fibrose bij IPF.

Het belang van verschillende methoden om de micro-omgeving van de long drie dimensionaal (3D) na te bootsen, vormt de hoofdboodschap van **Hoofdstuk 4**, waarin verschillende state-of-the-art kweekmodellen (*in vitro* modellen) worden besproken met betrekking tot hun voordelen, nadelen en uitdagingen. Deze modelsystemen, namelijk longplakjes, longorganoïden (mini-longetjes in een petrischaal), long-ECM-afgeleide hydrogels en lung-on-chip-systemen, bieden mogelijkheden om de micro-omgeving van de longen *in vitro* na te bootsen. Hoewel er verschillende uitdagingen moeten worden overwonnen vanwege de menselijke oorsprong van deze modellen, kan het vertaalvermogen van *in vitro*-onderzoek voor preklinisch longonderzoek aanzienlijk worden verbeterd door de bestaande modellen te verbeteren, nieuwe en innovatieve alternatieven te ontwikkelen en creatieve combinaties van deze systemen te onderzoeken.

Hoofdstuk 5 omschrijft onderzoek met een van de 3D-modellen, namelijk longorganoïden, om de regeneratie van de epitheelcellen te onderzoeken. Primaire longblaas (alveolaire) epitheelcellen, geïsoleerd uit menselijke IPF longen en ondersteund door mesenchymale fibroblasten, kunnen uitgroeien tot organoïden wanneer ze worden ingebed in een hydrogel die de omgeving in de long nabootst. Vergelijking van het aantal en de grootte van organoïden gevormd door de epitheelcellen in de aan-en afwezigheid van lokale cellen uit de micro-omgeving (de stroma) onthulde de belangrijke invloed van de stromacellen bij de vorming van organoïden en liet ook zien dat deze wisselwerking tussen alveolair epitheel en de stromacellen verstoord is bij IPF. Deze resultaten benadrukken dat de epitheelcellen mogelijk niet intrinsiek defect zijn bij IPF, maar dat de regeneratie-ondersteunende capaciteit van stromacellen in de longen van patiënten met IPF mogelijk verstoord is.

Een belangrijk aspect in nieuwe *in vitro*-modellen is de aanwezigheid van een ECM-nabootsende stof. Aangezien long-ECM van vitaal belang is voor de reguliere functies van de longen, hebben deze modellen geschikte materialen nodig om de complexe samenstelling en/of architectuur van longweefsel na te bootsen. **Hoofdstuk 6** demonstreert het gebruik van verschillende materialen voor *in vitro* modellen in de context van longgezondheid en -ziekte. ECM-afgeleide eiwitten, zoals collageen of gelatine, zijn al herhaaldelijk gebruikt als een ECM-nabootsende substantie in *in vitro* modellen. In de afgelopen twee decennia heeft het veld echter een transformatie doorgemaakt naar een meer accurate weergave van de micro-omgeving van de longen, hetzij door gebruik te maken van longweefsel zonder cellen

of hydrogels gemaakt van dit natuurlijk longweefsel dat was ontdaan van zijn cellen (long-ECM). In dit hoofdstuk wordenbirecente ontwikkelingen met betrekking tot dergelijke modellen samengevat, evenals de uitdagingen die gepaard gaan met het gebruik van modellen met een verschillende samenstelling en complexiteit. **Hoofdstuk 7** bouwt voort op de basis van **Hoofdstuk 6** en geeft het perspectief van long-ECM-afgeleide hydrogels als een geavanceerd en innovatief hulpmiddel voor het nabootsen van de micro-omgeving van de longen. Deze hydrogels die zijn afkomstig van natuurlijke long-ECM, en behouden het grootste deel van de complexe biochemische samenstelling. Hiermee lijken deze hydrogels wat betreft de mechanische eigenschappen veel op het longweefsel waar ze van gemaakt zijn. Hoewel long-ECM-afgeleide hydrogels voordelig zijn in vergelijking met eenvoudigere hydrogels, zijn er verschillende uitdagingen, zoals het verlies van ECM-geassocieerde groeifactoren of beperkingen met betrekking tot 3D-beeldvorming. Het is duidelijk dat het maximale potentieel van deze hydrogels nog moet worden bereikt en alleen zal worden bereikt door in multidisciplinaire teams te werken.

Hoofdstuk 8 presenteert een van de voorbeelden voor het bevorderen van het nabootsingsvermogen van long-ECM afgeleide hydrogels beschreven in **Hoofdstukken 4**, **6** en **7**. Historisch gezien werden mechanische eigenschappen bepaald door de concentratie en samenstelling van een ECM-poeder. Door het toepassen van UV-licht kunnen ook stijvere hydrogels worden geproduceerd zonder de biochemische samenstelling te veranderen. Deze methode, namelijk verstijving door de stof ruthenium te gebruiken, bleek niet toxisch voor de cellen, zoals getest met humane longfibroblasten. Verhoogde stijfheid, vergezeld van veranderde vezelorganisatie, veroorzaakte de overgang van de fibroblasten die op deze cel groeiden naar myofibroblasten (verantwoordelijk voor fibrotische processen). De toegepaste methodologie in dit hoofdstuk bood een nieuwe en cel-vriendelijke manier om de mechanische eigenschappen van de ECM-afgeleide hydrogels te veranderen om *in vitro* een zieke longmicro-omgeving na te bootsen.

Een ander voorbeeld van het gebruik van long-ECM-afkomstige hydrogels voor geavanceerde *in vitro* modellering werd onderzocht in **Hoofdstuk 9**. De hydrogels van longen van IPF- en niet-IPF-donoren werden gebruik voor het kweken van fibroblasten uit IPF- of niet-IPF-longen. Hoewel deze cellen geen waarneembare verandering in het totale collageen- of glycosaminoglycaangehalte in de hydrogels veroorzaakten, werden de collageenvezelorganisatie en mechanische eigenschappen van de hydrogels drastisch veranderd door de fibroblasten die in IPF-hydrogels waren gezaaid. Door de reacties van beide soorten fibroblasten in beide soorten micro-omgevingen te karakteriseren en de ECM-structureringsreacties van deze

fibroblasten te vergelijken met de bestaande verschillen tussen de IPF en niet-IPF long-ECM-afgeleide hydrogels, was het mogelijk om aan te tonen dat zowel de cel- als micro-omgeving een cruciale rol spelen bij het aansturen van de ECM-herstructurering door fibroblasten.

Dit proefschrift heeft ons begrip van de complexe wisselwerking tussen cellen en de ECM bevorderd en toont aan dat de fibrotische ECM een overheersende rol heeft in het fibrotische proces. Nieuwe mechanismen zijn ontdekt waarmee de fibrotische ECM cellen beïnvloedt en er zijn ook innovatieve, geavanceerde technieken ontwikkeld om de micro-omgeving van de longen in vitro na te bootsen.

ACKNOWLEDGEMENTS

A heartfelt confession is quite ideal to start this chapter: I had a feeling, I was scared to write this chapter. Considering I have had the privilege of working in teams with amazing people for all the content in this book (and some more outside) and here I only have couple of (maybe ten?) pages, to fill only with words to be able to sufficiently express my gratitude to everyone contributed to my journey. I did know that this chapter would have to be the most difficult one as it is the one I have to write all by myself. What an amazing journey it was, and now I would like to at least attempt to express my gratitude to every colleague, mentor, friend and family of mine.

"There and back again..." *– J. R. R. Tolkien.*

I would like to start with my supervision team, who started this journey with me, who taught me and allowed me to see different directions towards which I could grow even more. Having four strong personalities in one room every week Tuesday at 15:00 wasn't easy at times, but we managed to look past differences and built a strong team spirit, creating a positive and harmonious atmosphere for our collaborative efforts. And ultimately, it was this unique combination of you three and me that delivered our projects as you each showed me something only you can teach.

Dear **Janette**, I am overwhelmingly grateful to have met you and join your team back in 2018. I did not know what I was getting in as just a Master's student, certainly didn't have any long term plans to stick around – if only if that man could see now! Every time I knocked your door, every time I heard your voice saying "Come in!", I felt welcomed, I felt appreciated and I felt respected. I want to thank you for creating and sustaining such a positive environment for my personal and professional development. Since the beginning, you have set an amazing example and a role model for me, both with your words and your actions. I can only hope and trust that I have been able to appreciate all the opportunities you provided by having stepped up to the challenges and shown you that I could handle it. Maybe I couldn't then but I now can, thanks to you.

Dear **Irene**, I still vividly remember the day I met you in my first EXPIRE group meeting. It was my first time joining that meeting, and I did not know you beforehand. I remember feeling impressed in that first time, and I have developed a great deal of respect during all of our interactions over the years. You set a great example of how a professor can be dedicated to their work but also still stayed connected to the team. Your strong approach for how a scientific project needs to be organized from the initiation to the execution taught me I should place my milestones and

research questions, in advance and perhaps on paper. When the team faced with challenges and setbacks regarding the project, your steadfast belief in me and your willingness to offer guidance and encouragement have provided an additional source of motivation.

Dear **Barbro**, I'd like to start by thanking you for your very calm approach to everything we have done together. Thanks to your calmness, I have got to learn to relax a tiny bit more when things are not going in the direction I originally intended for them to go. I am also grateful for how approachable you were, especially when you once said "Just call me", instead of arranging another online meeting or so. It inevitably and ultimately made me realize that, some things don't have to be complicated for them to work out, so thank you for that. Over the years, not only I have enjoyed every conversation with you regardless of the topic, but also I often found myself being impressed by how effortlessly you can convey your thoughts to me or anyone else. I hope I will be able to follow your example to be able to a good communicator.

I would like to thank to my thesis assessment committee members, **Prof. R.A. Bank**, **Prof. G. Westergren-Thorsson** and **Prof. M. Kolb**, thank you for your valuable time and efforts you've put into this thesis through your suggestions and feedback.

I also would like to thank to couple of additional professors with whom we crossed paths during my PhD trajectory. Dear Prof. **Marco Harmsen**, a long time has passed since I joined to the (then) little 3D meeting group where I met you, and I cannot remember any chat we had that was dull. We sometimes agreed and sometimes agreed to disagree in a friendly way but it always ended being productive. Thank you Marco for always keeping me on my toes with our scientific sword fights! Dear Prof. **Wim Timens**, I'd like to thank you not only for sharing your endless knowledge about the lung diseases with us but also your extreme efforts to optimize the protocol for fibrotic tissue distribution. I always appreciated your feedback on my manuscripts we wrote together and always learned something new in every exchange. Dear Prof. **Daniel Weiss** – Dan, thank you for a warm welcome and including me in your nice group for the last couple of months of my PhD. I am truly happy and grateful for the opportunity to collaborate with you and your team, and I have really enjoyed discussing science with you.

As a 2+2 industrial PhD candidate, our collaboration with Boehringer Ingelheim (both Biberach and Ridgefield campuses) was quite important and fruitful. I would like to start by thanking to Prof. **Matthew Thomas** for always being supportive and enthusiastic about our project(s) since the initiation 4 years ago. Another big "thank

you" would have to go to Prof. **Eric White**, not only for kindly providing precious human donor samples but also giving critical and crucial feedback on how to improve our messages, even about the most challenging analyses. Dear **Marco**, although you have stepped out of the collaboration rather shortly after the start, I genuinely enjoyed the initial phases of the project where we brainstormed to improve the project. Dear **Karim**, I always appreciated your supportive and approachable attitude towards our collaboration. I also would like to thank the hands-on collaborators **Caro**, **Dani** and **Julia** for fruitful discussions on methodology and results. I'm looking forward to finalizing the studies we have started together. Moreover, I would like to thank to **Coralie** for her guidance towards optimizing the tissue dissociation protocol for fibrotic tissues (which seemed to have lasted for a century), to **Marina** and **Alex** for their kind invitation to the Ridgefield campus and a day full of immunohistochemical staining pilot experiments, to **Praveen** and **Fidel** for their help with data analysis, to **Alec**, **Diana** and **David** for their technical and logistical help.

It truly took a village to reach to this milestone, and this village would be none other than the Experimental Pulmonology and Inflammation Research (EXPIRE) Lab – partially because we are quite crowded! Dear **Martijn**, thank you for setting an amazing example for professors from Groningen when we met in Uppsala in 2017. The memory of you teaching me how to drink cognac and your advice on taking the provided challenges head on is vividly alive in my mind! Who would have known that only a year after that, I would be joining to the lab you co-lead with my two of my main supervisors?! I enjoyed our chats, whether it's about science or daily stuff, and I am happy that I got a chance to work in a scientific project with you. I'd like to continue expressing my gratitude with the current and past members of the "Tech Team". **Marnix,** thank you for everything, starting with your help when I first joined the lab as a Master's student and anything and everything that came after that! I was initially hesitant or even scared to approach you but your willingness to help and sense of humor were always there and I, for one, appreciated your support every day in lab! (Although I am still scared to see you angry!). **Taco,** what a roller coaster two years we had! You joined to the collaboration just when things were picking up pace and Godspeed we had! Thank you for all the cell culture and tissue processing days where we started before seeing the daylight. You have helped improving many aspects of the project and things wouldn't have been the same without you. **Marissa**, we had lots of fun in and out of the lab, didn't we? Thank you for sharing the pain of optimizing lots of protocols with me, but also thank you for being with me when we were walking in the middle of nowhere in rural parts of a small German town, in the middle of the night! **Theo**, or The Magician, as I would like to call you, thank you for always being kind to me (and to everyone else, I'm sure). Your kind attitude and

willing to help are two things I would like to take with me, I would also appreciate receiving your magical speed in taking care of stainings, imaging or image analysis, but I know that it's impossible to replace or replicate your years of experience and expertise. I also would like to thank to the rest of the team, not only for their support and help in day-to-day things but adding value to my journey: to **Jacobien**, for the guidance in the lab and most importantly for showing trust when needed; to **Djoke**, for not hesitating to go out of your way to help me and others; to **Ilse**, for your ever-positive attitude to brighten the day and all the giggles; to **Leonie**, for your expertise in single-cell sequencing and amazing baked goods (a unique combination!); to **Petra**, for your friendly chats.

Before moving on with the colleagues from EXPIRE lab, I would like to thank to my paranymphs **Roderick** and **Mugdha**, who were not only from the lab, but also very good friends along the road. Thank you both for your help and support in the last stages of my PhD, and I am very happy with you two joining me for my defense. **Roderick**, it's been a long journey from the days that you hated when I called you *senpai* to the days that you cheerfully responded to me saying that. You were my supervisor first, then a valued team member and then a good friend; at each step we took together I appreciated your help, support and friendship. Your mischievous and relaxed approach taught me to take things easy (sometimes!). Thank you for your amazing support in answering my endless questions at the initial stages of my PhD, going for thousands of coffee breaks and drinks and dinners and always being open and approachable no matter what. Once a part of GelBoyz, always a part of GelBoyz. **Mugdha,** or also more widely-known as **Mugdy**, look where we are now! I'm truly grateful to our friendship, started in the early stages of our PhDs. Next to our friendship, we had numerous chances to collaborate and I have learned a lot from you (even if I don't readily show this at times). Outside the lab we had lots of adventures together regardless whether it is enjoying cocktails on a rainy afternoon in Copenhagen or walking in the streets of Lisbon, hearing fado from every open door, or singing karaoke in Utrecht. Our passion towards desserts will always lead us to new bakeries or home-baked goods and good coffee, both of which are always accompanied by a chat filled with laughter. I also would like to thank you for initiating "Project Office Door", it contributed to our office spirit and made us all closer. I wish you both the best of luck for finalizing your theses, not that you guys need it!

Next, I would like to thank my PhD or post-doc colleagues among past and present colleagues from EXPIRE lab. Dear **Kaj**, my Australian mate from Apeldoorn, we had a great time together – both in and out of the lab. Whether it was making gels together or grabbing a drink outside, I appreciated your friendship a lot. Although I miss you

and your presence in the office, I'm so glad to see you happy in Australia and looking forward to seeing you again! Dear **Maunick**, look how much things have changed since we started (and since you left us to go to the US)! Now we are finishing together, and I am grateful to have you as a friend, colleague and office-mate during this journey. The second part of our long-waited collaboration arrived way too late to be part of either of our books, but I am still looking forward to doing great science together. Dear **Qing**, your kind and supportive approach to everyone else around you is admirable and I, for one, am grateful to your friendship during the last couple of years. I wish you the best of luck in the next chapter of your life! To the current members of *Project Office Door*, i.e. my office-mates: **Jelmer**, my first student! Thank you for your initial contribution to my PhD trajectory, even unbeknownst to you, you helped me see the importance of having a clear plan ready as early as three weeks in! I am happy to see you now as a fellow PhD candidate in the same office. Thank you for the chats with or without the science (but usually with coffee). **XinZi**, thank you for always being available for a chat when needed. Also I always appreciated you always being your true honest self - I still find it extremely refreshing. Last but not least - thank you for the continuous supply of snacks from China! **Akash** – the young blood in the office! Your hunger for knowledge (and also various types of cheese) is impressive! I want to thank you for keeping me (or usually the whole office) entertained, either laughing with or at you while always being kind and grounded. Dear **Ayla**, you and I have a weird match in our senses of humor, which brought us together through random chitchat online or in the office. Thank you for all the fun exchanges and holding the Metallica fort of the office with me! You are all wonderful and hardworking people - I wish you all guys the best of luck with the rest of your projects!

Moving on to the other members of EXPIRE lab: dear **Akshaya**, starting the PhD at the exact same time created a special bond between us! Your willingness to help and support your friends impressed me a lot and I am very happy to have spent these past 4 years together as fellow PhDs. I still do not regret forcing you to take the rides in the fair with me; quite the opposite I am looking forward to doing so in more occasions! Thank you for sharing your endless love for arepas, all the nice memories and the support when needed. Dear **Aurore**, we had lots of fun: from the work-from-Forum Wednesdays to sightseeing in Washington in the US. Our masterpiece photo from the bar in Utrecht is going to stay alive as a very fun memory for a very long time. Thank you for the fun times we had together! Dear **Brady**, I think the years passed since our GelBoyz days only helped our friendship to evolve and get better – from colleagues with friendly banter to friends with safe havens to share and shelter. Thank you for being authentically you, sharing your fun facts and completely random information – no matter how grumpy I might have looked, I enjoyed them. Dear **Yanzhe**, your

positive attitude towards everything you do is admirable and I felt your contagious energy whenever we encountered in the corridor. Thank you for brightening those days and being a great colleague! Dear **Nataliya**, thank you for your willingness to contribute to the team despite the challenging start you had during the major lockdown or going to and coming back from the US.

I also would like to thank to the rest of the EXPIRE team members from past and present: to **Dennis**, for bringing an interesting angle to many conversations we had in the coffee room; to **Maud**, for adding positivity and kindness to every room you are in; to **Gwenda**, for setting a good example of a hardworking and detailed-oriented scientist starting from my early days; to **Martin**, for your cheerful chats during lunches as well as your help and guidance in bioinformatics analyses; to **Marijn**, for converting our coffee breaks to a baking festival; to **Kingsley**, for your availability and support, despite our limited direct interaction after you moved to Canada; to **Daan**, for very good and on-point advices since the beginning of my trajectory and for being a good role model of successful young investigator; to **Laura**, for showing that checking in with people no matter what doesn't cost you anything; to **Merel**, for going out of your way to kindly help us; to **Mirjam**, for the help when I was a Master's student and in the initial stages of my PhD; to **Sjoers** and **Lei**, for the nice chats in the last couple of months. I wish you all best of luck in finalizing your projects, whether it's a PhD or a post-doc project.

To my students over the last four years: **Jelmer** (again), **Hilde** & **Adrianne**, **Rhode**, **Mallak** and **Frederique**. thank you for joining me long the road. Thanks to you, I discovered numerous ways to improve the scientist, mentor and colleague in me.

During the four years of my PhD trajectory, I have interacted with different groups and departments, which all helped me directly or indirectly to improve myself in various ways. In the **Lung Pathology** group: Dear **Machteld**, I would like start by thanking you for including me in your collaborative project on 3D bioprinting with Marco and Janette back when I was looking for a group to join in Groningen. Thanks to your initiative, I was introduced to the Lung Pathology and EXPIRE teams. I would also like to thank you for your feedback and suggestions on our projects during the group meetings. Dear **Corry-Anke**, I would like to thank you for all of your input in different projects over the years. Whether you were directly involved in the projects or not, your constructive criticism helped us improve our projects. Dear **Roy**, thank you for nice and fruitful scientific chats as well as for always willing to help. Dear **Marjan** and **Wierd**, thank you for your kind help over the years with whatever random question I had to ask. Thanks to your immense efforts, some of the studies containing

precious patient samples were possible to be completed. Dear **Niek**, thank you for your ever-positive attitude and interesting questions during the meetings. Dear **Rhode**, it's so nice to see you as a PhD candidate in the group now, and thank you for your amazing work on the image analysis you did during your internship with us. To the other previous and current members of the Lung Pathology group, thank you for your input in the meetings and providing a safe scientific environment for everyone.

I also would like to thank my past and present colleagues from the **Medical Biology** section of the department of Pathology and Medical Biology. **Francisco**, we always worked on similar topics and having scientific chats in the 3D Meeting was always fun with you, it's a shame that we never got to collaborate. Thanks for everything! **Jolien**, your dedication and time management skills impressed and inspired me! Thank you for the nice chats in the office and showing me the fact that a 9-5 PhD would still work (or 8-4 in your case!)! **Fenghua**, you are very hard-working and eager to learn more, thank you for your contribution in the Ruthenium paper and looking forward to continuing to collaborate. Other past and current members of the X, Z and U labs: **Meng**, **Linda**, **Vasilena**, **Guido**, **Josee**, **Pytrick**, **Marja**, **Peter**, **Matthijs B.**, **Anita N.**, **Anita M.**, **Timara**, **Bart**, **Rianne**, **Wendy**, **Sandra**, **Matthijs L.**, **Theo**, **Johan**, thank you for making the labs and the department a fun place to work! Moreover, I would like to extend my thanks to **Carolien**, **Johanna** and **Hans** as they have supported and me (and the whole department) in our endless paperwork, questions and problems.

My colleagues from the Weiss group in the University of Vermont in Burlington, Vermont, USA: **Bennett**, **Chika**, **Joy**, **Katina**, **Will** – thank you for showing me around in the lab and in the campus as well as nice chats and fun! I enjoyed my time in Burlington even more thanks to you, I wish you success in your careers moving forward.

The colleagues from the department of **Molecular Pharmacology**: dear **Rosa**, our PhD trajectories were quite alike both topic- and organization-wise. How nice that we could take this a step further and collaborate on two different projects to cross the paths! Despite the experiments and results being frustrating, thank you for your proactiveness and your help in these projects. Dear **Reinoud**, I'm grateful to the opportunities we had to interact and collaborate. I consider your kindness and humble attitude as a quite remarkable personality trait, which I will aim to take as an example. I also would like to thank to the other members of the department: **Shanshan**, **Habibie**, **Marina** and **Sophie** for their willingness to help both for the projects and for when I was (possibly) wandering around the department cluelessly.

I also would like to thank the members of **Groningen Research Institute of Asthma and COPD (GRIAC)**. Over the four years, I have a proud member of GRIAC and thanks to all the colleagues here, I had the opportunity to talk about my science to a broader scientific community as well as to contribute others' trajectories. Dear **Maaike**, I'd like to thank you for your efforts in providing a safe space for young investigators in the GRIAC YI meetings, and your help in initiating the poster reformatting focus group. Dear **Judith**, I cannot appreciate your willingness enough, whether it is to lend a hand in complicated statistical analyses as or to provide constructive feedback on how to make scientific stories accessible to everyone with different backgrounds. I also would like to extend my thanks to the GRIAC Poster Reformatting Focus Group: **Sharyn**, **Tatiana**, **Brady**, **Niek** and **Rhode** – it is very nice that our efforts realized a new and accessible poster format for our institute. To the past and present members of GRIAC, thank you for your input during the Young Investigator meetings.

From the Department of Biomedical Engineering, dear **Prashant**, I would like to thank you for your patience and extensive efforts regarding the mechanical analyses we performed in many different studies. It was very nice to collaborate with you. Dear **Patrick**, although we did not get to collaborate on a research project, you were involved in the macrophage–stroma interactions review and I would like to thank you for your feedback during that writing exercise.

Some of the friends who supported me throughout my PhD journey had little to do with the lab or the topics I worked on. I would like to thank **İdil** for the chats, chats about having coffee and never giving up on the idea of meeting soon again. Considering we lived in the same cities with same friend circles for 10+ years, I think us meeting this many times in the last couple of years is already a great success! It was nice to talk in my native language, once in a while. I wish you the best in finalizing your PhD too, and hope to see you more (this time for real!). **Erika** and **Alejandro**, my *Donderdag* trio. **Erika**, I still cannot believe that I am writing these lines for you, after our very rocky start years back. But we have learned from mistakes, learned how to look past the disagreements and discovered how alike we are in the end. Thank you for your continuous and unconditional cheering in the last couple of years, I really appreciated it. Hoping to see you was the reason most of the time I aimlessly passed the door between the X lab and U lab. **Alejandro** (Alex!), every time we met for coffee or drinks, your care and genuine interest in others amazed me! I am so happy to have our friendship and know that we can be there for each other for both bad and good days. Thank you both for making Thursday evenings great, when we didn't have to postpone it to Fridays or Wednesdays!

Parts of the scientific output I have generated ended up as the chapters in this thesis; however, some of them did not. Still, this did not take anything away from my gratitude to each and every co-author with whom I have had chance to work with on different manuscripts. I would like to thank **Sai Sneha Priya Nemani**, **Markus Weckmann**, **YiWen Fan**, **Janesh Pillay**, **Catarina Almeda**, **Jorge Otero**, **Linda Elowsson**, **Anne-Karin Callerfelt**, **Isabelle Dupin**, **Pauline Henrot**, **Lisette van Os**, **Olivier Guenat**, **Ramon Farre**, **Joris van Dongen**, **Harold de Bruin**, **Karla Arevalo Gomez**, **Nick ten Hacken**, **Geke Teitsma**, **Michael Schuliga**, **Daryl Knight**, **Vasilena Getova**, **Meng Zhang** for the manuscripts we worked on together.

I also would like to express my appreciation to the committees/councils I've had the privilege to get involved with: giving back to the scientific community (mostly PhDs) together with you was fulfilling and fun at the same time! To my dear GUIDE PhD Council members: **Matthijs**, **Rita**, **Yehya**, **Juan**, **Noura**, **Yang**, **Sara**, **Erika** and **Mugdha**, thank you for making and keeping every first Thursday of the month interesting with our discussions and brainstorming. I wish you all the best in finalizing your PhDs! To the Dutch Society for Matrix Biology (NVMB) Early Stage Researcher Committee members: **Niek**, **Matthew**, **Josette**, **Mugdha** and **Abdullah**, thank you for adding an additional source of fun to the annual meetings we had in the last couple of years. To the Industry Perspectives in Medicine (IPIM) Summer School Organizing committee members from 2020 and 2021 editions: **Gerben**, **Eline S.**, **Eline J.**, **Ariel** and **Freek**, I have had a blast in organizing and running the two summer schools with you guys.

I also would like to thank to the Dutch Society for Matrix Biology (NVMB), Netherlands Respiratory Society (NRS) and Stitching Bestrijden Asthma (SAB) for the financial support during my PhD trajectory. I am also grateful to **Junko Hashiguchi** for the help with the original quote and translation in the dedication text.

There are two people, who are in the same journey as I have been since the very beginning, from our undergraduate study years. Regardless of the distance and time differences, we have been many things to each other: a safe haven for venting, a shoulder to cry, a critical eye when needed and unconditional support. **Bilge** and **Muge**, I am extremely grateful to your helps over the last not four but ten years. I know for sure that many things became easier and possible thanks to your support, and I appreciate our efforts to stay in touch both personally and academically between the different combinations of Turkey-Germany-Sweden-Netherlands-USA. Thank you for all you've done, and for all you've contributed.

Family is essential for such long journeys, and it's great to have their support throughout. Being away from where my family lives was difficult at times because of this reason, because sometimes text messages and video calls were not just enough. For these times, I would like to thank my partner's mother **Madalena** and her husband **Eddy**, for the nice weekend getaways and good company. I truly felt at home whenever we visited you guys, and those visits provided a nice breaks during the four years.

To my family in Turkey, I would like to express my gratitude in Turkish: biricik **anneciğim Ayşegül**, bu zamana kadar benim için yaptığın her şeye gerçekten tüm kalbimle minnettarım. Biliyorum ki bütün bu yıllar boyunca bana ve benim eğitimim için elinden geleni ardına koymadan sarf ettiğin efor ve zamanın karşılığını vermek çok zor. Canım **babam Fatih**, senin de tüm bu yıllar boyunca verdiğin destek ve teşvik icin çok teşekkür ederim. Yine de, umuyorum ve düşünüyorum ki bu tez ile ikiniz de de gurur duyacaksınız ve emeklerinizin sonucunu herkese iftiharla gösterebileceksiniz. Sevgili kardeşim **Kaan**, evin küçüğü olmana rağmen ben yokken benim sorumluluklarımın sana kaldığının farkındayım ve bu zamana kadar yaptıkların için teşekkürler. Yakından ve uzaktan, bu zamana kadarki eğitim hayatıma direkt ya da dolaylı olarak destek olan geniş ailem, herkesin ismini tek tek yazamayacağım kadar çok büyük bir aileyiz ve hepinize destekleriniz icin teşekkür ediyorum.

And finally, I would like to attempt to write couple of sentences for my dear partner, **Albano**. For the last four years during this journey, you were extremely supportive whether it was something to celebrate, something frustrating, something unfair or something surprising. You helped me see reason, you helped me calm down, you helped me decide. You were there to listen when I blabber about experimental details or paperwork. Thank you for your patience, support, time and effort in this PhD. It's not just a cliché, this thesis would not be finished without you and your grandiose involvement. As if your involvement by proxy as a partner wasn't enough, you crafted this amazing cover for this thesis and beautifully visualized our ideas for the introduction and discussion chapters in addition to professionally helping for most of the figures of almost all chapters in this thesis (and other scientific manuscripts). Meeting you was the major reason when I was trying to decide whether I wanted to stay in the Netherlands, being with you was/still is the major factor helping me succeed in finishing this journey. It's most likely not enough to say just a thank you, but even most beautifully-formed sentences would fail to describe how grateful I am. I hope I made us proud.

CURRICULUM VITAE

Mehmet Nizamoglu was born on 29 June 1992 in Kadikoy, Istanbul. He obtained his bachelor's degree in Molecular Biology and Genetics with high honors from Middle East Technical University (METU) in Ankara, Turkey, in 2016. In 2017, he was granted a full scholarship to participate in the Erasmus Mundus Joint Master's Degree program, International Master's in Innovative Medicine (IMIM). He pursued his studies at Uppsala University in Sweden, specializing in Medical Research for his Master's Degree. His Master's thesis research focused on developing alternative crosslinking strategies for methacrylated gelatin hydrogels at the Department of Polymer Chemistry in Chemistry-Angstrom. Subsequently, he joined the University of Groningen in the Netherlands for the Medical and Pharmaceutical Drug Innovation (MPDI) Master's program, where he conducted research at the Department of Pathology and Medical Biology in the University Medical Center Groningen (UMCG). His research at UMCG aimed to develop alternative methods for generating hydrogels from native tissue by exploring alternatives to pepsin digestion. In the summer of 2019, he finalized his double degree with a *cum laude* distinction in his Master's in Medical and Pharmaceutical Drug Innovation.

In September 2019, Mehmet embarked on a 2+2 Industrial PhD project with the Experimental Pulmonology and Inflammation Research (EXPIRE) group, a collaborative project between UMCG and Boehringer Ingelheim. Throughout his PhD trajectory, he presented his research at national and international scientific congresses. In addition to his scientific contributions, he actively participated in various roles within the academic community. He served as a member of the organizing committee for the Industry Perspectives in Medicine (IPIM) Summer School and successfully organized two editions of the summer school in 2020 and 2021. In 2021, he became involved with the PhD council of the Groningen University Institute of Drug Exploration (GUIDE) and assumed the role of chair in 2022. Mehmet also joined the Early Stage Researchers' committee of the Dutch Society for Matrix Biology (NVMB) in 2022, eventually becoming a board member as the representative for early stage researchers. After concluding his PhD, he transitioned to a new career as a project manager at UMCG Research BV within the UMCG in Groningen, the Netherlands.

LIST OF PUBLICATIONS

Wisman, M.*, **Nizamoglu, M.***, Noordhoek, J. A., Timens, W., Burgess, J. K. & Heijink I. H. (2023). Dysregulated cross-talk between alveolar epithelial cells and stromal cells in IPF reduces epithelial regenerative capacity. Frontiers in Medicine, 10. https://doi.org/10.0.13.61/fmed.2023.1182368

Harmsen, M. C., Getova, V., Zhang, M., Zhao, F., van Dongen, J., Martinez Garcia, F.D., **Nizamoglu, M.**, & Burgess J.K. (2023). Organ-derived ECM hydrogels: versatile systems to investigate impact of biomechanics and biochemistry on cells in disease pathology. In Handbook of the Extracellular Matrix. Springer Press *(Accepted: April 2023)* (Invited book chapter).

Nizamoglu, M.*, Joglekar M.M.*, Almeida C.A., Larsson Callerfelt, A.K., Dupin, I., Guenat, O.T., Henrot, P., van Os, L., Otero, J., Elowsson, L., Farre, R,. & Burgess, J.K. (2023). Innovative 3D models for understanding mechanisms underlying lung diseases: powerful tools for translational research. European Respiratory Review 2023; 32: 230042 https://doi.org/10.1183/16000617.0042-2023

Nizamoglu, M., & Burgess, J. K. (2023). Current possibilities and future opportunities provided by three-dimensional lung ECM-derived hydrogels. *Frontiers in Pharmacology,* 14, [1154193]. https://doi.org/10.3389/fphar.2023.1154193 (Invited perspective article).

Blokland, K. E. C., **Nizamoglu, M.,** Habibie, H., Borghuis, T., Schuliga, M., Melgert, B. N., Knight, D. A., Brandsma, C-A., Pouwels, S. D., & Burgess, J. K. (2022). Substrate stiffness engineered to replicate disease conditions influence senescence and fibrotic responses in primary lung fibroblasts. *Frontiers in Pharmacology*, 13, [989169].https://doi.org/10.3389/fphar.2022.989169

Joglekar, M. M.*, **Nizamoglu, M.*,** Fan, Y., Nemani, S. S. P., Weckmann, M., Pouwels, S. D., Heijink, I. H., Melgert, B. N., Pillay, J., & Burgess, J. K. (2022). Highway to heal: Influence of altered extracellular matrix on infiltrating immune cells during acute and chronic lung diseases. *Frontiers in Pharmacology*, 13, [995051]. https://doi.org/10.3389/fphar.2022.995051

Nizamoglu, M., Joglekar, M. M., de Hilster, R. H., Ngassie, M. L. K., Teitsma, G. J., Migulina, N., ... & Burgess, J. K. (2022). Three dimensional lung models-Three dimensional extracellular matrix models. In *3D Lung Models for Regenerating Lung*

Tissue (pp. 109-131). Academic Press. https://doi.org/10.1016/b978-0-323-90871-9.00012-7 (Invited book chapter).

Nizamoglu, M.*,de Hilster, R. H. J.*, Zhao, F., Sharma, P. K., Borghuis, T., Harmsen, M. C., & Burgess, J. K. (2022). An in vitro model of fibrosis using crosslinked native extracellular matrix-derived hydrogels to modulate biomechanics without changing composition. *Acta Biomaterialia*, 147, 50-62. https://doi.org/10.1016/j.actbio.2022.05.031

Nizamoglu, M., & Burgess, J. (2022). The Multi-Faceted Extracellular Matrix: Unlocking Its Secrets for Understanding the Perpetuation of Lung Fibrosis. *Current Tissue Microenvironment Reports*. https://doi.org/10.1007/s43152-021-00031-2 (Invited review).

Kruk, D. M., Wisman, M., Noordhoek, J. A., **Nizamoglu, M**., ... & Heijink, I. H. (2021). Paracrine Regulation of Alveolar Epithelial Damage and Repair Responses by Human Lung-Resident Mesenchymal Stromal Cells. *Cells*, 10(11), [2860]. https://doi.org/10.3390/cells10112860

Vasse, G. F.*, **Nizamoglu, M.*,** Heijink, I. H., Schlepütz, M., van Rijn, P., Thomas, M. J., Burgess, J. K., & Melgert, B. N. (2021). Macrophage-stroma interactions in fibrosis: Biochemical, biophysical, and cellular perspectives. *Journal of Pathology*, 254(4), 344-357. https://doi.org/10.1002/path.5632 (Invited review, highlighted in the 2021 Annual Review Issue of The Journal of Pathology).


GRIAC
Groningen